

AKO 3111.1-PTCF

AD-A281 261



HIGH RESOLUTION SPECTROSCOPY

POSTCONFERENCE EDITION

DTIC
ELECTE
JUL 12 1984
S F D



Sponsored by
Optical Society of America

In Cooperation with
American Physical Society

1993 TECHNICAL DIGEST
SERIES VOLUME 1

JANUARY 18-21, 1993
SALT LAKE CITY,
UTAH

This document has been approved
for public release and sale; its
distribution is unlimited.

AD-A281 261

1993 OSA Technical Digests

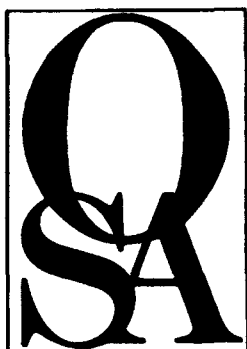
- Vol. 1** High Resolution Spectroscopy Salt Lake City, UT (January 18-21)
Postconference edition: ISBN 1-55752-273-1 [U.S. List Price: \$66 / OSA Member Price: \$43]
- Vol. 2** Compact Blue-Green Lasers New Orleans, LA (February 2-4)
Postconference edition: ISBN 1-55752-278-2 [U.S. List Price: \$75 / OSA Member Price: \$48]
- Vol. 3** Ophthalmic and Visual Optics AND Noninvasive Assessment of the Visual System
Monterey, CA (February 19-23)
Postconference edition: ISBN 1-55752-280-4 [U.S. List Price: \$92 / OSA Member Price: \$60]
- Vol. 4** Optical Fiber Communication Conference & International Conference on Integrated Optics and Optical Fiber Communication San Jose, CA (February 21-26)
Postconference edition: ISBN 1-55752-282-0 [U.S. List Price: \$92 / OSA Member Price: \$60]
- Vol. 5** Optical Remote Sensing of the Atmosphere Salt Lake City, UT (March 8-12)
Postconference edition: ISBN 1-55752-284-7 [U.S. List Price: \$92 / OSA Member Price: \$60]
- Vol. 6** Spatial Light Modulators and Applications Palm Springs, CA (March 15-17)
Postconference edition: ISBN 1-55752-288-X [U.S. List Price: \$75 / OSA Member Price: \$48]
- Vol. 7** Optical Computing Palm Springs, CA (March 16-19)
Postconference edition: ISBN 1-55752-290-1 [U.S. List Price: \$75 / OSA Member Price: \$48]
- Vol. 8** Quantum Optoelectronics Palm Springs, CA (March 17-19)
Postconference edition: ISBN 1-55752-292-8 [U.S. List Price: \$75 / OSA Member Price: \$48]
- Vol. 9** Optical Design for Photonics Palm Springs, CA (March 22-24)
Postconference edition: ISBN 1-55752-294-4 [U.S. List Price: \$75 / OSA Member Price: \$48]
- Vol. 10** Integrated Photonics Research Palm Springs, CA (March 22-25)
Postconference edition: ISBN 1-55752-296-0 [U.S. List Price: \$92 / OSA Member Price: \$60]
- Vol. 11** Conference on Lasers and Electro-Optics Baltimore, MD (May 2-7)
Postconference edition: ISBN 1-55752-300-2 [U.S. List Price: \$92 / OSA Member Price: \$60]
- Vol. 12** Quantum Electronics and Laser Science Baltimore, MD (May 2-7)
Postconference edition: ISBN 1-55752-301-0 [U.S. List Price: \$92 / OSA Member Price: \$60]
- Vol. 13** Soft X-Ray Projection Lithography Monterey, CA (May 10-12)
Postconference edition: ISBN 1-55752-304-5 [U.S. List Price: \$66 / OSA Member Price: \$43]
- Vol. 14** Light and Color in the Open Air University Park, PA (June 16-18)
Postconference edition: ISBN 1-55752-305-3 [U.S. List Price: \$66 / OSA Member Price: \$43]
- Vol. 15** Optical Amplifiers and Their Applications Yokohama, Japan (July 4-6)
Postconference edition: ISBN 1-55752-310-X [U.S. List Price: \$75 / OSA Member Price: \$48]
- Vol. 16** Nonlinear Guided Wave Phenomena Southampton, UK (September 19-22)
Postconference edition: ISBN 1-55752-312-6 [U.S. List Price: \$75 / OSA Member Price: \$48]
- Vol. 17** OSA Annual Meeting Toronto, Canada (October 3-8)
Postconference edition: ISBN 1-55752-314-2 [U.S. List Price: \$75 / OSA Member Price: \$48]
- Vol. 18** Organic Thin Films for Photonic Applications Toronto, Canada (October 6-8)
Postconference edition: ISBN 1-55752-316-9 [U.S. List Price: \$75 / OSA Member Price: \$48]

(All Technical digests and Postconference editions are paperback.)

Order by phone, fax, or mail. To charge by phone, call (202) 416-1907.
(We accept VISA, MasterCard, Diner's Club, and AMEX.) Fax your order and
charge information to (202) 416-6120. Mail your order to: OSA Publications Dept.,
ATTN: Susan Borst, 2010 Massachusetts Ave., NW, Washington, DC 20036-1023.
Orders are accepted up to six months in advance of the meeting.



REPORT DOCUMENTATION PAGE			Form Approved OMB No. 0704-0188	
Public reporting burden for this collection of information is estimated to average 1 hour per response, including the time for reviewing instructions, searching existing data sources, gathering and maintaining the data needed, and completing and reviewing the collection of information. Send comments regarding this burden estimate or any other aspect of this collection of information, including suggestions for reducing this burden, to Washington Headquarters Services, Directorate for Information Operations and Reports, 1215 Jefferson Davis Highway, Suite 1204, Arlington, VA 22202-4302, and to the Office of Management and Budget, Paperwork Reduction Project (0704-0188), Washington, DC 20503				
1. AGENCY USE ONLY (Leave blank)	2. REPORT DATE May 1994	3. REPORT TYPE AND DATES COVERED Final 10 Dec 92-14 Jan 94		
4. TITLE AND SUBTITLE High Resolution Spectroscopy			5. FUNDING NUMBERS DAAH04-93-G-0056	
6. AUTHOR(S) Jarus W. Quinn				
7. PERFORMING ORGANIZATION NAME(S) AND ADDRESS(ES) Optical Society of America Washington, DC 20036-2571			8. PERFORMING ORGANIZATION REPORT NUMBER	
9. SPONSORING/MONITORING AGENCY NAME(S) AND ADDRESS(ES) U.S. Army Research Office P.O. Box 12211 Research Triangle Park, NC 27709-2211			10. SPONSORING/MONITORING AGENCY REPORT NUMBER ARO 31111.1-PH-CF	
11. SUPPLEMENTARY NOTES The views, opinions and/or findings contained in this report are those of the author(s) and should not be construed as an official Department of the Army position, policy, or decision, unless so designated by other documentation.				
12a. DISTRIBUTION/AVAILABILITY STATEMENT Approved for public release; distribution unlimited.			12b. DISTRIBUTION CODE	
13. ABSTRACT (Maximum 200 words) The postconference edition of the High Resolution Spectroscopy conference contains summaries of the papers presented at the meeting. The sessions at the conference included double resonance techniques, intra- and intermolecular interactions, sub-doppler techniques, condensed phase spectroscopy laboratory astrophysics and atoms and radicals.				
14. SUBJECT TERMS High Resolution Spectroscopy, Conference, Molecular Interactions, Sub-Doppler Techniques, Spectroscopy, Astrophysics			15. NUMBER OF PAGES 198	
			16. PRICE CODE	
17. SECURITY CLASSIFICATION OF REPORT UNCLASSIFIED	18. SECURITY CLASSIFICATION OF THIS PAGE UNCLASSIFIED	19. SECURITY CLASSIFICATION OF ABSTRACT UNCLASSIFIED	20. LIMITATION OF ABSTRACT UL	



High Resolution Spectroscopy

*Summaries of papers presented at the
High Resolution Spectroscopy
Topical Meeting*

January 18–21, 1993
Salt Lake City, Utah

1993 Technical Digest Series
Volume 1

POSTCONFERENCE EDITION

Sponsored by
Optical Society of America

In Cooperation with
American Physical Society

Optical Society of America
2010 Massachusetts Avenue, NW
Washington, DC 20036-1023

Accession For	
NTIS CRA&I	<input checked="" type="checkbox"/>
DTIC TAB	<input type="checkbox"/>
Unannounced	<input type="checkbox"/>
Justification	
By	
Distribution /	
Availability Codes	
Dist	Avail and/or Special
A-1	

94-21157
392 813

94 7 11 159

Articles in this publication may be cited in other publications. In order to facilitate access to the original publication source, the following form for the citation is suggested:

Name of Author(s), "Title of Paper," in High Resolution Spectroscopy Technical Digest, 1993 (Optical Society of America, Washington, D.C., 1993), Vol. 1, pp. xx-xx.

ISBN Number

Conference Edition	1-55752-272-3
Postconference Edition	1-55752-273-1
(Note: Postconference Edition includes postdeadline papers.)	
1993 Technical Digest Series	1-55752-317-7

Library of Congress Catalog Card Number

Conference Edition	92-62707
Postconference Edition	92-62708

Copyright © 1993, Optical Society of America

Individual readers of this digest and libraries acting for them are permitted to make fair use of the material in it, such as to copy an article for use in teaching or research, without payment of fee, provided that such copies are not sold. Copying for sale is subject to payment of copying fees. The code 1-55752-317-7/93/\$2.00 gives the per-article copying fee for each copy of the article made beyond the free copying permitted under Sections 107 and 108 of the U.S. Copyright Law. The fee should be paid through the Copyright Clearance Center, Inc., 21 Congress Street, Salem, MA 01970.

Permission is granted to quote excerpts from articles in this digest in scientific works with the customary acknowledgment of the source, including the author's name and the name of the digest, page, year, and name of the Society. Reproduction of figures and tables is likewise permitted in other articles and books provided that the same information is printed with them and notification is given to the Optical Society of America. Republication or systematic or multiple reproduction of any material in this digest is permitted only under license from the Optical Society of America; in addition, the Optical Society may require that permission also be obtained from one of the authors. Address inquiries and notices to Director of Publications, Optical Society of America, 2010 Massachusetts Avenue, NW, Washington, DC 20036-1023. In the case of articles whose authors are employees of the United States Government or its contractors or grantees, the Optical Society of America recognizes the right of the United States Government to retain a nonexclusive, royalty-free license to use the author's copyrighted article for United States Government purposes.

Printed in U.S.A.

CONTENTS

Agenda of Sessions	v
MA Double Resonance Techniques	1
MB Poster and Postdeadline Session 1	13
TuA Intra- and Intermolecular Interactions	35
TuB Sub-Doppler Techniques	55
WA Condensed Phase Spectroscopy	69
WB Poster and Postdeadline Session 2.....	89
ThA Laboratory Astrophysics	121
ThB Atoms and Radicals.....	131
Key to Authors and Presiders.....	149

TECHNICAL PROGRAM COMMITTEE

Laura A. Phillips, Chair
Cornell University

Geoffrey A. Blake, Chair
California Institute of Technology

Mark C. Abrams
Jet Propulsion Laboratory

Phillip R. Bunker
Herzberg Institute

Peter M. Felker
University of California, Los Angeles

H. Jeffrey Kimble
California Institute of Technology

John H. Lacy
University of Texas, Austin

Andrzej W. Miziolek
U.S. Army Laboratory

Janice Reutt-Robey
University of Maryland

Alec M. Wodtke
University of California, Santa Barbara

SUNDAY, JANUARY 17, 1993

COTTONWOOD ROOM

5:30 pm–8:00 pm REGISTRATION

SALON C

6:30 pm–8:00 pm INFORMAL OPENING RECEPTION

MONDAY, JANUARY 18, 1993

COTTONWOOD

7:30 am–12:00 m REGISTRATION AND SPEAKER CHECK-IN

SALON D

**7:55 am–8:00 am
OPENING REMARKS**

Laura A. Philips, *Cornell University*

8:00 am–11:45 am

MA, DOUBLE RESONANCE TECHNIQUES

Laura A. Philips, *Cornell University, Presider*

8:00 am (Invited)

MA1 Laser induced fluorescence probing of highly vibrationally excited acetylene: vibrational state mixing in the ground and electronically excited states, F. Fleming Crim, *Univ. Wisconsin–Madison*. Vibrational overtone excitation and laser-induced fluorescence detection identify the mixing of vibrations in the ground electronic state and determine the vibrational structure in the excited state, including the frequencies of all the ungerade vibrations. (p. 2)

8:45 am (Invited)

MA2 Selectivity, sensitivity, speed, and sub-Doppler resolution are not incompatible, Michael C. McCarthy, Hideto Kanamori, Mingguang Li, Robert W. Field, *Massachusetts Institute of Technology*. The combination of magnetic rotation, electro-optic frequency modulation, and sub-Doppler $\Delta M_J = 2$ Zeeman resonance tunable laser techniques yields J, ΔJ , and g, presorted spectra at near shot-noise-limited sensitivity. (p. 3)

SALON C

9:30 am–10:00 am COFFEE BREAK

MONDAY, JANUARY 18, 1993—Continued

SALON D

10:00 am (Invited)

MA3 High-resolution stimulated Brillouin gain spectroscopy, Richard A. MacPhail, W. Tandy Grubbs, *Duke Univ.* Several examples are presented to illustrate the application of high-resolution stimulated Brillouin gain spectroscopy to liquids, supercooled liquids, and glasses. (p. 4)

10:45 am

MA4 Stimulated emission pumping (SEP) spectroscopy of propynal: an example of "sparse" IVR at high vibrational state density, C. A. Rogaski, J. Price, A. M. Wodtke, *UC–Santa Barbara*. SEP spectra of propynal are recorded and rotational constants obtained. The SEP spectra are simple and show perturbations due to anharmonic resonances. The SEP results are discussed in the context of IVR. (p. 7)

11:15 am

MA5 Time-resolved optical double resonance spectroscopy in acetylene: exploring rovibrational energy transfer at various levels of excitation, A. P. Milce, H.-D. Barth, B. L. Chadwick, B. J. Orr, *Macquarie Univ., Australia*. Time-resolved infrared–ultraviolet and Raman–ultraviolet double resonance spectroscopy enables state-selective studies of rotationally resolved vibrational energy transfer in gas-phase acetylene, emphasizing the role of intramolecular perturbations. (p. 8)

11:45 am–8:00 pm FREE TIME

COTTONWOOD

7:30 pm–10:00 pm REGISTRATION AND SPEAKER CHECK-IN

SALON B

8:00 pm–10:00 pm

MB, POSTER AND POSTDEADLINE SESSION 1

MB1 Substituted ethanes: a study of vibrational mode-coupling, C. Cameron Miller, H. Li, Laura A. Philips, *Cornell Univ.* Presented is a comparison of mode-coupling involving torsions in substituted ethanes and the puckering mode in cyclobutane as studied via high resolution infra-red spectroscopy. (p. 14)

MB2 Inverse Raman spectroscopy measurements of line-shift coefficients in hydrogen perturbed by argon, J. W. Forsman, R. L. Farrow, L. A. Rahn, *Sandia National Laboratories*. Measurements of the Raman Q branch line-shift coefficients in H₂-Ar mixtures show a rotational dependence which compares qualitatively with calculations for D₂ in Ar. (p. 17)

MONDAY, JANUARY 18, 1993—Continued

MB3 High-resolution electronic spectroscopy of ZnCH₃ and CdCH₃, Timothy M. Cerny, Xue-Qing Tan, Eric S. J. Robles, Andrew M. Ellis, James M. Williamson, Terry A. Miller, *Ohio State Univ.* The high-resolution (~ 0.0033 cm⁻¹) laser-induced fluorescence spectra of ZnCH₃ and CdCH₃ have been recorded and analyzed. Fine and hyperfine structure are observed. (p. 20)

MB4 Tunable far-infrared laser spectroscopy of hydrogen bonds, Paul Stockman, Sakae Suzuki, Geoffrey A. Blake, *California Institute of Technology*. Sub-doppler far-infrared vibration-rotation-tunneling spectra of several water- and ammonia-containing clusters will be presented. Intermolecular potential energy surfaces derived from these spectra will also be discussed. (p. 24)

MB5 Stimulated emission pumping (SEP) studies of energy transfer in highly vibrationally excited oxygen, J. A. Mack, J. M. Price, Alec M. Wodtke, *UC-Santa Barbara*. Rate constants for the collisional deactivation of SEP prepared O₂(v'' = 18–25) by O₂(v'' = 0) have been determined from the pressure dependent lifetimes of each probed vibrational level at temperatures of 295 and 395 K. Implications of the measured rates for atmospheric chemical reactions are discussed. (p. 25)

MB6 Renner-Teller and spin-orbit perturbations in triatomic molecules, Alexander Alijah, *Univ. Bielefeld, Germany*; Geoffrey Duxbury, *Univ. Strathclyde, Scotland*. A method of calculating the effects of Renner-Teller and spin-orbit coupling in triatomic dihydrides has been developed. Examples are given of radiative lifetime variations. (p. 26)

MB7 Electronic surface state and plasmon-phonon coupled excitations at the surface of modulation-doped GaAs/AlGaAs multiquantum wells: a study of high-resolution electron-energy-loss spectroscopy (HREELS), R.H. Yu, *Central Washington Univ.* We have used a modulated doping profile, including an accumulation or a depletion surface layer, in our self-consistent calculations of potential and carrier density profile. The plasmon-phonon coupled carrier excitations associated with the Tamm states have been studied via the calculated electron-energy-loss spectrum within the random-phase-approximation. (p. 28)

MB8 Growth and detection of an antitropic spectral hole in tetraphenylporphyrin derivatives by polarization spectroscopy, Luo Xiao, Zhao Youyuan, *Fudan Univ., China*. We report a high-resolution technique which detects the dynamic of a polarized hole with signal-to-noise 30 times greater than that of absorption spectroscopy. Dynamic equations are developed to account for the dichroism and birefringence of the hole. (p. 29)

MB9 Deconvolution method used in the analysis of a-C Raman spectrum, Qi Wang, D. D. Allred, *Brigham Young Univ.* Deconvolution is introduced into the analysis of amorphous carbon Raman spectrum. The deconvolution is based on the modified Van Cittert' method. (p. 30)

TUESDAY, JANUARY 19, 1993

COTTONWOOD

7:30 am–12:30 pm REGISTRATION AND SPEAKER CHECK-IN

SALON D

8:00 am–12:15 pm
TuA, INTRA- AND INTERMOLECULAR INTERACTIONS
Geoffrey A. Blake, *California Institute of Technology*,
President

8:00 am (Invited)
TuA1 Spectroscopic studies of weakly bound molecular complexes, William Klemperer, *Harvard Univ.* Recent studies of the species ArL₂, ArHCN, ArHF, and (HF)₂ are discussed, in terms of molecular structure and photodissociation dynamics. (p. 36)

8:45 am (Invited)
TuA2 Infrared molecular beam spectroscopy: the study of weakly bound molecular complexes as a probe of potential energy surfaces and molecular dynamics, R. E. Miller, *Univ. North Carolina*. The experiments reported in this talk were carried out using the optothermal detection method. A number of systems are discussed which illustrate some of the different types of wide amplitude motions that are typical of these systems. The influence of these internal motions on vibrational predissociation is also discussed. (p. 39)

9:30 am
TuA3 High-resolution electronic spectroscopy of hydroxyl-rare gas complexes, Bor-Chen Chang, James M. Williamson, James R. Dunlop, Terry A. Miller, *Ohio State Univ.* We have observed and analyzed the rotational, fine, and hyperfine structure in the high-resolution (0.008 cm⁻¹) laser-induced fluorescence spectra of Ar·OH/D and Ne·OH/D. (p. 40)

SALON C

10:00 am–10:30 am COFFEE BREAK

SALON D

10:30 am
TuA4 Conformational interchange in the 10- μ m and 3- μ m infrared spectra of propargyl amine, Anne M. Andrews, Gerald T. Fraser, Brooks H. Pate, *National Institute of Science and Technology*. The propargyl amine spectrum was observed using an electric resonance optothermal spectrometer coupled to a CO₂ laser-microwave sideband system for measurement of 10- μ m spectra and to a color center laser for 3- μ m spectra. (p. 44)

11:00 am (Invited)
TuA5 Molecular collisions at very low temperature, Frank C. De Lucia, *Ohio State Univ.* A new technique, collisional cooling, for the study of molecular collisions at very low temperatures will be described, and experimental and theoretical results presented. (p. 48)

TUESDAY, JANUARY 19, 1993—Continued

11:45 am

TuA6 First rotational analysis of the infrared spectrum of dimethylacetylene, P. R. Bunker, J. W. C. Johns, A. R. W. McKellar, C. Di Lauro, *Univ. Degli Studi di Napoli, Italy*. The spectrum around 10 μm of cooled dimethylacetylene has been rotationally analyzed. Internal rotation splittings and intramolecular vibrational coupling effects have been resolved and interpreted. (p. 52)

12:15 pm–8:00 pm FREE TIME

COTTONWOOD

7:30 pm–10:30 pm REGISTRATION AND SPEAKER CHECK-IN

SALON C

8:00 pm–11:00 pm CONFERENCE RECEPTION

SALON D

8:30 pm–10:00 pm

TuB, SUB-DOPPLER TECHNIQUES

Peter Felker, *University of California at Los Angeles, Presider*

8:30 pm

TuB1 Nearly degenerate four-wave mixing lineshapes in gases, Larry A. Rahn, *Sandia National Laboratories*. Expressions for nearly degenerate four-wave mixing lineshapes are presented and compared with high-resolution measurements on OH molecules in a flame. (p. 56)

9:00 pm

TuB2 Doppler-free spectroscopy of molecular iodine near 532 nm, Ady Arie, Robert L. Byer, *Stanford Univ.* Two frequency-doubled diode-pumped Nd:YAG lasers are used to study the hyperfine spectrum of $^{127}\text{I}_2$ by heterodyne spectroscopy. Hyperfine constants for eight ro-vibrational transitions are obtained. (p. 60)

9:30 pm

TuB3 Stark quantum-beat spectroscopy: the electric dipole moment of NO (A), J. A. Gray, R.L. Farrow, J. L. Durant, Jr., L. R. Thorne, *Sandia National Laboratories*. We observe fluorescence quantum beats in fields ≤ 22.5 kV/cm. Fourier analysis yields narrow (2 MHz) Stark/hyperfine frequencies which are fit to a model Hamiltonian. (p. 64)

WEDNESDAY, JANUARY 20, 1993

COTTONWOOD

7:30 am–12:00 m REGISTRATION AND SPEAKER CHECK-IN

SALON D

8:00 am–11:45 am

WA, CONDENSED PHASE SPECTROSCOPY

Janice Reutt-Robey, *University of Maryland, Presider*

8:00 am (Invited)

WA1 Dynamics in glasses probed with optical nonlinear line-narrowing experiments, Michael D. Fayer, *Stanford Univ.*

Optical nonlinear experiments, including hole burning, picosecond photon echoes, and the first psec infrared photon echo measurements of vibrational dephasing are used to probe solute-solvent interactions and multi-time-scale dynamics in organic glasses. (p. 70)

8:45 am (Invited)

WA2 Applications of high-resolution coherent Raman spectroscopy, Joseph W. Nibler, *Oregon State Univ.*

The development of a system for high-resolution (0.001 cm^{-1}) CARS and stimulated Raman spectroscopy will be described. The use for study of torsional splittings in ethane and the spectral and phase properties of small to large molecular clusters of aco_2 formed in jet expansions are discussed. (p. 72)

SALON C

9:30 am–10:00 am COFFEE BREAK

SALON D

10:00 am (Invited)

WA3 Time-resolved probes of adsorbate-substrate energy transfer, Richard R. Cavanagh, *National Institute of Standards and Technology*.

Subpicosecond pump-probe techniques are applied to study adsorbate energy transfer in CO/Pt(111). The coupling strength of CO($v=1$) to platinum, and of optically excited platinum to low-frequency Pt-CO modes are shown to be comparable. (p. 76)

10:45 am

WA4 Optimization of Raman signal enhancement in Kretschmann configuration, N. Primeau, J. L. Coutaz, *LEMO-ENSERG, France*; L. Abello, *LIES-ENSEEG, France*.

The influence of the metal film thickness on surface plasmons-enhanced Raman scattering in Kretschmann geometry is experimentally determined for the first time. At the optimum thickness, an enhancement factor of the order of 10^4 has been observed. (p. 80)

WEDNESDAY, JANUARY 20, 1993—Continued

11:15 am

WA5 High resolution spectroscopy on single molecules, Jerzy Sepiol, Frank Cüttler, Marco Pirotta, Alois Renn, Urs P. Wild, *Swiss Federal Institute of Technology, Switzerland*. Using the solid p-terphenyl as a trap, Stark shifts, and the dependence of the fluorescence intensity on the polarization of the exciting laser light has been determined for single pentacene molecules. (p. 84)

11:45 am–8:00 pm FREE TIME

COTTONWOOD

7:30 pm–10:00 pm REGISTRATION AND SPEAKER CHECK-IN

SALON B

8:00 pm–10:00 pm

WB, POSTER AND POSTDEADLINE SESSION 2

WB1 Low-pressure measurements of line-broadening coefficients in CH_3F , M. Nischan, D. Clark, D. Guerin, A. W. Mantz, *Franklin and Marshall College*. Plotting the measured unblended line halfwidth squared versus pressure squared produces a linear plot at all pressures. Both laser linewidth and broadening coefficient may be accurately determined this way. (p. 90)

WB2 Measurement of collision cross section and line broadening coefficient for $2p_8 \leftrightarrow 4d_4$ transition in neon, P. R. Sasi Kumar, S. S. Harilal, V. P. N. Nampoori, C. P. G. Vallabhan, *Cochin Univ. Science and Technology, India*. The collision cross section and broadening coefficient for $2p_8 \leftrightarrow 4d_4$ transition in neon has been evaluated by high-resolution optical-galvanic spectroscopy using a single mode ring dye laser. (p. 92)

WB3 Position, shape, and polarization dependence of resonances in the laser photoionization spectrum of aligned $\text{Ca } 4s5p \ ^1P_1$, D. W. Duquette, K. W. McLaughlin, D. S. Eschliman, O. P. Francis, *Univ. Nebraska*. The relative photoionization cross section of an excited level of calcium is measured as a function of energy and polarization of the ionizing photons. (p. 97)

WB4 Production of high-intensity beams of ultracold atoms for high-resolution spectroscopy, E. Korsunsky, D. Kosachiov, *St.-Petersburg State Technical Univ., Russia*; Yu. Rozhdestvensky, *Vavilov State Optical Institute, Russia*. We suggest the collimation technique to get the collimated atomic beam practically without intensity loss and discuss the production of the intensive beam using the two-zone interaction scheme. (p. 101)

WEDNESDAY, JANUARY 20, 1993—Continued

WB5 Velocity selection technique for high-resolution spectroscopy, E. Korsunsky, D. Kosachiov, *St.-Petersburg State Technical Univ., Russia*; Yu. Rozhdestvensky, *Vavilov State Optical Institute, Russia*. In the velocity selection method the formation of lower recoil velocity structures is performed not only by the counterpropagating, but also by co-propagating light waves. This fact allows formation of two-dimensional velocity distribution. Resultant two-dimensional selection permits accumulation of the atoms that are unique for high-resolution spectroscopy. (p. 105)

WB6 New spectroscopic techniques on the basis of elliptically polarized pumping, Igor I. Gancheryonok, Yasuo Kanematsu, Takashi Kushida, *Osaka Univ., Japan*. We present new spectroscopic methods that exploit pump ellipticity dependence of polarization alterations of the probe wave. Independence of the parameters to be obtained on the pump intensity can considerably enhance the accuracy of measurements. (p. 109)

WB7 Very high resolution spectrometer at the National Institute of Standards and Technology, John Fortna, Harry Morgan, Hailemichael Seyoum, *Univ. District of Columbia*; Araya Asfaw, *Howard Univ.*; David C. Humm, *St. Mary's College of Maryland*. The very high resolution spectrometer at the Synchrotron Ultraviolet Radiation Facility has been upgraded with improved beamline throughput, instrument control, and data acquisition. (p. 113)

WB8 Precise pulsed laser spectroscopy in the visible and fuv region: toward the measurement of the 1^1S - 2^1S interval in atomic helium, S. Gangopadhyay, N. Melikechi, E. E. Elyer, *Univ. Delaware*. The frequency evolution of laser radiation produced during amplification and by doubling is studied. A scheme for the generation of vuv radiation is also reported. (p. 117)

THURSDAY, JANUARY 21, 1993

COTTONWOOD

7:30 am–12:30 pm **REGISTRATION AND
SPEAKER CHECK-IN**

SALON D

8:00 am–9:45 am
ThA, LABORATORY ASTROPHYSICS
John H. Lacy, *University of Texas, President*

8:00 am (Invited)
ThA1 Carbenes in the interstellar gas, Patrick Thaddeus, *Harvard-Smithsonian Center for Astrophysics*. The identification of one of the most abundant and widespread interstellar carbenes, the cyclopropenylidene ring, C_3H_2 , is described, together with recent laboratory work on the excited vibrational states of this molecule and on the geometrical structure of one of its isomers, the carbon chain carbene H_2C_3 . (p. 122)

8:45 am
ThA2 Infrared laser spectroscopy of jet-cooled carbon clusters: the structure and spectroscopy of $^3\Sigma C_n$, Hyun-Jin Hwang, Alan K. Van Orden, Keiichi Tanaka, Erica W. Kuo, James R. Heath, Richard J. Saykally, *UC Berkeley*. This paper will describe the application of the Berkeley supersonic cluster beam apparatus for diode laser spectroscopy to the characterization of linear C_n . (p. 123)

9:15 am
ThA3 Near-threshold structure of molecular hydrogen at the $1s + 2I$ dissociation limit, E. E. Eyler, B. F. Catching, N. Melikechi, *Univ. Delaware*. Both bound-state and continuum structure have been studied in the region near the second dissociation limit of the H_2 , HD, and D_2 molecules. Fine and hyperfine interactions result in surprisingly complex spectra. (p. 127)

SALON C

9:45 am–10:15 am **COFFEE BREAK**

SALON D

10:15 am–12:15 pm
ThB, ATOMS AND RADICALS
Andrzej W. Miziolek, *U.S. Army Laboratory, President*

10:15 am
ThB1 b-Dipole transitions in \tilde{X}^1A' t-HOCO observed by FIR laser magnetic resonance, Trevor J. Sears, H. E. Radford, Mary Ann Moore, *Harvard Smithsonian Center for Astrophysics*. b-dipole transition frequencies in hydroxyformyl depend directly on the A rotational constant, and analysis improves the structural parameters for this important species. (p. 132)

THURSDAY, JANUARY 21, 1993—Continued

10:45 am
ThB2 Infrared Fourier transform and diode laser spectra of formaldoxime, R. Bannai, G. Duxbury, *Univ. Strathclyde, Scotland*. Vibrational, rotational, and intensity parameters of formaldoxime have been derived from the analysis of Fourier transform and diode laser in the 5–14 μm region. (p. 136)

11:15 am
ThB3 Ultranarrow velocity distributions of slow atoms produced with the Zeeman tuning technique, S. C. Zilio, V. S. Bagnato, *Univ. Sao Paulo, Brazil*. We have produced an atomic beam with a very narrow velocity distribution through the use of the Zeeman tuning technique together with a stimulated Raman transition. (p. 138)

11:45 am
ThB4 Laser preparation and probing of initial and final angular momentum states in the collision-induced energy transfer $Ca(4s4p^3P_1) + He \rightarrow Ca(4s4p^3P_2) + He$, Eileen M. Spain, Christopher J. Smith, Mark J. Dalberth, Stephen R. Leone, *Univ. Colorado*. State-to-state relative cross sections are measured for the collision-induced near-resonant electronic energy transfer process $Ca(4s4p^3P_1) + He \rightarrow Ca(4s4p^3P_2) + He$. Laser preparation and probing of the initial and final m sublevels of the $J=1 \rightarrow J=2$ collisional transfer are performed using linearly and circularly polarized laser light in a crossed-beam apparatus. (p. 142)

12:15 pm–12:20 pm
CLOSING REMARKS
Geoffrey A. Blake, *California Institute of Technology*

Monday, June 18, 1993

Double Resonance Techniques

MA 8:00am–11:45am
Salon D

Laura A. Philips, *Presider*
Cornell University

**Laser Induced Fluorescence Probing of Highly Vibrationally
Excited Acetylene: Vibrational State Mixing in the Ground
and Electronically Excited States**

**F. Fleming Crim
University of Wisconsin—Madison
Department of Chemistry
Madison, WI 53706**

Vibrational overtone excitation and laser induced fluorescence detection identify the mixing of vibrations in the ground electronic state and determine the vibrational structure in the excited state, including the frequencies on all the ungerade vibrations.

**Selectivity, Sensitivity, Speed, and Sub-Doppler
Resolution Are Not Incompatible**

**Michael C. McCarthy, Hideto Kanamori,
Mingguang Li, Robert W. Field
Massachusetts Institute of Technology
Cambridge, MA 02173**

The combination of magnetic rotation electro-optic frequency modulation, and sub-Doppler $\Delta M_J = 2$ Zeeman resonance tunable laser techniques yields J , ΔJ , and g_J presorted spectra at near shot-noise-limited sensitivity.

High Resolution Stimulated Brillouin Gain Spectroscopy

W. Tandy Grubbs and Richard A. MacPhail
Department of Chemistry
Duke University
Durham, NC 27708
(919) 660-1536

Brillouin spectroscopy has been an important source of information about the collective dynamics of molecules in liquids.^{1,2} In a conventional Brillouin experiment, a Fabry-Perot interferometer is used to measure the spectrum of laser light scattered at an angle θ by spontaneous density fluctuations in a sample. The Brillouin peaks in the spectrum arise from the acoustic wave component of these density fluctuations, and accordingly the shift of the Brillouin peaks from the elastic Rayleigh scattering peak corresponds to the acoustic frequency, while the width of the Brillouin peaks corresponds to the acoustic damping rate. By varying θ , and thus the scattering wavevector, one can determine the dispersion in the speed of sound and the acoustic attenuation, which in turn characterize the elastic and viscous responses of the fluid. A more detailed analysis of the spectral lineshape with the aid of generalized hydrodynamic theories allows one to determine the values of transport coefficients that describe the molecular dynamics.¹

In recent years much attention has focussed on the Brillouin spectra of supercooled, viscoelastic liquids, whose dynamics are inherently more complicated and interesting than those of simple liquids.² Whereas at high temperatures the fluid dynamics and Brillouin spectrum can usually be described in terms of a few coupled exponentially relaxing variables, in the supercooled regime many liquids exhibit complex dynamical behavior and highly non-exponential relaxation. These dynamics are reflected in the dispersion of the Brillouin shifts and widths, and also through additional features in the spectrum, such as the "Mountain mode"^{1,2} which arises from coupling between the acoustic waves and structural relaxation processes that slow down as the glass transition is approached. In order to characterize these dynamics fully, it is crucial to obtain Brillouin spectra over a wide dynamic range, i.e. over a wide range of scattering angles, and over a wide range of temperatures. Unfortunately, limitations on the finesse and contrast of conventional interferometers make such measurements particularly difficult in the supercooled liquid and glassy regimes where the Brillouin lines are narrow, the Brillouin shifts large, and the elastic scattering strong.

One way to address these instrumental limitations is to turn from spontaneous light scattering techniques to coherent, stimulated scattering techniques. While stimulated Brillouin scattering was discovered quite some time ago,^{3,4} only recently has it been exploited to perform truly high resolution spectroscopy in either the frequency⁵⁻¹¹ or time domain.^{12,13} In the frequency domain, cw stimulated Brillouin gain (SBG) spectroscopy is perhaps the most attractive method for high resolution Brillouin spectroscopy. This technique, essentially a version of the cw stimulated Raman spectroscopy methods pioneered by Owyong,¹⁴ has now been demonstrated

for gases,⁶ optical glass,⁷ and a variety of liquids.⁸⁻¹¹ In this four-wave mixing experiment, two lasers are used to stimulate and probe hypersonic sound waves in the sample. As in stimulated Raman gain spectroscopy, the resolution is determined by the linewidths of the lasers employed. Our own SBG apparatus employs low power, frequency-stabilized cw lasers for maximum resolution, and spectra with good signal-to-noise are obtained through the use of balanced detection and double modulation.⁸⁻¹¹ A confocal reference etalon, which is locked to the HeNe probe laser frequency, is used to linearize the frequency scans of our pump laser, a ring dye-laser, so that highly accurate measurements of Brillouin shifts can be made.^{10,11}

Building on the work of Jacobsen and Shen⁵ and of She and coworkers,⁶ we recently provided the first demonstration of high resolution cw SBG spectroscopy applied to liquids.⁸ The Brillouin shifts and widths measured in a backscattering geometry for thirteen different liquids were perfectly consistent with previous spontaneous scattering results, but as expected the resolution of the cw SBG spectra is much higher. In addition, because of the weighting of the spectral density in the SBG spectrum, the Rayleigh peak is absent and the inherent contrast against elastic scattering is high. Even so, the presence of the central "Mountain mode" feature in the SBG spectrum of carbon tetrachloride (which in this case arises from coupling of the acoustic modes to internal vibrational relaxation in the molecules) can be detected.

We have also carried out a systematic study of the scattering angle dependence of the SBG spectra of liquid carbon disulfide that illustrates the feasibility of such measurements and also some limitations of our apparatus.⁹ SBG spectra obtained at angles between 1 and 179° showed an increase in the Brillouin shift by almost two orders of magnitude, a large dynamic range for Brillouin measurements. Unfortunately, the peak gain falls off rapidly as the angle decreases from 179°, by a factor of 20 at forward scattering angles. In addition, the forward scattering linewidths are limited by instrumental broadening from the laser linewidths and from the uncertainty in the scattering wavevector that results from focusing the laser beams. These measurements indicate the need for improved signal-to-noise in future scattering angle studies, which can be obtained through the use of higher power lasers.

In two other recent applications of high resolution SBG spectroscopy, we have gone beyond demonstrations of the technique to show how its advantages can be fruitfully applied to new problems in liquids. The first of these studies¹⁰ addresses the existence of a "structural transition" within the liquid state of benzene, which has been postulated on the basis of an unusual temperature dependence observed in depolarized light scattering intensities and Brillouin shifts.¹⁴ Our high precision, high accuracy SBG measurements (with Brillouin shifts on the order of 6.5 GHz measured to $\pm 0.1\%$) show conclusively that both the Brillouin shifts and widths vary smoothly with temperature, with no sign of any "structural transition." In a second study of liquid carbon disulfide¹¹ we have observed for the first time an unusual asymmetry in the Brillouin lineshapes that arises from the coupling between the translational and rotational motions of the molecules. The physical origin of the asymmetry is an acoustically-induced birefringence, which can be quantitatively described with theories developed to understand related effects in depolarized light scattering spectra.¹⁵ The observation of this asymmetry vividly demonstrates the power of

high resolution SBG spectroscopy to uncover new and subtle effects in the lineshapes of Brillouin spectra.

Finally, we have obtained spectra of the glass-forming liquids glycerol and 2,4,6-trimethylheptane that clearly illustrate the advantages of cw SBG spectroscopy over interferometry in studies of supercooled liquids. For example, in the SBG spectrum of glycerol at 170K, near the glass transition, the elastic scattering peak is completely suppressed and the measured Brillouin shifts and half-widths are 19 GHz and 21 MHz, respectively. A comparable measurement with spontaneous Brillouin scattering methods would require a high contrast interferometer with a finesse of better than 1000.

¹B. J. Berne and R. Pecora, *Dynamic Light Scattering* (Wiley, New York, 1976).

²G. D. Patterson and A. Munoz-Rojas, *Ann. Rev. Phys. Chem.* **38**, 191 (1987).

³R. Y. Chiao, Ch. H. Townes, and B. P. Stoicheff, *Phys. Rev. Lett.* **12**, 592 (1964).

⁴W. Kaiser and M. Maier, in *Laser Handbook*, ed. by F. T. Arrecchi and E. O. Schulz-Dubois (North-Holland, Amsterdam, 1972), p. 1077.

⁵A. G. Jacobsen and Y. R. Shen, *Appl. Phys. Lett.* **34**, 464 (1979).

⁶S. Y. Tang, C. Y. She, and S. A. Lee, *Opt. Lett.* **12**, 870 (1987).

⁷G. W. Faris, L. E. Jusinski, M. J. Dyer, W. K. Bischel and A. P. Hickman, *Opt. Lett.* **15**, 703 (1990).

⁸K. Ratanaphruks, W. T. Grubbs and R. A. MacPhail, *Chem. Phys. Lett.* **182**, 371 (1991).

⁹W. T. Grubbs and R. A. MacPhail, *J. Chem. Phys.* **97**, 19 (1992).

¹⁰W. T. Grubbs and R. A. MacPhail, *J. Phys. Chem.*, in press.

¹¹W. T. Grubbs and R. A. MacPhail, *J. Chem. Phys.*, in press.

¹²Y. -X. Yan and K. A. Nelson, *J. Chem. Phys.* **87**, 6240, 6267 (1987).

¹³S. M. Silence, S. R. Goates, and K. A. Nelson, *Chem. Phys.* **149**, 233 (1990).

¹⁴P. Esherick and A. Owyong, in *Advances in Infrared and Raman Spectroscopy*, ed. by R. J. H. Clark and R. E. Hester (Heydon, Philadelphia, 1982), Vol. 9, p. 130.

¹⁴N. B. Rhozhdestvenskaya and L. V. Smirnova, *J. Chem. Phys.* **95**, 1223 (1991).

¹⁵D. Kivelson and P. A. Madden, *Ann. Rev. Phys. Chem.* **31**, 523 (1980).

Stimulated Emission Pumping(SEP) Spectroscopy of Propynal: An Example of "Sparse" IVR at High Vibrational State Density.

C. A. Rogaski, J. Price and A. M. Wodtke
Department of Chemistry, U. C. Santa Barbara, Santa Barbara CA 93106
Telephone: (805) 893-8552

SEP spectra were recorded for the overtones of the C=O stretch(ν_4) up to $\nu_4=5$ and one combination band with three quanta of C=O stretch and one quanta of in plane C=C-C bend(ν_9). The experiments were performed in a molecular beam, using two excimer pumped dye lasers with etalons for the PUMP and DUMP steps giving an experimental resolution of 0.04 cm^{-1} . The resulting SEP spectra are simple and assignable to a near prolate asymmetric top. Anharmonic perturbations manifest themselves in the SEP spectra for $\nu_4=4$ and 5 as extra transitions. Anharmonic perturbations from unobserved levels appear in the rotational constants for $\nu_4=2$ and 3.

Perturbations in the overtone spectra of polyatomic molecules are very common¹, propynal isn't any different. What is remarkable about propynal is the lack of multiple state mixing at high vibrational state densities. The highest vibrational state density probed is $300 \text{ states/cm}^{-1}$ where "intermediate" intramolecular vibrational redistribution(IVR) is expected²; however, what is observed is explainable in the context of a simple fermi resonance, i.e. the "sparse" IVR limit. A comparison to other SEP experiments on aldehyde containing molecules^{3,4,5} provides evidence that molecular structure plays a dominant role in the IVR process.

¹G. Herzberg, *Infrared and Raman Spectra*, pp.239-271

²B. Pate, Doctoral Thesis, Princeton University

³H. L. Dai, C.L. Korpa, J.L. Kinsey, and R.W. Field, *J. Chem Phys.*, **82**(4), 1688 (1985)

⁴S.A. Reid, H. L. Kim, and J. D. McDonald, *J. Chem. Phys.*, **92**(12), 7079 (1990)

⁵Hong L. Kim, Scott Reid, and J. D. McDonald, *Chem. Phys. Letters*, **139**(6), 525 (1987)

Time-resolved optical double resonance spectroscopy in acetylene : exploring rovibrational energy transfer at various levels of excitation

A. P. Milce, H.-D. Barth, B. L. Chadwick and B. J. Orr

*School of Chemistry and Centre for Lasers & Applications,
Macquarie University, Sydney 2109, Australia*

Phone: 61-2-805-8289 / -8275; Fax: 61-2-805-8313

Time-resolved optical double resonance (DR) techniques are useful not only for high-resolution spectroscopy, but also for studies of the mechanisms by which molecules transfer energy from one distinct rovibrational quantum state to another, thereby elucidating aspects of chemical reactivity and energetics. The DR approach employs tunable laser excitation to prepare a molecule in a specific state and a second laser absorption step *either* to characterise that excitation *or* to probe resulting state-to-state molecular energy transfer. Typically, we use *either* infrared (IR) absorption *or* coherent Raman excitation for state preparation and ultraviolet (UV) laser-induced fluorescence (LIF) for detection. The emphasis in this work is on high state-specificity and sensitivity, to enable detailed modeling of the resulting spectroscopic and kinetic data and to provide insight into the intermolecular and intramolecular energy transfer processes involved. Figure 1 depicts the LIF-detected Raman-UVDR and IRUVDR excitation schemes.

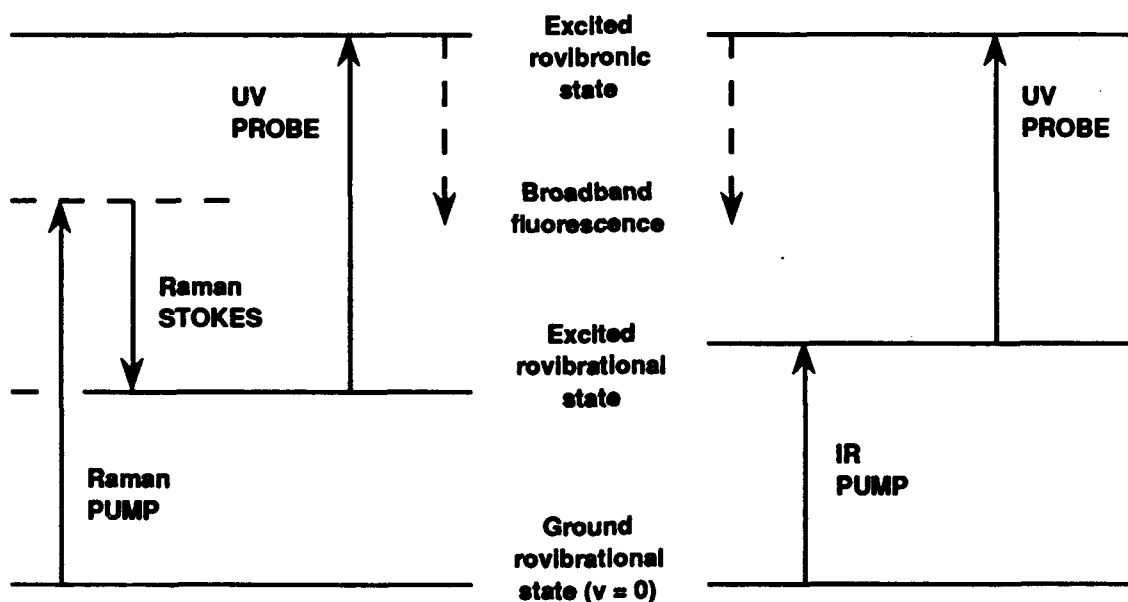


Figure 1: LIF-detected excitation schemes for time-resolved optical double resonance spectroscopy. The Raman-UVDR scheme (left) employs coherent Raman excitation by pulsed PUMP and STOKES laser beams to select a particular rovibrational state. In IRUVDR spectroscopy (right), a pulsed tunable infrared laser source (*e.g.*, a CO₂ laser or a Raman-shifted dye laser) provides the PUMP radiation to select a particular rovibrational state. In both schemes, a pulsed tunable UV PROBE laser and LIF detection are used to monitor the population of the directly excited rovibrational state and subsequent state-to-state energy transfer. Varying the PUMP/PROBE delay interval and sample pressure provide corresponding state-specific kinetic information. In the case of acetylene, the UV PROBE accesses bands in the $\bar{A} \leftarrow \bar{X}$ vibronic system, a *trans*-bent \leftarrow linear transition.

The spectroscopic potential of Raman-UVDR spectroscopy of acetylene is now well documented.¹ As a specific example, we have realised both broadband and narrowband Raman excitation of particular rovibrational states of C₂H₂ in a skimmed molecular beam.² The Raman-UVDR spectra shown in Fig. 2 were recorded by pumping the Q branch of the ν_2 (C≡C stretching, 1974 cm⁻¹) band and scanning the UV PROBE through the region of the 242-nm $\tilde{A} \leftarrow \tilde{X} 2_1^0 3_0^1$ band. This shows the promise of LIF-detected Raman-UVDR as a means of state-selecting skimmed molecular beams in state-to-state collision dynamics studies.

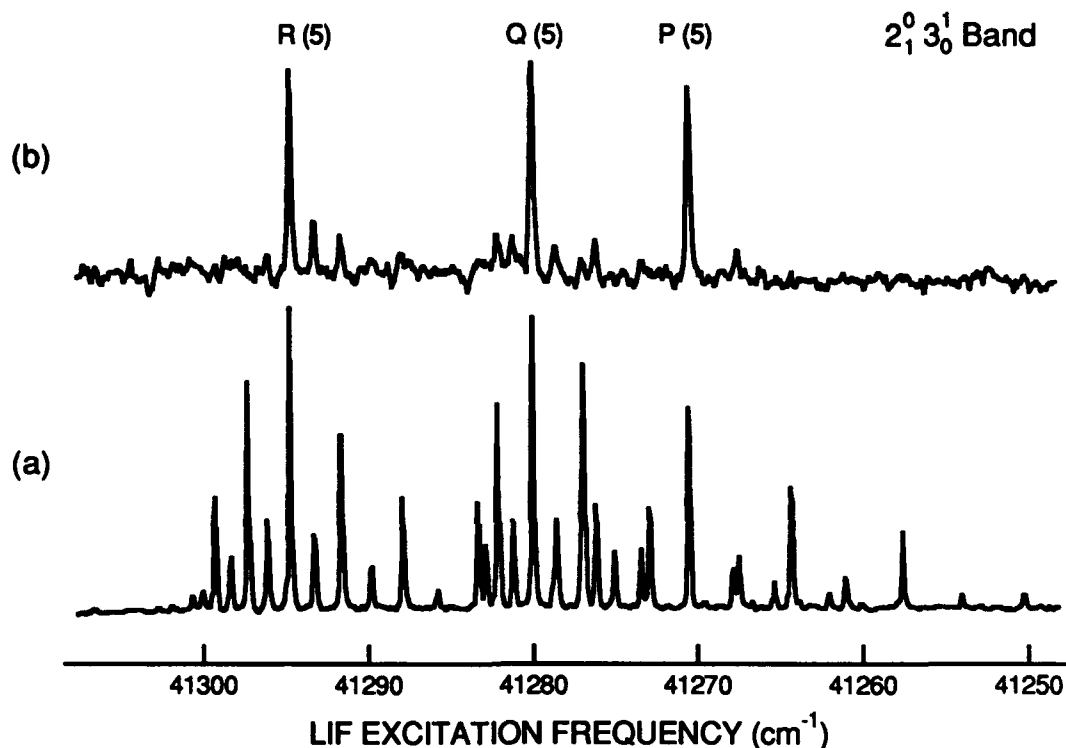


Figure 2: Raman-UVDR spectra² of the 242-nm $\tilde{A} \leftarrow \tilde{X} 2_1^0 3_0^1$ rovibronic band of C₂H₂ in a skimmed molecular beam at a rotational temperature of ~ 60K. The lower trace (a) is a 'multiple-J' Raman-UVDR spectrum recorded with broadband (effective bandwidth $\Delta\nu = 0.3$ cm⁻¹) Raman excitation in the ν_2 -band Q branch, centred on $J = 5$. The upper trace (b) is a 'single-J' Raman-UVDR spectrum recorded with narrowband ($\Delta\nu = 0.08$ cm⁻¹) Raman excitation, isolating rovibronic spectral features due to $J = 5$. The three laser pulses are coincident in time and their typical energies and durations are: 532-nm PUMP, 50 mJ, 15 ns; 594-nm STOKES, 16 mJ, 12 ns; 242-nm PROBE, 0.5 mJ, 20 ns.

Collision-induced intermolecular vibrational energy transfer of the form, C₂H₂(2₁4₁) + C₂H₂($\nu=0$) → C₂H₂(2₁) + C₂H₂(4₁), where ν_4 is the 612-cm⁻¹ *trans*-bending vibrational mode, has been investigated by Raman-UVDR with coherent Raman excitation in the ($\nu_2 + \nu_4 - \nu_4$) hot band. The UV PROBE monitors *either* the directly excited 2₁4₁ level *or* (after a delay to enable V-V transfer) the 2₁ level. In the latter case, UV probing of the $\tilde{A} \leftarrow \tilde{X} 2_1^0 3_0^1$ band, shows population growth due to V-V transfer, with a second-order rate constant of 1.73 μs^{-1} Torr⁻¹.

Raman-UVDR spectroscopy has also been used by our group¹ and others³ to investigate collision-induced rotational energy transfer (RET) within the 2₁ rovibrational manifold of C₂H₂(g). IRUVDR studies⁴⁻⁶ provide complementary information on RET in various other vibrational states of acetylene.

A wide range of IRUVDR experiments have now been performed to characterise rovibrational energy transfer in acetylene at various levels of vibrational excitation, from relatively low energies to the congested high-overtone region: 4_15_1 (1040 cm^{-1} , in C_2D_2);⁷ $3_1/2_14_15_1$ (3290 cm^{-1});⁵ 3_2 (6560 cm^{-1});⁸ 3_3 (9640 cm^{-1});^{8, 9} 3_4 (12680 cm^{-1}).⁸ Various parts of the 11000 to 16000 cm^{-1} region have also been explored using stimulated emission pumping.¹⁰

We are currently exploiting IRUVDR to investigate rovibrational energy transfer in the 2_13_3 region (11600 cm^{-1}), which is highly congested with numerous overlapping vibrational levels coupled by Darling-Dennison, Fermi-resonance and Coriolis perturbations.¹¹ In these IRUVDR experiments, a pulsed, Raman-shifted dye laser operating at $0.86\text{ }\mu\text{m}$ prepares acetylene molecules in a single rovibrational state of the 2_13_3 manifold and the UV PROBE pulse scans a chosen region of the rovibronic spectrum at several time delays and pressures. This produces IRUVDR LIF excitation spectra exemplified by Fig. 3. Relaxation of the 'parent' peaks is evident, but the absence of RET satellites is attributable to strongly J-dependent Franck-Condon factors, which peak markedly at $2_13_3, J = 5$.

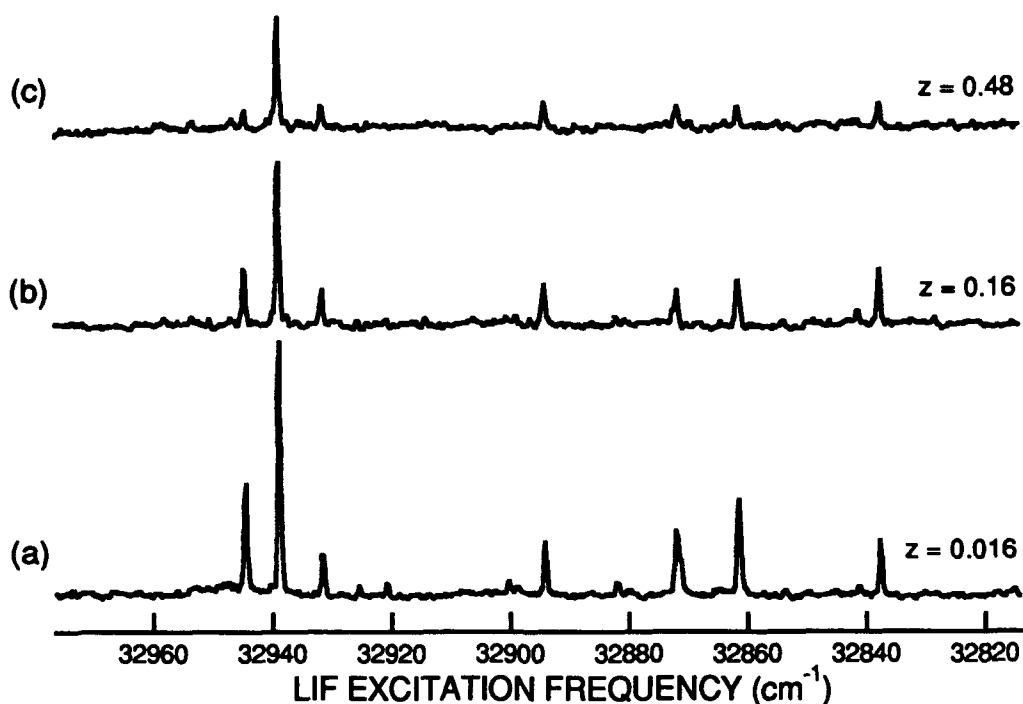


Figure 3: IRUVDR LIF excitation spectra of the $\tilde{A} \leftarrow \tilde{X}$ absorption system of $\text{C}_2\text{H}_2(\text{g})$ at 100 mTorr in the vicinity of 304 nm , recorded with a UV PROBE bandwidth of 0.4 cm^{-1} . The wavelength of a Raman-shifted dye laser is fixed to select a single 2_13_3 rovibrational state ($J = 5$) and the population changes are monitored after delays of (a) 10 ns , (b) 100 ns and (c) 300 ns ; these yield collision numbers z (referred to the Lennard-Jones collision rate constant) as indicated.

An alternative approach, illustrated in Fig. 4, is to park the pulsed UV PROBE on a particular feature in the rovibronic spectrum and to scan the IR PUMP wavelength through the corresponding $(\nu_2 + 3\nu_3)$ -band rovibrational spectrum. IR-scanned IRUVDR spectra recorded at various PUMP-PROBE delay intervals then show the collision-induced growth of RET satellites corresponding to $\Delta J = \pm 2, \pm 4, \dots$. There is evidence that the decay of the R(4) and P(6) rovibrational

intensities is not entirely balanced by the growth of RET satellite intensities, owing to competition with an efficient intramolecular vibrational redistribution (IVR) process. The kinetics of rovibrational population decay and growth in this region appears to be a combination of first-order (*i.e.*, collision-free) and second-order (*i.e.*, collision-induced) energy-transfer processes.

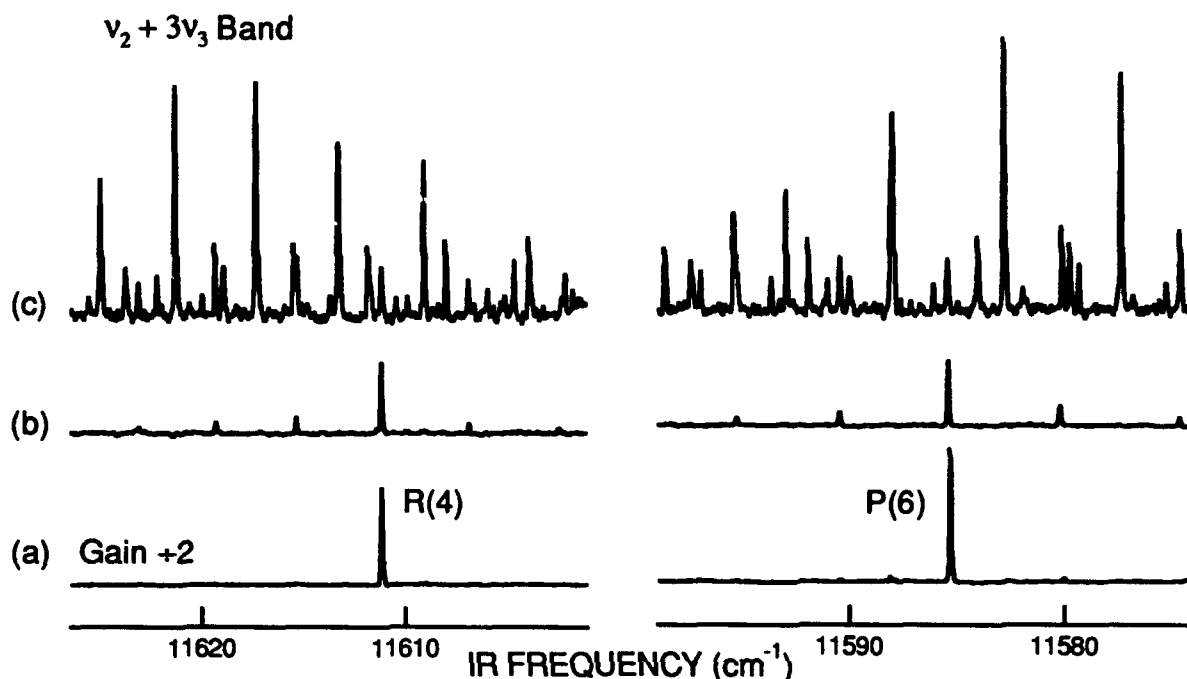


Figure 4: IRUVDR difference spectra (a, b) and photoacoustic absorption (c) spectra of the $0.86\text{-}\mu\text{m}$ $\nu_2 + 3\nu_3$ band of $\text{C}_2\text{H}_2(\text{g})$ at 100 mTorr, recorded with an IR PUMP bandwidth of 0.08 cm^{-1} . With the UV PROBE wavelength fixed at 32938.6 cm^{-1} to monitor the $2_13_3, J=5$ state, IRUVDR (a, b) projects the R(4) and P(6) rovibrational features out of the thermal-equilibrium spectrum (c). Collision-induced RET satellites grow as the collision number z increases from 0.016 (a) to 0.48 (b).

Further work is in progress in this context, with emphasis on spectroscopic assignment and understanding of the intramolecular processes which cause the IRUVDR spectroscopic intensities to peak extraordinarily sharply around the $J = 5$ rotational state in the 2_13_3 vibrational manifold of acetylene.

References

1. B.L.Chadwick & B.J.Orr, *J. Chem. Phys.*, **97**, 3007 (1992).
2. H.-D.Barth, A.P.Milce, B.L.Chadwick & B.J.Orr, *J. Chem. Soc. Faraday Trans.*, **88**, 2563 (1992).
3. R. Dopheide, W. B. Gao and H. Zacharias, *Chem. Phys. Lett.*, **182**, 21 (1991).
4. H.-D.Barth, B.L.Chadwick, A.P.Milce & B.J.Orr, to be published.
5. M.J.Frost & I.W.M.Smith, *Chem. Phys. Lett.*, **191**, 574 (1992).
6. E.Carrasquillo, A.L.Utz & F.F.Crim, *J. Chem. Phys.*, **88**, 5976 (1988); J.D.Tobiason, A.L.Utz & F.F.Crim, *J. Chem. Phys.* (in press, 1992).
7. B.L.Chadwick & B.J.Orr, *J. Chem. Phys.*, **95**, 5476 (1991).
8. A.L.Utz, J.D.Tobiason, E.Carrasquillo, M.D.Fritz & F.F.Crim, *J. Chem Phys.*, **97**, 389 (1992).
9. H.-D.Barth, B.L.Chadwick, J.G.Haub, M.J.Johnson, A.P.Milce & B.J.Orr, to be published.
10. Y.Chen, S.Halle, D.M.Jonas, J.L.Kinsey & R.W.Field, *J. Opt. Soc. Am. B*, **7**, 1805 (1990); K.Yamanouchi, N.Ikeda, S.Tsychiya, D.M.Jonas, J.K.Lundberg, G.W.Adamson & R.W.Field, *J. Chem. Phys.*, **95**, 6330 (1991).
11. B.C.Smith & J.S.Winn, *J. Chem. Phys.*, **94**, 4120 (1991).

Monday, January 18, 1993

Poster and Postdeadline Session 1

MB 8:00pm–10:00pm
Salon B

Twist and Strain: A Study in Vibrational Mode-Coupling

C. Cameron Miller, Hao Li, Laura A. Philips

Department of Chemistry, Cornell University, Ithaca, New York, 14853-1301

A homologous series of small organic molecules are used to explore the role of low frequency, large amplitude motion in vibrational mode coupling and in photochemically induced isomerization reactions. From the variation in structure in a series of substituted ethanes and strained ring systems, we can begin to link aspects of structure with the propensity for vibrational mode coupling. The molecules to be discussed include 2-fluoroethanol (2FE), 1,2-difluoroethane (DFE), 1-chloro,2-fluoroethane (CFE), and cyclobutane.

High resolution infrared spectroscopy in a molecular beam is used to measure the vibrational mode coupling of high frequency C-H stretching modes to other vibrational modes in these molecules. Vibrational mode coupling is observed as the departure of the predictions of the rigid rotor/harmonic oscillator model of the experimental spectrum. The perturbations in the spectra vary from minor deviations in transition frequencies to fragmentation of the individual rotational transitions into clumps of peaks in the spectrum. The magnitude of the vibrational mode coupling varies with many of the structural characteristics of the various molecules. Important characteristics include the density of states at the C-H stretching frequency and the intramolecular attractive interactions that restrict the low frequency, large amplitude motion.

The number of coupled states varies in the set of molecules under study. In 2FE, the density of coupled states exceeds the total density of vibrational states. The vibrational mode coupling in this molecule is evidenced by large clumps of peaks where single rotational transitions are

expected. In DFE, the vibrational mode coupling is dominated by the C-H stretch coupling to one additional state. The mode coupling in this case is manifested as doublets and triplets in lieu of the clumps of peaks observed in 2FE. The spectra of both of these molecules indicate that the spectrum is produced by the gauche conformer of each molecule. Similarly, some fragmentation is observed in the spectrum of the CFE gauche conformer. In contrast, in the spectrum of the trans conformer of CFE, no fragmentation of the rotational structure is observed.

Cyclobutane offers an interesting comparison to the substituted ethanes. The hindering of the torsional motion in the substituted ethanes is taken to the extreme by covalently bonding the two ends of the molecule together. The ring puckering motion in cyclobutane can be compared to the hindered torsions of the substituted ethanes. In the same manner that the torsional motion is the reactive coordinate for conformational isomerization, the puckering motion is the coordinate to take cyclobutane from one puckering conformation to the equivalent but opposite puckering conformation. The complicated spectrum of cyclobutane suggests that the vibrational mode coupling is dominated by coupling to a single second state as in the case of DFE, but clumps of peaks also occur as in the spectrum of 2FE. The extent of the mode coupling in cyclobutane is made more dramatic by the fact that the density of vibrational states at the C-H stretching frequency is comparable to that of DFE and CFE, and significantly less than 2FE.

The magnitude of the vibrational mode coupling in this series of molecules allows us to speculate about the relationship between intramolecular attractive interactions and vibrational mode coupling. In 2FE there is a strong bond dipole-bond dipole attractive interaction between the O-H and the C-F bond dipoles that acts to stabilize the gauche conformer. The

gauche conformers of CFE and DFE are stabilized by weaker intramolecular attractive interactions. In contrast, the CFE trans conformer does not have this intramolecular attractive interaction. The extent of the vibrational mode coupling, as observed in the high resolution spectra, appears to correlate with the magnitude of the intramolecular attractive interactions. Cyclobutane could be thought to fit into this model of vibrational mode coupling as well. Covalently bonding is the attractive interaction present in cyclobutane which could act to stimulate vibrational mode coupling of the C-H stretch to the ring puckering coordinate. The strong attractive interaction correlates with the strong vibrational mode coupling.

Additional molecules in both the family of substituted ethanes and strained ring systems are needed to develop the connection between molecular structure and vibrational mode coupling. The results to date will be discussed in the context of relating molecular structure, conformational isomerization and vibrational mode coupling.

Inverse Raman Spectroscopy Measurements of Line-Shift Coefficients in Hydrogen Perturbed by Argon

J. W. Forsman, R. L. Farrow, and L. A. Rahn
Combustion Research Facility
Sandia National Laboratories
Livermore, California 94551-0969
510-294-2095

High resolution Raman studies of the Q branch in H₂ perturbed by Ar are relevant to combustion diagnostics and for tests of the intermolecular potential. The use of spectroscopic techniques to study combustion requires accurate models for the line shapes, which can range from Lorentzian to Gaussian to more complicated profiles¹ depending on the perturber species, perturber concentration, density and temperature. Calculations with these models require estimates of the speed dependence of the line-shift and line-broadening coefficients. Modern theories are now able to predict the shifting and broadening resulting from collisions but are hampered by uncertainties in the interaction potential. One of the most studied potentials is that of H₂-Ar, which has the advantage of being theoretically tractable for line shape computations. Furthermore, since the masses of Ar and molecular O₂ and N₂ are similar, spectral features depending on the perturber's mass are expected to be similar. We report preliminary measurements of the density shift of the Q branch lines in H₂ as a function of rotational state and temperature.

The line shifts due to Ar were measured with inverse Raman spectroscopy² with the molar concentration of H₂ set at 2%. The quasi-CW inverse Raman spectrometer had a resolution of $2 \times 10^{-3} \text{ cm}^{-1}$. The total density was normally 10 amagat, but higher densities and densities as low as 0.33 amagat were also investigated. The H₂-Ar mixture was contained in an internally heated, temperature controlled furnace. We minimized the

perturbations in the shift and the line shape due to the Stark effect³ by using peak pump powers less than 90 kW. It was estimated that the Stark shifts were less than $1.5 \times 10^{-3} \text{ cm}^{-1}$.

A least squares method was used to fit Lorentzian profiles to the observed spectra. The narrowest linewidths (HWHM) observed in 2% H₂ mixtures at 295 K were approximately $6 \times 10^{-3} \text{ cm}^{-1}$ at a density of 0.55 amagat. The shifts, shown in Fig. 1, were computed from measurements of the transition frequency at 10 amagat for the temperatures studied except at 295 K where the dependence of the transition frequency on density was investigated. The two methods were self-consistent within the uncertainty of $\pm 2 \times 10^{-3} \text{ cm}^{-1}/\text{amagat}$.

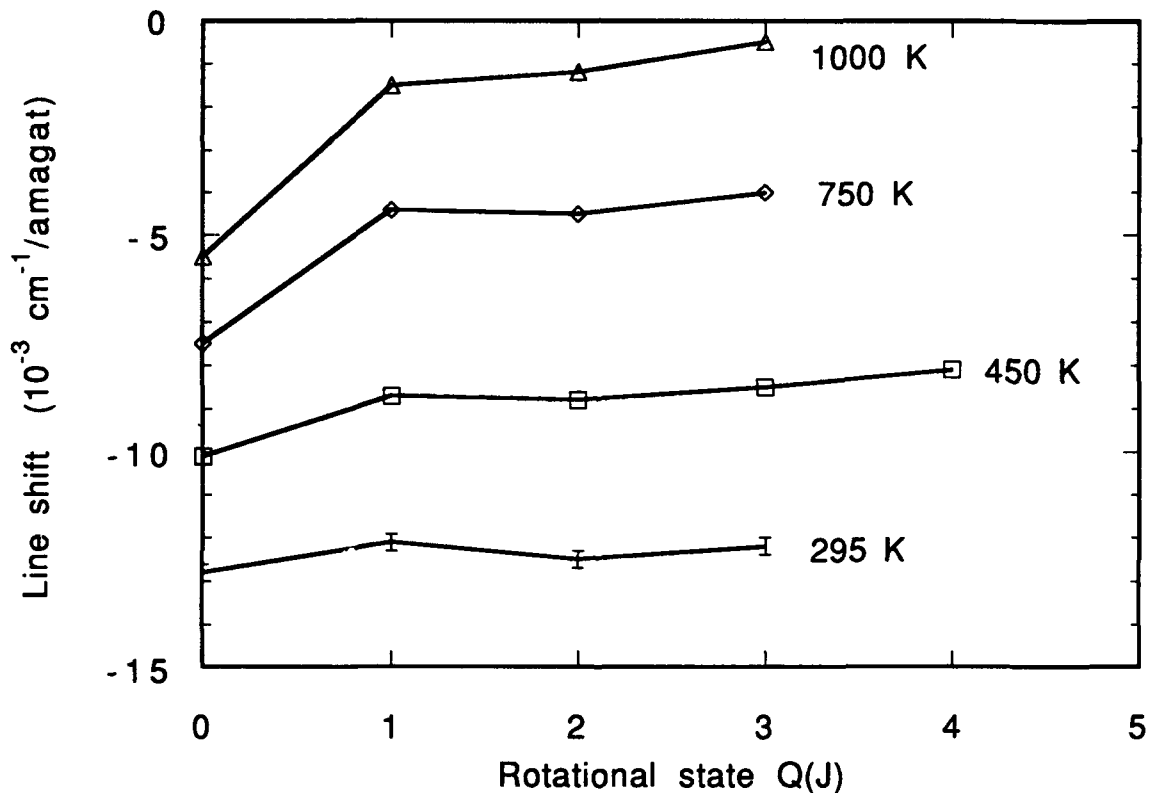


Fig. 1. Q branch line-shift coefficients as a function of temperature and rotational state for a 2% concentration of H₂ in Ar. Error bars are shown for the data at 295 K.

At 295 K the Ar line-shift coefficients were independent of the rotational state within the estimated errors. However, at elevated temperatures, Ar had a much larger influence on the Q(0) transition compared to the other Q-branch lines. The behavior of the line-shift coefficients for H₂ qualitatively agrees with rotational dependence found in calculations for D₂ in Ar.⁴

We also monitored the asymmetry attributed to speed-changing collisions.¹ For 1:1 mixtures of H₂ and Ar the asymmetry was small and changed signs as the density was reduced. For this mixture the asymmetry was zero within the noise in the signal at intermediate densities. In 2% H₂-Ar mixtures the asymmetry was larger and the sign was unchanged at densities less than 10 amagat. The sign of the asymmetry in both mixtures was the same at low densities. Asymmetries persisted at densities as low as 0.5 amagat (below the Dicke minimum in the linewidth) in 2% and 50% mixtures at 295K.

Final values for the line-shift coefficients of H₂ perturbed by Ar will be presented. The homogeneous line-broadening coefficients are being determined with the use of a speed-changing model.¹

This research is supported by the U. S. Department of Energy, Office of Basic Energy Sciences, Division of Chemical Sciences. J. W. Forsman acknowledges a Natural Sciences and Engineering Research Council of Canada post-doctoral fellowship.

References

1. R. L. Farrow, L. A. Rahn, G. O. Sitz, and G. J. Rosasco, Phys. Rev. Lett. **63**, 746 (1989).
2. L. A. Rahn and R. E. Palmer, J. Opt. Soc. Am. B **3**, 1164 (1986).
3. H. Moosmüller, C. Y. She, and W. M. Huo, Phys. Rev. A **40**, 6983 (1989).
4. S. Green, J. Chem. Phys. **93**, 1496 (1990).

High Resolution Electronic Spectroscopy of ZnCH₃ and CdCH₃

Timothy M. Cerny, Xue-Qing Tan, Eric S. J. Robles, Andrew M. Ellis,
James M. Williamson and Terry A. Miller

Laser Spectroscopy Facility

Department of Chemistry

The Ohio State University

120 West 18th Avenue

Columbus, Ohio 43210

(614) 292-2949

The number of organometallic free radicals studied spectroscopically in the gas phase has been very limited until quite recently. Application of Broida oven, laser photolysis and laser photolysis/vaporization techniques to synthesize these transient species has significantly enlarged the number of reports over the past few years. This research group's contribution to the area have been a series of reports by Robles, Ellis and Miller detailing electronic and vibrational structures ($\sim .5 \text{ cm}^{-1}$ resolution) of 15 species of the form M-R (M = Mg, Ca, Zn and Cd; R = cyclopentadienyl (Cp), pyrrolyl (Py) and methylcyclopentadienyl (MCp)) and M-CH₃ (M = Ca, Zn and Cd), many of them observed for the first time.¹⁻⁸ These molecules are more than simply novel constructs. The methyl and Cp derivatives are recognized as important intermediates in metal deposition processes while the metal-Py species are found as subunits in several chemical substances of biological importance. Metal-ligand bonding sites, vibrational frequencies, spin-orbit splittings and barriers to internal rotation are some of the types of information that this work has yielded. To augment this work, a rotationally resolved study is presented here which confirms the electronic state symmetry assignments given in earlier studies,

and more importantly, determines rotational constants and other interaction parameters of these radicals.

This rotationally-resolved study, in particular, examines ZnCH_3 and CdCH_3 . Preliminary characterization of the $\tilde{A} \leftarrow \tilde{X}$ band was accomplished in a number of low resolution (> 1 nm) studies.⁹⁻¹² Our previous work on these systems served to clarify the vibrational levels for the \tilde{A} and \tilde{X} states and investigated reports of dispersed fluorescence patterns characteristic of emission from excited vibrational levels in the \tilde{A} state of CdCH_3 to those in its \tilde{X} state.^{2,5} In addition to the previously mentioned benefits of a rotational study, there are two other substantive motivations for conducting this work. First, some questions remain about the electronic symmetry of the \tilde{A} state of CdCH_3 . This is due to the absence of clear spin-orbit structure one would expect for a 2E state. To explain this lack of structure, Ellis *et al.* have proposed the existence of a non-radiative decay channel based on a series of lifetime measurements in the \tilde{A} state vibrational manifold.⁵ Confirmation by the present study of the 2E character of the state strongly supports this argument. Second, X-CdCH_3 ($\text{X} = \text{He, Ne, Ar, Kr, Xe}$) complexes have been observed that demonstrate very unusual vibrational structure.^{2,13} Further high resolution studies of these species require a complete understanding of the bare molecule.

The radicals in this experiment were generated by ArF photolysis (193 nm) of the stable dimethyl precursors seeded in carrier gas (Ne 70%, He 30%) at the throat of a pulsed, supersonic free jet expansion. The cooled species are then probed ~ 2.5 cm downstream with the continuous-wave output of an Ar^+ pumped ring dye laser ($< .0001$ cm^{-1} linewidth). The laser induced fluorescence (LIF) is collected with a quartz $f/1$ optic and imaged onto a photomultiplier tube. The resulting electronic signal is integrated, then digitized and averaged in a Coherent 699-29 Autoscan data acquisition system. The spectra obtained had linewidths (FWHM) of $.0033$ cm^{-1} which can be attributed to Doppler broadening, laser power broadening and unresolved hydrogen hyperfine structure.

Figure 1 displays the 0_0^0 band spectrum of the ${}^2E_{1/2} \leftarrow {}^2A_1$ transition of ZnCH_3 which is typical of the $\tilde{A} \leftarrow \tilde{X}$ bands observed for ZnCH_3 and CdCH_3 . The spectrum consists of 3 overlapped rotational sub-bands ($K' \leftarrow K'' = 2 \leftarrow 1, 1 \leftarrow 0$ and $0 \leftarrow 1$). Rotational transitions exhibit spin-rotation splittings in the \tilde{X} state for each isotope of Zn. Additionally, in the spectrum of CdCH_3 , hyperfine structure is clearly observed for those isotopes having non-zero nuclear spin

(^{111}Cd and ^{113}Cd). Both spin-orbit components of ZnCH_3 and the only assigned spin-orbit component of CdCH_3 have been fit to a symmetric top (C_{3v}) rotational model that includes spin-orbit, electronic Coriolis, Jahn-Teller, and spin-rotation interactions. The hamiltonian and the matrix elements have been discussed by Hougen¹⁴ and Endo *et al.*¹⁵

For $^{64}\text{ZnCH}_3$, a global fit from both spin-orbit components containing 88 lines was performed. The fit has a standard deviation of 51 MHz, which is comparable to our experimental accuracy. The ${}^2E_{1/2} \leftarrow {}^2A_1$ transition of $^{114}\text{CdCH}_3$ was successfully fit to the previously discussed model,^{14,15} confirming initial assignments. A total of 45 lines were fit with a standard deviation of 55 MHz. Other significant isotopes have been fit for both ZnCH_3 and CdCH_3 . Theoretical details of this fit and the determined parameters, with their physical interpretation, will be presented. Work is currently in progress to fit the hyperfine structure of $^{111}\text{CdCH}_3$ and $^{113}\text{CdCH}_3$.

REFERENCES

1. A.M. Ellis, E.S.J. Robles and T.A. Miller, *J. Chem. Phys.*, **94**, 1024 (1991).
2. E.S.J. Robles, A.M. Ellis and T.A. Miller, *Chem. Phys. Lett.*, **178**, 185 (1991).
3. E.S.J. Robles, A.M. Ellis and T.A. Miller, *J. Phys. Chem.*, **96**, 3248 (1992).
4. E.S.J. Robles, A.M. Ellis and T.A. Miller, *J. Phys. Chem.*, **96**, 3259 (1992).
5. A.M. Ellis, E.S.J. Robles and T.A. Miller, *Chem. Phys. Lett.*, **190**, 599 (1992).
6. E.S.J. Robles, A.M. Ellis and T.A. Miller, *J. Chem. Soc., Faraday Transactions*, **88**, 1927 (1992).
7. E.S.J. Robles, A.M. Ellis and T.A. Miller, *J. Am. Chem. Soc.*, **114**, 7171 (1992).
8. E.S.J. Robles, A.M. Ellis and T.A. Miller, *J. Phys. Chem.*, accepted.
9. P.J. Young, R.K. Gosari, J. Connor, O.P. Strausz and H.E. Gunning, *J. Chem. Phys.*, **58**, 5280 (1973).
10. C.F. Yu, F. Youngs, K. Tsukiyama and R. Bersohn, *J. Chem. Phys.*, **85**, 1382 (1986).
11. R.L. Jackson, *Chem. Phys. Lett.*, **174**, 53 (1990).
12. A. Penner, A. Amirav and R. Bersohn, *Chem. Phys. Lett.*, **176**, 147 (1991).
13. A.M. Ellis, E.S.J. Robles and T.A. Miller, *J. Phys. Chem.*, submitted.
14. J.T. Hougen, *J. Mol. Spectrosc.*, **81**, 73 (1980).
15. Y. Endo, S. Saito and E. Hirota, *J. Chem. Phys.*, **81**, 122 (1984).

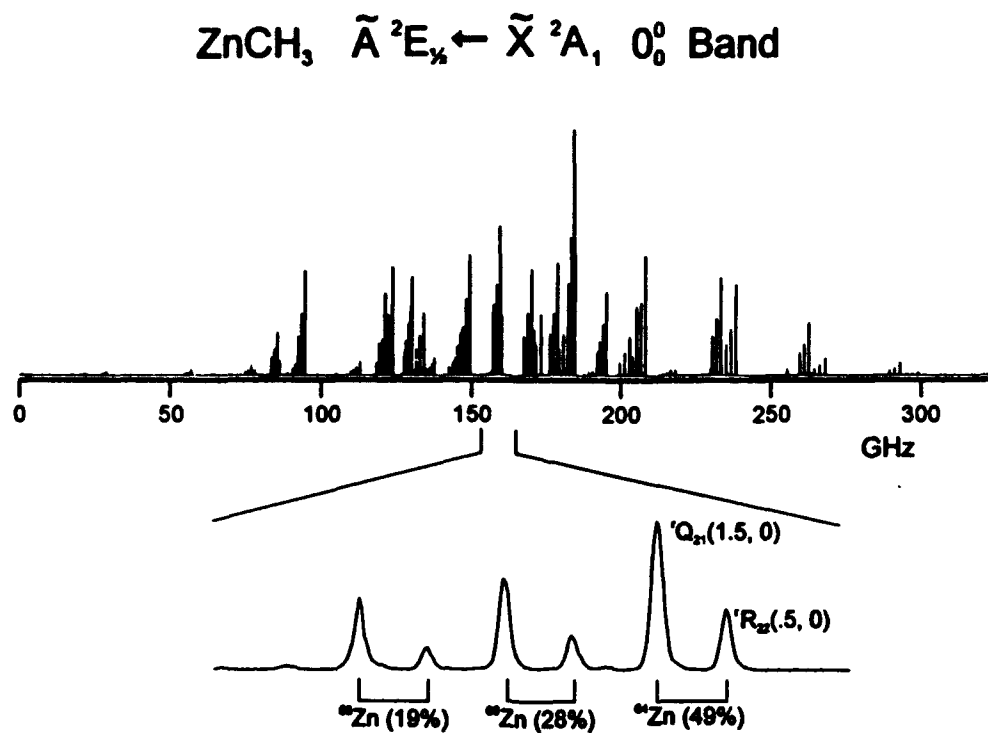


Figure 1. The high resolution ($\sim .033 \text{ cm}^{-1}$) LIF spectrum of ZnCH_3 recorded at 417.5 nm. The magnified section shows spin rotation splitting in the ground state for each of the significant nuclear spin-free isotopes of zinc. The spin orbit pair to this band was acquired at 413.2 nm with similar resolution.

Tunable Far-Infrared Laser Spectroscopy of Hydrogen Bonds

**Paul Stockman, Sakae Suzuki, Geoffrey A. Blake
California Institute of Technology
Pasadena, CA 91109**

Sub-Doppler far-infrared vibration-rotation-tunneling spectra of several water- and ammonia-containing clusters will be presented. Intermolecular potential energy surfaces derived from these spectra will also be discussed.

Stimulated Emission Pumping (SEP)¹ Studies of Energy Transfer in Highly Vibratonally Excited Oxygen.

J.A. Mack, J.M. Price and Alec M. Wodtke ^{a,b,c}

A.M. Wodtke, Dept. of Chemistry, University of California, Santa Barbara

Santa Barbara, CA. 93106

Phone: (805) 893-8552

Fax: (805) 893-4120

Recent results have shown that highly vibrationally excited O₂ is formed in significant quantities from the ultraviolet photolysis of ground state ozone. An important question for understanding the balance of O₃ in the upper atmosphere is the lifetime of these highly vibrationally excited molecules which are proposed² to be a photolytic source of odd oxygen atoms. In this work we report the rate constants for the collisional deactivation of SEP prepared O₂(v^{*}=18-25) by O₂(v^{*}=0), at temperatures of 295 and 395 K. The experiments are analogous to the "Pump", "Dump" and "Probe" studies carried out by Yang et al on NO.³ A pulsed tunable Argon Fluoride laser is used to "PUMP" O₂ from X³Σ_g⁻ ground electronic state to a specific rovibrational level of the B³Σ_g⁻ excited electronic state via the well known Schumann-Runge bands⁴. A Xenon-Chloride pumped tunable dye laser system then stimulates, or "DUMPS" the O₂ back to a specific excited rovibrational level of the ground electronic state. A second tunable dye laser system then "PROBES" the vibrationally excited O₂ population by Laser Induced Fluorescence. By varying the time delay between the DUMP and PROBE lasers, the time dependant occupation of the prepared vibrational level is monitored. The collisional quenching rate constant for a given vibrational level is then determined from the pressure dependance of the lifetime. Implications of the measured rates for atmospheric chemical reactions are discussed.

a) Camille and Henry Dreyfus Teacher-Scholar

b) Alfred P. Sloan Research Fellow

c) National Science Foundation Presidential Young Investigator

¹ Kittrel, C., Abramson, E., Kinsey, J.I., MacDonald, S.A., Reisner, D.E., Feild, R.W. and Katayama, D.H., 1981, J.Chem.Phys. 75, 2056

² Slanger, T.G., Jusinski, Black, G., Gadd, G.E., Science 241, 945 (1988)

³ Yang, X., Kim, E.H., and Wodtke, A.M., J.Chem.Phys. 93,4483 (1990)

⁴ Creek, D.M., Nicholls, R.W., Proc.R.Soc.Lond.A. 341, 517 (1975)

Renner Teller and Spin-orbit Perturbations in Triatomic Molecules

Alexander Alijah, Facultat fur Chemie, Universitat Bielefeld, D-4800 Bielefeld, Federal Republic of Germany.

Geoffrey Duxbury, Department of Physics and Applied Physics, University of Strathclyde, John Anderson Building, 107 Rottenrow, Glasgow G4 0NG, Scotland.

Telephone 44-41-552-4400 ext 3271
FAX 44-41-552-2891

Recent high resolution experimental studies of the electronic spectra of triatomic dihydrides and their ions have provided a severe test of current models of electronic orbital angular momentum-nuclear - vibrational angular momentum coupling. This coupling is associated with the breakdown of the Born-Oppenheimer separation of electronic orbital and nuclear motion, the Renner-Teller effect, and also with spin-orbit coupling.

We describe an extension to our current modelling of these interactions (Alijah and Duxbury¹, Duxbury and Jungen²), which is based on the approach developed by Barrow, Dixon and Duxbury³, and Duxbury and Dixon⁴. The extensions include the calculation of ro-vibronic lifetimes, and of perturbations associated with spin-orbit coupling. The improved model has been recently used to interpret new laser spectroscopic results on SiH₂⁵, SiH₂⁺⁶ and CH₂⁷. We will present further comparisons of results of the new calculations with experimental data on NH₂, PH₂, CH₂, and PH₂⁺.

In the NH₂ $\bar{A}, ^2A_1 - \bar{X}, ^2B_1$ system we are concerned with high vibrational levels of the ground state and high angular momentum states associated with rotation about the nearly linear molecule axis, whereas in the analogous system of PH₂ we have calculated radiative lifetimes and the vibronic dependence of the spin-orbit coupling. The iso-electronic molecules CH₂ and PH₂⁺ exhibit an interesting interplay of Renner-Teller and spin-orbit coupling causing intersystem crossing in CH₂, and to spin forbidden predissociation in PH₂⁺.

1) A. Alijah and G. Duxbury, Mol. Phys. 70, 605 (1990)

- 2) G. Duxbury and Ch. Jungen, *Mol. Phys.* 63, 981 (1988)
- 3) T. Barrow, R.N. Dixon and G. Duxbury, *Mol. Phys.* 27, 1217-1234 (1974)
- 4) G. Duxbury and R.N. Dixon, *Mol. Phys.* 43, 255-274 (1981)
- 5) G. Duxbury, A. Alijah and R. Treurling, Submitted to *J Chem. Phys.* (1992)
- 6) D.I. Hall, A.P. Levick, P.J. Sarre, C.J. Whitham, A. Alijah and G. Duxbury submitted to *Faraday Communications* (1992)
- 7) I Garcia-Moreno, E.R. Lovejoy, C. Bradley-Moore and G. Duxbury, Submitted to *J. Chem. Phys.* (1992)

Abstract for the High-Resolution Spectroscopy Conference**Electronic Surface State and Plasmon-Phonon Coupled Excitations at the surface of Modulation-doped GaAs/AlGaAs Multiquantum Wells: A Study of High-Resolution Electron-Energy-Loss Spectroscopy(HREELS)****R. H. Yu****Department of Physics, Central Washington University, Ellensburg, WA 98926**

A selfconsistent framework for study of the surface electronic structure of finite superlattices has been proposed. Our emphasis is on the influence of accumulation or depletion layer on the surface states (Tamm states). We have used a modulated doping profile, including an accumulation or a depletion surface layer, in our selfconsistent calculations of potential and carrier density profile. We have found the existence of Tamm states above(depletion layer) or below(accumulation layer) the superlattice miniband. One of the Tamm states found crosses the Fermi energy in the energy gap when the depletion effect, resulting from dangling bonds, defects, impurities, etc, near the surface increases. In our case, near the top layer of the superlattice the depletion region was formed as a result of the pinning of the Fermi level below its position in intrinsic GaAs due to the midgap surface states.

The plasmon-phonon coupled carrier excitations associated with the Tamm states have been studied via the calculated electron-energy-loss spectrum(EELS) within the random-phase-approximation(RPA). Both intra- and interminiband excitation modes as well as the plasmaron modes due to the Tamm states have been found. At low temperature, the Tamm state below the miniband(accumulation layer) is more heavily populated than the Tamm state above the miniband. We have found several strong plasmaron modes due to the surface localized state emerged from the other modes, their strength reflects the heavy carrier population while their departure from the other modes signals the spatial confinement of the Tamm state. Large depolarization effect due to the localization of the Tamm state was also found in the interminiband plasmaron excitation spectrum. The temperature dependence of the electronic level structure as well as plasmaron excitation modes will be discussed.

Persistent spectral hole burning in organic materials

**Li Jianzhao, Chen Lingbing
Zhao Youyuan and Li Fuming**

Laser Physics Laboratory

Department of Physics, Fudan University

Shanghai 200433, P.R.China

Tel. (021)5492222 Ext. 2374

As a technique for high resolution spectroscopy one-photon and photon-gated persistent spectral hole burning was realized in our organic materials. Hole shape, properties and quantum efficiency of hole formation were investigated. Hole growth dynamics and theory for it were given.

The Deconvolution Method Used In The Analysis Of a-C Raman Spectrum

Qi Wang and D. D. Allred

*Department of Physics and Astronomy, Brigham Young University
Provo, Utah 84602*

It is believed that the Raman spectrum of amorphous carbon (a-C) is a kind of broadened version of the phonon density of states (PDOS) of graphite¹. To further verify this relation and to extract more information from the Raman spectrum of a-C, we introduce the deconvolution method into the analysis of a-C Raman spectrum .

Deconvolution used in spectrum analysis is based on the assumption that the observed spectrum i is related to the "object" or ideal spectrum o through the convolution

$$i = s \otimes o, \quad (1)$$

where s is the spread function caused by certain physical effects. Deconvolution is the process of finding the best estimate of o for the measured spectrum i and an estimate of the spread function, s . We have chosen the "constrained nonlinear method" to conduct the deconvolution since it has been well developed for the spectrum analysis. The constrained nonlinear deconvolution we used is based on P. A. Jansson's² modification of Van Cittert's method.

To test the method we picked up a known spectrum as o and convoluted it with the Gaussian shaped spread function, s , to obtain i and then deconvoluted i by using the method described above. Our approach in the deconvolution process is to change one parameter at a time while keeping

the others constant. Comparison of the result of the deconvolution, $\hat{o}^{(k)}$, with the known original spectrum, o , gives information about how that parameter effects the deconvolution. The parameters tested are: number of iterations and width of the spread function. We also studied the effects of noise reduction and relaxation function. Fig. 1 shows the test result. From Fig. 1(b) it can be seen that the convolution makes some of the basic features of the original spectrum submerged in the broad curve. After deconvolution the two-peak feature in the 1300-1450 cm^{-1} region is revealed clearly (see Fig. 1(c)). The half width of the peak at about 1600 cm^{-1}

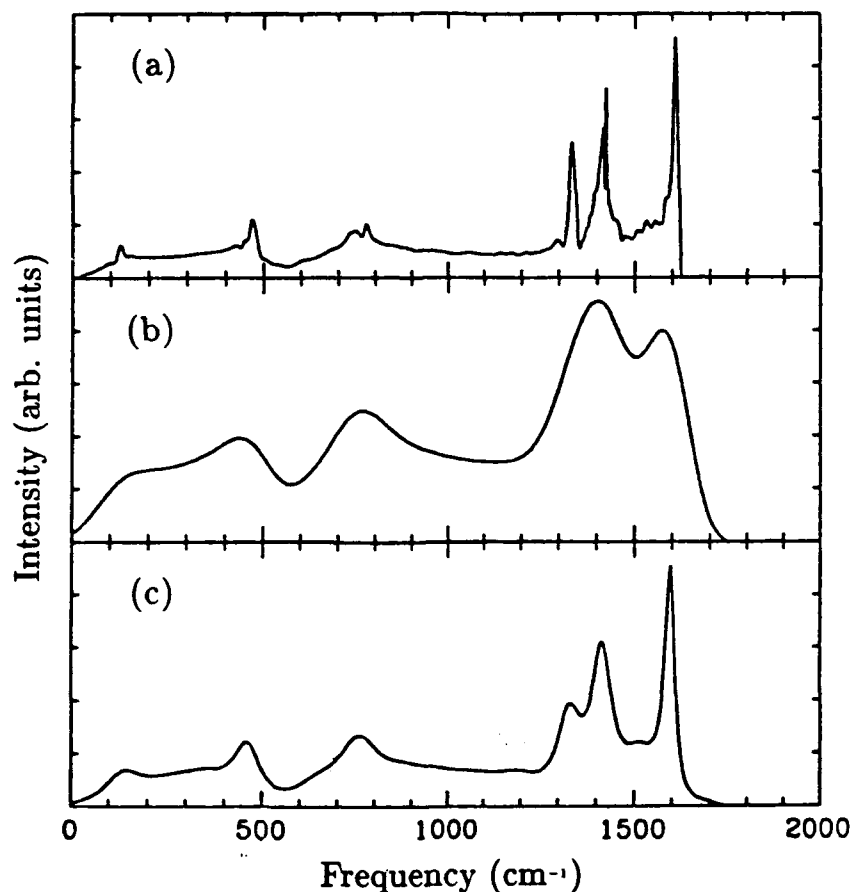


Fig. 1. (a): PDOS from Ref. 3. (b): Convolution of the curve in (a) with a Gaussian function. (c): Deconvolution result of the spectrum in (b).

is narrowed down to less than 50 cm^{-1} . The relative positions of the features in the spectrum remain accurate. Another important thing about the method is that it works on spectra with complex shapes. Deconvolution is capable of recovering the basic characteristics of the original spectrum.

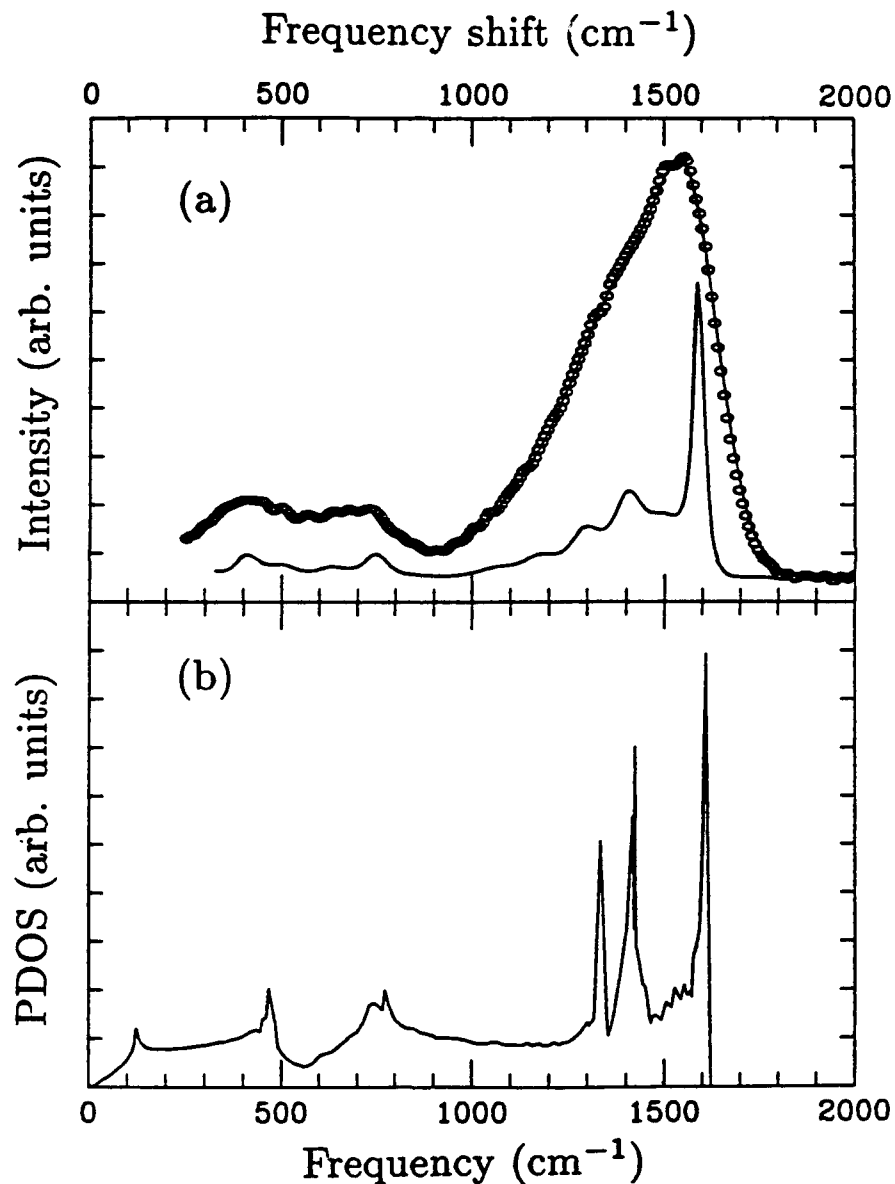


Fig. 2. (a): Circles are measured a-C Raman data. The lower curve is the deconvolution result of the measured data and the upper curve is the convolution result of the lower curve. The same Gaussian function was used in both deconvolution and convolution. (b): Phonon density of states of graphite calculated by Nicklow *et al.*³

The limitations of the deconvolution method are as follows. First, due to the basic assumption that all the features in the original spectrum are broadened in the same manner and to the same extent, this method can only remove the part of the expansion which is common to all features. Second, this method is very sensitive to noise. Obtaining high quality measurements in the first place is critical to the success of the deconvolution method. The third limitation concerns the relative intensities of features in the deconvolution result. The relative intensities of the features can change with the changes of the parameters in the deconvolution.

We have applied the deconvolution method in the analysis of a-C Raman spectrum. The deconvolution results for as-deposited a-C sample are displayed in Fig. 2(a). As a test of the hypothesis that the Raman spectrum of a-C is a broadened version of the phonon density of states of graphite, the PDOS data from R. Nicklow *et al.*³ is displayed in Fig. 2(b). The agreement of our results with Nicklow's data is noteworthy.

Reference

- ¹ N. Wada, P. J. Gaczi, and S. A. Solin, *J. Non-Cryst. Solids* **35 & 36**, 543 (1980).
- ² P. A. Jansson, *Deconvolution with Application in Spectroscopy* (Academic Press, Orlando 1984).
- ³ R. Nicklow, N. Wakabayashi, and H. G. Smith, *Phys. Rev. B* **5**, 4951 (1971).

Tuesday, January 19, 1995

Intra- and Intermolecular Interactions

TuA 8:00am-12:15pm
Salon D

Geoffrey A. Blake, *Presider*
California Institute of Technology

Spectroscopic Studies of Weakly Bound Molecular Complexes

William Klemperer Harvard University

We present recent results of the studies on the following systems. ArI₂ (With M.L.Burke), ArHCN (with S.Drucker and A.L. Cooksy) and ArHF and (HF)₂ (with H. Chang).

Optical spectra recorded with Ar and I₂ in a He expansion exhibit fluorescence from an excitation continuum through a broad region of the discrete B—X transitions of I₂ and I₂-Ar. This fluorescence emanates from B state I₂ and arises from excitations of a bimolecular I₂-Ar van der Waals complex. These results were obtained in order to test a proposed mechanism for the one-atom cage effect in I₂-Ar, whereby continuum excitation to the repulsive Π_U state precedes coupling onto the B state, association of the complex, and fluorescence from B state I₂. The variation of the relative intensity of the observed fluorescence with excitation wavelength can be adequately reproduced with this model, but the Π_U -X transition is much too weak (factor of 20) to explain the observed absolute intensities. We propose the existence of a linear I₂-Ar isomer in the expansion along with the well documented T-shaped isomer. Large geometry changes for the linear isomer upon B —X excitation would result in highly dispersed Franck-Condon factors and thus split this stronger transition over a continuum. Both absolute intensities and wavelength dependences observed for fluorescence from continuum excitation fit well to the linear isomer model. The linear isomer is probably responsible for the one-atom cage effect observed at the higher excitation energies which access the B state continuum.

The isomer of the I₂-Ar complex which yields discrete bands in the B—X spectrum is shown, as expected, to be T-shaped on the basis of the rotational structure observed in the vibronic bands. Precise fluorescence quantum yields for I₂-Ar relative to I₂ were measured via simultaneous acquisition of absorption and fluorescence excitation spectra in a slit nozzle expansion. These fluorescence quantum yields provide vibrational predissociation efficiencies for B state I₂-Ar as a function of vibrational state, from v' of 15 to 26. This is an oscillating function with local maxima at v' of 16, 22, and 26. For v=22 and 26, 73±3% of the complexes undergo vibrational, rather than electronic, predissociation. Fluorescence intensities of combination bands with excitation in the van der Waals modes were also found to have oscillating v' dependences, with patterns nearly identical to that for the bands without van der Waals mode excitations. Thus, these oscillations must arise from the electronic predissociation channel, rather than the vibrational predissociation

channel. Deconvolution of the lifetime of B state I_2 -Ar into vibrational and electronic lifetimes indicates that the similar overall lifetimes at v' of 18 and 21 result from a two-fold increase in the electronic lifetime at $v=21$, which compensates for a decrease in the vibrational lifetime. Assumption of a smooth v' dependence for the vibrational lifetime leads to oscillatory predicted overall lifetimes of 35, 77, 82, 51 and 30 ps over the v' range of 20 to 24, respectively. Based on symmetry arguments, as well as the observed vibrational predissociation efficiencies, the electronic predissociation of I_2 -Ar must arise from coupling of the B state to the Π_g state. This coupling may also be the dominant channel for collisional quenching of B state I_2 .

The lowest excited bending states, Σ_1 and Π_1 , of the ArHCN complex have been measured by millimeter-wave electric resonance optothermal spectroscopy. The principal molecular constants determined for the Σ_1 state are: $\nu_0 = 164890.790(12)$ B = 1958.8571(37) D = -0.07523(29) ; $eq_{aa}Q = 0.825(27)$ MHz; and $\mu_a = -0.521(30)$ D. For the Π_1 state, the constants are: $\nu_0 = 181984.4126(47)$; B = 2031.3624(17) D = 0.15335(16) $eq_{aa}Q = 0.904(11)$ MHz; and $\mu_a = 0.27302(63)$ D. The leading $\Sigma_1 - \Pi_1$ coupling constants are the Coriolis coefficient $\beta_0 = 1016.998(13)$ MHz and the transition dipole moment $\mu_b = 2.2535(57)$ D. The rotational constants for the two bending states indicate that the average separation between the argon and the HCN center of mass contracts by roughly 0.5 Å compared to the linear ground state. This is consistent with the nearly T-shaped average geometry for each state established by analysis of the dipole moments and quadrupole coupling constants. Agreement between this work and prior theory confirms attribution of the anomalous distortion and isotope effects in the ground state to extreme angular-radial coupling. The relative sign of the dipole moments for the Σ_1 and Π_1 , states is resolved in this work, allowing an unambiguous interpretation of the angular information. Assuming Laguerre angular distributions, we obtain that the Σ_1 wavefunction has a maximum at 108° with a halfwidth of 49° , and that the Π_1 state maximum is at 80° with a halfwidth of 37° . This Σ_1 state angular distribution indicates that although the state is not antilinear (ArNCH), as was expected, it does approach this configuration. The Π_1 state is nearly a free rotor eigenstate, showing that the angular part of the potential surface near 90° is extremely flat. The combined data from the Σ_0 , Σ_1 and Π_1 states reflect virtually the entire angular coordinate along the radial minimum of the potential.

Laser induced fluorescence is used to obtain the second overtone spectrum of ArHF. The method exploits intracavity circulating power of a Ti-sapphire ring laser to pump the weakly bound complex generated in a supersonic slit jet from $v = 0$ to $v = 3$. Fundamental ($\Delta v = -1$) emission is monitored using an infrared PbS detector. Intense fluorescence allows recording of the rotationally resolved sub-Doppler spectra of (3000) — (0000), (3100) - (0000) and (3110)— (0000) transitions. We determine vibrational band origins of $\nu_0 = 11339.034$, 11412.438 , 11422.378 cm^{-1} and rotational constants of $B = 0.10330$, 0.10276 , 0.10118 cm^{-1} for the (3000), (3100) and (3110) bands respectively. Both the band origins and the rotational constants indicate that the weak Ar-HF van der Waals bond is strengthened as the HF stretch is vibrationally excited to higher states. All the observations are in near perfect accord with extrapolations of related constants in the HF stretching states of $v = 0 - 2$.

The spectrum of $v=3$ free HF in $(\text{HF})_2$ is measured. Two subbands $K=0$ and $K=1$ are observed. The tunneling splitting of -0.002cm^{-1} shows the complete quenching of interconversion. The constants for this state are

$$\nu_0 = 11273.501 \quad \frac{B+C}{2} = 0.221177 \quad \frac{B-C}{2} = 1.9 \times 10^{-3} \quad A = 26.570$$

$$D_{JK} = -8.4 \times 10^{-4} \quad D_J = 2.02 \times 10^{-6} \text{ cm}^{-1}.$$

The values of these constants are found to fit smooth extrapolations from those of $v=0 - 2$. The Lorentzian broadening of the lines in the $K=0$ subband is obtained from fitting the Voigt profile as 45(10) MHz. The Lorentzian broadening of the lines in the $K=1$ subband is observed directly to be 1900 (200) MHz. No discernable variation with J is seen in either subband. These linewidths are entirely different than expected from simply extending $v=1$ and 2 observations. In particular the $K=0$ width is a factor of three smaller than that observed in $v=2$. The dramatic variation of width with K was not found in $v=2$. The results are interpreted as a specific coriolis induced interaction with the $v=3$ bonded HF stretching state plus the HFF bend.

**INFRARED-MOLECULAR BEAM SPECTROSCOPY:
THE STUDY OF WEAKLY BOUND MOLECULAR COMPLEXES AS A PROBE OF
POTENTIAL ENERGY SURFACES AND MOLECULAR DYNAMICS**

**Roger E. Miller
Department of Chemistry
University of North Carolina
Chapel Hill, North Carolina**

Infrared laser spectroscopy has become a powerful tool in the study of weakly bound molecular complexes. The molecular constants obtained from these spectra can be used to determine the "structure" of the complex, for systems where this is a meaningful concept, while, in complexes which undergo wide amplitude excursions from their equilibrium geometries, the spectroscopy is often sensitive to the details of the intermolecular potential energy surface. In many cases, these spectra are sensitive to both the internal dynamics of the complex and the vibrational predissociation dynamics that result from the excitation process.

The experiments reported here are based upon the use of the optothermal detection method. A number of rare gas-polyatomic molecule systems are discussed which illustrate some of the types of wide amplitude motions that can occur in these systems, and comparisons are made between the experimental results and those obtained using either *ab initio* theory or semi-empirical methods for constructing intermolecular potentials.

The application of high resolution cw pump-probe methods to the study of the vibrational predissociation dynamics of these systems will also be discussed.

High Resolution Electronic Spectroscopy of Hydroxyl-Rare Gas Complexes**Bor-Chen Chang, James M. Williamson, James R. Dunlop, and Terry A. Miller**

Laser Spectroscopy Facility

Department of Chemistry

The Ohio State University

120 West 18th Avenue

Columbus, Ohio 43210

(614) 292-2949

For many years, scientists have studied the spectroscopy of van der Waals complexes in past to understand intermolecular interactions and potential energy surfaces. There are abundant experiments and theoretical calculations on the closed-shell van der Waals complexes.^{1,2} Relatively speaking, the open-shell complexes have attracted much less attention until recently. The sparsity of information is due to both the difficulty of preparing the species and the complexity of their spectroscopy, which involves both unquenched electronic orbital and spin angular momenta. In the past four years, there have been several experimental and theoretical papers centered on Ar•OH/D and Ne•OH/D.^{3,4} However, except for one microwave experiment⁵ the previous works lack information about fine and hyperfine structure due to the resolution limit of dye laser used in the laser-induced fluorescence (LIF) studies.

In our laboratory, the LIF probe laser system is an Ar⁺-pumped ring dye laser with an excimer-pumped optical amplifier. This system gives resolution an order of magnitude better than previous experiments. Moreover, hydroxyl radicals are produced by ArF (193 nm) laser photolysis of nitric acid at the throat of a slit jet expansion. This slit jet expansion offers a minimal Doppler line width, and a rotational temperature in these spectra of approximately 2 degrees Kelvin. Based upon these advantages, we have observed the high resolution (0.008cm⁻¹)

LIF spectra of Ar•OH/D and Ne•OH/D. These high resolution spectra reveal very interesting fine and hyperfine structure of these species as well as more accurate rotational constants.^{6,7,8}

In the spectrum of Ar•OH, there are two distinct types of transitions. The bands without any bending excitation in the \tilde{A} state are called "A bands", and those with one-quantum bending excitation are called "U bands". These two types of bands have very distinct rotational structure as well as the fine and hyperfine structure. Figure 1 shows the difference between the spectrum of an A band and the spectrum of a U band. The top trace was assigned to the $\tilde{A} (0, 1^1, 3) \leftarrow \tilde{X} (0, 0^0, 0)$ transition (U band), and the bottom trace was assigned to the $\tilde{A} (0, 0^0, 3) \leftarrow \tilde{X} (0, 0^0, 0)$ transition (A band). Clearly, there is a J-independent doublet for each rotational transition of the bottom trace. In contrast, the top trace shows a J-dependent splitting for each rotational transition. We conducted an analysis including rotational, fine, and hyperfine interactions on these bands. From the fitting results, the Fermi contact hyperfine parameter of the Ar•OH \tilde{A} state is 700(12) MHz, which is approximately 10% less than the corresponding value in OH (775 MHz). This implies an electronic rearrangement in the OH moiety caused by the interaction with the Ar atom. In other words, the van der Waals interaction between Ar atom and OH radical is somewhat "chemical" rather than purely "physical". On the other hand, the high resolution spectrum of Ne•OH gives a Fermi contact parameter of 761(15) MHz, which is within experimental error identical to the corresponding value in OH.

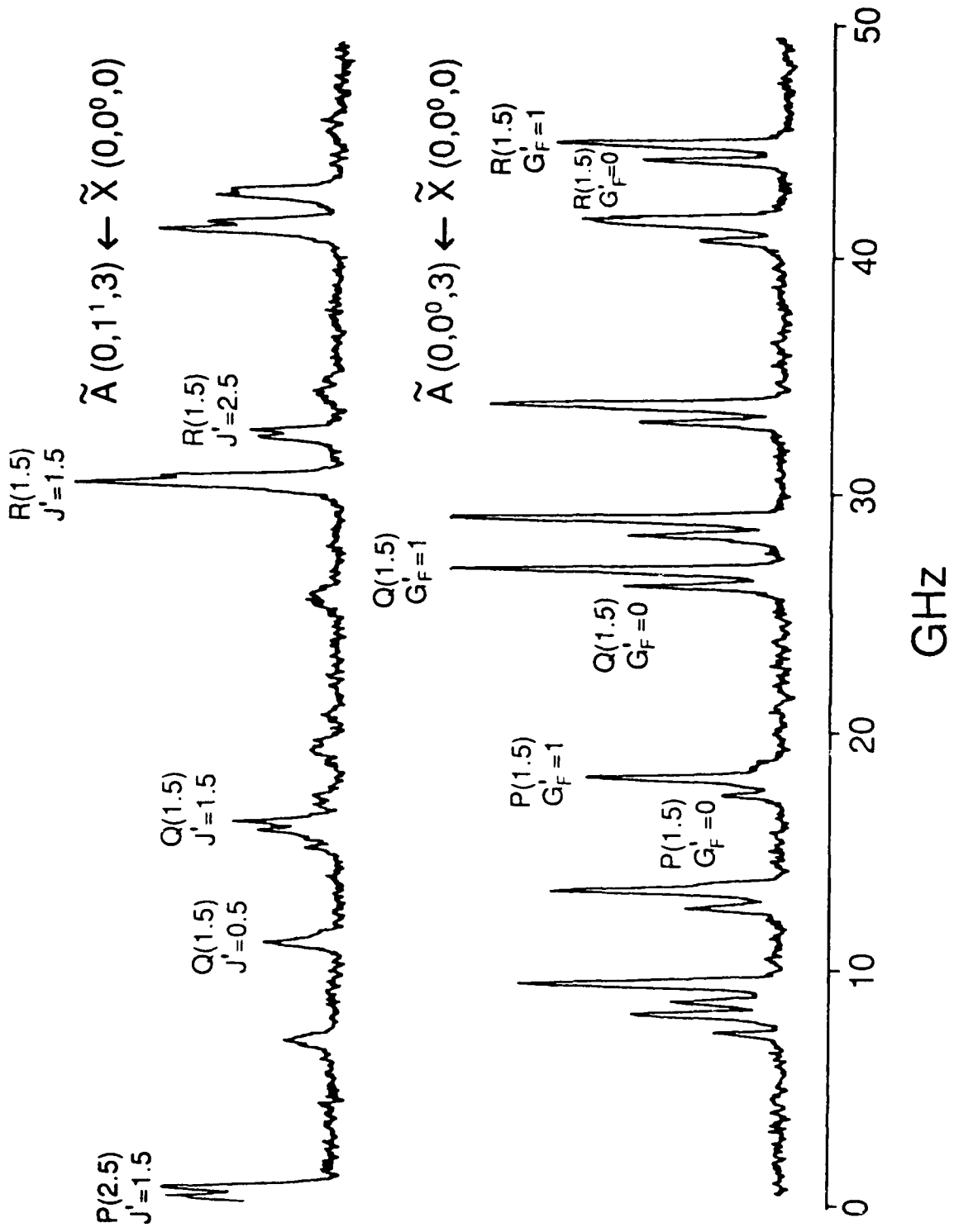
The spin-rotational structure in A bands and U bands is very different. In the case of an A band, the spin-rotational structure can be described by a single effective (diatomic) parameter of 46(12) MHz, which is very close to the value predicted from the corresponding value of OH based upon second-order perturbation theory. In contrast, the U bands show a spin-rotational splitting of a few GHz. In fact, this variation causes different angular momentum coupling schemes for the upper states of the A bands (case (b)_{βS}) and those of the U bands (case (b)_{βI}), and creates very different splitting patterns.

Furthermore, the parity splitting in the \tilde{X} state of the complexes were also determined. The parity splitting parameter in Ne•OH/D is approximately a factor of 10 larger than the corresponding value in Ar•OH/D. This implies that the potential anisotropy of the Ne complexes are quite different from that of the Ar complexes. Details of the experiment and analysis will be presented.

REFERENCES

1. R. C. Cohen and R. J. Saykally, *J. Phys. Chem.* **96**, 1024 (1992) and references therein.
2. M. D. Schuder, D. D. Nelson, Jr., and D. Nesbitt, *J. Chem. Phys.* **94**, 5796 (1991) and references therein.
3. M. C. Heaven, *Ann. Rev. Phys. Chem.*, in press and references therein.
4. M.-L. Dubernet, D. Flower, and J. M. Hutson, *J. Chem. Phys.* **94**, 7602 (1991) and references therein.
5. Y. Ohshima, M. Iida, and Y. Endo, *J. Chem. Phys.* **95**, 7001 (1991).
6. B.-C. Chang, L. Yu, D. Cullin, B. Rehfuss, J. Williamson, T. A. Miller, W. M. Fawzy, X. Zheng, S. Fei, and M. C. Heaven, *J. Chem. Phys.* **95**, 7086 (1991).
7. B.-C. Chang, D. W. Cullin, J. M. Williamson, J. R. Dunlop, B. D. Rehfuss, and T. A. Miller, *J. Chem. Phys.* **96**, 3476 (1992).
8. B.-C. Chang, J. M. Williamson, J. R. Dunlop, and T. A. Miller, *J. Chem. Phys.*, accepted.

Ar•OH



Conformational Interchange in the 10 μm and 3 μm Infrared Spectra of Propargyl Amine

Anne M. Andrews, Gerald T. Fraser and Brooks H. Pate
Molecular Physics Divison, NIST, Gaithersburg, MD 20899

The propargyl amine spectrum was observed using an electric resonance optothermal spectrometer coupled to a CO_2 laser-microwave sideband system for measurement of 10 μm spectra and to a color center laser for 3 μm spectra. Three bands were recorded in the 10 μm region; all were characterized by doubling of the transitions with a 3:1 intensity ratio, which is attributed to a torsion-inversion tunneling motion interchanging the two amine hydrogen atoms. The 3 μm band was greatly fractionated due to IVR. From double resonance experiments, each IVR component could be associated with one of the two tunneling states observed in the 10 μm spectrum.

Introduction

Propargyl amine ($\text{H}-\text{C}\equiv\text{C}-\text{CH}_2-\text{NH}_2$) in the gas phase has been observed as a mixture of *trans* and *gauche* conformers, with the *trans* conformer as the dominant component. An *ab initio* study by Riggs produced the potential function for rotation about the C-N bond shown in Figure 1.¹ The *trans* form is predicted to be more stable than the *gauche* form by $\approx 920 \text{ cm}^{-1}$ with a barrier to *trans-gauche* interconversion of $\approx 1427 \text{ cm}^{-1}$.

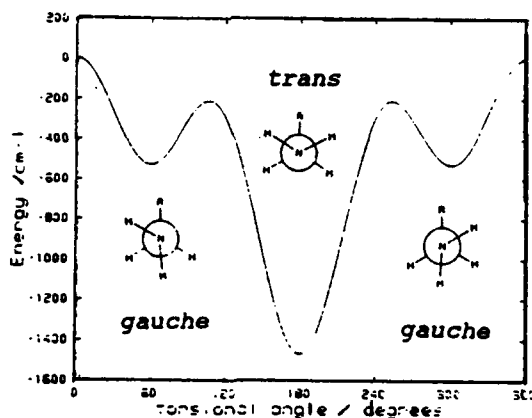


Figure 1. *Ab initio* potential for rotation about the C-N bond of propargyl amine.

There is no evidence of non-rigidity in the ground state spectrum of propargyl amine. However, it has been observed in a number of systems that vibrational excitation will provide

sufficient energy that tunneling can occur through a barrier insurmountable in the ground state. Additionally, it has been observed in matrices that isomerization between rotamers can be achieved through excitation of specific vibrational modes. The motivation for the $10\ \mu\text{m}$ study was in part to see whether evidence of such effects would be observed in propargyl amine in the gas phase. Additionally, at $3\ \mu\text{m}$, the region of the acetylenic C-H stretch, propargyl amine has a high density of states and displays evidence of intramolecular vibrational relaxation (IVR).² This is of interest for comparison with IVR studies of related molecules with $\text{-C}\equiv\text{C-H}$ chromophores.³

Spectrum at $10\ \mu\text{m}$

The EROS spectrometer used to obtain the spectra has been described in detail previously.⁴ At $10\ \mu\text{m}$ three bands were observed for propargyl amine. In all the bands the transitions were doubled with a 3:1 relative intensity ratio. The magnitude of the splitting showed a very strong K dependence and a slight J dependence. Figure 2 shows the K=3 Q-branch for one of the bands.

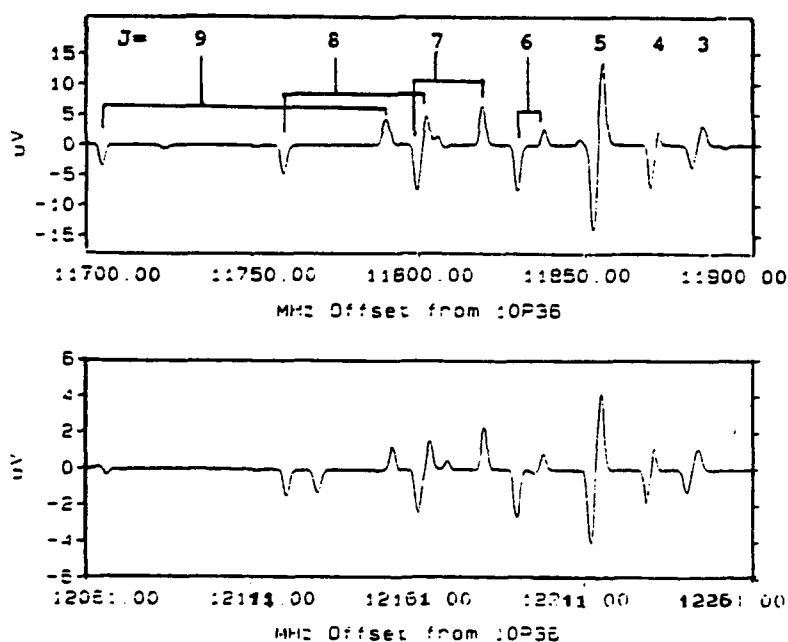


Figure 2. K=3 Q-branch from the $10\ \mu\text{m}$ spectrum of propargyl amine showing the two states observed and their relative intensities. The intensity scale on the lower trace ($I_H=0$) is one third that of the upper trace ($I_H=1$). The frequency scale is the offset (in MHz) on the positive sideband of the 10P36 CO_2 laser line at $929.01743596\ \text{cm}^{-1}$.

The intensity scale of the weaker band is one third that of the stronger band. The 3:1 relative intensities are characteristic of the nuclear spin statistical weights associated with the interchange of two hydrogen atoms. Since the amine group is the only part of the molecule likely to have a low barrier to proton interchange and further because vibrational transition involved is the NH_2 wag at 931 cm^{-1} , it seems reasonable to attribute the upper state splitting to the interchange of the two amine protons. Interchange of the $-\text{CH}_2-$ protons would involve inversion of the methyl group and seems unlikely. The strong state corresponds to the $I_{\text{H}}=1$ nuclear spin modification, while the weak state corresponds to the $I_{\text{H}}=0$, where I_{H} is the resultant nuclear spin function of the protons on NH_2 . Additionally, one of the bands displays severe perturbations while the other two are slightly perturbed.

Several interesting observations can be made about the tunneling motion. The first is that the barrier to the motion is probably in the neighborhood of 1000 cm^{-1} . This arises because the absorption of a 931 cm^{-1} photon propels the molecule from the bottom of the potential where no tunneling occurs to a region near enough to the barrier height that tunneling becomes possible. Second, the pathway required to account for the interchange of the two amine protons is not a simple one-dimensional coordinate: both an umbrella-like inversion motion and torsion about the C-N bond leave one with a different conformation from the starting structure. Therefore, the interchange must arise from a pathway involving the coupling of both motions; for example, an inversion followed by an internal rotation of 180° about the C-N bond would interchange the NH_2 protons. Finally, such a pathway implies that the molecule, which is *trans* in both minima, samples the *gauche* conformation during the tunneling process.

Spectrum at $3 \mu\text{m}$

In the 3300 cm^{-1} region, the acetylenic C-H stretch was observed. The R(1) transition is shown in Figure 3. Double resonance with the $10 \mu\text{m}$ band was used to assign the J, K and I_{H} quantum numbers. Each IVR component is associated with either an $I_{\text{H}}=1$ or $I_{\text{H}}=0$ tunneling state similar to the $10 \mu\text{m}$ band, indicating that the spin degeneracy of the bath states is lifted, presumably due to large torsional-inversion splittings. Further, the IVR widths and centers of gravity ($\sum I_i v_i / \sum I_i$, where I_i is the intensity and v_i is the frequency of the transition) for the singlet and triplet states differ significantly. The widths corresponds to IVR lifetimes of $\tau = 400 \text{ ps}$ for $I_{\text{H}}=0$ and $\tau = 250 \text{ ps}$ for $I_{\text{H}}=1$. Although the cause of this difference is not obvious, the fact that the torsional-inversion wavefunctions sample different spatial parts of the potential may play a role. The barrier to rotation about the C-N bond implies that the two functional groups sense the presence of one another. At present, how the C-H group senses the motion of the NH_2 group is unclear. For R(1), the centers of gravity are separated by about 200 MHz, which is a significant fraction of the

total IVR width. This points to a strong coupling to a background state outside the IVR width which has a large singlet/triplet splitting. Because the torsion inversion splittings at $10\ \mu\text{m}$ exhibit J and particularly K dependence, it is expected that a similar dependence will be observed in the $3\ \mu\text{m}$ spectrum. This appears to be the case and we are attempting to further address this issue.

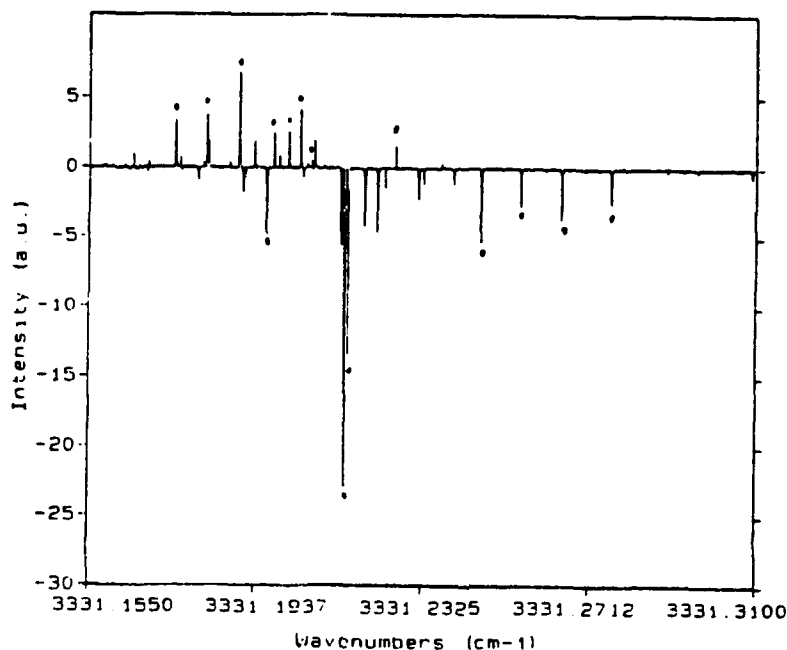


Figure 3. The R(1) transition of the acetylenic C-H stretch of propargyl amine showing fractionation from IVR. Each of the components is associated with either the $I_H=1$ or $I_H=0$ tunneling state observed in the $10\ \mu\text{m}$ spectrum. The $I_H=1$ transitions are marked with (•) while the $I_H=0$ are unmarked. The centers of gravity of the $I_H=1$ and $I_H=0$ bands are separated by 200 MHz.

References

1. N.V. Riggs, *Aust. J. Chem.*, 1987, **40**, 435-41.
2. B. H. Pate, Doctoral thesis, 1991.
3. B. H. Pate, K. K. Lehmann, and G. Scoles, *J. Chem. Phys.*, 1991, **85**, 3891-3916.
4. G. T. Fraser, R. D. Suenram and L. Coudert, *J. Chem. Phys.*, 1989, **90**, 6077-85; G. T. Fraser and A. S. Pine, *J. Chem. Phys.*, 1989, **91**, 637-45.

Molecular collisions at very low temperature

Frank C. De Lucia

Department of Physics, 174 W 18th Ave., The Ohio State University, Columbus, OH 43210

I. INTRODUCTION: We have reported a number of investigations in which a newly developed collisional cooling method was used to investigate collisional processes between gas phase atoms and molecules at very low temperatures.¹⁻⁷ In these studies the molecules are effectively in thermodynamic equilibrium with their collision partners, but at temperatures far below their freezing points. Used in conjunction with conventional equilibrium cells, measurements over the entire 1 - 1000 K region can be made. This range makes possible both the observation of new collision phenomena at low temperature and the study of collisions over a wide enough range to consider the collisions *spectroscopically*.

At some fundamental level there is an intimate connection between the familiar radiative spectroscopy and collisional spectroscopy. In the former, molecules are subjected to essentially dipolar radiative fields derived from spectroscopic sources; usually for the purpose of investigating energy level spacings, but also in principle for determining transition rates induced between levels by the interaction between the radiative field and the electric dipole moment of the molecule. In the latter, an electromagnetic field also mediates the interaction; but in a more intimate manner, with higher order multipole moments playing a significant role and the continuous spectrum produced by the collision replacing the essentially monochromatic radiation of conventional spectroscopy. This results in a much more complex interplay between the two partners.

Additionally, we have noted that the collisional cooling technique can be used for a number of other spectroscopic applications in both the microwave and infrared and that it should prove to be an attractive alternative to free expansion jets for many applications. These include the simplification of complex spectra, studies of weakly bound species and clusters, simulations of the interstellar medium and atmospheres of the outer planets, and studies of reaction dynamics at low temperature. Recently, Barnes et al.⁸ have used this technique (which they refer to as 'diffusive trapping') for infrared observations of CO₂ at 77 K. They too conclude that it is a 'versatile and economical device' and preferable to supersonic jet cooling for some applications.

II. EXPERIMENTAL: Central to the experiment is the collisionally cooled cell, shown in Figure 1. It is immersed in a bath of liquid helium or thermally connected to a helium pot, and the temperature varied by pumping on the helium. The spectroscopic gas is cooled to ~5 K by first filling the cell with a background of helium or hydrogen gas which quickly cools to the same temperature as the walls of the cell. The warm sample gas enters at the top of the cell via vacuum insulated needle tubing. After entering the cell the sample gas molecules cool by collisions with the cold background gas, eventually random walking their way to the walls where they condense. The key to the success of the technique is that while at 10 mTorr pressure it takes about 10000 collisions for a typical molecule to travel the 5 cm to the cell walls, it takes fewer than 100 collisions to effectively cool a molecule to the temperature of the background gas.

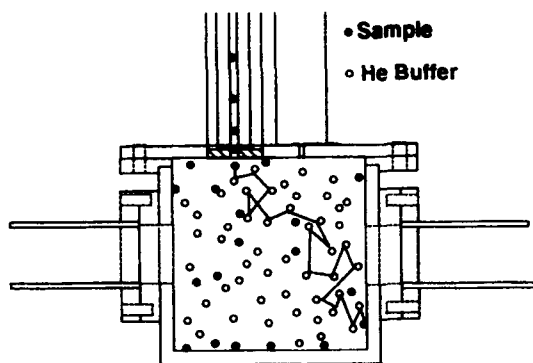


Figure 1. The collisionally cooled cell

H₂ slows and cools the injected molecules less efficiently than the heavier He. It is also noteworthy that smaller linewidths at these low temperatures begins to make the hyperfine structure marginally resolvable. As a result the data plotted in the figure were recovered via a Voigt fit to the six hyperfine components of this transition. We have also used this concept to develop systems cooled by liquid nitrogen, which are especially suitable for collisional studies involving the atmospheric gases N₂ and O₂.

Figure 2 shows a plot of the linewidth of the $1_{10} - 1_{01}$ transition of H₂S broadened by He at 12.3 K. Below ~2 mTorr the data show an upward hook. This is due to the incomplete cooling at the lowest pressures and is larger for collisions with H₂ than with He because the smaller mass of

For quantitative measurements it is important that the sample gas be very dilute. The absorption coefficient for a rotational transition is given by

$$\alpha = \left[\frac{8\pi^2\nu}{3ch} \right] |\langle m | \mu | n \rangle|^2 \left[\frac{N}{\Delta\nu} \right] \left[1 - e^{-\frac{h\nu}{kT}} \right] \left[\frac{1}{Q_r} \right] \left[e^{-\frac{E_l}{kT}} \right]$$

where $\langle m | \mu | n \rangle$ is the transition moment, N the number density, $\Delta\nu$ the linewidth, Q_r the rotational partition function, and E_l the energy of the lower state of the transition. This equation has been factored in order to separate the temperature dependent terms according to their physical origins. Three of the terms (the linewidth, Boltzmann difference between upper and lower states, and rotational partition function) depend strongly upon the rotational/translational temperature, while (for low lying rotational states) the energy of the lower state depends primarily upon the energy of the vibrational state which contains it. Near 5 K these factors represent about five orders of magnitude gain in the absorption coefficient in the microwave and perhaps three in the infrared. Thus, it is customary that dilution ratios between 10^{-4} and 10^{-6} produce signals that are observable in real time on an oscilloscope.

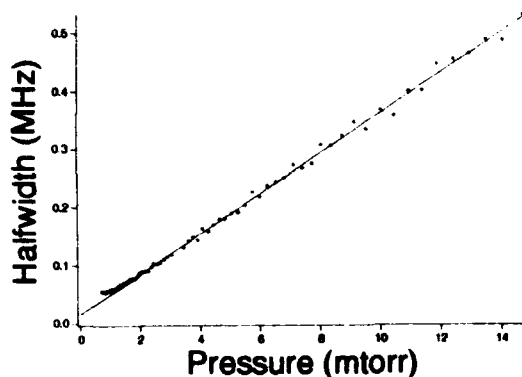


Figure 2. Linewidth of H_2S as a function of pressure.

Because of the large cross section for rotational energy transfer, it is well known that except under unusual circumstances the rotational temperature in a system follows closely its translational temperature. Because of the large number of collisions in the systems considered here, it would be expected that a single rotational/translational temperature would be established. The vibrational temperature of the spectroscopically active molecules is much more problematic, depending both upon the much smaller and widely varying cross sections for vibrational relaxation and the pressure of the cooling gas. Thus, in many circumstances it is possible to separately control the vibrational and rotational temperatures by judicious choice of the injector temperature, the bath temperature, and the pressure of the cooling gas. In the final analysis heat energy is very cheap and provides an interesting alternative to vibrational heating via laser pumping or discharges.

III. THEORETICAL CONSIDERATIONS: Because the physical origin of the cross sections for the molecular collisions considered here changes with collision energy, it is useful to begin with a consideration of measures of how *classical* or *nonclassical* an interaction might be. Consider the Correspondence Principle:

"The predictions of the quantum theory for the behavior of any physical system must correspond to the prediction of classical physics in the limit in which the quantum numbers specifying the state of the system become very large."

For collisional systems the appropriate quantum numbers are those specifying the internal states of the molecule and its collision partner and the orbital angular momentum associated with the collisional velocity and impact parameter. An additional consideration is the angular momentum associated with energetically open channels and the averaging over these channels which must take place before any experimentally observable quantity results.

Consider a He atom with a kinetic energy corresponding to 300 K and impact parameter 3 \AA colliding with a CO molecule. For this case a simple calculation shows that $L = 30 \hbar$. Similarly, the energy associated with 300 K corresponds to about $J = 10$ for CO, providing many energetically open channels. From this it is easy to conclude that ambient collisions between CO and He should in many respects be classical and be describable by classical or semiclassical theories. An experimental verification of this expectation is provided by the work of Nerf and Sonnenberg,⁹ who measured the collision cross section for CO broadened by He at 294 K, 195 K, and 77 K and found them essentially equal. We have found similar results for a wide range of molecules.¹⁰

It is useful to first consider semiclassical collisions in the context of Anderson like theories.¹¹⁻¹³ The interaction potential between a molecule and its collision partner can be considered to be of the form

$$V(t) = \frac{K}{r(t)^n}$$

where $r(t)$ is the time varying distance between collision partners, and K and n are constants characteristic of the multipole moment(s). If ω_{ab} is the transition frequency between two levels, substituting $x = r/b$ and $k = (b/v)\omega_{ab}$

into time dependent perturbation theory gives the matrix element for the collision induced transition probability as

$$\langle a|P|b\rangle = \frac{2\pi K}{hb^{n-1}v} \int_{-\infty}^{\infty} \frac{e^{ikx}}{(1+x^2)^{n/2}} dx$$

This equation is in the form of a Fourier integral and shows the interaction of the multipole moments of the molecule with the spectrum of the collision. For $k \gg 1$, the Fourier components of the radiation produced in the collision do not reach the transition frequencies ω_{ab} and the contribution to broadening or transition probability is small. In this context it is useful to note that hydrogen and helium have the largest thermal velocities, thereby leading to the smallest k 's and the highest frequency Fourier components. Furthermore, a hard sphere has in effect $n = \infty$ for that class of molecules which come within the sphere's radius R , thereby producing $P = 1$ and the classical collisional cross section $\sigma = \pi R^2$. More exact treatments additionally consider the internal energy levels and multipole moments of the collision partner and orientation effects.

At lower collision energies new phenomena which are beyond the context of semiclassical models become important. Although several distinguishable cases can be identified, for our purposes they can all be associated with quasibound states. At high collision energies the molecules effectively bounce off of each other's strong repulsive core in a fashion represented by the semiclassical theory discussed above. However, at lower energies the existence of a shallow attractive well gives rise to the formation of intermediate states during the collision. In this regime much more exact (and computationally costly) methods are required which quantize the entire problem, including the angular momentum of the molecular trajectories.^{14,15}

An especially interesting calculation has been done by Palma and Green¹⁶ for CO - He collisions and the results

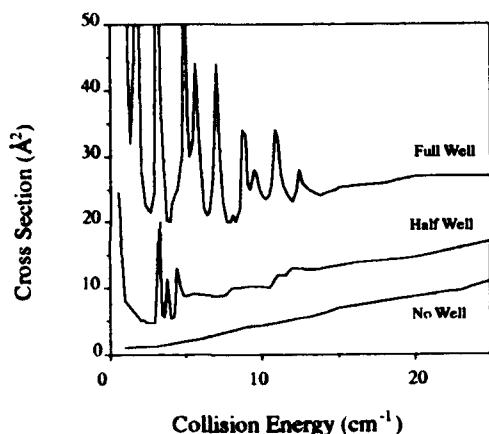


Figure 3. Pressure broadening cross section for the full, half and no well modifications of the potential.

are shown in Fig. 3. Using a potential obtained by *ab initio* techniques, the pressure broadening cross section was calculated as a function of collision energy. This result is shown as the upper line in the figure. At the lowest energies, large resonances associated with the quasibound states are important. These slowly decrease in size with increasing collision energy, and finally approach the 'classical' plateau associated with higher energy collisions. Palma and Green then reduced the depth of the attractive well by a factor of two and repeated the calculation, producing the results shown by the middle line. The lower line was obtained by completely eliminating the attractive well. These results are extremely useful, providing a basis for substantial qualitative understanding of low energy processes. They show the importance of the shallow attractive well in the formation of the resonances which increase the experimentally observable cross sections. Furthermore, in the case of no well the approach toward zero cross section at zero energy is intuitively satisfying.

IV. RESULTS: A variety of phenomena in a large number of systems, including CO, NO, CH₃F, H₂S, DCl, HDO, OCS, and CH₂F₂, have now been studied.

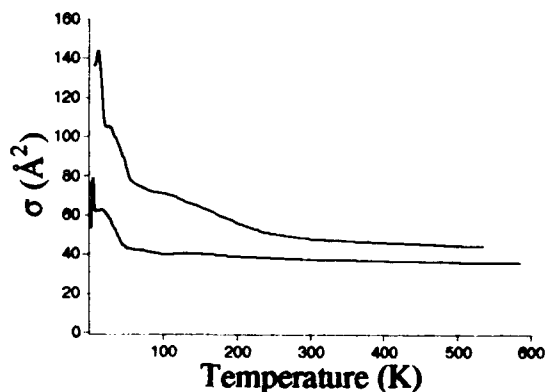


Figure 4. Pressure broadening cross sections for the CH₃F - H₂ (upper) and CH₃F - He (lower) systems

Figure 4 shows the pressure broadening cross sections for collisions between CH₃F and He and H₂. Both show the large increase in cross section at low temperature associated with the formation of the quasibound states. Additionally, at higher temperature the cross section for collisions with He are essentially constant as predicted by semiclassical theory, while those for collisions with H₂ are not. This effect in the CH₃F - H₂ system is caused by the relation between the Fourier spectrum of the collision and the internal energy levels of the molecules.

Figure 5 is a collection of pressure broadening cross sections measured in the nonclassical region between 1.5 and 5 K. In this figure the measured cross sections are normalized to their respective values at 300 K. This variety of spectroscopic types has been selected in order to illustrate

the relation between spectral density of states and the formation of quasibound states which increase observed cross sections. Species, such as CH_3F , which have level spacing $\sim kT$ show increases in observed cross sections above their classical 300 K values; while those like H_2S and DCI , with spacings wide in comparison to kT , show reduced cross sections.

There are many spectroscopic applications, especially those associated with the assignment of complex spectra, in which the rotational and vibrational temperatures of the spectroscopic gas are important considerations. Because

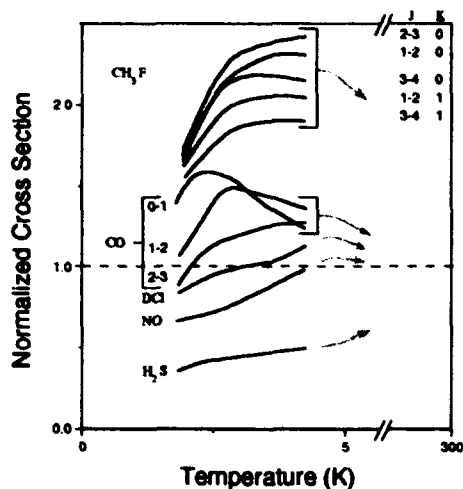


Figure 5. Normalized broadening cross sections.

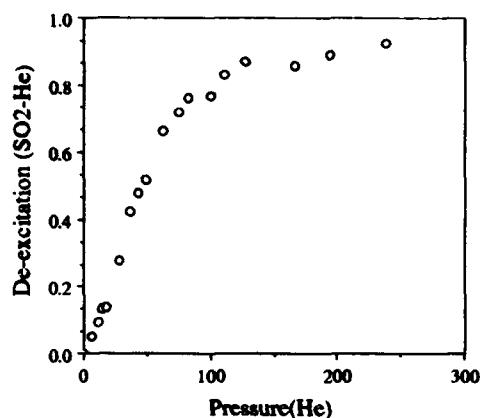


Figure 6. Vibrational deexcitation factor for SO_2 -He collisions at 77 K.

vibrational relaxation is ordinarily orders of magnitude slower than rotational relaxation, it is not uncommon for the rotational and vibrational temperatures to be decoupled. In a common limit of collisional cooling experiments, the temperature of the injector should determine the vibrational temperature and the background gas the rotational temperature. For the CH_3F we have confirmed this expectation by observing the intensities of rotational transitions in the ground, ν_3 , $2\nu_3$, and $3\nu_3$ vibrational states for injector temperatures between 300 and 600 K.¹⁷ However, for molecules with lower vibrational energy, we have found that by adjustment of the pressure of the cooling gas (and thereby the number of collisions, which varies as the square of the pressure), the vibrational temperature can be continuously 'tuned' from the temperature of the injector to the temperature of the cooling gas.¹⁷ This is illustrated in Fig. 6 for the ν_3 state of SO_2 . This independent adjustment of the vibrational and rotational temperatures by appropriate choice of cooling gas and injector temperatures will be important for many spectroscopic applications.

REFERENCES:

1. J. K. Messer and F. C. De Lucia, *Phys. Rev. Lett.* **53**, 2555 (1984).
2. D. R. Willey, R. L. Crownover, D. N. Bittner, and F. C. De Lucia, *J. Chem. Phys.* **89**, 1923 (1988).
3. D. R. Willey, R. L. Crownover, D. N. Bittner, and F. C. De Lucia, *J. Chem. Phys.* **89**, 6147 (1988).
4. D. R. Willey, D. N. Bittner, and F. C. De Lucia, *Mol. Phys.* **67**, 455 (1989).
5. D. R. Willey, D. N. Bittner, and F. C. De Lucia, *J. Mol. Spectrosc.* **133**, 182 (1989).
6. D. R. Willey, D. N. Bittner, and F. C. De Lucia, *J. Mol. Spectrosc.* **134**, 240 (1989).
7. D. R. Willey, T. M. Goyette, W. L. Ebenstein, D. N. Bittner, and F. C. De Lucia, *J. Chem. Phys.* **91**, 122 (1989).
8. J. A. Barnes, T. E. Gough, and M. Stoer, *Rev. Sci. Instrum.* **60**, 406 (1989).
9. R. B. Nerf and M. A. Sonnenberg, *J. Mol. Spectrosc.* **58**, 474 (1975).
10. T. M. Goyette and F. C. De Lucia, *J. Mol. Spectrosc.* **143**, 346 (1990).
11. P. W. Anderson, *Phys. Rev.* **76**, 647 (1949).
12. C. J. Tsao and B. Cumutte, *J. Quant. Spectrosc. Radiat. Transfer* **2**, 41 (1962).
13. C. H. Townes and A. L. Schawlow, *Microwave Spectroscopy*, McGraw-Hill, New York, 1955.
14. A. M. Arthurs and A. Dalgarno, *Proc. R. Soc. London* **256**, 540 (1962).
15. S. Green and P. Thaddeus, *Astrophys. J.* **205**, 766 (1976).
16. A. Palma and S. Green, *J. Chem. Phys.* **85**, 1333 (1986).
17. T. M. Goyette, W. L. Ebenstein, and F. C. De Lucia, *J. Mol. Spectrosc.* **140**, 311 (1990).

The First Rotational Analysis of the Infrared Spectrum of Dimethylacetylene

P. R. Bunker, J. W. C. Johns, and A. R. W. McKellar

*Herzberg Institute of Astrophysics
National Research Council of Canada
Ottawa, Ontario, K1A 0R6, Canada,
Telephone: (613) 990-0738*

and

C. Di Lauro

*Facolta di Farmacia
Universita Degli Studi di Napoli
80131 Naples, Italy.
Telephone: (081) 546-4311*

I. INTRODUCTION

The perpendicular fundamental bands of dimethylacetylene have long been of interest to spectroscopists. This is because it is in these bands that two interesting effects manifest themselves. The first of these effects is the splitting of certain rotational lines caused by the small barrier to internal rotation. And the second effect is the shift of intensity within the band due to the coupling (through the acetylene bond) of the perpendicular methyl vibrations from one end of the molecule to the other.

We have recorded the infrared spectrum of the methyl-rocking fundamental band around $10\ \mu\text{m}$, and have rotationally analysed a significant number of sub-bands. We have identified splittings caused by internal rotation, and shifts due to the end-to-end vibrational coupling. This is the first time that any infrared spectrum of dimethylacetylene has been rotationally analysed, and these effects quantitatively understood.

II. EXPERIMENT

The two important experimental features are the use of our modified double-pass BOMEM FT spectrometer, and the use of a cooled multiple-pass absorption cell.

The resolution of our BOMEM DA3.002 FT spectrometer has been essentially doubled by replacing the moving plane mirror with a moving roof-top reflector and a fixed plane mirror. The maximum optical path difference has been increased to 4.45 m and, as a result, the full width at half height of the instrument function has been decreased to 0.0014 cm^{-1} . Also the 'optical moving mirror' has now become stationary, and it has been possible to transfer the dynamic alignment mechanism to this mirror. Thus misalignments caused by imperfections in the movement of the roof-top are corrected in the moving-arm of the interferometer and are always referred to the truly fixed arm.

The absorption cell used in the experiment is a cooled, large aperture, multipass cell. The cell has a length of 0.5 m, and up to 40 traversals are possible. The aperture of the cell is $f/4$, and it consequently uses all of the light from the BOMEM. The cell is made of stainless steel and is cooled by flowing refrigerated liquid through coils around it; it is vacuum insulated and can be cooled to 130 K. In our experiment we cooled the dimethylacetylene to 213 K, used a pressure of 1.6 Torr, and used 16 traversals to achieve a path length of 8 m.

The Doppler width in the $10 \mu\text{m}$ region of the spectrum of dimethylacetylene at 213 K is 0.0014 cm^{-1} . Without the increased resolution of the BOMEM, and without cooling the sample from 300 K, we would have been unable to resolve the very congested spectrum.

II. THEORY

The perpendicular fundamental band of a 'normal' symmetric top molecule consists of sub-bands, and the most prominent features are the Q -branches which in a first approximation are equally spaced with a separation of $2[A(1 - \zeta^2) - B]$. The Q -branches can be labelled by the value of $K\Delta K$, where K is the value of K in the ground state of the transition and $\Delta K = \pm 1$ is the change in K . In Dimethylacetylene there is practically free internal rotation and every rotational level has torsional fine structure labelled by the torsional quantum number K_i . As a result, the number of Q -branches in the band is greatly increased and now they must be labelled by $K\Delta K$ and $K_i\Delta K_i$. The spectrum is very congested with these Q -branches occurring in 'bunches'. The centres of the bunches are separated by $2[2A(1 - \zeta^2) - B]$ and the separation of the Q -branches within the bunches is

only $2B$ ($\approx 0.22 \text{ cm}^{-1}$).

One of the particularly interesting features about dimethylacetylene is its very low barrier to internal rotation. This barrier could be determined from fine structure in the perpendicular fundamental bands. The Q -branches having $K_i \Delta K_i = \pm 3$ are split by the V_3 term in the torsional potential, and if such a splitting could be resolved we could determine the height of the torsional barrier from it. The second interesting fact about dimethylacetylene concerns the nature of the perpendicular fundamental vibrations such as the methyl-rocking vibration studied here. These methyl group vibrations become localized in one end of the molecule or the other as a result of the torsional motion. The torsional motion prevents the perpendicular displacements from being transferred through the acetylene bond from one end of the molecule to the other. A careful study of the positions of the Q -branches will reveal the extent of this uncoupling.

III. RESULTS

The spectrum is congested with thousands of resolved and partly resolved lines, as well as many regions where the rotational structure is unresolved. We have concentrated on the region from 1000 cm^{-1} to 1100 cm^{-1} where the methyl rocking perpendicular fundamental band occurs. We have been able to assign many Q -branch features in this region. For the 16 most prominent sub-bands we have assigned the Q -branches and P - or R - branch lines with J values up to about 60. From the ground state combination differences formed we could determine accurate values for the ground state constants B , D_J , and $D_{JK} = D_{JK_i}$. More interestingly we could identify a Q -branch that is split by the ground state torsional barrier, and therefore determine this barrier. We could identify a series of Q -branches to excited state levels having $K_i = 0$ in which the end-to-end coupling of the methyl group vibrations occurs. The shift caused by this coupling is accurately determined from the spectrum.

Eventually a complete analysis of all the perpendicular fundamental bands will show how the barrier to internal rotation changes with vibrational state, and how the extent of the end-to-end coupling of the vibrations depends on the nature of the vibration.

Tuesday, February 17, 1998

Sub-Doppler Techniques

TuB 8:30pm–10:00pm
Salon D

Peter Felker, *Presider*
University of California at Los Angeles

Perturbative Nearly-Degenerate Four-Wave Mixing Lineshapes in Gases

Larry A. Rahn

Combustion Research Facility, Dept. 8354

Sandia National Laboratories

Box 969

Livermore, CA 94551-0969

(510)294-2091

Nearly-degenerate four-wave mixing (NDFWM) spectroscopy¹ and the closely related tunable-laser-induced grating spectroscopies² have proved to be valuable tools in the study of nonlinear optical interactions. The NDFWM spectral lineshape provides information concerning the lifetimes,³ and therefore the identities, of multiphoton scattering mechanisms. In addition to the great number of investigations in liquids and solids, considerable research has focused on wave-mixing in resonant atomic gases for phase conjugation applications.⁴ Although many special cases have been discussed, general expressions that include the effects of molecular motion for the NDFWM lineshape in gases have not been previously reported. The present study is motivated by an interest in understanding the mechanisms contributing to degenerate four-wave mixing (DFWM) spectroscopy in molecular gases for application to combustion and chemical physics research.

In this study, expressions for the NDFWM lineshape have been developed for nearly forward- and counter-propagating collinear pump-beam geometries. The lineshapes have been derived by applying the velocity integration methods used by Lam and Abrams⁵ for the phase-conjugate DFWM to the perturbation-theory expressions developed by Tretout, et al.⁶ for resonance coherent anti-Stokes Raman spectroscopy (CARS). The resultant expressions thus include the effects of molecular degeneracy on the polarization characteristics of $\chi^{(3)}$.

The NDFWM susceptibility expression for the forward near-collinear pump geometry is the most simple and reveals the sensitivity to population lifetimes. We consider monochromatic pump (ω_1, ω_3) and probe (ω_2) laser beams incident near resonance with a transition from ground state (a) to excited state (n) producing a signal at ω_4 . In this case we find

$$\chi_{\text{fwd}}^{(3)} \propto (\mu_{13} + \mu_{31}) [(\delta + i\gamma_a)^{-1} + (\delta + i\gamma_n)^{-1}] \\ \times \left[-\frac{1}{2} (\delta + i\gamma_{an})^{-1} \{ Z(\Delta + \delta + i\gamma_{an}) + Z(-\Delta + \delta + i\gamma_{an}) \} \right. \\ \left. + \delta^{-1} \{ Z(-\Delta + \delta + i\gamma_{an}) - Z(-\Delta + i\gamma_{an}) \} \right],$$

where the detunings are defined by $\delta = \omega_1 - \omega_2$ and $\Delta = \omega_{na} - \omega_1$. The function Z represents the plasma dispersion function⁵ while μ_{13} and μ_{31} represent the product of the four relevant dipole-moment matrix elements⁶ for the two permutations of pump-photon time ordering. Damping is represented in the customary way with the dephasing and population decay rates described by doubly-indexed and singly-indexed γ 's, respectively. The frequencies are all normalized to ku_0 where k is the pump wavevector and u_0 is the most probable molecular speed.

The NDFWM experiment is performed by measuring the signal versus δ with Δ fixed, while DFWM experiments measure the signal *versus* Δ with δ set to zero. We note, then, that the first two resonant denominators in $\chi_{\text{fwd}}^{(3)}$ cause the population lifetime influence on the NDFWM spectrum (δ tuned) while the DFWM spectrum (Δ tuned) is sensitive to the dephasing rate and the Doppler effect (through Z).

Comparison to high resolution NDFWM and DFWM measurements on the $R_1(9)$ transition of OH in an atmospheric pressure H_2-O_2 flame are made in Fig. 1. The NDFWM data in Fig. 1(a) were measured with cross-polarized pump and probe beams and fit using the dephasing rate ($\gamma_{an} = 6 \times 10^{-2} \text{ cm}^{-1}$) from earlier backward DFWM and Doppler-free saturated absorption measurements.⁷ Assuming that $\gamma_a = \gamma_n$, the population decay rate found from the fit is $3.7 \times 10^{-2} \text{ cm}^{-1}$. The NDFWM data in Fig. 1(b) were measured with all laser polarizations parallel. In this case, an intensity grating is formed, giving rise to a very narrow feature near

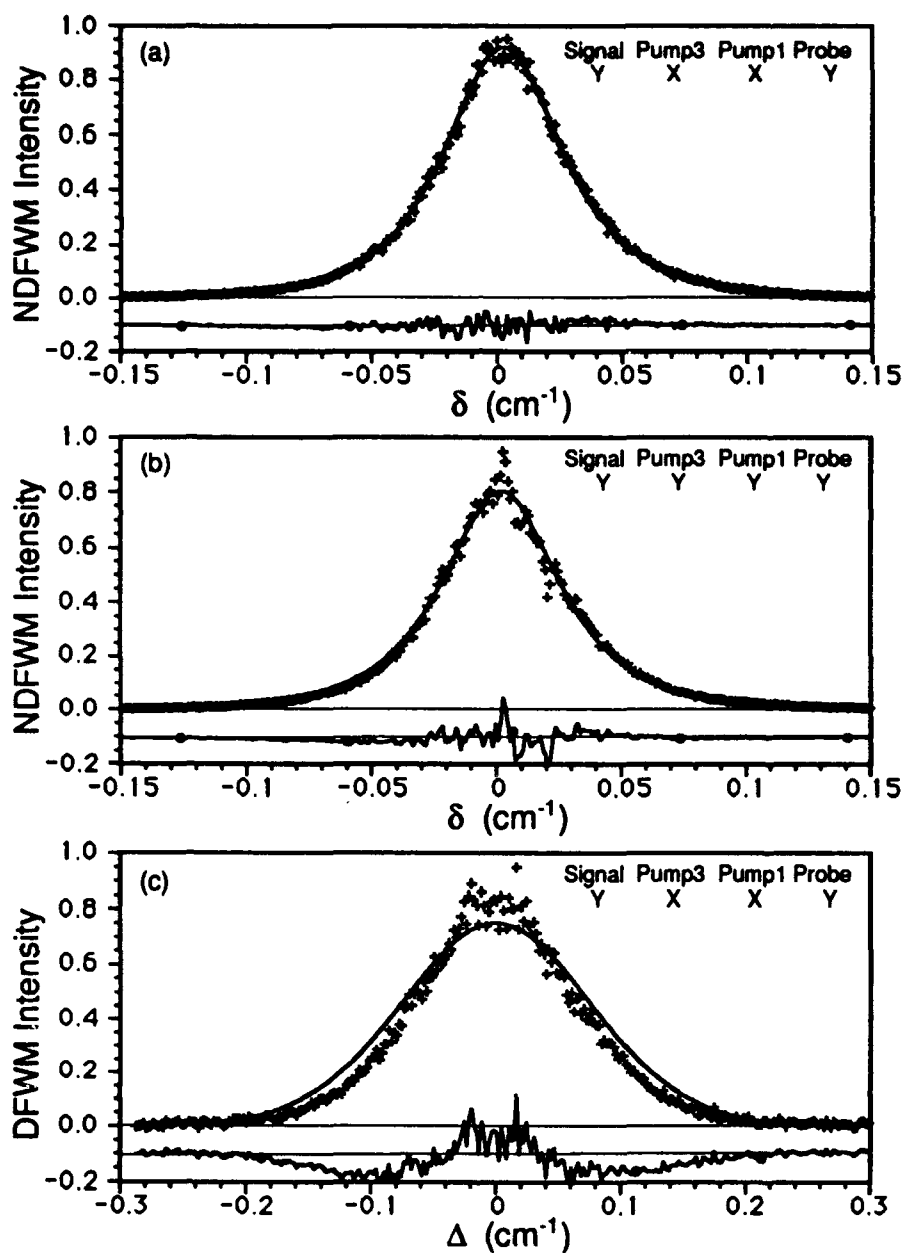


FIG. 1 NDFWM, in (a) and (b), and DFWM, in (c), measurements (symbols) of the $R_1(9)$ transition of OH in a flame. The lineshapes are compared to theory (solid line) that was fit to the data in (a). The difference between theory and experiment is plotted offset below in each case.

zero detuning attributed to the formation of a thermal grating. The line is calculated from the parameters derived from the fit in Fig. 1(a). The data of Fig. 1(c) are DFWM measurements of the same transition and are also compared to theory calculated from the parameters derived from

the fit in Fig. 1(a). Note that, although the line is considerably broader, it is still narrower than the theoretical prediction. This difference is attributed to velocity-changing collisions that cause a degree of motional narrowing of the Doppler effect.

This research is supported by the U. S. Department of Energy, Office of Basic Energy Sciences, Division of Chemical Sciences.

References

1. J. Nilsen and A. Yariv, *J. Opt. Soc. Am.* **71**, 180 (1981).
2. R. Trebino, C. E. Barker, and A. E. Siegman, *IEEE J. Quantum Electron.* **QE-22**, 1413 (1986).
3. P. R. Berman, D. G. Steel, G. Khitrova and J. Liu, *Phys. Rev. A* **38**, 252 (1988).
4. R. L. Abrams, J. F. Lam, R. C. Lind, D. G. Steel and P. F. Liao, in *Optical Phase Conjugation*, R. A. Fisher ed. (Academic Press Inc., New York, 1983).
5. J. F. Lam and R. L. Abrams, *Phys. Rev. A* **26**, 1539 (1982).
6. B. Attal-Trétout, P. Monot and K. Müller-Dethlefs, *Mol. Phys.* **73**, 1257 (1991).
7. M. S. Brown, L. A. Rahn and T. Dreier, *Opt. Lett.* **17**, 76 (1992).

Doppler-Free Spectroscopy of Molecular Iodine Near 532 nm

Ady Arie and Robert L. Byer

Edward L. Ginzton Laboratory, Stanford University, Stanford CA 94305

Telephone: (415) 723-0161

Molecular Iodine exhibits a very rich absorption spectrum¹ near 532 nm. Frequency-doubled monolithic diode laser pumped Nd:YAG lasers, having narrow linewidths and relatively wide tuning range, provide an excellent tool to investigate these transitions. Furthermore, we have recently shown that the Nd:YAG laser frequency can be absolutely stabilized to the Doppler-free lines of Iodine². In this paper we utilize the ability to lock two lasers to Iodine hyperfine transitions in order to measure precisely the hyperfine frequency splitting by heterodyne spectroscopy. These results are then used to determine the hyperfine constants of the measured transitions.

The experimental setup is shown in Fig. 1. We used two Lightwave Electronics model 122 Nd:YAG monolithic diode laser-pumped non-planar ring lasers, emitting 300 mW at 1064 nm. The laser frequency was externally doubled using MgO:LiNbO₃ monolithic crystal resonator, heated to its phase matching temperature (~108 °C). To provide high conversion efficiency with a fixed output power, the resonator was frequency locked to the pump frequency by a servo which controls the LiNbO₃ resonator temperature. More than 100 mW of green power can be generated at the optimal phase matching temperature, but the typical operating powers were in the range of 10-20 mW. The 532 nm output of the doubler was the source for FM Doppler-free saturation spectroscopy of Iodine. The FM signal from a hyperfine component was fed back into the PZT frequency actuator of the laser through a servo amplifier, thereby locking the laser frequency to a hyperfine line of the Iodine. We used 10 and 15 cm long ¹²⁷I₂ cells, held at a temperature of 0°C.

Eight relatively strong ro-vibrational transitions in the range³ 18787 - 18789 cm⁻¹, as well as a few weaker lines are observed within the tuning range of the laser. Using vibrational band head energies and rotational constants⁴ we have assigned the vibrational and rotational numbers for these lines, see enclosed table. The line numbers and measured frequencies are taken from Reference 3. Note that lines 1109 and 1111 each contain two ro-vibrational transitions.

Two completely independent systems have been built, with each laser locked to its own Iodine cell. The heterodyne beatnote signal between the lasers was measured at 1064 nm using a photodetector followed by a frequency analyzer. The stability of the locked lasers was calculated using the Allan variance². Fig. 2 shows the root Allan variance as a function of measurement time, τ , when both lasers are locked to the a₁ line of R(56)32-0. At $\tau=1$ s the the two-sample frequency deviation is

185 Hz (root Allan variance of $6.5 \cdot 10^{-13}$), and the lowest frequency deviation of 70 Hz is obtained at $\tau=32$ s (root Allan variance of $2.5 \cdot 10^{-13}$). This represents an order of magnitude improvement in the frequency stability with respect to our previous results². The main improvements in the experimental system are: Cooling and temperature stabilizing the Iodine cells and eliminating the interferometric noise between the scattered pump and probe by acousto-optic modulation of the pump beam.

Line No.	Measured (cm^{-1})	Calculated (cm^{-1})	Assignment
1106	18787.1285	18787.1270	P(119)35-0
1107	18787.2800	18787.2792	R(86)33-0
1108	18787.3389	18787.3378	R(106)34-0
1109	18787.8042	18787.7807 18787.8008	R(134)36-0 P(83)33-0
1110	18788.3371	18788.3345	R(56)32-0
1111	18788.4454	18788.4345 18788.4417	P(103)34-0 P(53)32-0

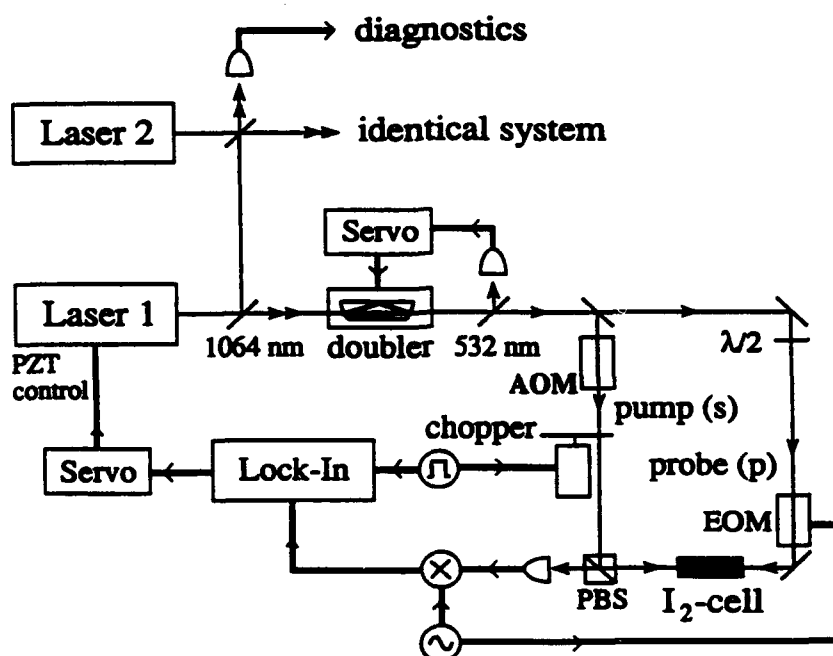


Fig. 1: Experimental set-up. PBS is a polarizing beam splitter, AOM is an acousto-optic modulator and EOM is an electro-optic modulator.

In order to measure the hyperfine frequency splitting we have locked one of the lasers to an isolated hyperfine component. This laser served as a frequency reference, while the second laser was locked each time to a different hyperfine component, and the beat frequency was measured by taking the average of 30 successive 4 s measurements. Fig. 3 shows the hyperfine spectrum and measured frequencies of line R(56)32-0.

We used the measured Iodine spectra to determine the difference in the hyperfine constants for these transitions. We follow the procedure outlined by Foth and Spieweck [5]: The Hamiltonian of the hyperfine interactions can be written as:

$$H_{\text{hfs}} = H_{\text{EQ}} + H_{\text{SR}} + H_{\text{SSS}} + H_{\text{TSS}}$$

where H_{EQ} (eQq), H_{SR} (C), H_{SSS} (A), H_{TSS} (δ) represent the electric quadrupole, spin-rotation, scalar spin-spin and tensor spin-spin interactions, respectively, and the symbols in parenthesis denote the constants of each of these interactions. For the electric quadrupole interactions we have also considered rotational levels separated by ± 2 , where the rotational energy spacings were taken from Ref. 4. The differences in the constants between the upper and lower levels were used as fitting parameters to the experimental measurements. As an example, we obtained a theoretical fit to the measurement with a standard deviation of 35 kHz for the R(56)32-0 line using the following hyperfine constants: $\Delta eQq = 1908.21 \pm 0.06$ MHz, $\Delta C = 86.44 \pm 0.1$ kHz, $\Delta A = -26.18 \pm 2$ kHz, $\Delta \delta = -28.16 \pm 1.7$ kHz. ΔeQq and ΔC are, respectively, 1.76 MHz higher and 7.3 kHz lower than the values predicted using empirical formulas⁶.

In conclusion, we have measured the spectra and determined the hyperfine constants of 8 different ro-vibrational transitions near 532 nm. These transitions occur between the lowest vibrational level in the ground (X) state and the vibrational levels 32-36 in the B state. The determination of the hyperfine constants may provide insight for the dependence of the hyperfine constants on the vibrational number. The high level of stability that can be obtained with Iodine-stabilized Nd:YAG laser, as well as its small size, excellent beam quality and high reliability, makes this laser an attractive source for precision metrology, e.g. a new optical length standard for the realization of the meter.

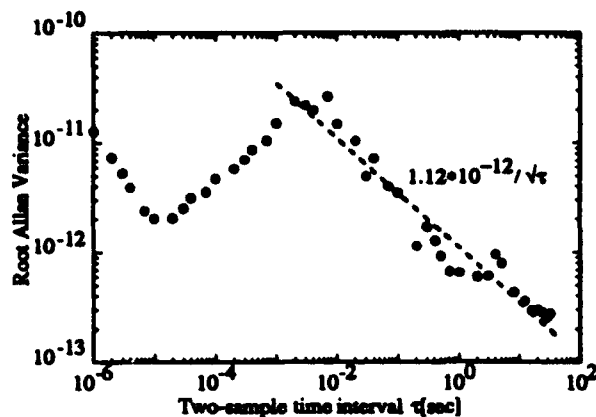


Fig. 2: The root Allan variance of the beatnote between 2 lasers locked to a₁ line of R(56)32-0. Number of samples=100, optical frequency=281.63 THz.

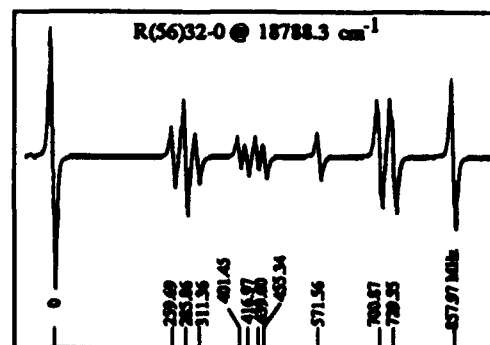


Fig. 3: FM saturated absorption spectrum of the R(56)32-0 transitions. The lines at 285.86, 700.87 and 729.55 MHz each contain 2 unresolved hyperfine transitions.

References

1. S. V. Kruzhlov, V. A. Parfenov, L.N. Pakhomov and V. Yu Petrun'kin, *Sov. Tech. Phys. Lett.* **11**, 111 (1985); P. Esherick and A. Owyong, *J. Opt. Soc. Am. B* **4**, 41 (1987)
2. A. Arie, S. Schiller, E.K. Gustafson and R.L. Byer, *Optics Letters* **17**, 1204 (1992).
3. S. Gerstenkorn and P. Luc, Atlas Du Spectre D'Absorption de la Molecule D'Iode, (Editions du CNRS, Paris, 1978).
4. S. Gerstenkorn and P. Luc, *J. Physique* **46** 867 (1985).
5. H.J. Foth and F. Spieweck, *Chemical Physics Letters* **65**, 347 (1979).
6. M. Glaser, *Optics Communication* **54**, 333 (1985).

Stark quantum-beat spectroscopy: The electric dipole moment of NO ($A^2\Sigma^+$)

J. A. Gray, R. L. Farrow, J. L. Durant, Jr. and L. R. Thorne
Department 8354
Combustion Research Facility
Sandia National Laboratories
Livermore, California 94551-0969
(510) 294-3676

The γ -system ($A^2\Sigma^+ \leftrightarrow X^2\Pi$) of nitric oxide (NO) is observed in many environments including combustion and atmospheric applications. Molecular properties of the $A^2\Sigma^+$ state are thus important in collision theories used to predict A-X radiative efficiencies. These theories often involve electric-multipole expansions,^{1,2} in which the permanent electric dipole moment of $A^2\Sigma^+$ (μ_A) is the leading term for long-range interactions. Moreover, μ_A is a basic property of the molecular charge distribution and has often been used to gauge the accuracy of *ab initio* quantum chemistry calculations.³⁻⁶ Here we describe measurements of Stark quantum beats in the fluorescence of NO from which we derive a precise value for μ_A in $v'=0$. This is the vibrational level most often excited in laser-based methods for detecting NO. Bergeman and Zare,⁷ using a radio frequency-optical double-resonance technique, provide the only other measurement of μ_A in a different vibrational level ($v'=3$). We thus also determine the change in μ_A with v' , which provides a sensitive test of computed dipole moment functions.

The fine and hyperfine structure of the $A^2\Sigma^+$ state add considerable complexity to the Stark effect in NO, requiring the use of narrow-bandwidth lasers to provide selective excitation. Molecular quantum-beat spectroscopy makes it possible to obtain extremely high resolution using nanosecond-pulsed laser sources

that are tunable at deep UV wavelengths. We obtain linewidths of ~ 2 MHz in the present Stark quantum-beat (SQB) studies using a laser whose Fourier-transform limited bandwidth is ~ 120 MHz, even though the Doppler width for the NO A-X system is ~ 3000 MHz at 300 K. To derive the dipole moment from SQB spectra, we formulate a Hamiltonian to predict the energies of six degenerate pairs of M_F hyperfine sub-levels in electric fields up to 22.5 kV/cm.

SQB measurements were conducted between polished stainless-steel plate electrodes mounted in a 3-inch diameter Pyrex cell. NO was flowed slowly through the cell at pressures of < 6 mTorr maintained by a mechanical pump. Three pairs of Helmholtz coils were mounted around the cell to reduce stray magnetic fields in the test region to < 30 mGauss. An argon-ion pumped cw dye laser operating near 574 nm was pulse amplified by the frequency-doubled output of an injection-seeded Q-switched Nd:YAG laser. The pulsed dye output was frequency doubled and sum-frequency mixed with the residual output of the Nd:YAG fundamental to produce 1 mJ, 8-ns pulses having a bandwidth of < 120 MHz near 226 nm. The probe laser was tuned to $44\,197.83\text{ cm}^{-1}$ to excite the $Q_1(1)$ transition in the (0,0) band, attenuated to an energy less than 10 μJ , and directed through the Stark plates with the laser polarization oriented perpendicular to the Stark field. LIF was collected along the direction of laser polarization by a PMT, and a digitizing oscilloscope averaged the decay profile for 2000 laser pulses at each electric-field setting. Figure 1 shows the weak beat modulation typically observed in these experiments.

The data was analyzed by subtracting an exponential decay waveform and taking the Fourier transform to obtain SQB spectra. The observed line widths, 2 MHz FWHM, correspond entirely to the natural lifetime of $\tau=215$ ns. The optical selection rules ($\Delta M_F=\pm 1$) cause excitation of $\Delta M_F=2$ quantum beats. Using estimates of the Stark energies,⁷ we assigned nearly all of the observed features to 8 of the 9 allowed transitions between the 6 degenerate pairs of M_F hyperfine sub-levels in

$N'=1, J'=3/2$. The intensities of resolved features in the SQB spectra varied smoothly with the electric field, aiding in assignment of the transitions. A total of 178 beat frequencies were measured at various field strengths and are shown in figure 2.

The Stark effect of a $^2\Sigma^+$ state with hyperfine structure has been described by Bergeman and Zare.⁷ We use their formulae to generate matrix elements between the $27 |M_F|$ states for $N'=0, 1, \text{ and } 2$ in a $|N J F M_F\rangle$ basis. We consider only the lowest rotational levels because of the congestion in SQB spectra at higher N . The observed and predicted beat frequencies are then input to a non-linear least-squares fitting routine. Magnetic and quadrupole hyperfine coupling constants are determined primarily from the zero-field beat frequencies. Final values for the dipole moment μ_A and the hyperfine constants in the $A^2\Sigma^+ v'=0$ state will be presented.

References

1. J. A. Gray, P. H. Paul and J. L. Durant, *Chem. Phys. Lett.* **190**, 266 (1992).
2. J. W. Thoman, J. A. Gray, J. L. Durant and P. H. Paul, *J. Chem. Phys.*, to be published.
3. S. Green, *Chem. Phys. Lett.* **13**, 552 (1972).
4. S. Green, *Chem. Phys. Lett.* **23**, 115 (1973).
5. S. P. Walch and W. A. Goddard, *Chem. Phys. Lett.* **33**, 18 (1975).
6. S. R. Langhoff, J. Bauschlicher C. W. and H. Partridge, *J. Chem. Phys.* **89**, 4909 (1988).
7. T. Bergeman and R. N. Zare, *J. Chem. Phys.* **61**, 4500 (1974).

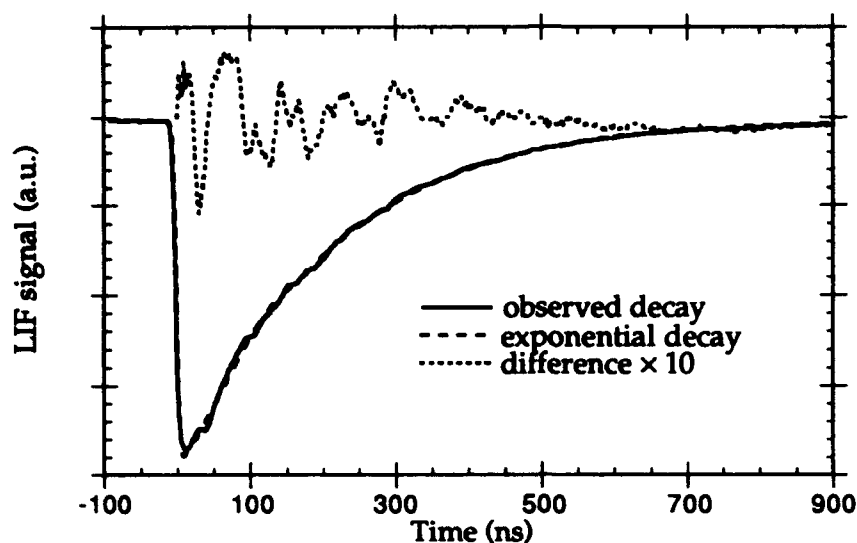


Fig. 1: Fluorescence quantum beats excited via the A-X (0,0) $Q_1(1)$ transition of NO at $44\,197.83\text{ cm}^{-1}$ in an electric field of 4.5 kV/cm . The exponential decay in the temporal waveform is removed before Fourier analysis.

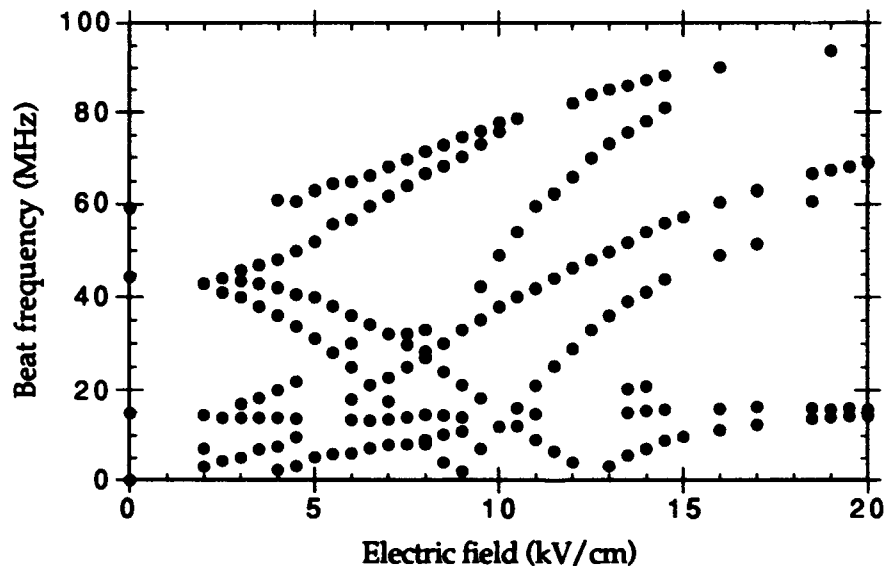


Fig. 2: Stark quantum-beat frequencies as a function of electric field. Zero-field frequencies result from ^{14}N hyperfine splitting in $N'=1, J'=3/2$. Eight $\Delta M_F=2$ transitions are observed over a range of field strengths and are analyzed to yield the electric dipole moment in the NO $A^2\Sigma^+ v'=0$ state.

Wednesday, January 20, 1993

Condensed Phase Spectroscopy

WA 8:00am–11:45am
Salon D

Janice Reutt-Robey, *President*
University of Maryland

DYNAMICS IN GLASSES AND LIQUIDS: OPTICAL NON-LINEAR LINE NARROWING EXPERIMENTS

Michael D. Fayer

Department of Chemistry, Stanford University, Stanford, CA 94305

Molecules in condensed phase systems are coupled to their environments through intermolecular interactions. These interactions influence the internal electronic and vibrational states of molecules. At any finite temperature, solvent molecules are in constant motion, even in a low temperature glass. Since intermolecular interactions are distance and orientation dependent, the motions of the solvent make the intermolecular interactions with solute molecules inherently time dependent. These time dependent interactions result in fluctuations in the solute's electronic and vibrational energy levels. Energy fluctuations are responsible for processes such as thermal activation of a chemical reaction.

The time dependent intermolecular interactions can be examined using optical dephasing experiments. Information can be obtained about the fluctuations of the solute's energy levels as well as about the nature of the solvents dynamics and the solute-solvent coupling mechanism. In principle, optical dephasing information can be obtained by measuring the spectroscopic line shape. However, in practice most systems are inhomogeneously broadened. Therefore, it is necessary to perform optical line narrowing experiments.

Complex condensed matter systems, such as glasses, liquids, proteins, and complex crystals, undergo dynamical processes which have a very broad distribution of rates. In glasses at low temperatures, dynamics can occur on time scales spanning picoseconds to kiloseconds. Recent theoretical and experimental advances show how to extract the distribution of dynamical rates by using a variety of nonlinear optical line narrowing experiments. Photon echo, stimulated photon echo, and nonphotochemical hole burning measurements have been made on dye molecules in organic glasses at very low temperatures. In systems such as cresyl violet in ethanol glass, below ~ 5 K, line broadening is dominated by the dynamics of the glass's two level systems (TLS). Homogeneous line widths as narrow as 100 MHz are observed. The temperature dependence is approximately linear in T , characteristic of TLS dynamics. At higher temperatures, the dynamics becomes exponentially activated.

It is observed that the photon echo experiments yield considerably narrower line widths than hole burning experiments on the same sample. The broadening of hole widths beyond the photon echo results is a measure of the slow spectral diffusion processes in a glass. The four time correlation functions for photon echo and hole burning experiments are different. In fact, the hole burning experiment is the frequency domain analog of the stimulated echo experiment, and

therefore it is sensitive to slow dynamics occurring out to the characteristic time scale associated with the hole burning experiment. Hole widths in the cresyl violet/ethanol glass system are observed to broaden with time. Measurements were made from 10 μ sec to 10,000 seconds. Using this data, the fluctuation rate distribution was determined.

In the experiments discussed above, electronic transitions of organic molecules were examined. We have recently performed the first infrared psec vibrational photon echo experiments in condensed matter systems. This extends the methods developed for electronic transitions to vibrational states of molecules. Therefore, it is now possible to examine the vibrational dephasing caused by the coupling of solvent dynamics to the vibrational states of a molecule.

In the experiments, we examined the CO stretch of $W(CO)_6$ in 2-meTHF glass and liquid. The vibrational transition is at 5.1 μ m (1960 cm^{-1}). The experiments were conducted with psec pulses produced by the Stanford super conducting linac pumped Free Electron Laser (FEL). The FEL provides a high rep rate source of tunable IR psec pulses. These experiments are the first IR non-linear experiments conducted with an FEL, although we have previously performed photon echoes in the visible with the Stanford FEL.

The vibrational dephasing was measured from 16 K through the glass transition temperature (90 K) to 140 K. The homogeneous line widths are remarkably narrow, even in the super cooled liquid. Pump-probe experiments were also performed to measure the vibrational lifetime. These are the first such measurements to follow a vibrational lifetime from the room temperature liquid through the glass transition temperature, and below. The data is remarkable in that the life time becomes shorter as the temperature is lowered from room temperature. The minimum life time is observed at the temperature where the liquid becomes super cooled. As the temperature is further lowered, the lifetime gradually lengthens.

Reference Publications

1. "Probing Organic Glasses at Low Temperatures with Variable Time Scale Optical Dephasing Measurements", L.R. Narasimhan, K.A. Littau, D.W. Pack, Y.S. Bai, A. Elschner, and M.D. Fayer, Chem. Rev. 90 439 (1990).
2. "Probing Low Temperature Glass Dynamics by Fast Generation and Detection of Optical Holes", K.A. Littau and M.D. Fayer, Chem. Phys. Lett. 176 551 (1991).
3. "Applications of Infrared Free-Electron Lasers: Basic Research on the Dynamics of Molecular Systems," D. D. Klott and M. D. Fayer, J. of Quant. Elec., 27, 2697 (1991).
4. "Optical Dephasing of a Near Infrared Dye in PMMA: Photon Echoes Using the Superconducting Accelerator Pumped Free Electron Laser," S. R. Greenfield, Y. S. Bai, and M. D. Fayer, Chem. Phys. Lett., 170, 133 (1990).

Applications of High Resolution Coherent Raman Spectroscopy

Joseph W. Nibler
 Department of Chemistry
 Oregon State University
 Corvallis, OR 97331
 (503) 737-6715

In recent years, the development of improved laser sources of high power and narrow linewidth has led to significant advances in high resolution Coherent Raman spectroscopies such as CARS (Coherent Anti-Stokes Raman Spectroscopy) and SRS (Stimulated Raman Gain/Loss Spectroscopy). The apparatus at Oregon State University is representative of current capabilities and consists of a cw ring dye laser whose output is increased in a three-stage dye amplifier pumped by the 532 nm output of a seeded, single frequency Nd:YAG pulsed laser. The resolution is thus limited by the Fourier transform of the amplifying pulse which is 5-10 ns for most commercial Nd:YAG lasers. Very recently, we have extended this using a custom long-pulse Nd:YAG laser of 30-50 ns 532 nm pulse duration.¹

Figure 1 illustrates the performance of this laser in a Doppler-free polarization spectrum taken of the hyperfine structure for the R(86) 33-0 line of I₂. This spectrum was recorded by temperature scanning a diode-pumped cw Nd:YAG laser used to seed the pulsed system. The observed hyperfine widths of 16 MHz are in good agreement with the 10 MHz predicted for the 45 ns experimental pulsewidth plus 6 MHz produced by the dithering mechanism used to hold the pulsed laser cavity length constant.

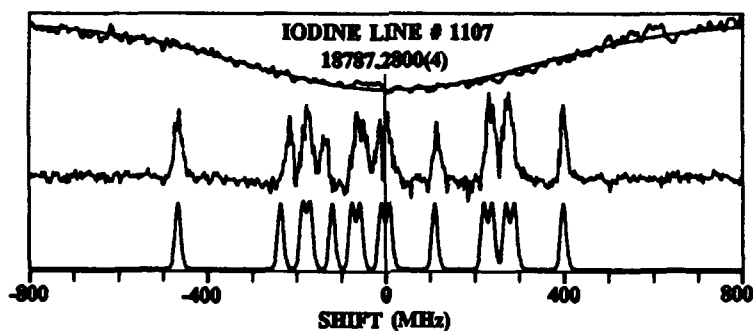


Figure 1 Doppler free polarization spectrum of iodine R(86) 33-0 line (middle trace). Calculated spectrum is shown below, Doppler broadened spectrum above.

For high resolution CARS applications, the Nd:YAG 532 nm beam serves as one of the sources driving the molecular resonance and it is necessary to hold the Nd:YAG frequency constant. We have found that this can be done to ± 8 MHz by simply locking to the side of a Doppler broadened line such as that

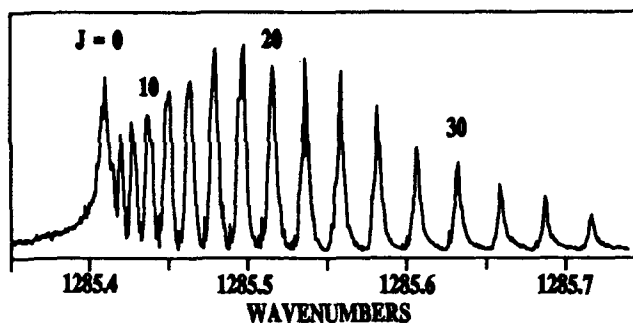


Figure 2 CARS spectrum of the $2\nu_2$ Q-branch of CO_2 at 2 Torr and 298K.

shown at the top of Fig. 1. Figure 2 demonstrates the resolution achieved in a CARS spectrum of the $2\nu_2$ Q-branch of CO_2 at 2 Torr. By deconvolving Doppler and collisional widths, we obtain a value of 45 MHz for the effective instrumental resolution of the combined 532 nm and Stokes beams, slightly more than a value of 33 MHz predicted from the measured pulse durations.

High resolution coherent Raman spectroscopy finds its most natural use in the study of low density gases although, as shown later, it is also valuable in examining low temperature solids and liquids where the linewidths can often be quite narrow. Because the interaction period is short, studies of reactive transient species such as CH_3 , formed by photolysis of CH_3I , are also feasible.³ High resolution is especially useful in molecular beam studies, where Doppler widths are greatly narrowed due to the low translational temperatures. As an example, Fig. 3 shows the rich CARS Q-branch structure observed for the ν_3 CC stretch of ethane in a static cell (a. 34 Torr, 298K) along with the narrowing and simplification that occurs in expansions (b. neat jet, $\sim 60\text{K}$), (c. 50% C_2H_6 in He jet, $\sim 50\text{K}$).

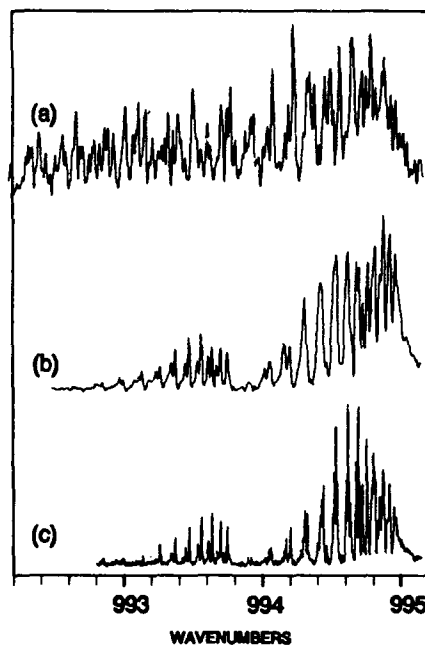


Figure 3 CARS Q-branch spectra of C_2H_6 in the ν_3 region.

A complex mixture of four band systems is seen, a consequence of Fermi resonance interactions causing the predicted four torsional sublevels of this state to separate as depicted in Fig. 4. CARS spectra of jet-cooled samples proved crucial in the assignment of the spectrum and the four torsional components of this transition were determined as 994.973 (E_{3s}), 994.878 (E_{3d}), 994.864 (A_{1s}) and 993.791 cm^{-1} (A_{3d}). The rotational analysis of this band and also of the pure rotational transitions from 0 to 100 cm^{-1} lead to A and B rotational constants for several states and these have been combined with *ab initio* calculations to characterize the structural changes that occur on excitation of the torsional mode or the CC stretch.² The results suggest that the V_3 torsional barrier for the $\nu_3 = 1$ state is about 3% smaller than for the ground state.

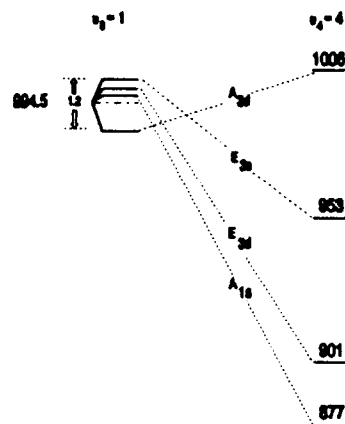


Figure 4 Energy levels and primary Fermi resonance interaction in the ν_3 region of C_2H_6 .

At high driving pressures, aggregation occurs quite readily in jet expansions, producing clusters ranging in size from dimers to small microunits of liquid or solid phases. We have

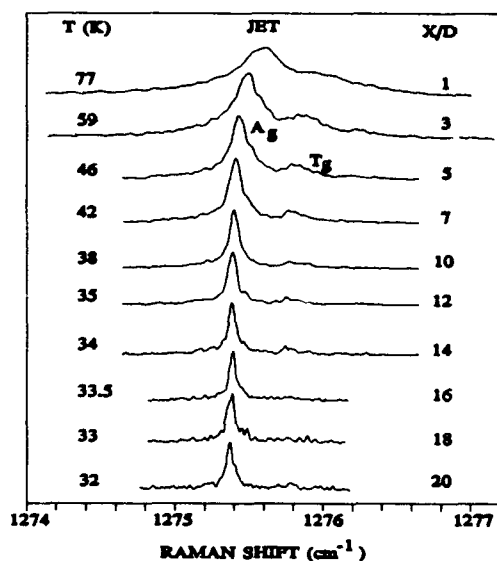


Figure 5 CARS $2\nu_2$ spectra of large CO_2 jet clusters.

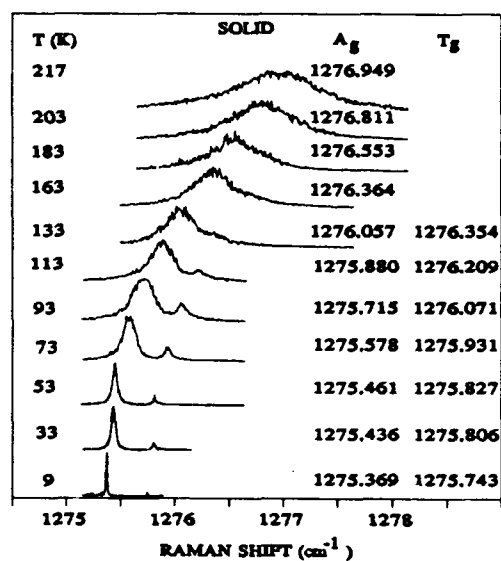


Figure 6 CARS $2\nu_2$ spectra for solid bulk CO_2 .

used high resolution CARS to examine this range for CO₂ clusters and show in Fig. 5 the 2ν₂ spectra of large aggregates. The large cluster peak at 1276 cm⁻¹ is seen to shift and sharpen significantly as cooling occurs along the expansion coordinate X/D. The trend mirrors the changes that we have measured precisely at high resolution for bulk solid in a variable temperature cryostat (Fig. 6) and the latter ν vs T bulk relation is the basis for the internal cluster temperatures displayed with the jet spectra. From models of the cooling rates in the expansion, the mean cluster size is estimated to be larger than 30 nm (>300,000 units) so the assumption of bulk behavior is justified. It is noteworthy that both A_g and T_g unit cell coupling components of the cubic solid are seen in the cluster spectra also, a clear indication that the aggregates are **crystalline** and not amorphous glasses. The sharp linewidths are also consistent with this and further suggest that the cluster size and temperature distributions are relatively narrow in the expansion.

At intermediate driving pressures of 5 to 25 atm., new spectral features appear between the solid and monomer extremes and these show structure which changes as the mean size of the clusters is altered. These features are **not seen** in bulk samples and we believe these intermediate features arise from vibrational modes of **surface layers** of CO₂, an idea suggested in recent infrared work⁴ and in calculations on CO₂ clusters⁵. The intensity of the surface bands, compared to that of the residual "core" feature near 1276 cm⁻¹, permits a rough estimate of mean cluster diameters of 3.5 nm (4000 units) and 0.9 nm (60 units) at driving pressures of 28 and 14 atmospheres. At still lower pressures, clusters with only surface modes are seen, corresponding to aggregates of about 10 units. Further manipulations of the expansion conditions to give even smaller clusters and, ultimately, mainly monomer with some dimer will be described.

1. J. A. Harrison, M. Zahedi and J. W. Nibler, "Use of Seeded Nd:YAG Lasers for High Resolution Spectroscopy", Optics Lett. In press.
2. A. Al-Kahtani, S. Montero and J. W. Nibler, "High Resolution Rotational and ν₃ Coherent Raman Spectra of C₂H₂", J. Chem. Phys. In press.
3. N. E. Triggs, M. Zahedi, J. W. Nibler, P. DeBarber, and J. Valentini, J. Chem. Phys. 96, 1822 (1992)
4. J.A. Barnes and T.E. Gough, J. Chem. Phys. 86, 6012(1987).
5. G.Cardini, V. Schettino, and M.L. Klein, J. Chem. Phys. 90, 4441(1989).

Time-Resolved Probes of Adsorbate-Substrate Energy Transfer

T.A. Germer, J.C. Stephenson, E.J. Heilweil, and R.R. Cavanagh
National Institute of Standards and Technology
Gaithersburg, Md 20899
(301) 975-2368

INTRODUCTION

Recent advances in time-resolved measurement techniques have provided new molecular level insights into energy transfer processes. Through pump-probe measurements of excited state recovery, direct measurements of lifetimes and energy transfer pathways have been achieved. In vapor, liquid, and condensed phase studies, these techniques have provided the capability of following the evolution of molecular processes. Application of similar techniques to clarify the timescales and pathways for energy transfer processes at surfaces is only now beginning to meet with success.^{1,2}

In this paper, the use of ultrafast infrared probes pulses to characterize the transient response of CO/Pt(111) is reported. Two different types of pump pulses are employed: an infrared pulse resonant with the CO($\nu=0 \rightarrow 1$) transition; and a visible pump resonant only with substrate excitations. In the case of infrared pumped CO, low lying electronic excitations in the metal have been implicated to be the source of the short excited state lifetime, while in the experiments where the pump pulse is coupled to substrate electronic states, it is shown that the transfer of energy from the substrate to the adsorbate can be accounted for by either a phonon or electron/hole pair model. By determining the time scale for transfer of energy between adsorbate degrees of freedom and the electronic levels of the substrate, the relative importance of these channels in maintaining equilibrium conditions can be ascertained.

EXPERIMENTAL

The laser system has previously been described.³ Briefly, the chirped and compressed output of a cw mode-locked Nd:YAG laser is frequency doubled and used to pump two tunable dye lasers. The second harmonic of a 20 Hz Nd:YAG regenerative amplifier is used to further amplify the dye laser pulses. Infrared pulses near 2106 cm^{-1} are generated through difference frequency mixing in LiIO_3 . For experiments where the infrared pulse is used both as pump and probe, a 5% reflection from a beam splitter serves as the probe. In experiments utilizing visible excitation, the residual amplified dye laser pulse at 660 nm is separated from the IR beam emerging from the LiIO_3 crystal and used as the pump beam. In all experiments the 1.0 ps duration pump and probe beams are incident at 87° from the platinum surface normal. The pump is p-polarized and the polarization of the probe is rotated approximately 45° out of the plane of incidence. The relative arrival times of the pump and probe pulse can be adjusted by a computer controlled delay stage.

The pump and probe beams are overlapped in time and space on a Pt(111) crystal mounted in an ultrahigh vacuum chamber ($\leq 10^{-8}$ Pa). The cleanliness of the substrate is routinely checked with Auger electron spectroscopy, and the homogeneity of the CO adlayer is assessed with Fourier Transform Infrared Spectroscopy. For the experiments in this paper, the CO coverage is 0.5 ML and the sample temperature is maintained at 150 K.

After emerging from the vacuum chamber, the reflected probe beam is propagated through an infrared monochromator with 1 cm^{-1} FWHM resolution. The monochromatized light is split into two beams which are measured by InSb photodiodes after passing through wire grid polarizers. The two polarizers are oriented such that one InSb detector samples p-polarized light, and the other samples s-polarized light. The ratio of these two detectors provides a shot-by-shot normalization of the sample response to the energy per unit band width. The transient response of the surface is then determined by comparing signals in the presence and absence of a pump beam. Transient difference spectra ($-\Delta\alpha$) are then obtained as $\ln(I_p/I_s)_{\text{pump}} - \ln(I_p/I_s)_{\text{no pump}}$. By varying the wavelength of the infrared monochromator, the spectral response at a fixed pump-probe time delay can be recorded over the spectral bandwidth of the IR probe. Alternatively, the temporal response at a fixed spectral position is characterized by varying the position of the delay stage.

RESULTS AND DISCUSSION

When IR pump pulses are used to excite the CO adlayer, the $\text{CO}(v=0 \rightarrow 1)$ transition is observed to broaden and shift to lower frequency. The magnitude of this shift decreases as the pump energy is reduced or as the arrival time of the probe is increased. Figure 1 displays characteristic transient spectra as a function of pump energy. Such transient behavior can be described using a model of strongly coupled anharmonic oscillators.⁴ Using this model of the spectral response, it has been possible to fit the temporal behavior of the transients to a single exponential decay model to extract the $\text{CO}(v=1)$ vibrational excited state lifetime, T_1 . The results indicate $T_1 = 2.2 \pm 0.2 \text{ ps}$.

A lifetime as short as 2.2 ps can only be attributed to a resonant decay process, in this case, the generation of electron-hole pairs. The $\text{CO}/\text{Pt}(111)$ lifetime is significantly shorter than the times found for CO stretch modes of metal carbonyls in the gas phase,⁵ in solution,⁶ or attached to SiO_2 supports.⁷ For those systems, the $\text{CO}(v=1)$ excited state lifetimes ranged from 100 to 1000 ps, and have been interpreted in terms of multiphonon relaxation processes. Comparison to the lifetime of the 2050 cm^{-1} Si-H($v=1$) mode on Si(111) is also of interest.⁸ The frequency of the Si-H stretch lies within the electronic gap of Si ($E_{\text{gap}} = 1.1 \text{ eV}$), so substrate mediated electronic resonance channels are not anticipated. The relatively long lifetime of several hundred picoseconds observed in the H/Si(111) system was interpreted with a multiphonon decay model.⁹ The dominance of 100-1000 ps decay times in the multiphonon relaxation mechanisms suggests that a resonant decay process is responsible for the $\text{CO}/\text{Pt}(111)$ result. Indirect support for this model can be found in two other CO adsorbate systems, $\text{CO}/\text{Cu}(100)$ ¹⁰ and $\text{CO}/\text{Pt}/\text{SiO}_2$.¹¹ In both

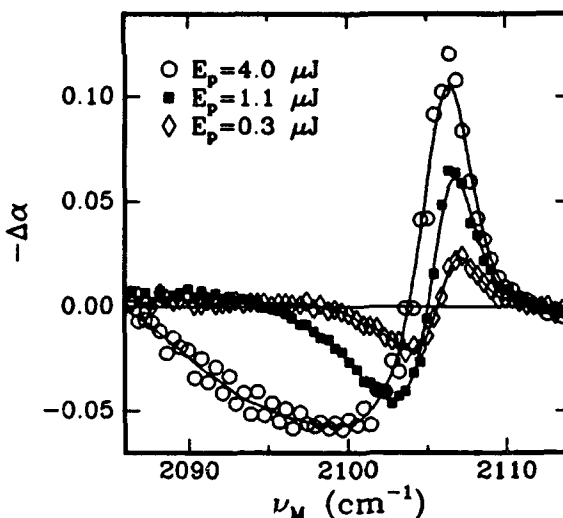


Figure 1 Transient difference spectra at $t_d = 0$ ps for different IR pump energies. Data is fit to a spline (data from Ref. 3).

of those systems, CO vibrational relaxation times of less than 10 ps have also been reported and attributed to relaxation mediated by electronic excitations near the Fermi level of the substrate.¹² In the absence of direct spectroscopic signals that can be attributed to newly born electron/hole pairs, the most compelling support for the role of these substrate electronic excitations comes from theoretical models of the relaxation process. While simple models have suggested the importance of electron/hole pair damping for these systems well over ten years ago,¹³ more recent efforts have attempted to model these effects in terms of nonadiabatic coupling of the normally unoccupied $2\pi^*$ CO levels.¹⁴

When using visible pulses to excite the system, a number of new excitation channels need to be considered. Based on other spectroscopies, there do not appear to be any adsorbed CO states with transitions near the 660 nm (1.9 eV) pump. Consequently, consideration will be restricted to the fate of the initially excited platinum electrons and their ability to couple to the adsorbed CO. Figure 2 shows the transient IR reflectivity of the CO/Pt(111) sample a long (6.7 ps) time after the arrival of a 660 nm pump pulse. Two aspects of this transient spectrum are significant: the baseline reflectivity has uniformly been reduced across the spectral width of the probe; and there is a pronounced shift in the CO($\nu=0\rightarrow 1$) absorption, evidenced in the derivative shape of $-\Delta\alpha$. Both of these features are consistent with laser heating of the system, the flat spectral shift is attributed to the temperature dependent reflectivity of Pt, while the sharp feature arises from the temperature dependence of the CO-stretch transition.¹⁵ In this case, the CO frequency shift is associated with activation of the 60 cm^{-1} frustrated translational mode, and does not reflect the presence of population in the CO($\nu=1$) level. Based on the thermal and optical properties of platinum, it is to be expected that the lattice and the electronic degrees of freedom should be described by a common temperature jump of approximately 45 K at the time delay of Fig. 2. At shorter time delays, when the electronic and lattice temperatures are distinct, it is important to distinguish whether coupling to the phonon or electron bath is responsible for the CO shift. Under the conditions of Fig. 2 the peak electronic and lattice temperatures are calculated¹⁶ to be 120 and 50 K, respectively.

Transient spectra recorded as a function of time delay have been analyzed using a density matrix treatment of the pump-induced CO($\nu=0\rightarrow 1$) frequency shift with a three temperature (T_{elec} , T_{lat} , and $T_{\text{f-trans}}$) model for the heating of the CO/Pt adlayer. The model correctly accounts for the perturbation of the probe's free induction decay signal induced by the transient change in the CO($\nu=0\rightarrow 1$) frequency. The results indicate that the time evolution of the 60 cm^{-1} frustrated translation temperature closely resembles that of the

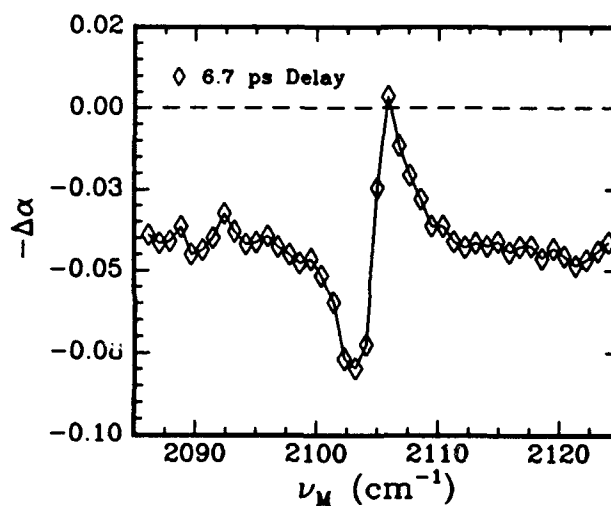


Figure 2 Transient difference spectra of CO/Pt(111) after 1 ps pump pulse at 660 nm. Solid line provided as a guide.

near-surface Pt lattice. This implies that either the 60 cm^{-1} frustrated translation is coupled to the hot electrons with a coupling time indistinguishable from that of the Pt lattice (1.5 ps), or that the frustrated translation is coupled to the lattice with a time constant of less than 1 ps. The comparable coupling times for phonon or electron mediated activation of the CO adlayer can be put into perspective by comparison to the electronic coupling responsible for damping the CO stretch mode ($T_1 = 2.2\text{ ps}$). It is evident that comparable coupling strengths are involved for damping of high lying adsorbate vibrations and for activation of the low lying adsorbate vibrations by substrate excitations.

CONCLUSION

These applications of time-resolved techniques to the transfer of energy between substrates and adsorbates are providing quantitative estimates of the coupling times between electronic excitation and nuclear motion. The ability to follow energy transfer processes at the molecular level is expected to provide new insights into chemical processes that occur at solid surfaces.

REFERENCES

1. R.R. Cavanagh, D.S. King, J.C. Stephenson, and T.F. Heinz, *J. Phys. Chem.* (in press).
2. J.D. Beckerle, M.P. Casassa, R.R. Cavanagh, E.J. Heilweil, and J.C. Stephenson, *J. C., Phys. Rev. Lett.* **64**, 2090 (1990).
3. J.D. Beckerle, R.R. Cavanagh, M.P. Casassa, E.J. Heilweil, and J.C. Stephenson, *J. Chem. Phys.* **95**, 5403 (1991).
4. J.C. Kimball, C.Y. Fong and Y.R. Shen, *Phys. Rev. B* **23**, 4946 (1981).
5. S.A. Angel, P.A. Hansen, E.J. Heilweil, and J.C. Stephenson, "Ultrafast Phenomena VII" **53**, 480 (1990).
6. E.J. Heilweil, R.R. Cavanagh, and J.C. Stephenson, *J. Chem. Phys.* **89**, 230 (1988).
7. E.J. Heilweil, R.R. Cavanagh, and J.C. Stephenson, *J. Chem. Phys.* **89**, 5342 (1988).
8. P. Guyot-Sionnest, P. Dumas, Y.J. Chabal, and G.S. Higashi, *Phys. Rev. Lett.* **64**, 2156 (1990).
9. P. Dumas, Y.J. Chabal, and G.S. Higashi, *Phys. Rev. Lett.* **65**, 1124 (1990).
10. M. Morin, N.J. Levinos and A.L. Harris, *J. Chem. Phys.* **96**, 3950 (1992); **96**, 6203 (1992).
11. J.D. Beckerle, M.P. Casassa, R.R. Cavanagh, E.J. Heilweil, and J.C. Stephenson, *J. Chem. Phys.* **90**, 4619 (1989).
12. E. Blaisten-Barojas and J.W. Gadzuk, *J. Chem. Phys.* **97**, 862 (1992); J.W. Gadzuk, *Appl. Phys. A* **51**, 108 (1990).
13. B.N.J. Persson and M. Persson, *Solid State Commun.* **36**, 175 (1980); A.G. Eguiluz, *Phys. Rev. B* **30**, 4366 (1984).
14. M. Head-Gordon and J.C. Tully, *J. Chem. Phys.* **96**, 3939 (1992); J.C. Tully, M. Gomez, and M. Head Gordon, *J. Vac. Sci. and Tech.* (in press).
15. E. Schweizer, B.N.J. Persson, M. Tüshaus, D. Hoge and A.M. Bradshaw, *Surf. Sci.* **213**, 49 (1989).
16. S.I. Anisimov, B.L. Kapeliovich, and T.L. Perel'man, *Zh. Eksp. Teor. Fiz.* **66**, 776 (1974); [*Sov. Phys. JETP* **39** 375 (1974)].

OPTIMIZATION of RAMAN SIGNAL ENHANCEMENT in KRETSCHMANN CONFIGURATION

N. Primeau , J.L. Coutaz and L. Abello*
LEMO-ENSERG, BP 257, 38016 Grenoble Cedex, France
* LIES-ENSEEG, BP 75, 38402 St Martin d'Hères, France

1. INTRODUCTION

Several experimental and theoretical studies [1,2,3] of Surface Plasmons Enhanced Raman Scattering (SPERS) in Kretschmann geometry (prism-metal-dielectric stacks) have demonstrated that it is possible to use surface plasmons (SP) to enhance Raman scattering from molecules adsorbed on a metal film. The enhancement process originates from two contributions: First, excitation of SP at pump frequency (ω_i) and second, excitation of SP at Stokes frequency (ω_s). To get the strongest Raman signal, scattered light must be detected on the prism side [3]. Indeed, the collected light comes from the outcoupling of SP at the Stokes frequency. In an experiment of SPERS, the Raman intensity depends on the distance of the active molecules to the metal surface [2]. Moreover, it has been suggested [3] that the thickness of the metal film deposited onto the prism should also be taken into account if one wants to *improve the limit of detection*.

The aim of this work is to study the dependence of Raman scattering from a thin coating layer on the thickness of the metal film in a Kretschmann configuration. This was done in order to optimize the Raman efficiency. Surprisingly, to the best of our knowledge, the Raman intensity dependence on the metal thickness *has not been reported yet* when dealing with delocalised SP. To perform this experiment, a silver film of thickness varying from 200Å to 700Å was evaporated onto a prism and was then covered by a thin copper phthalocyanine (CuPc) film. CuPc was selected as a test material because it is easy to deposit and it has a well-known Raman spectrum [4,5].

2. THEORY

The theoretical analysis is based on the matrix method first developed by Abelès [6] and used by Kurosawa *et al.* [7]. We consider an electromagnetic plane wave incident upon a n-layered structure bounded on each side by a homogeneous, semi-infinite medium. The expressions for the reflectivity R and the transmittivity T of the energy at the pump and Stokes frequencies are obtained by solving Maxwell's equations and matching the boundary conditions for a p-polarized wave. Our device (fig.1) is composed of a prism (medium 4 with dielectric constant ϵ_4), a thin silver film (medium 3, $\epsilon_3 = \epsilon_3' + i\epsilon_3''$ and variable thickness d_3) and a thin CuPc layer (medium 2, $\epsilon_2 = \epsilon_2' + i\epsilon_2''$ and d_2). Finally, air is considered as medium 1 (ϵ_1). For eight thickness regions of the Ag film, the reflectivity is measured in an Attenuated Total Reflection (ATR) experiment as a function of the angle of incidence. The numerical fitting of the reflectivity gives us the dielectric constants at both ω_i and ω_s and the thicknesses of the Ag regions and CuPc film.

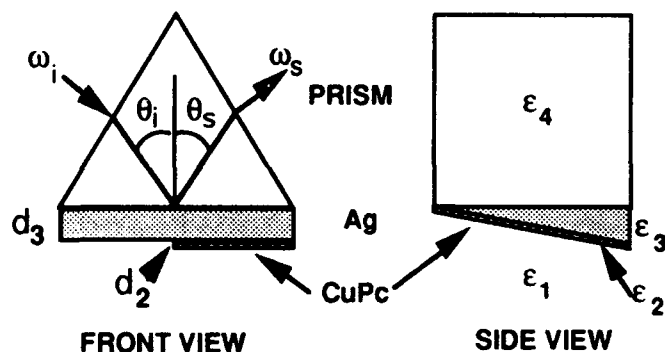


Fig.1 Kretschmann geometry used in this experiment with a Ag film of varying thickness (d_3) partly coated with a thin film of CuPc (d_2).

It has been shown by Kurosawa *et al.* [7] that the Raman intensity can be expressed as

$$I(\theta_i, \theta_s) = A T(\theta_i, \omega_i) T(\theta_s, \omega_s) \quad (1)$$

where A is a constant proportional to the intensity of the incident laser beam and to the scattering cross-section of the CuPc molecules, and T is the transmittivity at the interface. Hence, using the permittivity and thickness values we have measured, we calculate $T(\theta_i, \omega_i)$ and $T(\theta_s, \omega_s)$ at the interface between the Ag film and the CuPc layer for every Ag thickness region and then, we determine the Raman intensity I according to equation (1).

3. EXPERIMENT AND RESULTS

A silver film was evaporated on the prism (SF10 glass, $n = 1.7403$ for $\lambda = 5145 \text{ \AA}$) at 10^{-6} torr at a constant growth rate of about $30 \text{ \AA}/\text{sec}$ (monitored by a quartz oscillator gauge). In order to be able to characterize every thickness region by the same dielectric constant, the Ag film of varying thickness was deposited in one evaporation performed with a constant growth rate. Afterwards, a thin CuPc layer was evaporated onto both the silver coated prism and a bare glass slide.

Then, measurements of the ATR profile were performed for each region, using the 5145 \AA line of an argon laser (pump) and also a white lamp with a monochromator for the measurement at the Stokes wavelength (5585 \AA). The measured reflected light of the s-polarised beam is taken as the reference. Hence, in our calculation, the reflectivity is expressed as the ratio of the reflected light for a p-polarized beam and the reflected light for a s-polarized beam normalised by the s-polarized and p-polarized incident beams ratio.

At ω_i , for bare silver, the data fit gives us $\epsilon_3 = -10.18 + i0.435$ as the dielectric constant and the following thicknesses : 305 \AA , 350 \AA , 400 \AA , 440 \AA , 470 \AA , 490 \AA , 590 \AA , 650 \AA . For coated silver, we obtained $\epsilon_3 = -10.731 + i0.416$. Figure 2 shows the measured angular dependence of R and the calculated curves for three different Ag thicknesses. Notice that the difference in the dielectric constants that we obtained for the uncoated and the coated silver has already been observed and explained [9]. For the CuPc layer, we found $\epsilon_3 = 1.937 + i0.138 (\pm 0.002)$; which is in agreement with the value given in the literature [10]. The CuPc thickness was estimated at 31 \AA . At ω_s , we obtained for silver $\epsilon_3 = -12.3 + i0.56$ and for CuPc $\epsilon_2 = 0.95 + i0.22460 \text{ \AA}$. In figure 3, using the dielectric constants previously determined, we plot the thickness dependence of the reflectivity at the resonance angle for both ω_i and ω_s . We see that the Ag thickness corresponding to the maximum coupling of the light to the SP is different for the two frequencies. This was predictable since R is a function of ω . However, this effect is important here since the optical constants of CuPc change rapidly in the range of frequencies that we are interested in.

To perform the Raman scattering measurements, the light beam ($\lambda = 5145 \text{ \AA}$) is incident on the prism side at the resonance angle. A cylindrical lens ($f = 300 \text{ mm}$) focuses the light onto the Ag film. The outcoupled light at the Stokes frequency is collected with an achromatic lens ($f = 120 \text{ mm}$) and its polarisation is rotated since the spectrometer response is a factor of five greater for s-polarized light (the prism is taken as the reference). Then, using two mirrors, the light can be easily directed to the entrance slit of the spectrometer (Dilor multichannel XY equipped with a 1024 CCD array detector) and correctly processed.

The Raman signal is optimised by first adjusting the angle of incidence at ω_i and then by moving the two mirrors in order to fix the detection angle which must correspond to the SP emerging angle at ω_s . This optimization is performed for one thickness ($d_3 = 440 \text{ \AA}$) corresponding to the strongest Stokes intensity we could detect and then unchanged for the measurements at the other thicknesses. Such a procedure was chosen in order to limit the experimental errors. Thus, in our calculations (cf. eq. 1) of the Raman signal versus Ag thickness, the incidence and scattering angles are those corresponding to the experimental values ($d_3 = 440 \text{ \AA}$). In fig 4, we plot the measured Raman spectra obtained with an incident power beam of 50 mW and 2 mW . The spectra were obtained in 8 accumulations of an integration time of 10 seconds and for a slit width of 300 \mu m . For an incident power of 50 mW , we obtain all the lines that characterize CuPc, with some

variation in the lines intensity but no noticeable shift in the wavelengths. For an incident power of 2 mW, we still detect the strongest Raman lines. This result shows the high sensitivity of this SPERS experiment and confirms the fact that it can be used to detect very low quantity of matter. Indeed, we tried to measure the Raman spectra of the CuPc deposited directly on the glass slide using the same optics as for the SPERS experiment but we did not succeed. Therefore, on the basis of Raman spectra of CuPc we have previously measured elsewhere, we estimate the *enhancement factor* at more than 10^4 .

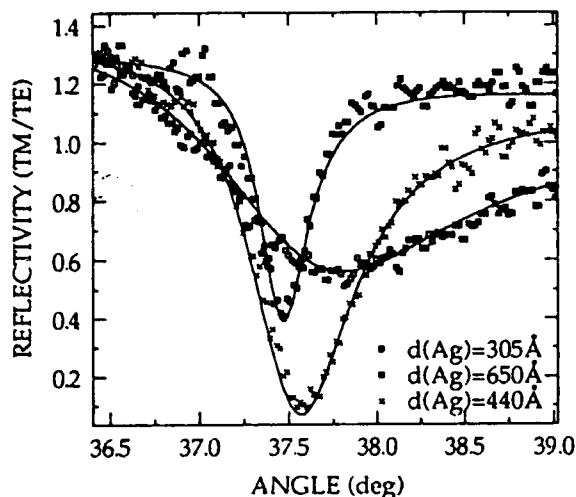


Fig. 2 Numerical fitting of ATR spectra versus the angle of incidence (θ_i) at 5145\AA , for three thicknesses of the Ag film coated with CuPc ($d_2=31\text{\AA}$). The solid curves show the data fits.

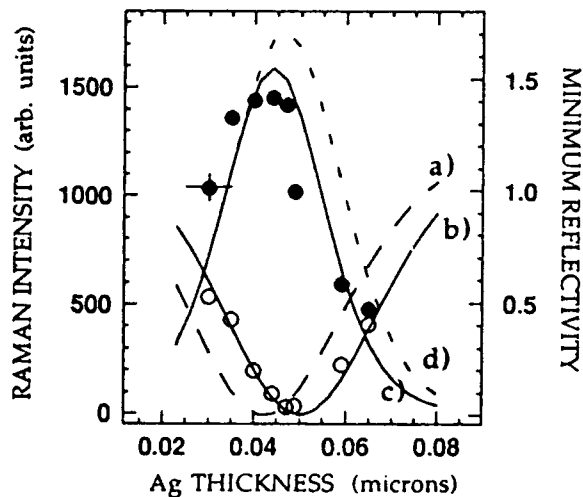


Fig.3 Maximum Raman intensity and reflectivity at the resonance angle versus the Ag thickness. Curves a) and b): numerical calculations of the minimum value in reflectivity at the resonance angle respectively at $\lambda=5585\text{\AA}$ and $\lambda=5145\text{\AA}$. Open circles: measured reflectivity at the resonance angle. Solid circles: maximum Raman intensity measured at fixed angles (resonance angles, θ_i and θ_s , for $d_3=440\text{\AA}$). Curves c) and d): calculations from eq. 1, respectively at fixed angles and at resonance angles ($\theta_{i,res}$ and $\theta_{s,res}$ for every Ag thickness).

Let us now consider the dependence of the Raman intensity on the metal thickness. Figure 3 shows the measured and calculated (eq. 1) intensity of the 1530 cm^{-1} line of CuPc for the different thicknesses of the Ag film. We see that the maximum Raman intensity occurs for a thickness of about 440\AA ($\pm 30\text{\AA}$) which lies in between the optimum coupling at ω_i and ω_s . As expected, the Raman intensity depends strongly on the metal film thickness. However, within a range of $\pm 40\text{\AA}$ around the optimum thickness of the Ag film, the change in the Raman intensity is very small.

We also calculate, using the dielectric constants we have determined previously, the dependence of the Raman intensity on the metal thickness when the signal is optimized at every Ag thickness; the result is shown on figure 3. In that case, we see that the maximum intensity occurs

for a thickness of the silver film of 470\AA . The optimised curve has almost the same shape as the measured one, but a shift of about 40\AA from the optimum thickness toward the larger thickness values. This can be explained by the narrowing of the dip in the reflectivity curve for thicknesses larger than the optimum one which makes more crucial the adjustment of the resonance angle.

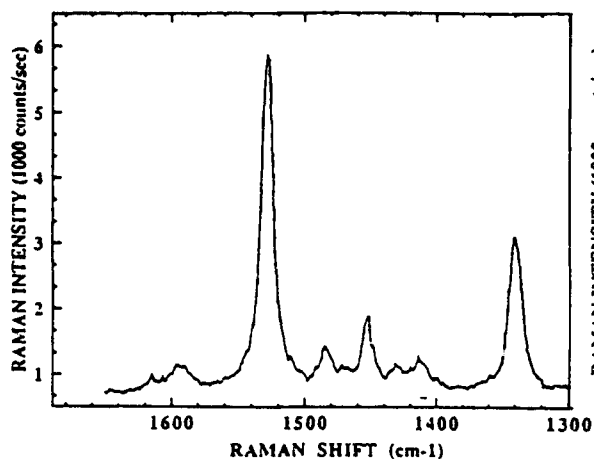


Fig.4 a) Raman spectra for an incident power of 50 mW

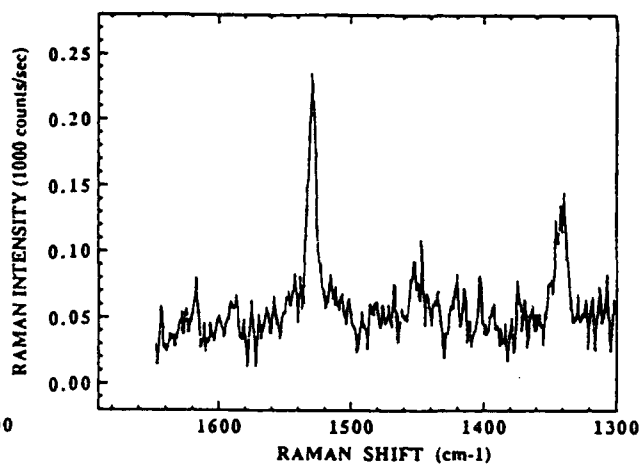


Fig.4 b) Raman spectra for an incident power of 2 mW.

4. CONCLUSION

We have shown the dependence of the Raman intensity on the thickness of the Ag film in an experiment of SP assisted Raman scattering in the Kretschmann geometry. This work confirms that the scattered light at the Stokes frequency also stimulates surface plasmons. Indeed, the shape of the experimental maximum Raman intensity curve versus the metal thickness is well described by the product of the coupling coefficients of the SP at both laser and Stokes frequencies. We have demonstrated that the maximum of Raman signal is obtained for an overall optimization of the coupling at both pump and Stokes lights. However, the overall optimization is not too difficult to achieve. Indeed, our results show that within a range of $\pm 50\text{\AA}$ around the optimum Ag thickness the variation in the intensity of the Raman signal is not of significant value. Hence, a large enhancement factor is obtained with no need to control exactly the thickness of the Ag film. This leads to the observation of the main lines of the Raman spectrum of a few (4 to 5) CuPc monolayers using only a 2 mW pump beam.

REFERENCES

1. Y.J. Chen, W.P. Chen, E. Burstein, Phys. Rev. Lett. **36**, 1207 (1976).
2. S. Ushioda, Y. Sasaki, Phys. Rev. **B 27**, 1401 (1983).
3. J. Giergiel, C.E. Reed, J.C. Hemminger, S. Ushioda, J. Phys. Chem. **92**, 5357 (1988).
4. S. Hayashi, M. Samejima, Surf. Science **137**, 442 (1984).
5. C. Jennings, R. Aroca, A. Ho, R.O. Loutfy, Anal. Chem. **56**, 2033 (1984).
6. F. Abelès, Ann. Phys. (Paris) **3**, 504 (1948); **5**, 596 (1950); **5**, 706 (1950).
7. K. Kurosawa, R.M. Pierce, S. Ushioda, J.C. Hemminger, Phys. Rev. **B33**, 789 (1986).
8. C.E. Reed, J. Giergiel, J.C. Hemminger, S. Ushioda, Phys. Rev. **B36**, 4990 (1987).
9. W.H. Weber, S.L. Mac Carthy, Appl. Phys. Lett. **25**, 396 (1974).
10. B.H. Schechtman, W.E. Spicer, J. of Molec. Spect. **33**, 28 (1970).

High Resolution Spectroscopy on Single Molecules

Jerzy Sepiol, Frank Güttler, Marco Pirotta, Alois Renn and Urs P. Wild

Physical Chemistry Laboratory

Swiss Federal Institute of Technology, ETH-Zentrum

CH-8092 Zürich, Switzerland

Tel. : +41 1 256 4387 ; Fax : +41 1 256 3402

Single particle spectroscopy has become a source of valuable information on fundamental interactions between light and matter. Whereas trapping and cooling of ions and atoms has been successfully achieved, single molecules, because of their multilevel structure (high number of internal degrees of freedom) have not been observed in electromagnetic traps so far. However due to the presence of zero phonon lines in conjunction with inhomogeneous broadening the spectroscopic isolation and detection of single molecules 'trapped in solids at very low temperatures' is made feasible [1,2]. Single molecule spectroscopy allows to study the distribution of molecular properties and not only the statistical average which is generally observed.

In this contribution we present the results of Stark-effect measurements and polarized fluorescence excitation spectra of single pentacene molecules in a solid matrix. Pentacene in *p*-ter

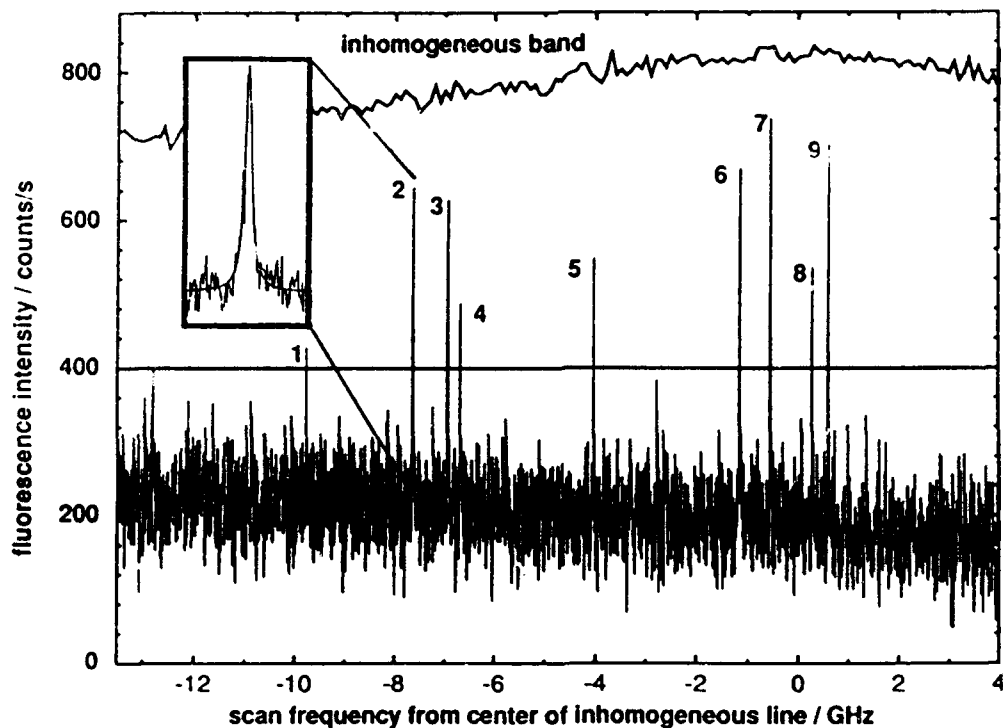


Fig. 1: Excitation scan of a part of the O_1 -site of pentacene in *p*-terphenyl showing resonant lines of single molecules (number 1-9). The inhomogeneous O_1 -band for a high concentration sample and an enhanced view of a single molecule signal is included in the figure.

phenyl was chosen because it is a well investigated system, it has a very low hole burning efficiency and of the high fluorescence quantum yield of the molecules in the O_1 - and O_2 -site. The sample preparation and the experimental method have been described elsewhere [3]. The crystal, containing the molecules to be studied in low concentration, was cooled to 1.8 K and illuminated through a 5 μm pinhole with a single mode tunable dye laser (Coherent, CR599-21, ~ 2 MHz bandwidth). The red-shifted fluorescence light of the guest molecule was collected through a set of lenses (N.A. 0.3) and detected by a cooled RCA C31034 photomultiplier which was connected to photon counting electronics. Optical cutoff filters (Schott RG 630) were used to suppress the intense Rayleigh scattered radiation. The experiment was controlled by a SUN 4/330 workstation.

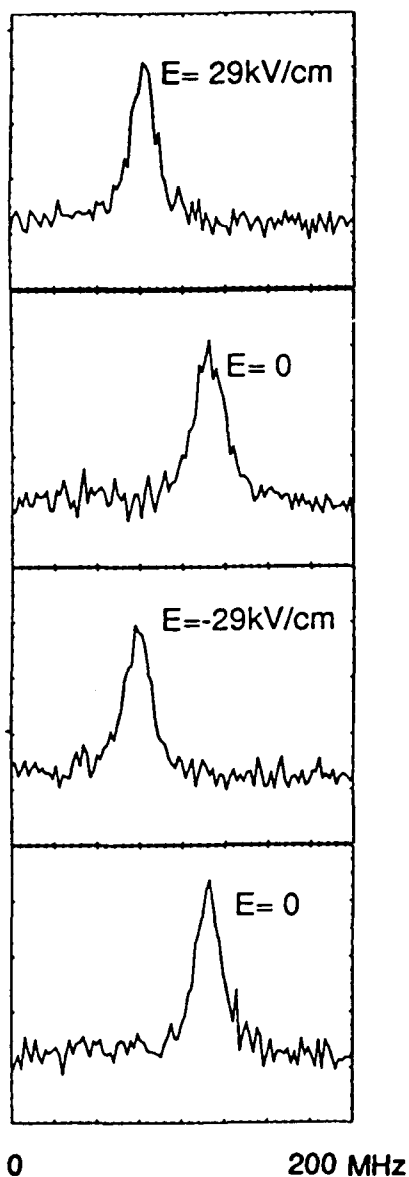


Fig. 2: Stark shift observed on a single pentacene molecule

Fig. 1 shows a 17.5 GHz frequency scan at the center of the inhomogeneous band with 9 peaks corresponding to isolated single molecules. The inhomogeneous O_1 absorption line at 592.322 nm measured with a high concentration sample is included in the picture.

The Stark shifted spectra were obtained by performing frequency scans of 200 MHz. At each frequency position the external electric field was switched to the values 29, 0, -29, 0 kV/cm in succession. Data were recorded individually at every value of the electric field for 0.5 s. This results in four different frequency spectra at the corresponding field values. The data obtained with in a single scan are plotted in Fig. 2 where the field strength E was 29 kV/cm.

Our measurements, also performed at different values of the electric field strengths, confirm the quadratic Stark effect reported by Wiersma et al. [4]. Most of the pentacene molecules showed this behavior, reflecting a highly symmetric environment of the molecules in the *p*-terphenyl crystal. Some molecules nevertheless exhibited a linear contribution to the energy shift which can be attributed to local crystal fields.

Crystallographic investigations confirmed that in our measurements the electric field was applied approximately parallel to the *c*-axis which approximately is the long axis of the embedded pentacene molecules. Thus, from our measured Stark shifts a value for the polarizability difference (field correction $f = 1.95$ [4]) of $\Delta\alpha_{LL} = 10 \times 10^{-24} \text{ cm}^{-3}$ to $\Delta\alpha_{LL} = 22 \times 10^{-24} \text{ cm}^{-3}$ can be deduced.

To get knowledge about the specific environment of a molecule it is helpful to determine the influence of the surrounding cage on the orientation of the transition dipole moment and the position of that molecule in its cage. For that we have performed the fluorescence excitation experiments with polarized light. Fig.3 shows excitation spectra obtained with linear polarized laser light at 4 different orientations of the polarization. The spectral region shown in this graph is located at the centre of the O_1 - site at about 592.32 nm. For several molecules (e.g. molecules 1 & 2) fluorescence signals vanish completely, other molecules have a small variation in the fluorescence intensity with respect to the polarization of the laser light (e.g. molecules 3 & 4).

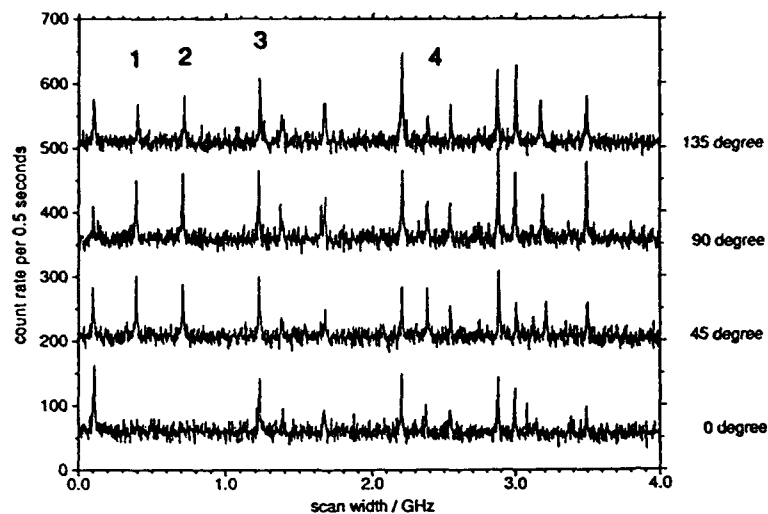


Fig. 3: Excitation spectrum in the center of the inhomogeneous band performed with 4 different orientations of the incoming linear polarized laser light.

More systematic measurements on 55 different pentacene molecules were performed in the spectral range 592.4 - 592.1 nm by setting the laser frequency to the centres of their absorption lines and rotating the polarization plane of the exciting light. All measured data were fitted with a sinusoidal function. Representative results, obtained by the above described method, of two molecules are shown in Fig. 4. Molecule A shows a very high modulation depth depending on the angle of the incoming polarized light. At specific orientations of the linear polarized laser light the fluorescence vanishes totally. The behaviour of molecule B is quite different from A, the modulation depth is smaller and there is a phase shift between the maxima of fluorescence of the two

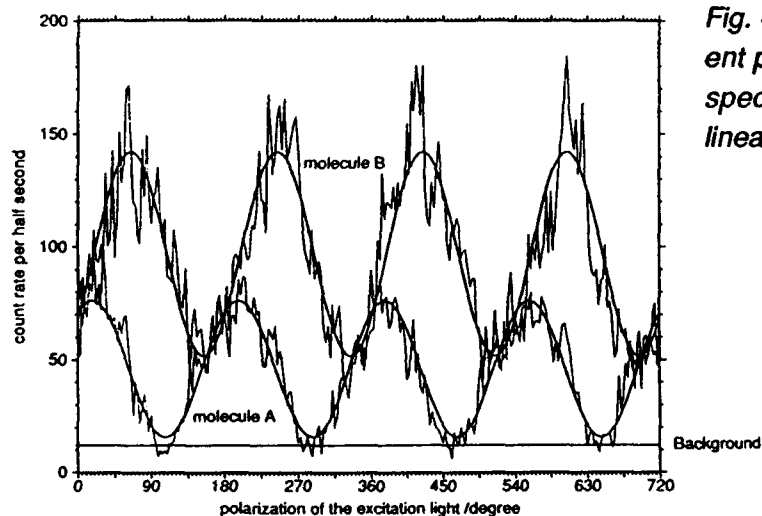


Fig. 4: Fluorescence signals of two different pentacene molecules plotted with respect to the orientation of the incoming linear polarized laser light.

molecules. From 55 molecules investigated so far 12 molecules have a highly modulated fluorescence. A correlation between spectral position of single molecules and direction of transition moments will be discussed.

In conclusion spectroscopic investigations at the single molecule level allows individual properties of isolated molecules in host systems to be distinguished. Molecular properties of the guest molecules exhibit variations from molecule to molecule. To understand this behaviour one has to keep in mind that we are dealing with molecules affected by their local environment. So a single molecule always has to be defined and characterized including its individual environment. Polarization measurements on single pentacene molecules in p-terphenyl crystal provides us to get information about the orientation of the transition dipole moment of the single molecule in its p-terphenyl cage.

- 1 W.E.Moerner and L.Kador, *Phys.Rev.Letters* 62 (1989) 2535.
- 2 M.Orrit and J.Bernard. *Phys.Rev.Letters* 65 (1990) 2716.
- 3 U.P.Wild, F.Güttler, M.Pirotta and A.Renn, *Chem.Phys.Letters* 193 (1992) 451.
- 4 J.H. Meyling, D.A. Wiersma, *Chem. Phys.* 17 (1976) 353.

Wednesday, January 30, 1993

Poster and Postdeadline Session 2

WB 8:00pm–10:00pm
Salon B

Low Pressure Measurements of Line Broadening Coefficients in CH₃F

M. Nischan, D. Clark, D. Guerin, and A. W. Mantz
Department of Physics and Astronomy
Franklin and Marshall College
Lancaster, PA 17604-3003

Interpretation of low pressure measurements of pressure broadened line widths is made difficult by the fact that Doppler line width and measurement laser line width both generally contribute significantly to the total line width. This is further complicated by the fact that the Doppler and Laser contributions are non linear in the low pressure regime when the line width is plotted as a linear function of pressure.

Townes and Schawlow (1) first showed that Doppler broadening, $\Delta v_{\text{Doppler}}$, and wall collision effects, $\Delta v_{\text{collision}}$, contribute to the measured line half width, Δv , for microwave transitions through the relation

$$\Delta v = ((\Delta v_{\text{Doppler}})^2 + (\Delta v_{\text{collision}})^2)^{1/2} . \quad (1)$$

We have found that the above relation may be generalized to include a finite laser line width ($\Delta\nu_{\text{laser}}$) as well as collisional ($\gamma P_{\text{foreign gas}}$) and self broadening ($\gamma_s P_{\text{self}}$) effects for rovibrational linewidths measured in the mid infrared as shown in equation (2) below

$$\Delta\nu^2 = (\Delta\nu_{\text{Doppler}})^2 + (\gamma_s P_{\text{self}})^2 + (\Delta\nu_{\text{laser}})^2 + (\gamma P_{\text{foreign gas}})^2 . \quad (2)$$

The primary benefit of this representation is the fact that a plot of squared line width versus foreign gas pressure squared is linear for a fixed P_{self} , and each contribution to the line width may be treated independently of the other effects. In the low pressure regime the pressure dependence is a linear function of pressure squared.

References

1. C. H. Townes and A. L. Schawlow, *Microwave Spectroscopy*, (McGraw-Hill, New York, 1955)

MEASUREMENT OF COLLISION CROSS SECTION AND LINE BROADENING
COEFFICIENT FOR $2p_8 \rightarrow 4d_4$ TRANSITION IN NEON

P R Sasi Kumar, S S Harilal
VPN Nampoori and CPG Vallabhan

Laser Division, Department of physics,
Cochin University of Science and Technology
Cochin-682022, INDIA.

ABSTRACT

The collision cross section and broadening coefficient for $2p_8 \rightarrow 4d_4$ transition in neon has been evaluated by high resolution optogalvanic spectroscopy using a single mode ring dye laser.

INTRODUCTION

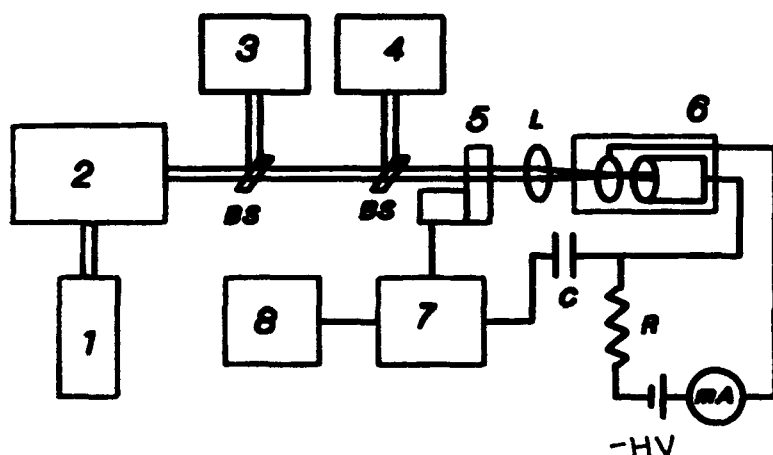
The width of spectral lines perturbed by collision with neutral atoms and charged particles in a discharge cell can provide useful information about interactions involving excited atomic states. As an alternative to conventional methods, collision processes in electrical discharges can be investigated using laser optogalvanic spectroscopy (LOGS). The application of LOGS to such studies offers far greater sensitivity and precision in these measurements.

LOG effect is essentially a change in electrical properties of a gas discharge by resonant absorption of laser radiation tuned to a particular transition of species in the discharge¹. Magnitude of the LOG signal is governed in a complex way by the life time of levels involved in the transition, collision processes in the discharge medium, the incident laser power density, discharge current and pressure of the gas. LOGS method has been successfully applied for the measurement of collision broadening and wavelength shift of spectral lines^{2,3}. It has been reported that spectral width and magnitude of the shift depend predominantly on pressure while their variation with discharge current has very little effect³. However one cannot rule out such variations in spectral characteristics due to discharge current, as an increase in the same will invariably cause an enhancement in the collision rate. In this paper we report the measurement of collision cross section and line broadening coefficient caused by increase in the discharge current for $2p_8 \longrightarrow 4d_4$ transition of neon at 17181.61cm^{-1} in a Ne/Mo hollow cathode by LOGS.

EXPERIMENT

Fig 1 shows the experimental set up employed to observe LOG effect. Radiation from a single mode ring dye laser (Spectra Physics, 380D) pumped by argon ion laser (Spectra Physics, 171) is focused into a Ne/Mo hollow cathode discharge tube (hcd). The laser power was maintained $240 (\pm 10)$ mW and the beam was mechanically chopped at 42Hz. The discharge was maintained by

applying a stable dc voltage through a ballast resistance (60K) in series with the cell. OG signal profile is recorded by scanning the dye laser at a rate of 15 GHz/min, through the absorption line using single mode scanning electronics. The LOG signal generated is coupled through a capacitor (0.1 μ F) to a lock in amplifier (EG&G 5208) and processed by a computer. The wavenumber of the laser beam was measured by a wavemeter (Burleigh WA 20VI) to an accuracy of 0.01 cm^{-1} . The OG signal was recorded and stored with computer. The results were highly reproducible at each value of the current.



1.Ar laser, 2.Ring dye laser, 3.wavemeter, 4.spectrum analyzer 5.chopper, 6.hollow cathode,7.lock in amp. 8.computer

Fig 1
Experimental setup

RESULTS AND DISCUSSION

The full width at half maximum (fwhm) for $2p_8 \rightarrow 4d_4$ transition of neon was studied as a function of discharge current. Fig 2 shows the plot of fwhm against the discharge current. Various broadening mechanisms lead to the observed width of the spectral line: pressure broadening will arise due to the collision of absorbing atoms with neutral and excited atoms and ions. Also in low pressure and low current

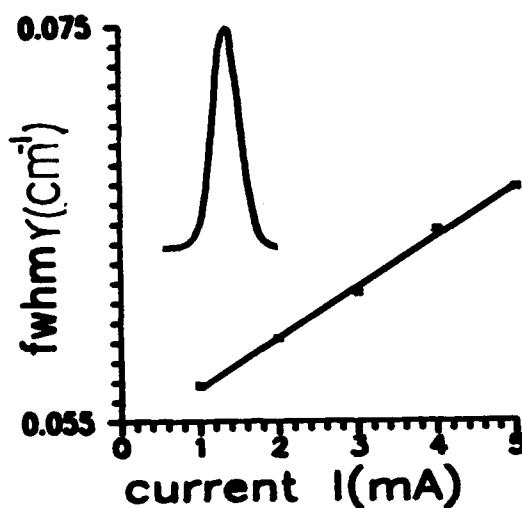


Fig 2. plot of fwhm (γ) verses current (I). The inset shows the line shape at 4mA

hcd lamps, the spectral width is determined by doppler effect. It is observed that the fwhm (γ) depends linearly on the current (I) according to the relation

$$\gamma = \gamma_0 + \alpha I \quad (1)$$

where $\alpha = 0.00297 \text{cm}^{-1}/\text{mA}$ is the slope of γ -I plot. From the behavior of equation (1) we can conclude that an increase of current produces an enhancement in the discharge temperature. Assuming doppler effect is the dominant line broadening process, the temperature (T) within the discharge can be calculated from the line width of the measured OG signal profile for various currents using the formula⁴

$$\Delta\nu = \frac{2\nu}{c}(2RT \log 2/M)^{1/2} \quad (2)$$

Here $\Delta\nu$ is the fwhm in Hz, ν is the frequency at line centre, M is the atomic weight of neon and R is the gas constant. Pressure of the gas in the hollow cathode was 10 torr and concentration at each current can be calculated from $N=p/kT$. The collision broadening coefficient is given by α/N and is listed in table 1

According to the theory of impact approximation⁵, interaction with neighboring atoms ions etc will perturb the state of the radiating atoms which will results into broadening of line. The spectral distribution of radiation is lorentzian with fwhm increasing according to

$$\beta = 2\sigma v \quad (3)$$

Here β is collision broadening coefficient in angular frequency units², σ is the collision cross section and $v = (16kT/\pi m)^{1/2}$, is the velocity of the absorbing atoms of mass m. In the range of current studied, average temperature calculated was 530K corresponding $v = 10.55 \times 10^4 \text{cm/sec}$ and $N = 1.852 \times 10^{17} \text{atoms/cm}^3$. The collision cross section calculated from this gives a value of $1.432 \times 10^{-15} \text{cm}^2$.

In conclusion ,fwhm of $2p_8 \longrightarrow 4d_4$ transition of neon in a Ne/Ne hcd lamp is found to vary linearly with discharge current. High resolution LOGS also gives the collision cross section and the broadening coefficient in this case.

ACKNOWLEDGEMENT

Financial assistances from Ministry of Human Resources Development (New Delhi) is gratefully acknowledged. PRS and SSH are indebted to University Grants Commission and Council for Scientific and Industrial Research (New Delhi) for research fellowship.

Table 1
Broadening coefficient for different discharge currents

discharge current (mA)	fwhm (cm^{-1})	broadening coefficient ($\text{cm}^{-1}/\text{atom cm}^{-3}$)
1	0.0571	1.338×10^{-20}
2	0.0598	1.471×10^{-20}
3	0.0626	1.606×10^{-20}
4	0.0663	1.830×10^{-20}
5	0.0687	1.942×10^{-20}

REFERENCES

1. R G Green ,R A Keller ,G G Luther ,P K Schenck and J C Travis, Appl. Phys. Lett. 29, 727 (1979).
2. K Naveedhullah, and Arther S Naqvi Optics Comm. 56, 117 (1985).
3. Takashi Masaki, Yukio Adachi and Chiaki Hirise, Appl Spectroscopy, 42, 54 (1988).
4. A C G Mitcell and M W Zemansky, University press, Oxford, (1961).
5. Alan Corney, Atomic and molecular spectroscopy, Oxford University press ,Oxford (1977).

The Position, Shape, and Polarization Dependence of Resonances in the Laser
Photoionization Spectrum of Aligned Ca $4s5p\ ^1P_1$

D.W. Duquette, K.W. McLaughlin, D.S. Eschliman, and O.P. Francis

Department of Physics and Astronomy, Behlen Laboratory of Physics
University of Nebraska, Lincoln, Nebraska 68588-0111 (402) 472-2783

Two-color spectroscopy using narrow-bandwidth pulsed lasers provides a powerful tool to study the near threshold photoionization spectrum of excited atomic states. By combining the energy and polarization selectivity afforded by pulsed dye lasers, it is possible to probe a number of different continua. Many of these would be unreachable from the ground state because of angular momentum and parity selection rules and also due to the lack of high resolution sources of photons at appropriate energies. Precise positions, shape profiles, and strengths of autoionizing resonances, as well as angular distributions of ejected photoelectrons are necessary for comparison with increasingly sophisticated calculations.

In this experiment, Ca atoms are excited from the $4s^2\ ^1S_0$ ground level to the $4s5p\ ^1P_1$ level and, after a short delay, the excited Ca atoms are ionized. Fluorescent photons from the $4s5p\ ^1P_1$ to $3d4s\ ^1D_2$ transition provide a relative pulse-to-pulse measurement of the excited level population. Photoelectrons are counted and the resulting photoelectron signal is normalized to the fluorescence and to the measured intensity of ionizing light.

Excitation and ionization photons are produced with two independently tunable dye lasers pumped by the same pulsed Nd:YAG laser at a pulse repetition rate of 10 Hz. Pulses from both dye lasers have a duration of 5 to 8 ns. The excitation dye laser operates 18365.8 cm^{-1} with a FWHM linewidth of approximately 0.1 cm^{-1} . This beam is frequency-doubled in BBO to 36731.6 cm^{-1} . The ionization dye laser operates over a range from 15000 cm^{-1} to 15500 cm^{-1} with a linewidth of less than 0.15 cm^{-1} . Stepper motors control the tuning elements in both dye lasers, resulting in an ultimate wavelength repeatability of less than half a linewidth. The ionizing dye laser pulses are optically delayed 15 ns so that the laser pulses do not overlap in time. The two beams are directed colinearly into the photoionization region where they cross a Ca atomic beam.

Ca atoms are produced in an outer vacuum chamber by an oven source at 460 to 530 °C. The uncollimated atomic beam is collimated by a 2 mm aperture as it enters a differentially pumped inner chamber. The collimated beam has a maximum angular divergence of approximately 11.5° , resulting in a transverse doppler width of 0.01 cm^{-1} at 15000 cm^{-1} .

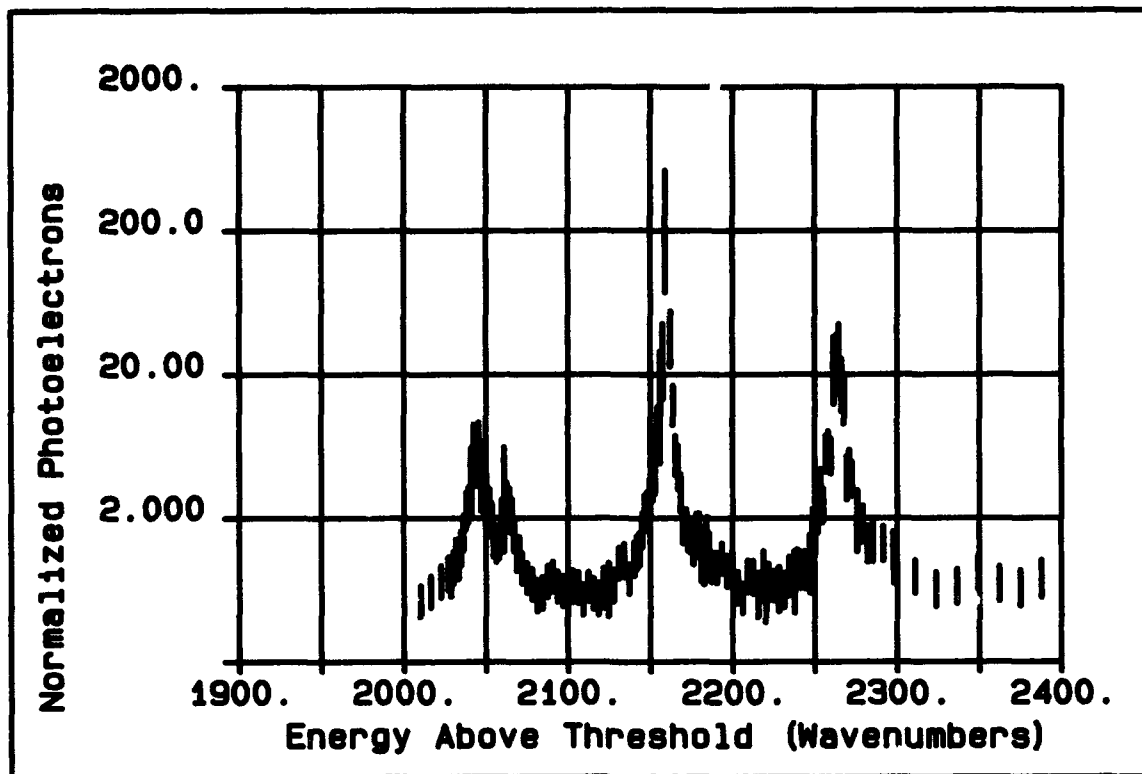


Figure 1. Total relative photoionization cross section as a function of ionizing photon energy above threshold. Excitation polarization linear, ionizing polarization circular.

The photoionization region consists of a 2 cm diameter Cu cylinder electrode and electrically isolated Cu endcap ring electrodes 1.2 cm apart. The entire interior is lined with Mo mesh. Fluorescent photons from the decay of the excited level and photoelectrons are collected in opposite directions along the cylinder axis. Photoelectrons leave the photoionization region through one endcap, enter a 10 cm long drift region, and are subsequently detected by a dual multi-channel plate detector. The photoionization region electrodes are maintained at a negative potential relative to the drift region to focus the photoelectrons onto the detector. Both regions are enclosed in a magnetic shield.

We detect angle-selected photoelectrons by applying a -50 V potential to all three photoionization region electrodes. Photoelectrons with energies above a few hundred mV propagate essentially freely in the small residual electric field and only those within the 38° acceptance angle of the drift region are counted. Alternatively, by shifting the potentials of the two cylinder endcaps to -65 V and -35 V, we create a weak electric field that is sufficient to pull all of the photoelectrons into the drift region.

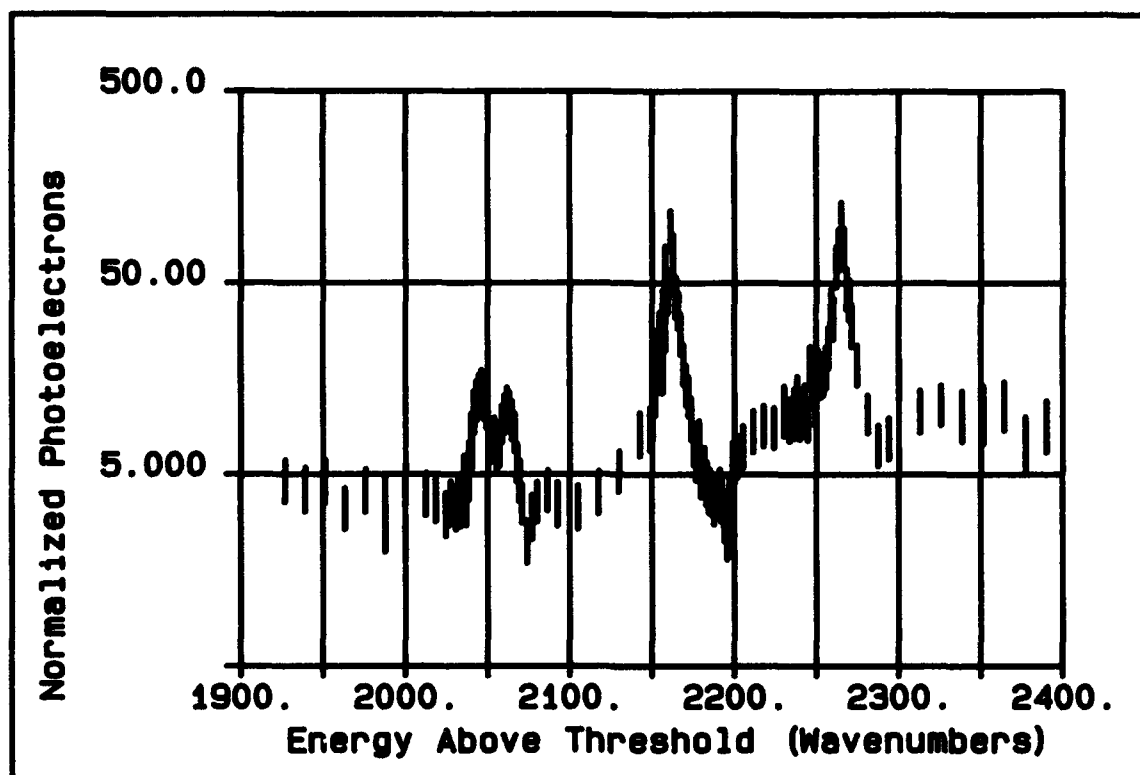


Figure 2. Angle-resolved relative photoionization cross section at 90° to excitation polarization axis as a function of ionizing photon energy above threshold. Excitation polarization linear, ionizing polarization circular.

In investigations so far completed, the polarization of the excitation laser is linear and vertical. We vary the polarization of the ionizing laser by inserting single or double Fresnel rhombs for circular polarization or linear polarization at chosen angles.

The photoionization spectrum of $\text{Ca } 4s5p \ ^1P_1$ from 1900 to 2400 cm^{-1} above threshold is obtained with ionizing photons between 15000 cm^{-1} and 15500 cm^{-1} . Both the total and angle-resolved relative cross sections observed using circularly polarized ionization clearly reveal 3 previously identified autoionizing levels: $3d4d \ ^3S_1$ and $3d4d \ ^3D_{1,2}$. In addition, there is a peak corresponding to new, previously unobserved autoionizing level. Initial calculations indicate a very narrow and strong $J=1$ resonance near this position.¹ The shapes and strengths of the observed resonances have not yet been compared with calculations in detail.

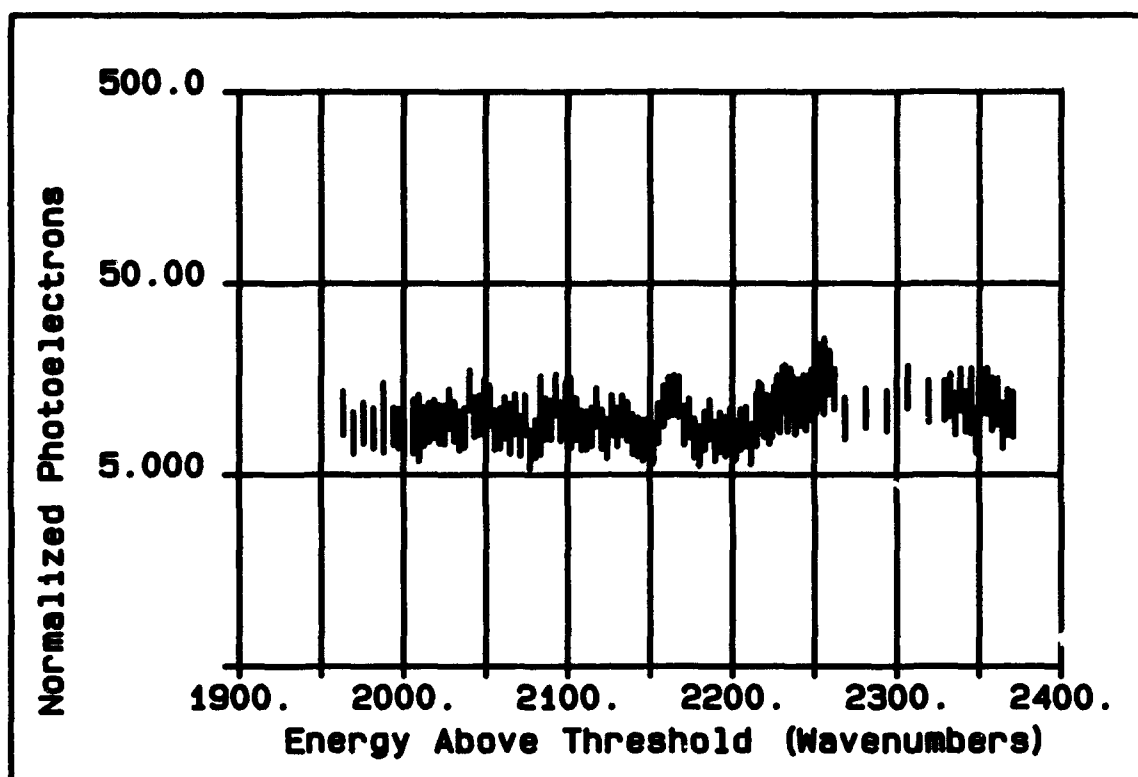


Figure 3. Angle-resolved relative photoionization cross section at 90° to excitation polarization axis as a function of ionizing photon energy above threshold. Excitation polarization linear, ionizing polarization linear and parallel.

The angle-resolved spectrum obtained with the ionizing laser linearly polarized parallel to the excitation polarization is remarkably free of any structure. This would appear to indicate that the photoelectrons are ejected quite preferentially along the polarization axis for all four resonances in this range. Initial measurements of the total photoionization cross section for parallel polarizations also indicate no resonances, in complete contrast to expectations. We will present the results of these ongoing measurements.

¹ C. Greene, private communication.

**PRODUCTION OF THE HIGH-INTENSIVE BEAMS OF ULTRACOLD
ATOMS FOR HIGH RESOLUTION SPECTROSCOPY .**

E. Korsunsky⁽¹⁾, D. Kosachiov⁽¹⁾ and Yu Rozhdestvensky⁽²⁾

⁽¹⁾ Department of theoretical physics , St.-Petersburg State
Technical University, 195251 St.-Petersburg, Russia

⁽²⁾ Vavilov State Optical Institute, 199034 St.-Petersburg,
Russia

The characteristic feature of the transversal cooling with CPT is that light pressure force F_z is of constant sign in a whole range of velocity variation [1,2]. Therefore , decelerating the atoms with $v_z < 0$, the same force accelerates the atoms with positive velocities , that leads to the considerable loss of final intensity of the atomic beam .

We suggest the collimation technique permitting to get the collimated atomic beam practically without intensity loss.

Production of the intensive beam is possible using the two-zone interaction scheme (Fig 1) . In the zone A the frequency detunings of the exciting fields are shifted so that the narrow CPT resonance is in region of positive velocities at $v_A = (\Omega_1 - \Omega_2) / 2k$. As a result the formation of the intensive peak in velocity distribution take place for $v_z \approx v_A$ (Fig. 2) . The peak accumulates the atoms with initial velocity $v_z < v_A$. In order to accumulate the whole Maxwellian distribution in this peak , values $v_A = (2$

- 3) Δv_1 (Δv_1 is the initial width of velocity distribution) are needed (2-3 m/sec for a Na beam with the initial width of velocity distribution corresponding to the Doppler limit). On the other hand , the atomic beam is now deviated after the interaction in the zone A . The return of the narrow peak of atoms to the region of small transversal velocities takes place in the zone B . Here the atomic beam interacts with the light fields , the wave vectors directions of which is opposite to those of zone A , and detunings are equal ($\Omega_1 = \Omega_2 = \Omega$). The light pressure force F_z in the zone B is negative and it has the CPT resonance in the zero-velocity region (Fig 2) . The effect of F_z leads to the shift of the velocity distribution peak formed in the zone A to the zero-velocity region and to its further narrowing. As it seen from Fig. 2 , almost all the atoms of the beam are accumulated to the narrow velocity region with $\Delta v_z \approx 10$ cm/sec near $v_z = 0$.

Note finally that the velocity diffusion unessentially affects the realization of suggested technique, since the atoms transit time through the zones A and B is small enough, hence the diffusion broadening of the transversal velocity distribution is slight.

1. V.G. Minogin , M.A. Olshany and S.U. Shulga : J.Opt.Soc. Am. B6 (1989) 2108
2. D.V. Kosachiov, B.G. Matisov and Yu.V. Rozhdestvensky , Kvantovaja Electr. 19 . N 7 .(1992) 713

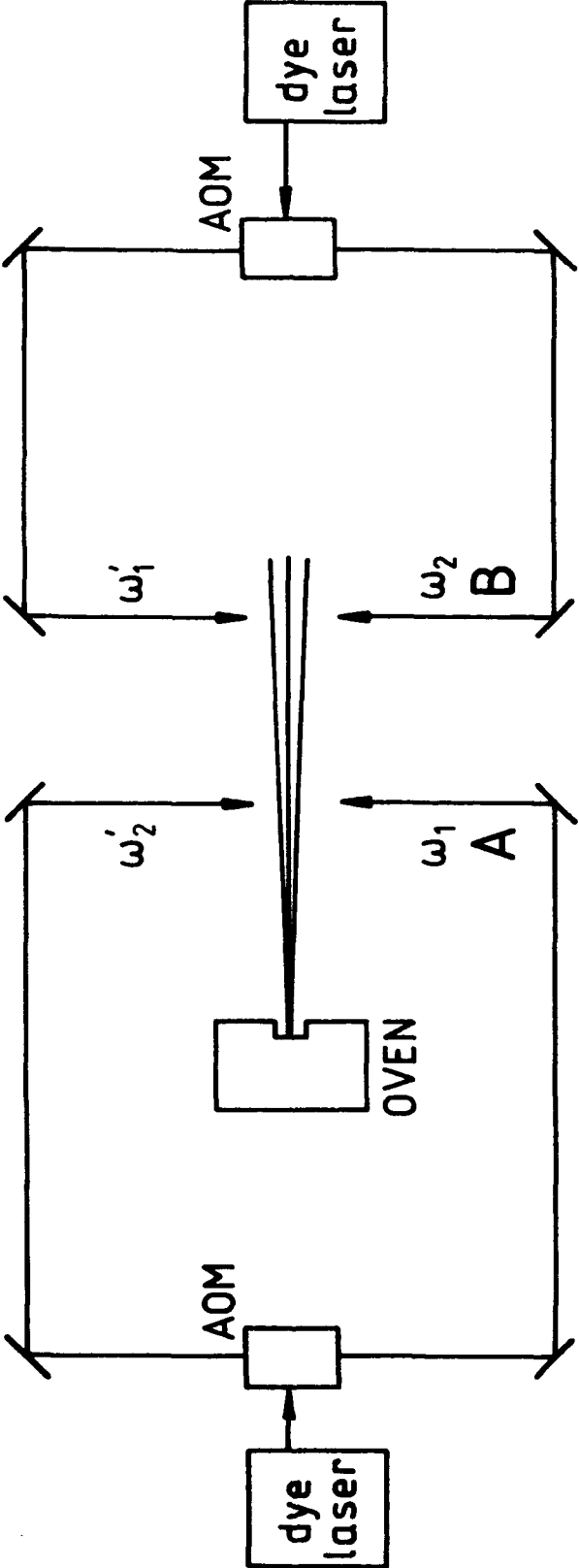


Fig.1 Two-zone scheme for production of an intensive Λ -atomic beam

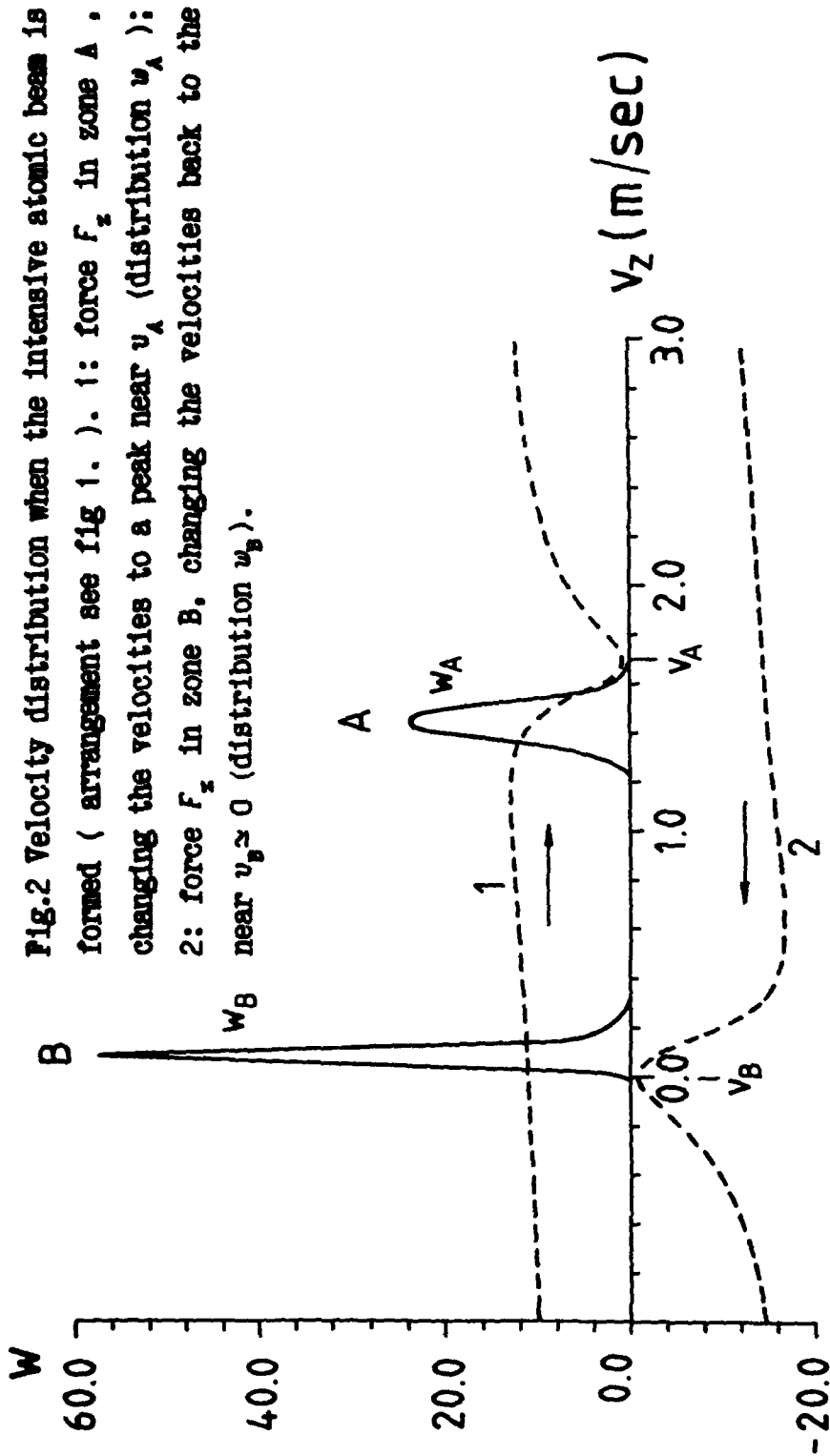


Fig.2 Velocity distribution when the intensive atomic beam is formed (arrangement see fig 1.). 1: force F_z in zone A , changing the velocities to a peak near v_A (distribution w_A) : 2: force F_z in zone B, changing the velocities back to the w_B near $v_B \approx 0$ (distribution w_B).

VELOCITY SELECTION TECHNIQUE FOR HIGH-RESOLUTION SPECTROSCOPY

E. Korsunsky⁽¹⁾, D. Kosachiov⁽¹⁾ and Yu. Rozhdestvensky⁽²⁾

⁽¹⁾ Department of theoretical physics , St.-Petersburg State Technical University, 195251 St.-Petersburg, Russia

⁽²⁾ Vavilov State Optical Institute, 199034 St.-Petersburg, Russia

It is known [1-3] , that the samples of atoms with a velocity spread much lower than the recoil velocity $v_R = \hbar k/M$ (k is the wave number of exciting light field, M is the mass of atom) can be obtained by use of velocity selection with stimulated Raman transitions. A theoretical analysis of the velocity selection method is presented in [2,3] . So , it was shown in [2] that the formation of such narrow velocity structures is performed not only by the counterpropagating , but also by co-propagating light waves. This fact allows to form the two-dimensional velocity distribution of the widths $\delta v_{x,y} \ll v_R$ by the velocity selection technique using laser configuration as in Fig.1b. The width of so formed velocity structure in the $|2\rangle$ state is determined by the Rabi frequency :

$$\delta v_x \approx \sqrt{2} \cdot g / (k \cdot \cos \varphi) \quad ,$$

$$\delta v_y \approx \sqrt{3} / \tau \approx \sqrt{6} \cdot g / (\pi \cdot k \cdot \sin \varphi) \quad , \quad (9)$$

and for $g \ll \omega_R$ can be much smaller than the recoil velocity v_R ($\delta v_x \approx \delta v_y \approx 10^{-1} + 10^{-2}$ cm/sec for $g \approx 0.1\omega_R$ for Na atoms)

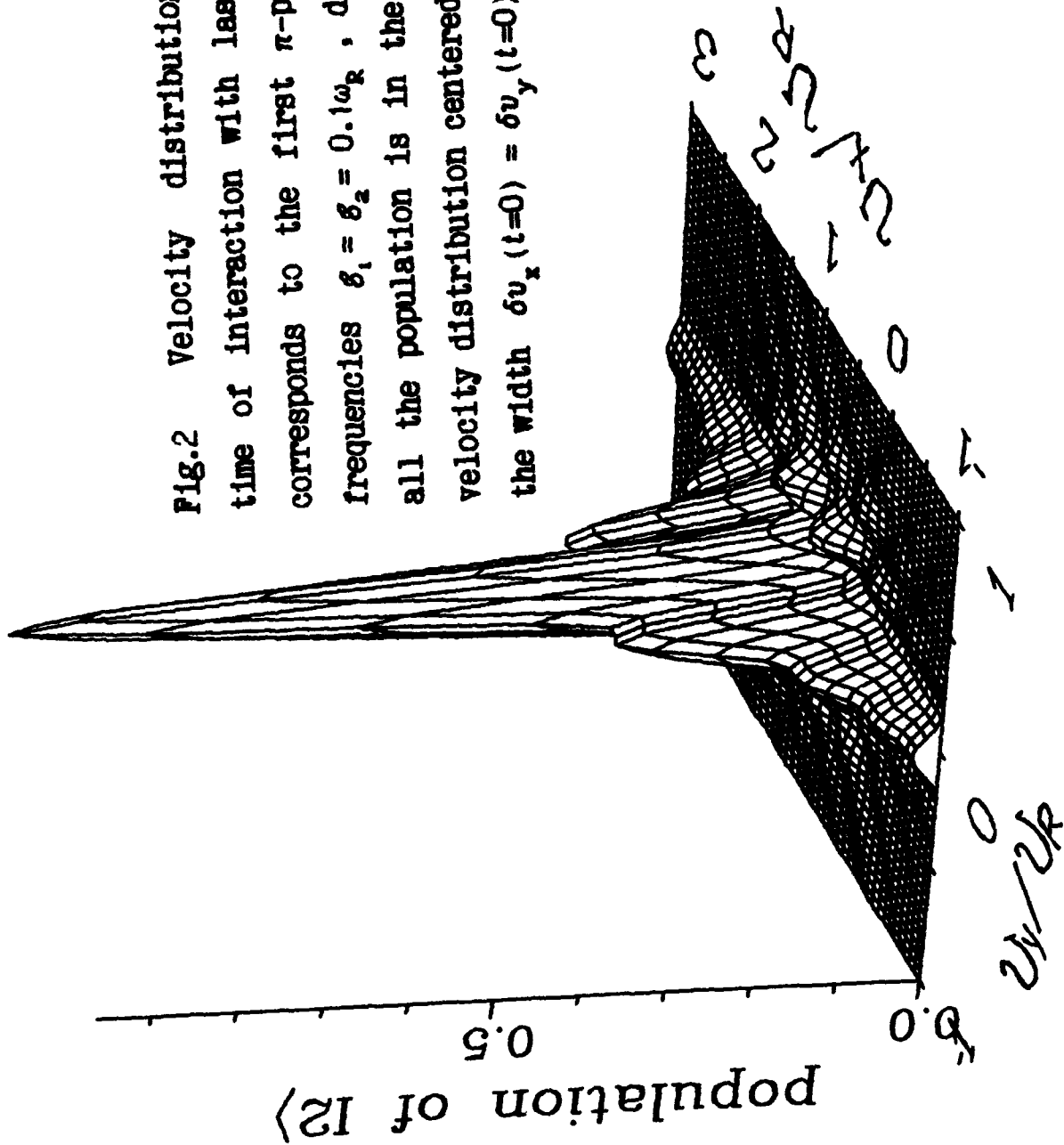
Fig.2 shows the typical shape of two-dimensional velocity structure in the $|2\rangle$ state formed by two-dimensional velocity selection technique considered here.

Realization of two-dimensional selection permits to accumulate in magnetic traps the atoms, which are in certain quantum state, with kinetic energy much less than recoil energy $R = \hbar^2 k^2 / (2M)$. Such atoms are the unique object for high resolution spectroscopy

References

1. M.Kasevich, D.S.Weiss, E.Riis, K.Moler, S.Kasapi and S.Chu, Phys.Rev.Lett. 66 (1991) 2297
2. E.A.Korsunsky, D.V.Kosachiov, B.G.Matisov and Yu.V. Rozhdestvensky , Pis'ma Zh.Eksp.Teor.Fiz 55 (1992) 313 (JETP Lett. 55 (1992) 311)
3. K.Moler, D.S.Weiss, M.Kasevich, S.Chu, Phys.Rev.A 45 (1992) 342

Fig.2 Velocity distribution of the $|2\rangle$ state after the time of interaction with laser fields $\tau = 22.2\omega_R^{-1}$, which corresponds to the first π -pulse in a Raman system. Rabi frequencies $\delta_1 = \delta_2 = 0.1\omega_R$, detunings $\Omega_1 = \Omega_2 = 0$. Initially all the population is in the $|1\rangle$ state and has a Gaussian velocity distribution centered at $v_{0x} = 0$, $v_{0y} = 0$, with the width $\delta v_x(t=0) = \delta v_y(t=0) = 5\hbar k/M$



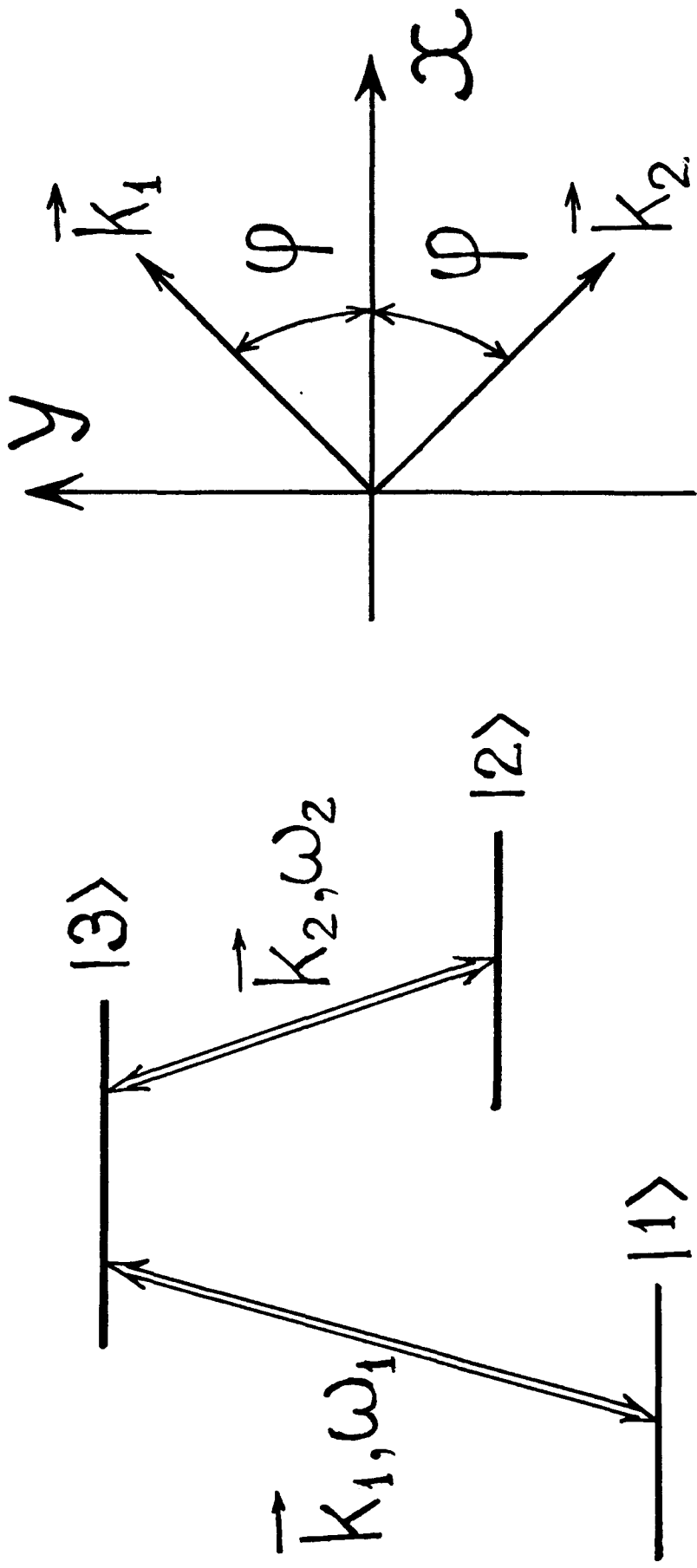


Fig.1 Configuration of selection light waves. Waves are linearly polarized along z axis. Wave with frequency ω_1 and wave vector k_1 excites only $|1\rangle \rightarrow |3\rangle$ transition, and wave with ω_2 , k_2 excites only $|2\rangle \rightarrow |3\rangle$ transition

**New Spectroscopic Techniques on the Basis of
Elliptically Polarized Pumping**

Igor I. Gancheryonok, Yasuo Kanematsu and Takashi Kushida

Department of Physics, Faculty of Science, Osaka University,
Toyonaka, Osaka 560, Japan (tel.: 06-844-1151 Ext. 4047)

When rather high-power polarized radiation (pump) propagates in an isotropic medium, an induced anisotropy may arise due to the nonlinear character of the interaction. This anisotropy can significantly affect the polarization of the probe field as well as its intensity. The cited effect lies in the basis of nonlinear polarization spectroscopy (NPS) and optically heterodyned polarization spectroscopy (OHPS). Usually the pump beam has linear or circular polarization and the probe one is linearly polarized. More general case occurs when pumping has elliptical polarization. In this paper we show how additional "degree of freedom" (pump ellipticity) of such a type of excitation can be advantageously applied to the investigation of initially isotropic substances.

Central to our theoretical consideration is the formalism for a tensor of light-induced anisotropy. It allows us to develop a general approach to description of the probe wave propagation effects in a medium within the framework of nonlinear optical spectroscopy. This tensor can be written in the following covariant form^{1,2}

$$\hat{S} = I + C_1 e \cdot e^* + C_2 e^* \cdot e,$$

where I is the unit tensor, e is the polarization vector of the pump field, the dot and asterisk denote the direct product and complex conjugate, respectively, and the complex parameters C_1 and C_2 are defined using the 3rd-order nonlinear susceptibility (3NS) as

$$C_1 = \frac{\chi_{1122}}{\chi_{1221}}, \quad C_2 = \frac{\chi_{1212}}{\chi_{1221}}.$$

Further, solving the corresponding vectorial beam propagation equation², we obtain the detected signal intensity behind the tilted analyzer as follows:

$$\Delta I = I_{10} [|u_a^* u_p|^2 + 2z \operatorname{Re} ((u_a u_p^*) A u_a^* \hat{S} u_p) + z^2 |A u_a^* \hat{S} u_p|^2]. \quad (1)$$

Here, the unit norm vectors u_a and u_p characterize the analyzer and polarizer respectively, I_{10} and z are the input intensity and distance along the direction of propagation of the probe beam, and

a complex parameter A is proportional to the pump beam intensity.

In NPS, generally, an initially linearly polarized probe beam is blocked by the exactly crossed linear analyzer ($\mathbf{u}_A \mathbf{u}_p = 0$) in order to observe only nonlinear contributions. Then, for the detected signal, we have

$$\Delta I_{NPS} = \frac{1}{4} z^2 |A|^2 |C_1 + C_2|^2 [(\cos 2\epsilon)^2 (\sin 2\phi)^2 + |q|^2 (\sin 2\epsilon)^2 - \text{Im} q \sin 4\epsilon \sin 2\phi], \quad (2)$$

$$q = \frac{(C_2 - C_1)}{(C_1 + C_2)},$$

where ϵ is the ellipticity angle of pumping such that the ellipticity $\eta = \tan \epsilon$, and ϕ is the azimuth of the probe wave. It is easy to see from eq. (2) that the NPS signal assumes its maximum and minimum values as a function of pump ellipticity. This theoretical result indicates the possibility of the determination of the ratio of two SNS components from the extreme values of ΔI_{NPS} and corresponding ϵ values obtained by tuning the ellipticity of the pump light. An important feature of such an experimental technique is the independence of the measured parameters on the pump beam intensity. This is particularly valuable when one uses pulsed lasers with intensities that experience, as a rule, appreciable fluctuations.

In Fig. 1 the NPS signal is plotted as a function of ϵ when $\phi = \pi/4$. Lines 1 and 2 are the calculated curves of the function defined by eq. (2) for the case of $C_1 = C_2$, and for the 992 cm^{-1} line of benzene.³ The experimental results of ref. 4 for crystal violet and methylene-blue in aqueous solutions are shown by the circles and triangles, respectively. They agree well with the theoretical curve 1, which indicates that $C_1 \approx C_2$ in these materials. Although Song et al.⁵ analyzed their experimental data for malachite green in water assuming the fourth power dependence of ΔI_{NPS} on $\cos 2\epsilon$, we believe that ΔI_{NPS} is almost proportional to the square of $\cos 2\epsilon$ for the majority of dye solutions.

Figure 2 shows a similar dependence in the case of atomic two-level systems when we neglect the effects of interatomic collisions and radiation trapping and assume that the decay constants of the upper (γ_a) and lower (γ_b) levels for the transition of the type ($J \leftrightarrow J-1$) are approximately equal. The latter assumption is omitted for the case indicated in Fig. 3, where the following magnitude is considered as a parameter

$$r = \frac{\Delta J}{|\Delta J|} \frac{\gamma_a - \gamma_b}{\gamma_a + \gamma_b}.$$

Thus, from Figs. 2 and 3 it can be easily seen that the line shape of ΔI_{NPS} exhibits rather strong J-dependence for low J values. Such a feature of the behavior of $\Delta I_{NPS}(\epsilon)$ may be used to identify the unknown transitions as in the case of a three-level cascade system.²

Instead of analysis of the behavior $\Delta I_{NPS}(\epsilon)$, we can measure the pump beam ellipticity dependence of the polarization parameters of the probe beam (induced rotation angle $\Delta \theta_1$ and ellipticity η_1).⁶ Figure 4 demonstrates the ϵ -dependence of $\Delta \theta_1$ (solid lines) and

η_1 (dashed lines) normalized to the linearly polarized pump case. The existence of specific ϵ values, when the effects of the laser-induced polarization alterations disappear, is clearly visible. It should be noted that these values are also independent of the pump beam intensity and can be expressed as

$$\tan 2\epsilon_{\Delta\theta_1=0} = -\frac{1}{q} \frac{\text{Im}\chi_{1221}}{\text{Re}\chi_{1221}} = -\frac{1}{qk},$$

$$\tan 2\epsilon_{\eta_1=0} = \frac{k}{q}.$$

Now, let us analyze the scheme of OHPS with elliptically polarized pumping. When the probe wave is linearly polarized at $\pi/4$ to the major axis of the pump polarization ellipse and position of the linear analyzer is defined by the angle $-\pi/4 \pm \beta$ ($\beta \ll 1$), the OHPS signal in the Kleinman symmetry case ($C_1=C_2=1$) is obtained as

$$\Delta I_{\text{OHPS}} = I_{10} [\beta^2 \pm 2\beta z \cos 2\epsilon \text{Re}A + (\cos 2\epsilon)^2 |A|^2 z^2]. \quad (3)$$

It can be seen from eq.(3) that the behavior of $\Delta I_{\text{OHPS}}(\cos 2\epsilon)$ has a clearly nonmonotonic character. The minimum of the OHPS signal is given as

$$\Delta I_{\text{OHPS}}^{\text{min}} = \frac{I_{10} \beta^2 k^2}{1+k^2}, \quad (4)$$

and this relationship can be used for measuring the k value (phase of 3NS). Moreover, eq.(3) shows two more potentially independent methods for measuring 3NS. One would be based on adjusting the analyzer; then the minimum of ΔI_{OHPS} and the corresponding value β_{min} allow to determine the real and imaginary parts of χ_{1221} , respectively. The second method would involve analyzing the minimum OHPS signal under tuning the pump beam intensity. In this case the final result is exactly the same as that described in the above eq.(4).

In conclusion, the new spectroscopic methods presented in this paper have the main advantage that the pump intensity fluctuations do not contribute to the uncertainties of the measurements. In consequence, the parameters to be determined can be measured with high accuracy. These methods yield also the information about 3NS as well as some spectroscopic parameters which are defined by q and r . Furthermore, they are fairly simple to employ (in comparison, for example, with a recently reported method⁷ for measuring the phase of 3NS) and can be applied for a large variety of materials.

References

1. L. I. Burov, I. I. Gancheryonok, *Opt. & Spectrosc.* **60**, 347 (1986).
2. I. I. Gancheryonok, *Rev. Laser Eng. (Japan)*, to be published.
3. I. I. Gancheryonok, *Jpn. J. Appl. Phys.*, to be published.
4. S. Saikan, J. Sei, *J. Chem. Phys.* **79**, 4149 (1983).
5. J. J. Song, J. H. Lee and M. L. Levenson, *Phys. Rev.* **A17**, 1439 (1978).
6. I. I. Gancheryonok, *Rev. Laser Eng. (Japan)* **20**, 502 (1992).
7. H. Ma et al., *Opt. Lett.* **16**, 630 (1991); **17**, 1052 (1992).

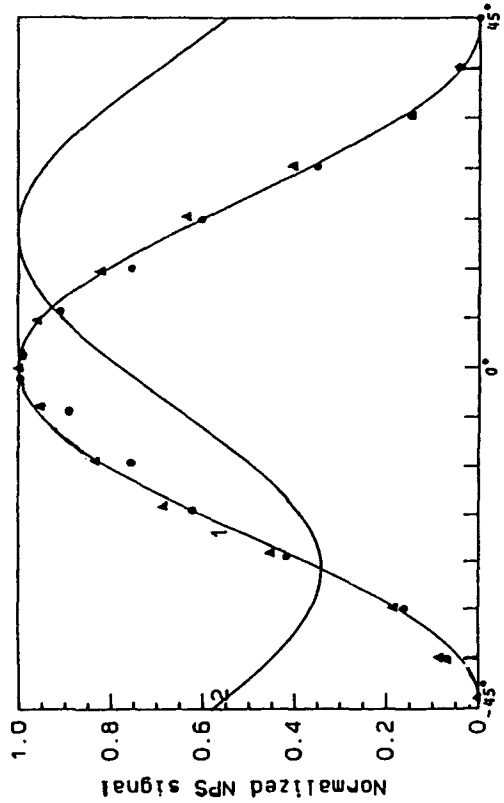


FIG. 1 Pump Beam Ellipticity Angle

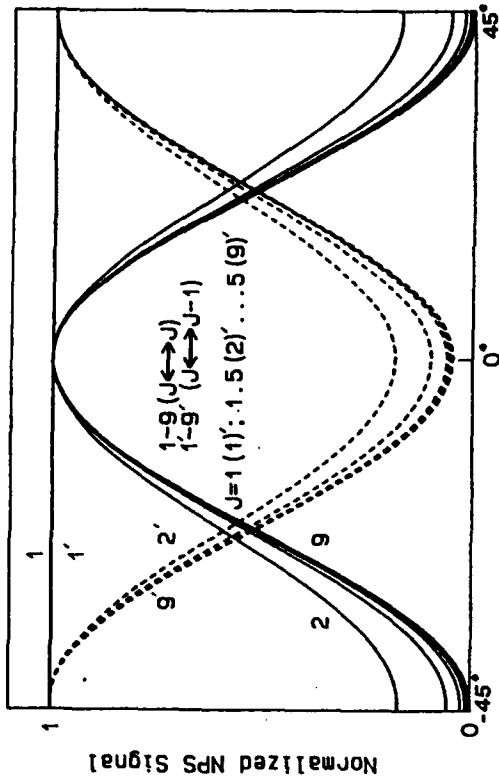


FIG. 2 Pump Beam Ellipticity Angle

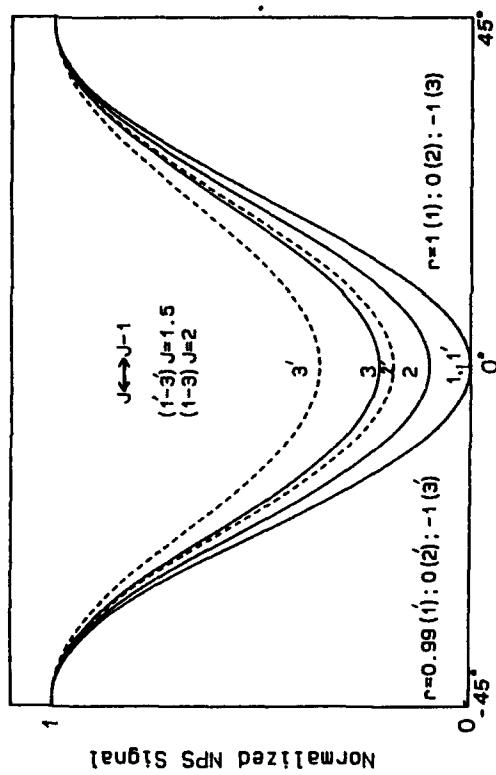


FIG. 3 Pump Beam Ellipticity Angle

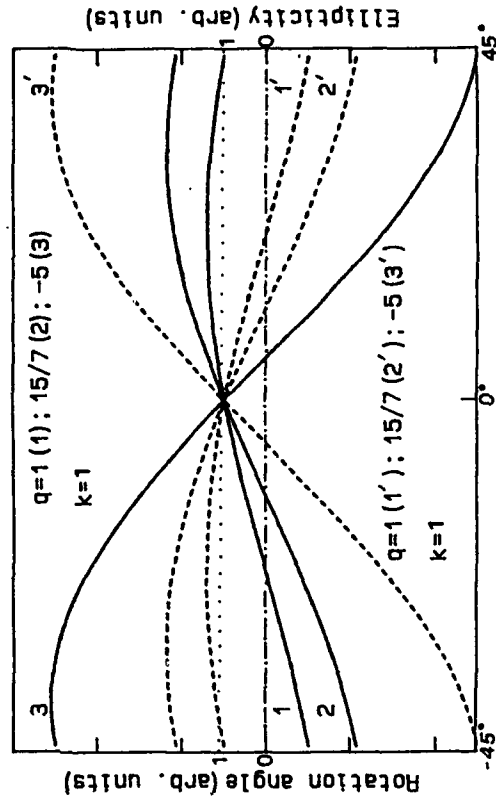


FIG. 4 Pump Beam Ellipticity Angle

Figs. 1-4. Pump beam ellipticity angle dependence of the indicated parameters. The symbols are defined in the text.

The Very High Resolution Spectrometer at the National Institute of Standards and Technology

John Fortna, Harry Morgan, Hailemichael Seyoum, University of the District of Columbia, Araya Asfaw, Howard University, Bldg 245, Rm B119, National Institute of Standards and Technology, Gaithersburg, MD 20899, 301-975-4527

David C. Humm, Division of Natural Science and Mathematics, Saint Mary's College of Maryland, Saint Mary's City, MD 20686, 301-862-0343

Mitchell L. Furst and Lanny R. Hughey, Bldg 245, Rm B119, National Institute of Standards and Technology, Gaithersburg, MD 20899, 301-975-6372

Of seven very high resolution spectrometers in the United States and Japan, two utilize electron storage ring light sources and provide photoelectric scanning of the vacuum ultraviolet spectrum.¹ These are the 6.65 m off-plane Eagle instrument connected to the Synchrotron Ultraviolet Radiation Facility storage ring at the National Institute of Standards and Technology (NIST)^{2,3} in Gaithersburg, Maryland, and the other is a similar instrument connected to the synchrotron at the Photon Factory in Tsukuba, Japan. The NIST spectrometer (Fig. 1) uses a 4800 l/mm gold-coated spherical mirror grating blazed at 900 Å with a radius of curvature of 6.65 m and a ruled area of 125 mm x 110 mm. The spectrometer uses this grating in the first order and at present has a full width half maximum resolution of ~10 mÅ and uses horizontal slits.

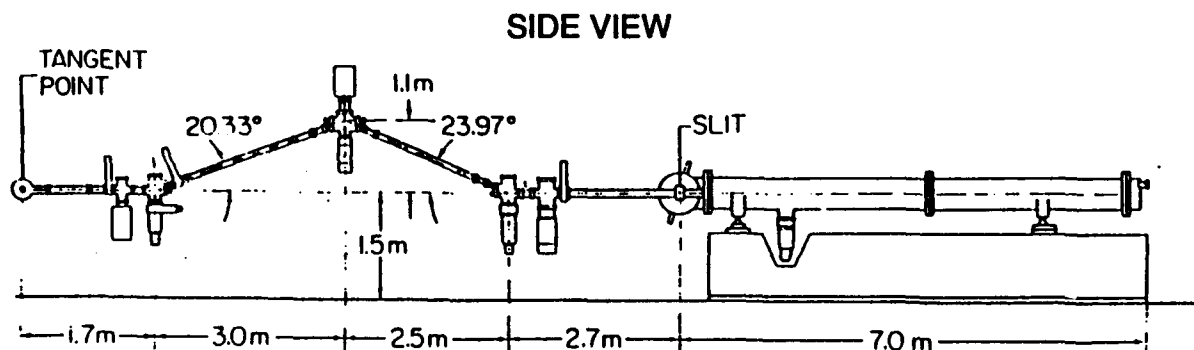


Figure 1

The beamline to the spectrometer entrance slit includes three silicon dioxide focusing mirrors at about 70° to 80° angle of incidence to provide both horizontal and vertical convergence of the beam at the f /number of the instrument, about $f/16$. The radiation is essentially horizontally polarized. The exit slit is the entrance to a 11.43 cm length absorption cell. With entrance and exit slits set at ~20 μm and the exit slit masked to 0.5 mm, the cell detector records about 10⁴ counts per second vacuum. Another, heated, absorption cell in front of the entrance slit is being designed. The entire volume of the spectrograph can be used as a 13.30 m length absorption cell.

Undergraduate students under NSF support help operate the instrument and the recording and on-line realtime presentation of its data through the control of a personal computer.

High resolution scans have been taken in absorption of Ar I in first order of the Beutler-Fano Rydberg window resonances at 466 - 424 Å and the Rydberg series at 876 - 786 Å, and of N2 and O II at 832, 833 and 834 Å.

Figure 2 shows the singly excited Rydberg series (Beutler-Fano window resonances) in Ar I converging onto the $3s3p^6\ ^2S_{1/2}$ level of Ar II. The resonances are associated with the $3s^23p^6\ ^1S_0 - 3s3p^6np\ ^1P_1$ series.⁴ The peaks included in the figure start at $n=16$ and can be seen through $n=29$. Resonances through $n=33$ (Fig. 3) can be seen on scans at longer count integration times and higher wavelength resolution. The feature at the series limit is the two electron resonance $3s^23p^6\ ^1S_0 - 3s^23p^4(^3P)4s(^2P_{1/2})4p$ at 424.23 Å.

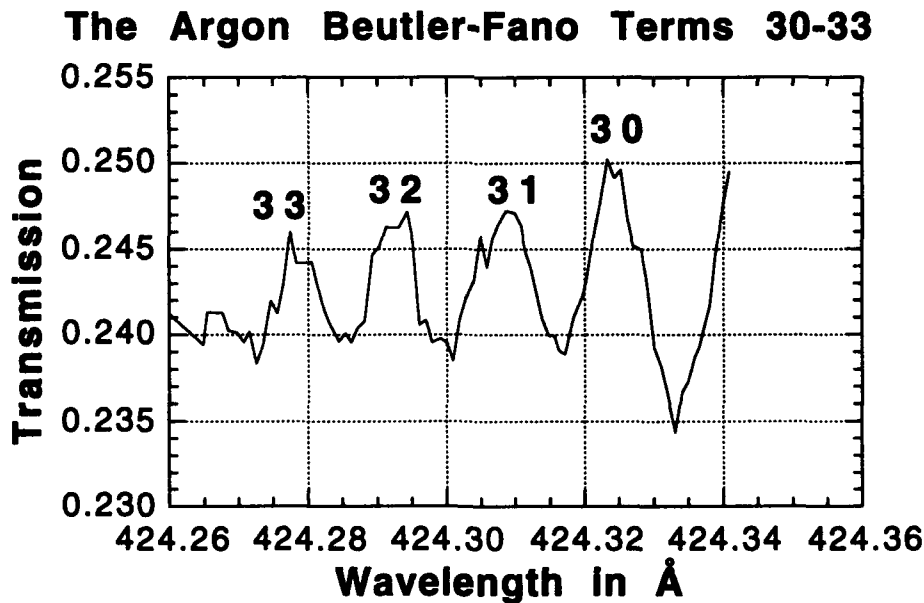
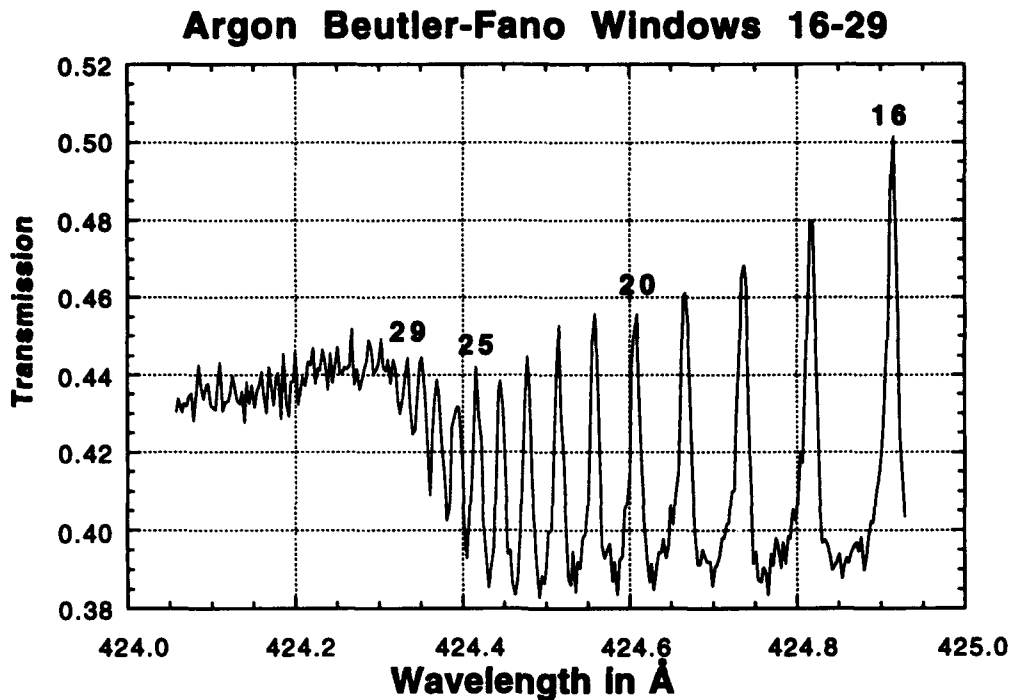


Figure 4 shows the $n=10$ transition at 426.89 \AA of the series in Fig. 2. The weaker feature at 826.99 \AA is the two electron resonance $3s^23p^6 \ ^1S_0 - 3s^23p^4(3P)4s(2P_{3/2})4p^4$ a separation of 100 m\AA , or about 10 times the resolution of the instrument. The "swelling" on the long wavelength side of the $n=10$ one electron resonance may be due to upper state $j-j$ coupling to the 1P_1 and the 3P_1 upper states of the two electron excitation.

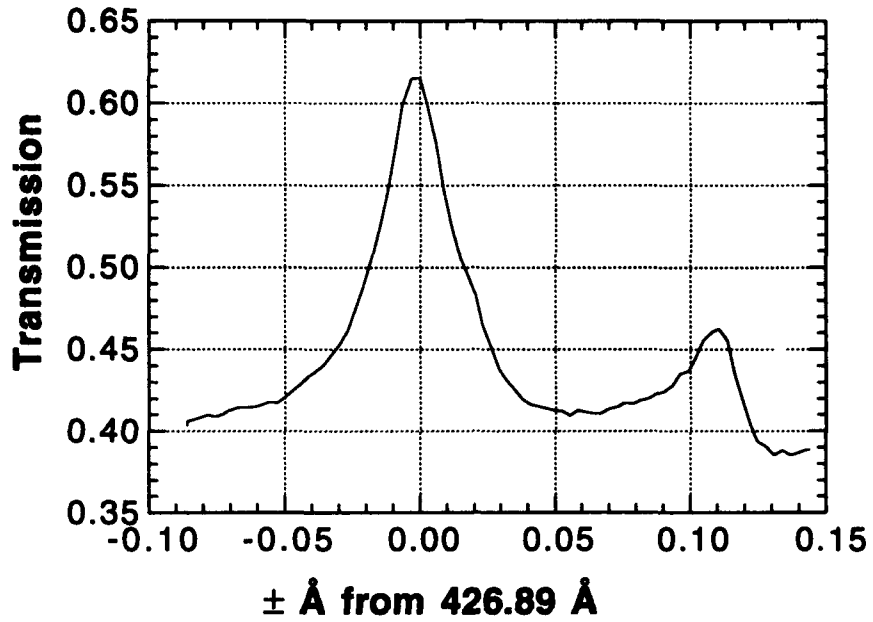
Beutler-Fano Window $n=10$ and $2e^-$ Resonance

Figure 4

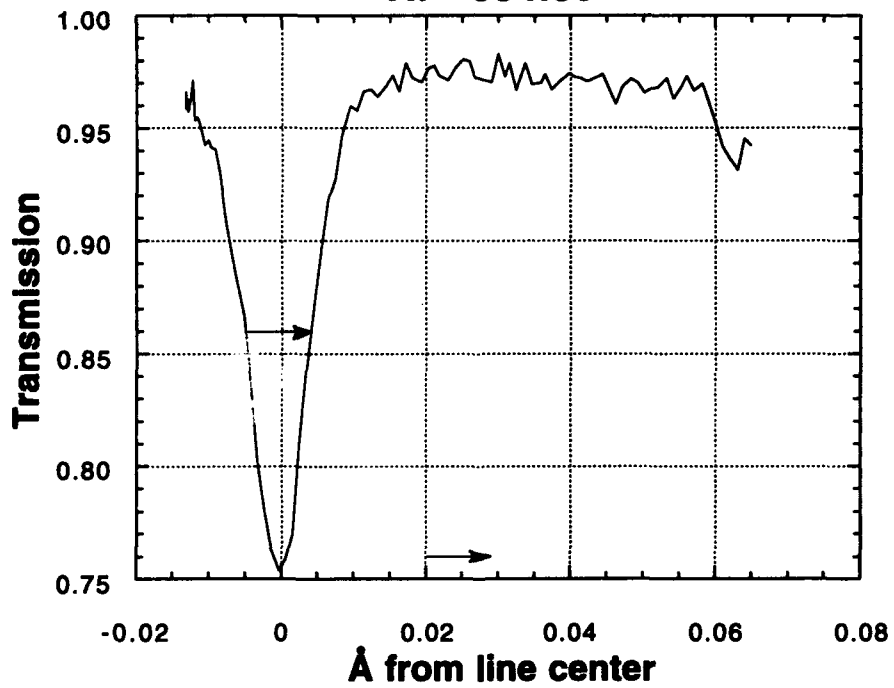
Ar 834.39

Figure 5

Figure 5 shows the $3s^23p^6\ ^1S_0 - 3s^23p^54d(3/2)_1^0$ member of the Ar I Rydberg series in absorption at $834.390\ \text{\AA}$ used as a wavelength calibration. The full width at half maximum measures $\sim 10\ \text{m\AA}$.

Figure 6 shows the highly resolved rotational transitions of N_2 in the $832\text{-}834\ \text{\AA}$ region of the spectrum. The locations reported by various investigators^{5,6,7,8} of the $834\ \text{\AA}$ member of the O II triplet are indicated by arrows, and the values of the N_2 absolute absorption cross-sections read at these points may be seen to vary significantly from one another. The separation of the N_2 rotational lines at $834\ \text{\AA}$ is about $20\ \text{m\AA}$.⁹

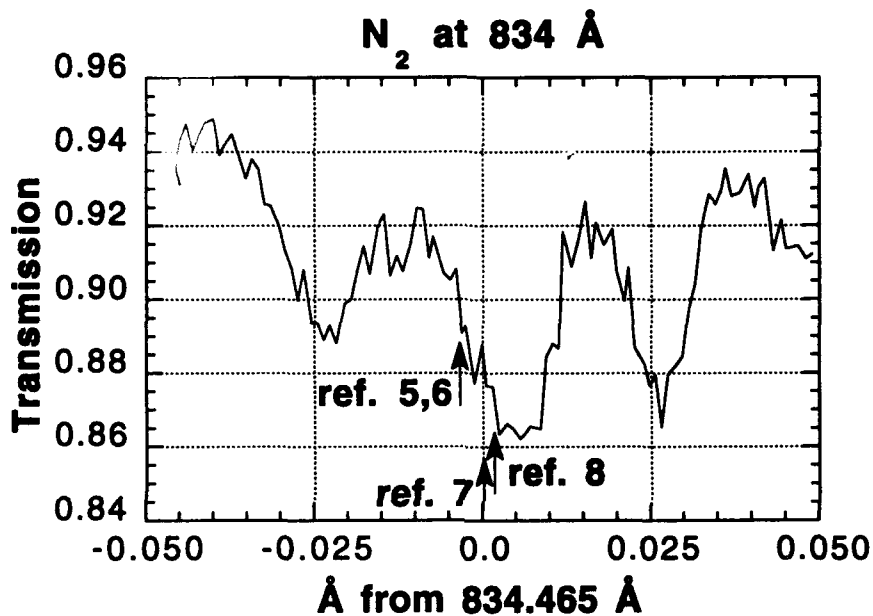


Figure 6

References

1. Ginter, M. L., Nucl. Instr. Meth., **A246**, 474 (1986).
2. Brown, C. M. and M. L. Ginter, Appl. Optics **23**, 4034 (1984).
3. Orth, F. B., M. L. Ginter, K. Yoshino and C. M. Brown, Appl. Optics **25**, 2218 (1986).
4. Madden, R. P., D. L. Ederer and K. Codling, Phys.Rev., **177**, 136 (1968).
5. Moore, C. L., Atomic Energy Levels as Derived From the Analyses of Optical Spectra, vol. 1, 48, U. S. Dept. of Commerce NTIS (1948).
6. Kelly, R. L., and L. J. Palumbo, Atomic and Ionic Emission Lines Below 2000 Angstroms; Hydrogen Through Krypton, 48 (U. S. Govt. 1973).
7. Yoshino, K. private communication, May (1992).
8. Zaidel', A. N. and E. Ya. Shreider, Vacuum Ultraviolet Spectroscopy, transl. by Z. Lerman, Halsted Press (1970).
9. Asfaw, Cleary, Humm, Morgan, Seyoum, Fortna, in publication.

Precise pulsed laser spectroscopy in the visible and far uv region: toward the measurement of the 1^1S - 2^1S interval in atomic helium

S. Gangopadhyay, N. Melikechi and E.E. Eyler
 Department of Physics and Astronomy
 University of Delaware, Newark, DE 19716
 Phone: (302) 831-3517

Precise optical measurements have so far been conducted mainly in the visible and near-uv part of the spectrum. Extension to the far uv region depends on the development of tunable coherent sources that provide high resolution, accurate wavelength metrology, and a large photon flux. As part of our ongoing effort to measure the ionization energy of atomic helium by two-photon excitation at 120.28 nm, we have developed improved methods for generating vuv radiation in the vicinity of 120 nm, and for accurately measuring the systematic frequency shifts that occur during amplification and nonlinear mixing of nanosecond laser pulses.

1. Frequency evolution of nanosecond pulse-amplified laser radiation and harmonic generation:

Pulsed amplification of single-mode lasers can cause both frequency shifts and time-dependent frequency chirps, since the gain and index of refraction of the amplifying medium are strongly time-dependent. We have begun a systematic investigation of these effects with the dual aim of understanding their origins and of reducing their impact on high-precision pulsed-laser spectroscopy.

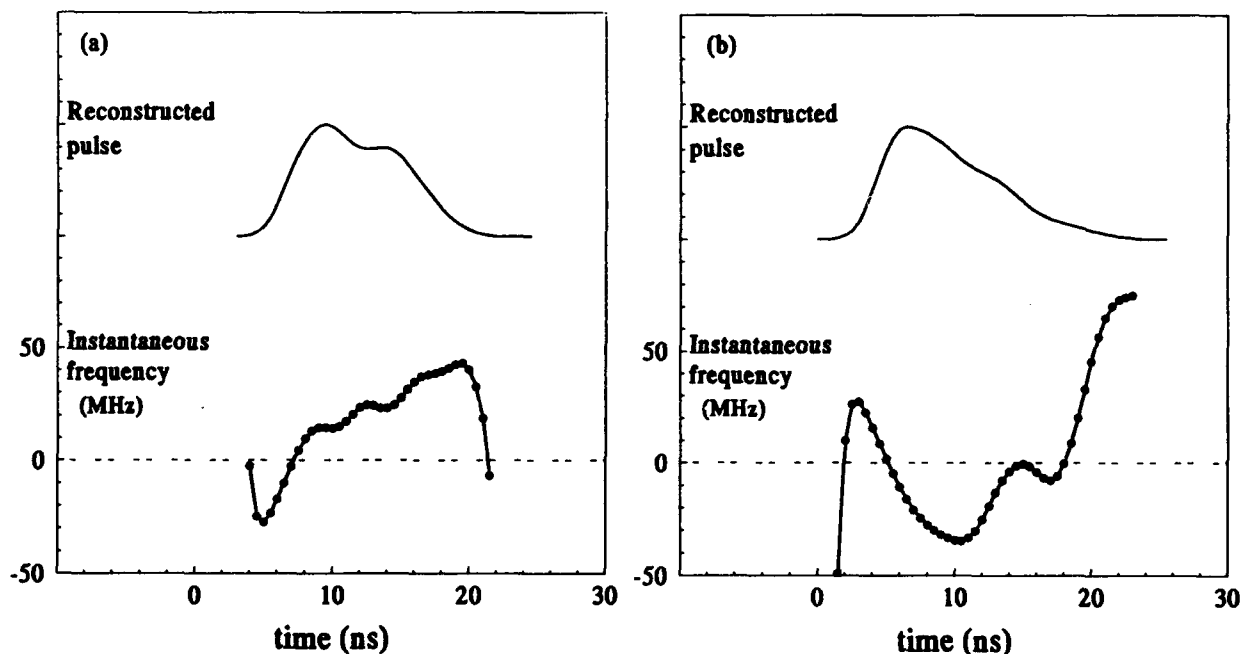


Fig. 1. Excimer-pumped pulsed dye amplifier: (a) two-cell chain, and (b) three-cell chain.

copy. Our experimental technique is similar to that developed by Fee, Danzmann and Chu.¹ The output of a single-mode cw ring dye laser is amplified in a series of dye cells pumped by either an excimer or a Nd:YAG laser. The resulting pulses are mixed with a frequency-shifted sample of the cw laser on a fast photodetector. The beat note is processed in the Fourier domain to obtain the phase and instantaneous frequency of the pulsed laser radiation.

We have extensively investigated the effects of amplifier chains constructed from two or three transversely pumped dye cells for wavelengths around 640 nm, and are currently undertaking a similar study for Bethune-type capillary dye cells. Each of the first two cells is pumped by about 10% of the pump beam, and the balance pumps the third cell when it is used. In the two-cell case,

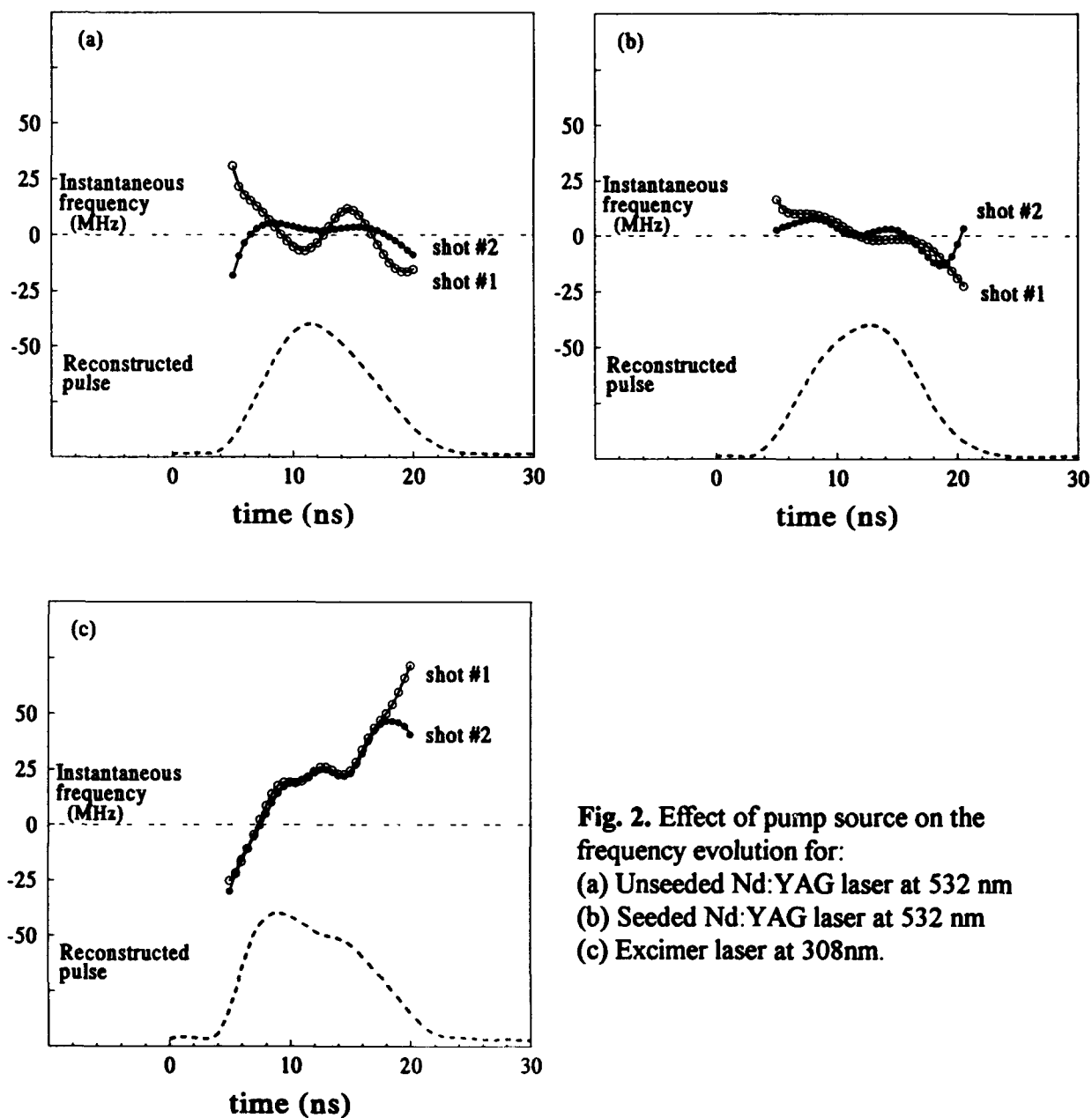


Fig. 2. Effect of pump source on the frequency evolution for:
 (a) Unseeded Nd:YAG laser at 532 nm
 (b) Seeded Nd:YAG laser at 532 nm
 (c) Excimer laser at 308 nm.

the frequency spectrum typically is shifted to the blue by about 20 MHz (Fig. 1(a)); in the three cell case, we see a red shift whose magnitude depends strongly on the alignment of the amplifier (Fig. 1(b)). This suggests that thermal effects alone cannot account for shifts and chirps in dye laser amplifiers. Depending on the alignment, considerable chirping of the frequency is seen as well.

There are substantial differences in the behavior of the instantaneous frequency and in shot-to-shot repeatability depending on the pump source. Shot-to-shot variations in the instantaneous frequency cover a range of up to 30 MHz for an unseeded Nd:YAG pumped amplifier. For pumping with an injection-seeded Nd:YAG laser or an excimer laser, these variations are reduced by a factor of 10 to 15 (Fig 2).

To study the time-dependence of pulsed second harmonic radiation, we frequency-double the pulse-amplified laser radiation in a KDP crystal. At the same time, cw uv radiation is obtained by intra-cavity frequency doubling of the single-mode ring dye laser, and a beat signal between the two uv beams is recorded. By acquiring both uv and visible beats under the same experimental conditions, we can directly compare the measured uv frequency behavior with predictions obtained by squaring the electric field of the measured visible signal.

We have observed that at low second-harmonic conversion efficiency, about 6%, the measured uv time-dependent frequency behavior matches that of the square of the visible pulse to within 3 MHz. Also, the observed and predicted pulse profiles match within 3%. However, as the conversion efficiency approaches saturation, about 10–15%, the measured uv pulse is broader than the predicted by 15 to 20%, and the time evolution of the instantaneous frequency is slightly altered, as shown in Fig. 3.

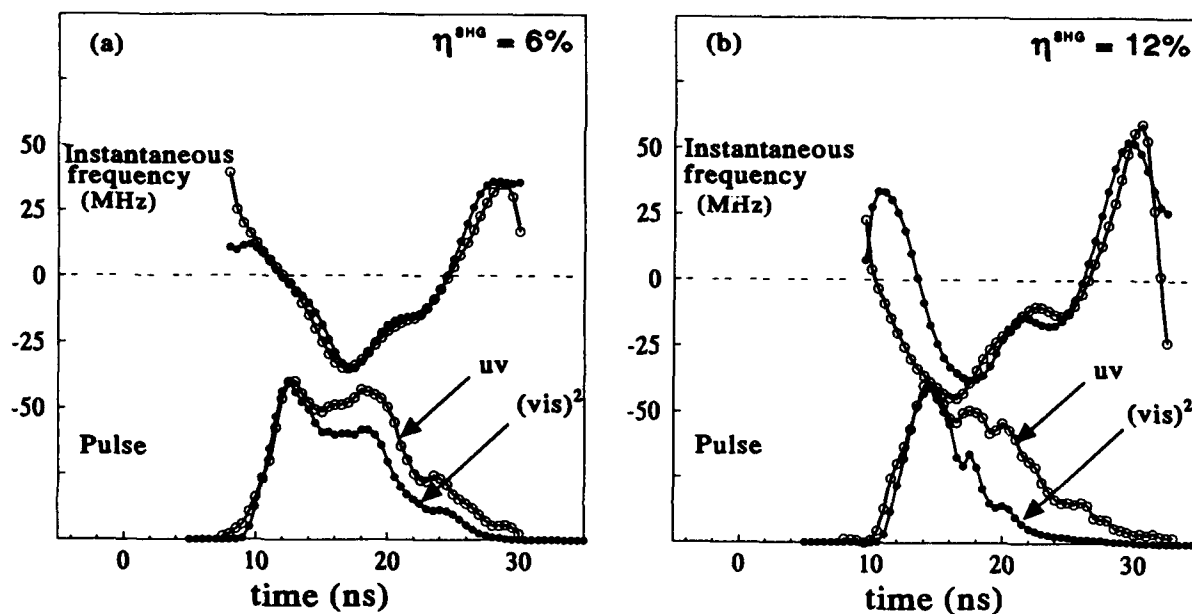


Fig. 3. Predicted ($(vis)^2$) and measured (uv) pulse shape and instantaneous frequency for a conversion efficiency of (a) 6%, and (b) 15%.

This is the first observation of the frequency evolution of uv radiation produced by doubling of a laser pulse in KDP. At laser intensities high enough for the doubling conversion efficiency to approach saturation, we observe appreciable deviations from the pulse shape and frequency evolution predicted from the measurement of the input pulse.

2. Progress towards measuring the 1^1S - 2^1S interval in atomic helium:

Recently, Sansonetti and Gillapsy² at NIST and Lichten, Shiner and Zhou³ at Yale have measured the 2^1S ionization potential of helium. The results reported agree to 9 digits with a small discrepancy of 3σ . In order to test our understanding of QED in multi-electron systems and encourage further theoretical work, a measurement of the 1^1S - 2^1S interval is in progress both at NIST and in our laboratory. This interval was last measured by Herzberg⁴ in 1958 to an accuracy of 0.15 cm^{-1} . Recent improvements in the theory made by Morgan *et al.*⁵ have reached an accuracy of to 0.002 cm^{-1} . Our goal is to improve on Herzberg's measurement and to ultimately match the theoretical accuracy.

We plan to measure the 1^1S - 2^1S interval using two-photon laser excitation at 120.28 nm. The key to this experiment is the production of intense narrowband vuv radiation at this wavelength. Recently, Strauss and Funk⁶ have reported a scheme for the generation of vuv radiation using resonant four-wave difference frequency mixing in molecular hydrogen. By mixing a dye laser radiation in the visible part of the spectrum with a 193 nm excimer laser in a hydrogen cell, they were able to generate vuv radiation in the range 117-150 nm. We have developed a similar scheme that has the advantage of using pulsed dye lasers, operating in the convenient red spectral region. One operating at a fixed 606 nm wavelength and the other tunable in the visible red region. The first laser is used to produce uv radiation that is two-photon resonant with the $\nu=0$, $N=0$ level of the EF state. The required 202 nm is generated by frequency tripling of 606 nm light, using frequency doubling in KDP and sum-frequency mixing in BBO. The second laser is a pulse-amplified cw laser tunable around 636 nm. The two beams are mixed in a molecular hydrogen cell and the vuv radiation is detected in an NO ionization cell. This allows for the quantitative detection of vuv radiation in the range 112-134 nm. With input powers of only about 10 kW at 202 nm and 500 kW for the tunable radiation, we obtain a conversion efficiency of about 10^{-5} . Detailed calculations show that about 1-10 W of vuv radiation at 120.28 nm is sufficient to detect a two-photon resonant, three photon ionization helium signal. Currently we are improving the arrangement by increasing the input pulse energies and by using Bethune-type dye amplifiers, giving a much-improved spatial mode.

References:

- ¹M.S. Fee, K. Danzmann and S. Chu, *Phys Rev. A* **45**, 4911 (1992)
- ²Sansonetti and J.D. Gillapsy, *Phys. Rev. A* **45**, 1 (1992)
- ³W. Lichten, D. Shiner, and Z.-X. Zhou, *Phys Rev A* **43**, 1663 (1991)
- ⁴G. Herzberg, *Proc. Roy. Soc. Ser A* **248**, 309 (1958)
- ⁵J. D. Morgan III, J.D. Baker, R.C. Forrey, R.N. Hill, M.Jeziorska, and J. Shertzer, *Bull. Am. Phys. Soc.* **37**, 1089 (1992)
- ⁶C.E.M. Strauss and D.J. Funk, *Opt. Lett.* **16**, 1192 (1991)

Thursday, January 21, 1993

Laboratory Astrophysics

ThA 8:00am–9:45am
Salon D

John H. Lacy, *Presider*
University of Texas

Carbenes in the Interstellar Gas

Patrick Thaddeus
Harvard-Smithsonian Center for Astrophysics
Cambridge, MA 02173

Carbenes are a significant trace constituent of the gas in the interstellar medium (and in the expanding shell around at least one star), representing about one-sixth of the molecular species that have been identified in space. The identification of one of the most abundant and widespread interstellar carbenes, the cyclopropenylidene ring, C_3H_2 , is described, together with recent laboratory work on the excited vibrational states of this molecule and on the geometrical structure of one of its isomers, the carbon chain carbene H_2C_3 . A number of additional free carbines which might be detected in space are considered. There are at least two reasons why carbenes are comparatively conspicuous in astronomical sources relative to other reactive molecules: one is their high polarity; a second is their production via the same ion-molecule reactions that make known stable species in space (or very similar reactions). Finally, it is pointed out that cumulene carbon chains somewhat longer than those so far detected in space are promising candidates for the carriers of the interstellar optical diffuse bands.

Infrared Laser Spectroscopy of Jet-Cooled Carbon Clusters:

The Structure and Spectroscopy of $^3\Sigma$ C₆

Hyun-Jin Hwang, Alan K. Van Orden, Keiichi Tanaka, Erica W. Kuo, James R. Heath, and Richard J. Saykally

Department of Chemistry, University of California, Berkeley, CA 94720
(510)642-1047

I. Introduction

Carbon clusters have been of interest for many years due to their astrophysical importance and their role in the chemistry of high temperature, carbon-rich environments.¹ Recent experimental and theoretical studies have been highly successful in elucidating the structure and bonding of small carbon clusters containing an odd number of atoms. The picture which has emerged is that odd clusters of three to nine atoms possess linear $^1\Sigma$ ground electronic states with cumulenenic bonding. One of the most fascinating characteristics of these odd clusters is their unusual bending motion. C₃, for example, has long been known to possess an extraordinarily low frequency, high amplitude bending mode, and indeed all of these linear chains are characterized by low bending frequencies.

The situation for even numbered carbon clusters containing four to ten atoms is less complete. *Ab Initio* theory predicts two low energy structural isomers - a $^3\Sigma$ linear chain and a singlet cyclic ring.¹ While all of the small odd clusters have been well characterized spectroscopically, until recently only the triplet form of C₄ had been detected in the gas phase.² No definitive evidence for the cyclic isomer of any even cluster currently exists. In this paper, we report the first gas-phase detection and characterization of the $^3\Sigma$ structure of C₆.

II. Experimental

The Berkeley supersonic cluster beam apparatus for mid-infrared diode laser spectroscopy has been described in detail elsewhere.³ Rotationally cold carbon

clusters are produced by 248nm excimer laser vaporization of graphite followed by expansion of graphite vapor through the slit of supersonic nozzle entrained in a high pressure pulse of argon. The cluster beam expands into a multipass cell where it intersects the path of a diode laser beam. Absorption signals are measured using boxcar detection, and absolute and relative frequency calibrations are performed by simultaneously recording the spectrum of a reference gas and a germanium etalon.

This apparatus produces carbon clusters with rotational temperatures in the range of 20-50K. The ultimate sensitivity is 2-3 parts in 10^5 , and the doppler limited resolution is about 50MHz. The diode laser spectrometer is tunable through 300-3000 cm^{-1} . Spectral features observed so far have occurred in the region of the asymmetric stretch of the linear chains, between 1500 and 2200 cm^{-1} .

III. Results and Discussion

The method described above has been applied to the first gas phase characterization of linear C_4 ,² C_5 ,⁴ C_6 ,⁵ C_7 ,^{3,6,7} and C_9 .⁸ In addition, the bending frequency of C_3 has been measured by far infrared laser spectroscopy in our laboratory.⁹ The bending motion of the longer chains can be characterized indirectly by measuring bending hot bands associated with the asymmetric stretch frequencies. This has been accomplished for C_5 ,¹⁰ C_7 ,³ and, most recently, C_9 .¹¹

The C_6 experiment was guided by the recent assignment of an Ar matrix absorption band to linear C_6 .¹² The region from 1957-1963 cm^{-1} was searched and about 120 absorption lines were observed, among which the 39 strongest lines were assignable to the $\nu_4(\sigma_u)$ asymmetric stretch. Triplet splittings were resolved for the P(5) through R(7) transitions (Figure 1). The experimental data were analyzed using the following Hamiltonian for both the ground and upper states.

$$H = B_v N^2 - D_v N^4 + \frac{2}{3} \lambda_v (3S_z^2 - S^2) + \gamma_v N \cdot S$$

where the first two terms account for the rotational energy, the third term for the spin-spin interaction, and the last term for the spin-rotation interaction. Calculated molecular constants (Table 1) are consistent with inert gas matrix experiments^{12,13} and *ab initio* studies of linear C₆.¹⁴

References

1. Weltner and Van Zee, *Chem. Rev.* **89**, 1713 (1989).
2. J.R. Heath and R.J. Saykally, *J. Chem. Phys.* **94**, 3271 (1991).
3. J.R. Heath and R.J. Saykally, *J. Chem. Phys.* **94**, 1724 (1991).
4. J.R. Heath, A.L. Cooksky, M. Gruebele, C.A. Schmuttenmaer, and R.J. Saykally, *Science* **244**, 564 (1989).
5. H.J. Hwang, A.K. Van Orden, K. Tanaka, E. Kuo, J.R. Heath, and R.J. Saykally, *Mol. Phys.* submitted.
6. J.R. Heath, R. Sheeks, A.L. Cooksky, and R.J. Saykally, *Science* **249**, 895 (1990).
7. J.R. Heath, A. Van Orden, E. Kuo, and R.J. Saykally, *Chem. Phys. Lett.* **182**, 17 (1991).
8. J.R. Heath and R.J. Saykally, *J. Chem. Phys.* **93**, 8392 (1991).
9. C.A. Schmuttenmaer, R.C. Cohen, N. Pugliano, J.R. Heath, A.L. Cooksky, K.L. Busarow, and R.J. Saykally, *Science* **249**, 897 (1990).
10. Moazzen-Ahmadi, McKellar, and Amano, *J. Chem. Phys.* **91**, 2140 (1989).
11. A.K. Van Orden, H.J. Hwang, E. Kuo, and R.J. Saykally, To be published.
12. Martin, Francois, and Gijbels, *J. Chem. Phys.* **93**, 8850 (1990).
13. Van Zee, Ferrante, Zeringue, Weltner, and Ewing, *J. Chem. Phys.* **88**, 3465 (1988).
14. Parasuk and Almlöf, *J. Chem. Phys.* **91**, 1137 (1989).

	Ground State ($v_4=0$)	Upper State ($v_4=1$)
$B(\text{cm}^{-1})$	0.048479(10)	0.048410(9)
$D(\text{cm}^{-1})$	$0.22(9)\times 10^{-7}$	$0.30(8)\times 10^{-7}$
$\lambda(\text{cm}^{-1})$	0.1875(16)	0.1854(16)
$\gamma(\text{cm}^{-1})^{\text{a}}$	-0.0001	-0.0001
$\nu_4(\text{cm}^{-1})$		1959.85852(18)

Table 1. Molecular Parameters for the $\nu_4(\sigma_u)$ fundamental of C_6 . Uncertainties in parentheses are 1σ . The standard deviation of the least squares fit was 0.00072 cm^{-1} .

a. γ'' and γ' were fixed to the value from ESR experiments in Ne matrix (Ref.13).

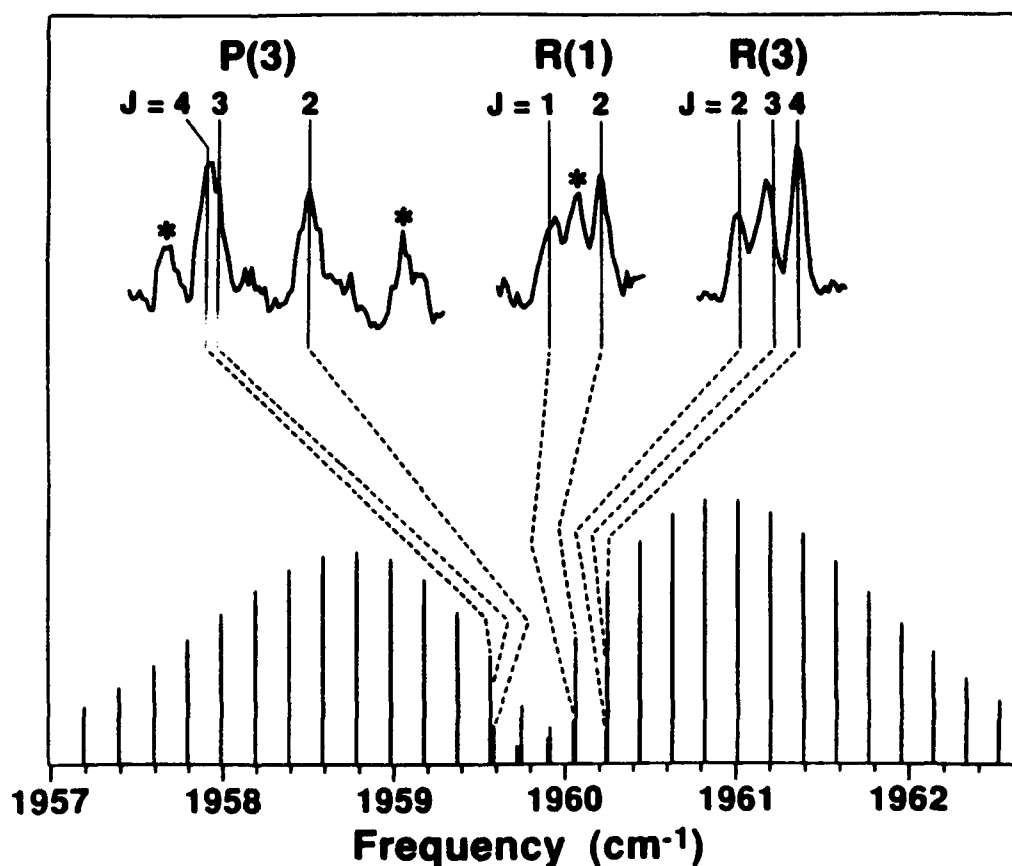


Figure 1. Typical experimental data and a stick spectrum of the $\nu_4(\sigma_u)$ asymmetric stretch fundamental of ${}^3\Sigma \text{C}_6$ calculated from a least square fit of observed frequencies and the estimated rotational temperature of 20K. The lines with asterisks are currently unassigned.

Near-threshold structure of molecular hydrogen at the $1s + 2l$ dissociation limit

E.E. Eyler, B.F. Catching, and N. Melikechi
Department of Physics and Astronomy
University of Delaware
Newark, DE 19716
(302) 831-3517

High-resolution measurements of molecular structure very near a dissociation limit can be used both to probe long-range atomic interactions and to make accurate determinations of dissociation energies. Our research group has investigated the $H(1s) + H(2s \text{ or } 2p)$ dissociation limit in molecular hydrogen using optical double resonance with single-mode lasers. Fig. 1 shows the general scheme of the experiment. Our measurements of bound states in H_2 , reported in Ref. 1, have now been extended to include the adjoining continuum and the other stable isotopomers, HD and D_2 . The most weakly bound levels to which transitions are seen are bound by only about 0.03 cm^{-1} , equivalent to about 40 mK. Very sharp continuum resonances are also observed in the region just above threshold.

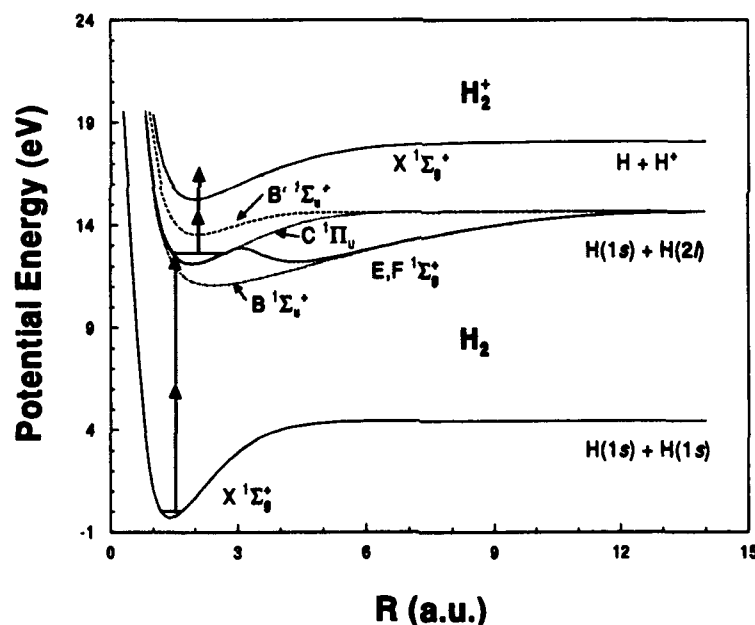


Fig. 1. Potential curves for H_2 , showing scheme for laser double-resonance excitation of near-threshold levels

Bound States

The bound vibrational levels, with outer turning points as large as 200-300 atomic units, would follow a simple pattern of energy level spacings if they could be accurately modeled as adiabatic levels in the B state potential well.² The actual situation is far more complex because of non-adiabatic couplings between the B , B' and C states, and because the atomic fine and hyperfine interactions are comparable in size to the total binding energy. In the H_2 isotope, numerous shifted and "extra" transitions are seen throughout the energy region

within 10 cm^{-1} of the threshold. No quantitative theoretical treatment yet exists, even though the various couplings are individually fairly well understood. Particularly interesting is the hyperfine mixing of *gerade* with *ungerade* levels.³ This perturbation is apparently responsible for the observed splitting of many of the highest bound levels in H_2 into two components spaced by $0.03\text{-}0.1 \text{ cm}^{-1}$.

The bound-state spectrum of D_2 is in general much simpler, as might be expected since the atomic hyperfine interaction is much smaller. No evidence is seen for closely-spaced doublets, nor is there any obvious fine-grained structure in the continuum. One unusual feature is an extremely strong bound-state transition that lies barely below the threshold excited from the $N=1$ level. Altogether 12 high-lying bound states have been measured, of which 3 are unidentified.

The mixed HD isotope is quite interesting. We have studied the threshold region from both the $N=0$ and $N=1$ levels of the EF state, and find strikingly different spectra, with a highly complex many-featured spectrum in from $N=1$ and a nearly featureless spectrum from $N=0$. Variations in the $B\text{-}B'$ configuration mixing are a possible explanation, since most of the adiabatic transition strength is to the B' state but most of the vibrational structure is in the B well. Of the 19 high-lying bound states we observe, 11 are unidentified. The $N=1$ spectrum is shown in Fig. 2.

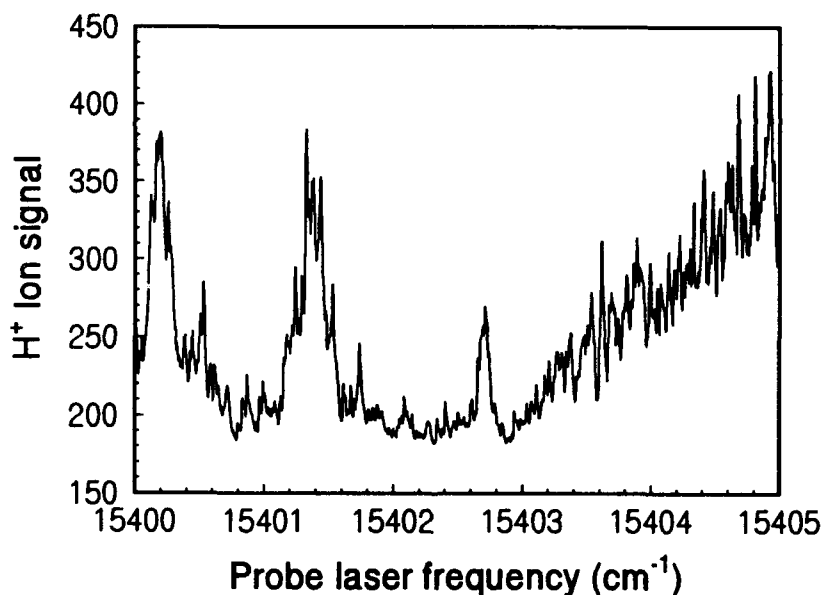


Fig. 2. Spectrum of HD near the $N=1$ dissociation limit. Noise in continuum is due to detector instabilities.

Continuum Structure

We have observed the vibrational continuum using several different detection schemes, including multiphoton ionization of the molecule, Lyman- α fluorescence from $n=2$ H atoms, and resonant multiphoton ionization of H and D atoms. In this last method, a Balmer- α laser is used to ionize the product atoms. When the Balmer- α laser pulse is delayed by 20-30 nsec

only H(2s) atoms are detected, but when it is simultaneous with the dissociation process we see both H(2s) and H(2p) atoms. The sum of 2s and 2p atom production can also be observed when the dissociating laser is sufficiently intense to cause resonant multiphoton ionization on its own. The threshold was investigated for at least two initial rotational levels of the EF state for each of the H_2 , D_2 , and HD isotopomers. In most cases the continuum is weak and appears to consist principally of 2s atoms. The near-threshold cross-sections show considerable deviations from the Wigner threshold law, which predicts a simple E^{2N+1} dependence in the absence of perturbations and shape resonances. In addition to overall deviations from the functional form of the Wigner law, fine-grained interference structure is seen in the H_2 and HD isotopomers. In a few cases, we observe prominent shape resonances associated with quasibound levels of the C state; their widths differ markedly from a recent calculation.⁴

An interesting exception to the typical behavior is the $N=1$ (ortho-hydrogen) threshold in H_2 . Here the continuum is strong, with about the same cross-section as the highest bound levels. Further, the threshold behaviors for H(2s) and H(2p) production are quite different. The region very near threshold is dominated by production of the atomic products H(1s) + H(2p). This 2p atom production has an extremely sharp threshold (of order 0.01 cm^{-1}) apparently associated with the broad long-range $1/R^3$ potential of the $B \ ^1\Sigma_u^+$ state. The B state continuum has a negligible cross-section for adiabatic excitation because of unfavorable Franck-Condon factors, but it can be excited through configuration mixing with the B' or C states. Only about 0.5 cm^{-1} above the continuum edge, production of H(2p) atoms is gradually replaced by H(2s) production, and the 2s channel then continues to dominate the photodissociation spectrum through the rest of the near-threshold region. Fig. 3 shows two scans over this region, one using Balmer- α detection of H(2s) atoms only, and the other using MPI to detect all resonances, including bound states, 2s atoms, and 2p atoms.

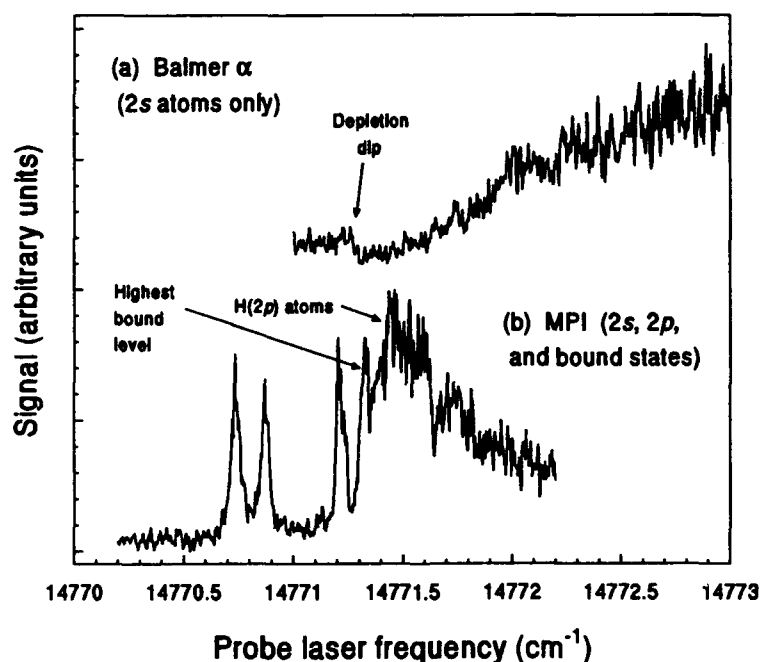


Fig. 3. H(2s) and H(2p) production just above the dissociation limit of H_2 .

Apart from the intrinsic interest of understanding this unexpectedly complex dissociation behavior, the thresholds can be used to determine the dissociation energy D_0 . Despite problems with noise and uncertainties about the functional form of the continuum onset, much-improved values for D_0 have been obtained from our existing data. The most accurate result is for H_2 , for which we obtain a preliminary value of $D_0=36118.039\pm 0.05\text{ cm}^{-1}$, to be compared with the theoretical value of 36118.088 cm^{-1} . All three isotopomers now show excellent agreement between theory and experiment, resolving a previous discrepancy. Our results also agree with highly accurate new measurements for the H_2 isotopomer by Stoicheff's group,⁵ who recently measured the $2s$ continuum by direct vuv single-photon excitation. These experimental values for D_0 are still far less accurate than our recent measurements of the ionization potentials, but are nevertheless sufficiently accurate to rigorously test the theory of relativistic and radiative corrections (of order 0.5 cm^{-1}) for this molecular system.

In cases where the threshold is extremely sharp, like the $N=1$ threshold for $2p$ atom production in H_2 , the current accuracy is limited only by technical problems. When MPI detection is used there is a problem with undesired overlap of bound-state lines with the continuum, and when resonant two-photon ionization by a Balmer- α laser is used, the threshold is shifted and broadened by the laser-induced broadening of the $H(2p)$ state. This problems can be eliminated using a somewhat different detection scheme, which we plan to adapt in our next runs.

This new arrangement will employ narrowband single-photon excitation of $H(2s$ or $2p)$ atoms to high Rydberg states, followed by pulsed field ionization. Since very little laser power is required for single-photon excitation of bound Rydberg states, this should permit a quantitative high-resolution study of cross sections for formation of atoms in each fine structure level. An absolute accuracy of 0.001 cm^{-1} for the dissociation energy is not unthinkable in a few years.

Outlook

A full coupled-state calculation will probably be necessary to fully understand these spectra. Configuration mixing, fine-structure perturbations, and hyperfine perturbations all play a major role. Even though the interaction of two hydrogen atoms is in some sense the simplest and best-understood molecular coupling, the very light mass and near-degeneracy of the atomic energy levels add complexity to the problem. It is fortunate that the sharpness of the dissociation threshold permits accurate determinations of the dissociation energies without a full understanding of the bound-state spectrum. We are particularly interested in using similar methods to investigate levels near the ion-pair threshold, where Rydberg-like states of the $H^+ + H^-$ system should be observable if the molecule is excited with sufficiently large internuclear separation. Similar techniques should also be applicable in other small molecules.

¹E. McCormack and E.E. Eyler, *Phys. Rev. Lett.* **66**, 1042 (1991).

²W.W. Stwalley, *Chem. Phys. Lett.* **6**, 241 (1970).

³J.P. Pique, F. Hartmann, S. Churassy, and R. Bacis, *J. Physique* **47**, 1909 (1986).

⁴J.R. Burciaga and A.L. Ford, *J. Mol. Spectrosc.* **149**, 1 (1991).

⁵A. Balakrishnan, V. Smith, and B.P. Stoicheff, *Phys. Rev. Lett.* **68**, 2149 (1992).

Atoms and Radicals

ThB 10:15am-12:15pm
Salon D

Andrzej W. Miziolek, President
U.S. Army Laboratory

***b*-Dipole Transitions in \tilde{X}^2A' *t*-HOCO Observed by FIR Laser Magnetic Resonance**

Trevor J. Sears¹, H. E. Radford², and Mary Ann Moore²

¹ Author for correspondence; Department of Chemistry, Brookhaven National Laboratory, UPTON, NY 11973. Phone (516-) 282 4374

² Harvard Smithsonian Center for Astrophysics, 60 Garden Street, CAMBRIDGE, MA 02138.

Summary

The HOCO radical is crucially important in combustion chemistry as the intermediate in the reaction between hydroxyl radicals and carbon monoxide. Studies of the temperature dependence of the rate constant for this reaction implied the existence of the radical intermediate¹ but only very recently was HOCO detected in the gas phase^{2,3}. Both the infrared spectrum³, which is due to the perturbed C=O stretching fundamental (ν_2), and the observed rotational spectrum² consist only of *a*-dipole transitions. Such transitions obey the selection rule $\Delta K_a = 0$ in this near prolate top rotor and as such contain no direct information on the spacings between energy levels of different K_a . The high precision of the millimeter wave data allowed an approximate value for the A rotational constant to be derived² however the accuracy with which it is known is much less than for B and C. Nonetheless, when combined with data for DOCO, it was possible to unequivocally attribute the spectra as due to the *trans*- geometrical isomer of the radical².

A more precise structural determination for this species require a more precise estimate of the A rotational constant, however μ_a has been calculated to be approximately half the size of μ_{bb} ⁴ and the *b*- dipole spectrum is sparse at the frequencies accessible using our millimeter wave spectrometer.

FIR laser magnetic resonance (LMR) offers a way around these difficulties being a very sensitive technique with wavelength coverage limited only by the number of accurately measured FIR laser frequencies. We have recorded and assigned LMR spectra of HOCO in its ground state using nine FIR laser lines between 235.6 μm and 669.5 μm . All of the assigned transitions are *b*- dipole in character and are relatively weak. Table I summarises the observations, and figure 1 shows an example of some of the best data, part of the spectrum obtained using the 305.7 μm CH₃OD laser line in parallel polarization. The strong resonances are due to M_j components of

the $J = 17/2 - 15/2$ fine structure component of the $9_{37} - 8_{26}$ rotational transition.

Table I: Summary of FIR Laser Lines Used and Observed Transitions in HOCO

Wavelength/ microns	Gas	Frequency/GHz	Wavenumber/ cm ⁻¹	Observed Transitions ^a
235.6	N ₂ H ₄	1272.6811	42.45207	8 ₄ - 7 ₃
305.7	CH ₃ OD	980.5916	32.70902	9 ₃₇ - 8 ₂₆ , 4 ₄ - 5 ₃
407.3	CF ₂ CH ₂	736.060	24.5523	11 ₂₉ - 10 _{1,10}
444.4	CD ₃ I	674.621	22.5029	10 ₂₉ - 9 ₁₈
461.3	HCOOD	649.9410	21.67970	5 ₃₂ - 6 ₂₅
513.0	HCOOH	584.3869	19.49305	8 ₃₅ - 9 ₂₈ , 5 ₂₃ - 4 ₁₄
515.1	CH ₃ OD	582.0264	19.41431	8 ₃₆ - 9 ₂₇
556.9	CD ₃ I	538.347	17.9573	3 ₂₁ - 2 ₁₂
669.5	HCOOH	447.7650	14.9358	11 ₂₉ - 11 _{1,10}

Footnote to Table I:

a. Notation is N_{K_aK_c}. Where no K_c value is given, the K-doubling was not resolved.

Some weaker components in the spectrum derive from the 4₄ - 5₃ ($J=7/2 - 9/2$) transition which coincidentally occurs at nearly the same zero field frequency in the radical. More typical data is shown in Figure 2 where the resonances on the 444.4 μ m CD₃I laser line are due to components of the 10₂₉ - 9₁₈, $J=21/2 - 17/2$ transition which is forbidden in zero field.

The LMR data have been fitted together with the previously reported millimeter wave observations² which were

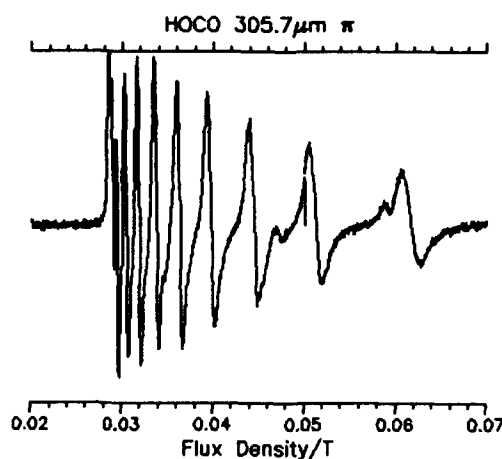


Figure 1: LMR spectrum of HOCO obtained in parallel polarization using the 305.7 micron CH₃OD laser line.

purely a - dipole in character. The molecular constants determined in this process are given in table II. They are significantly better determined than previously and it has been possible to determine values for the K dependent centrifugal distortion constants Δ_K and δ_K for the first time. Previously these had been fixed at values from a force field analysis which relied on *ab initio* estimates of the harmonic vibrational frequencies in the radical. Values of the other rotational and fine structure parameters are slightly modified from their earlier values.

Some of the LMR spectra show evidence of hyperfine splittings, particularly for the largest $|M_J|$ values. Analysis of these together with the fragmentary information available from the millimeter wave work² will give direct information on the electronic wavefunction. LMR spectra of DOCO have also been obtained. Their analysis will similarly improve the determination of the A rotational constant for DOCO and lead to a more accurate determination of the structural parameters for this important species.

Table II: Rotational and Fine Structure Parameters for t-HOCO

a. Rotational and Centrifugal Distortion			
Parameter	Value/cm ⁻¹	Parameter	Value/cm ⁻¹
A	5.5960782(64) ^b	$10^6 \Delta_N$	0.3303(18)
B	0.3813800(21)	$10^5 \Delta_{NK}$	-0.9882(11)
C	0.3564640(21)	$10^3 \Delta_K$	0.78689(33)
		$10^7 \delta_N$	0.410(11)
		$10^5 \delta_K$	0.367(89)
		$10^8 \Phi_{KN}$	-0.469(16) ^c

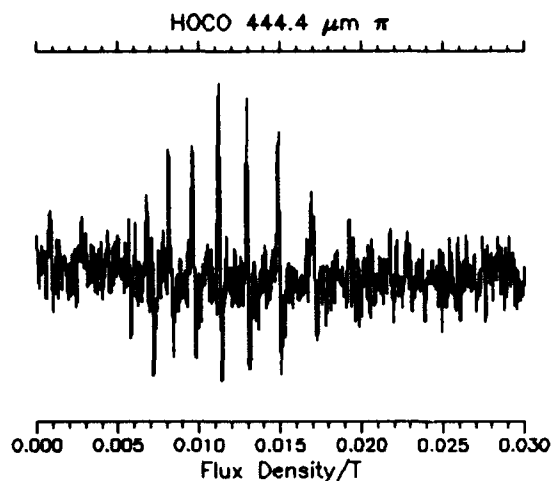


Figure 2: LMR spectrum obtained using the 444.4 μm CD₃I laser line.

Table II b. Spin-Rotational

Parameter	Value/cm ⁻¹
$10(\epsilon_{aa} + \epsilon_{bb} + \epsilon_{cc})^d$	0.510666(27)
$(2\epsilon_{aa} - \epsilon_{bb} - \epsilon_{cc})$	0.103919(53)
$10^2(\epsilon_{bb} - \epsilon_{cc})$	0.1234(17)
$10^4 \Delta_K^2$	-0.1802(70)

Footnotes for Table II:

- a. From a fit to 122 rotational transitions including 52 millimeter wave observations² and a representative sample of LMR data, appropriately weighted.
- b. Numbers in parenthesis are one standard deviation of the fit in units of the last quoted significant figure.
- c. All other sextic and higher centrifugal distortion parameters fixed at zero.
- d. Spin rotation tensor components are $\epsilon_{aa} = 0.051662$, $\epsilon_{bb} = 0.000320$, and $\epsilon_{cc} = -0.000915$. All other quartic and higher spin rotational parameters fixed at zero.

References

1. M. J. Frost, P. Sharkey and I. W. M. Smith, *Farad. Disc. Chem. Soc.* **91**, 305 (1991).
2. H. E. Radford, W. Wei and T. J. Sears, *J. Chem. Phys.* **97** 3989 (1992).
3. T. J. Sears, W. M. Fawzy and P. M. Johnson, *J. Chem. Phys.* **97** 3996 (1992).
4. A. D. McLean and Y. Ellinger, *Chem. Phys.* **94** 25 (1985).

Acknowledgement

Work at Brookhaven National Laboratory was performed under Contract No. DE-AC02-76CH00016 with the United States Department of Energy and supported by its Division of Chemical Sciences, Office of Basic Energy Sciences.

Infrared Fourier Transform and Diode Laser Spectra of Formaldoxime.

R.Bannai and G. Duxbury,
Department of Physics and Applied Physics,
University of Strathclyde, John Anderson Building,
107 Rottenrow, Glasgow G4 0NG, Scotland, U.K.
Telephone 44-41-552-4400 ext3271
FAX 44-41-552-2891

The infrared spectrum of the simplest oxime, CH_2NOH , was first obtained at low resolution in the gas phase by Califano and Lüttke¹. Subsequent high resolution spectroscopy by Duxbury et al.² and by Duxbury³ demonstrated that although the original vibrational analysis was correct, the directions of the transition moments derived from the analysis of low resolution band contours were not.

In order to extend the high resolution analysis to include the majority of the fundamental bands of CH_2NOH , we have obtained gas phase spectra in the region from 750 to 2000 cm^{-1} using both a Bomem Fourier transform spectrometer (FTS) and a diode laser spectrometer. The ν_4 , ν_5 , ν_6 and ν_8 A:B hybrid bands recorded using the FTS have been analysed in detail to yield both vibrational and rotational constants, and also intensity information related to the transition moments. The ν_7 band has also been partially analysed and has been shown to be predominantly B type rather than the A type inferred from the low resolution spectra¹.

The region of the ν_{11} band at 770 cm^{-1} exhibits a complicated structure. In earlier work², which relied on the interpretation of medium resolution Fourier transform spectra, this was all attributed to the ν_{11} band. However, a combination of higher resolution Fourier transform spectra with Doppler limited spectra obtained using a diode laser spectrometer, has allowed us to determine that the complications arise from the presence of two, almost degenerate, bands. One of these is ν_{11} which is of A" symmetry, and the other is an A:B hybrid band which we believe is due to the $2\nu_{12}$ overtone.

The A type 9Q branches of the latter band are well resolved using in the diode laser spectra. The complex structure observed in this spectral region is then ascribed to Coriolis coupling between these almost degenerate vibrational states, a situation which is known to occur in methyleneimine⁴. This places a value of $\sim 390 \text{ cm}^{-1}$ for the ν_{12} frequency, which is between that of $\sim 420 \text{ cm}^{-1}$ of Califano and Lüttke¹, and of $330 \pm 30 \text{ cm}^{-1}$ deduced by Levine⁵ from the intensity of the lines in the microwave pure rotation spectrum of the lowest frequency vibrational state.

The main results (in cm^{-1}) for the excited states identified in this study are:

Band	Symmetry	Type	ν_0	A	B	C
ν_4	A'	A	1639.477 ₆	2.24380 ₂	0.39349 ₉	0.33443 ₉
ν_5	A'	A	1410.422	2.26329 ₁	0.395582 ₈	0.33490 ₈
ν_6	A'	A	1318.977 ₀	2.26330 ₂	0.397150 ₃	0.335219 ₃
ν_7	A'	B	1157.28 ₂			
ν_8	A'	A	892.580 ₂	2.24368 ₀	0.39351 ₆	0.33450 ₆
$2\nu_{12}$	A'	A:B	778.47 ₅	2.22024 ₉	0.3955 ₈	0.3349 ₁
ν_{11}^2	A''	C	774.14			

It should also be noted that ν_4 is mainly due to the stretching of the $C=N$ bond. The observed frequency in the oxime is very close to that of 1638.298 cm^{-1} of the equivalent bond in CH_2NH^6 , and is a little lower than that of 1725.4 cm^{-1} reported by Jacox⁸ for the $C=N$ stretching frequency of the CH_2N free radical trapped in an argon matrix.

- 1) S. Califano and W. Lüttke, Z. Phys. Chem. 6, 83-104 (1956)
- 2) G. Duxbury, R.M. Percival, D. Devoy and M.R.M. Mahmoud, J. Mol. Spectrosc. 132, 380-392 (1988)
- 3) G. Duxbury, J. Mol. Spectrosc. 132, 393-406 (1988)
- 4) L. Halonen and G. Duxbury, J. Chem. Phys. 83, 2078-2090 (1985)
- 5) I.N. Levine, J. Mol. Spectrosc. 8, 276-284 (1962)
- 6) G. Duxbury, H. Kato and M.L. Le Lerre, Faraday Discuss. Chem. Soc. 71, 97-110 (1981)
- 8) M.E. Jacox, J. Phys. Chem 91, 6595-6600 (1987)

ULTRA-NARROW VELOCITY DISTRIBUTIONS OF SLOW ATOMS PRODUCED WITH THE ZEEMAN TUNING TECHNIQUE

S.C. Zilio and V.S. Bagnato

Instituto de Física e Química de São Carlos
Universidade de São Paulo
Caixa Postal 369, 13560-970 São Carlos, SP, Brazil

We report on the use of a stimulated Raman transition in a slowed atomic beam to produce a narrow velocity distribution of atoms in a selected electronic state, which could be used for atomic collisions studies in the low temperature regime⁽¹⁾. The velocity selection is part of the deceleration process and in this sense it is unique. The atomic beam is decelerated by the radiation pressure force exerted on the atoms by a counter-propagating laser beam. The resonance condition is maintained along the deceleration path because the changing Doppler shift is compensated by Zeeman tuning the electronic sublevels⁽²⁾ with a spatially inhomogeneous magnetic field. At the end of the slowing process, the initial Maxwell-Boltzmann distribution is compressed to a narrow velocity distribution ($\Delta v \sim 50$ m/s), centered close to $v = 0$. This velocity bunching⁽³⁾ increases considerably the number of atoms in each velocity class, allowing the use of velocity selection techniques as a feasible way of studying low velocity collisions.

Our experimental set-up has been fully described elsewhere⁽⁴⁾ and no details will be presented here. The slowing dye laser (power, 200 mW) is circularly polarized and tuned to the cooling transition $3S_{1/2}$ ($F = 2, m_F = 2$) \rightarrow $3P_{3/2}$ ($F' = 3, m_{F'} = 3$) of the sodium atom. A second dye laser (power, 30 μ W) crosses the atomic beam at an angle θ ranging from 2° to 60° , 30 cm after the solenoid end and the fluorescence at the crossing position allows one to monitor the velocity distribution and the population in each of the $3S_{1/2}$ ground state hyperfine sub-levels. The solenoid produces a field which in the deceleration

region is given by $B(z) = \{ 7.8 + 27 [1 - 0.01 (z - 20)^{\frac{1}{2}}] \} I$. At a low magnet current (≤ 30 A) the decelerating atoms follow the magnetic field adiabatically⁽⁶⁾ and at the end of the solenoid (small B) they are optically pumped to the $3S_{1/2}$ ($F = 1$) ground state hyperfine sub-level. Then, they stop interacting with the slowing laser.

A high resolution measurement of the peak of slow atoms in the $F = 1$ ground state presents the structure shown in Fig. 1. The broad bands (a, b and c) correspond to transitions between $3S_{1/2}$ ($F = 1$) and $3P_{3/2}$ ($F' = 1, 2$) levels at a position where the magnetic field is 10 G. As the probe laser is scanned through these transitions, the atoms are pumped back to the $F = 2$ ground state and come into resonance with the strong slowing laser, giving rise to the observed signal. The narrow peak (d) occurs in a frequency close to the transition $3S_{1/2}$ ($F = 1$) \rightarrow $3P_{3/2}$ ($F = 3$), which is not dipole allowed. Besides, its linewidth is subnatural, as shown in Fig. 2(a), suggesting that it comes from a stimulated Raman transition involving a Λ system composed of the two ground states and the $3P_{3/2}$ ($F' = 3$) excited state (Fig. 2(c)). The Raman process transfers the population from $F = 1$ to $F = 2$ and once the atom is again resonant with the strong slowing laser, it scatters many photons in the $3S_{1/2}$ ($F = 2$) \rightarrow $3P_{3/2}$ ($F' = 3$) transition before being repumped back to the $F = 1$ ground state. Since the transition $F = 1 \rightarrow F' = 3$ is not dipole allowed, the saturation is very high⁽⁶⁾ and the Raman transition is observed even when the slowing laser power is above 300 mW. For the usual stimulated Raman process involving allowed transitions in sodium, a low power (in the μW range) has to be used, otherwise the power broadening does not allow its observation.

For the resonant Raman transition described above only a very narrow velocity group participates and therefore this method constitutes a good way of preparing (or selecting) atoms with the purpose of collisions studies. The velocity can be selected by changing either the angle θ on the slowing laser frequency. The linewidth obtained (~ 2 MHz) is due to the use of two independent laser with uncorrelated jitter. If just one laser was used together with an electro-optical modulator to generate the probe frequency, much narrower lines (few KHz) are expected to be obtained since the jitters are now correlated.

In conclusion, we have presented a method of preparing a very narrow velocity distribution of slow atoms by using at the same time the Zeeman tuning technique as

the slowing tool and the stimulated Raman transition to select a specific velocity group. The conjugation of slowing and selection allows the collection of a fairly large amount of atoms in a narrow velocity group.

REFERENCES

1. P. Gould, P. Lett, P. Julienne, W. Phillips, H. Throshein and J. Weiner - Phys. Rev. Lett. 60, 788 (1988).
2. J.V. Prodan, W. Phillips and H. Metcalf - Phys. Rev. Lett. 49, 1149 (1982).
3. V.S. Bagnato, G. Lafyatis, A. Martin, K. Helmerson, J. Landry and D. Pritchard - J. Opt. Soc. Am B6, 2171 (1989).
4. V.S. Bagnato, C. Salomon, E. Marega Jr. and S.C. Zilio - J. Opt. Soc. am B8, 497 (1991).
5. R.J. Napolitano, S.C. Zilio and V.S. Bagnato - Opt. Commun. 80, 110 (1990).
6. J.E. Thomas, S. Ezekiel, C.C. Leiby Jr., R.H. Picard and C.R. Willis - Opt. Lett. 6, 298 (1981).

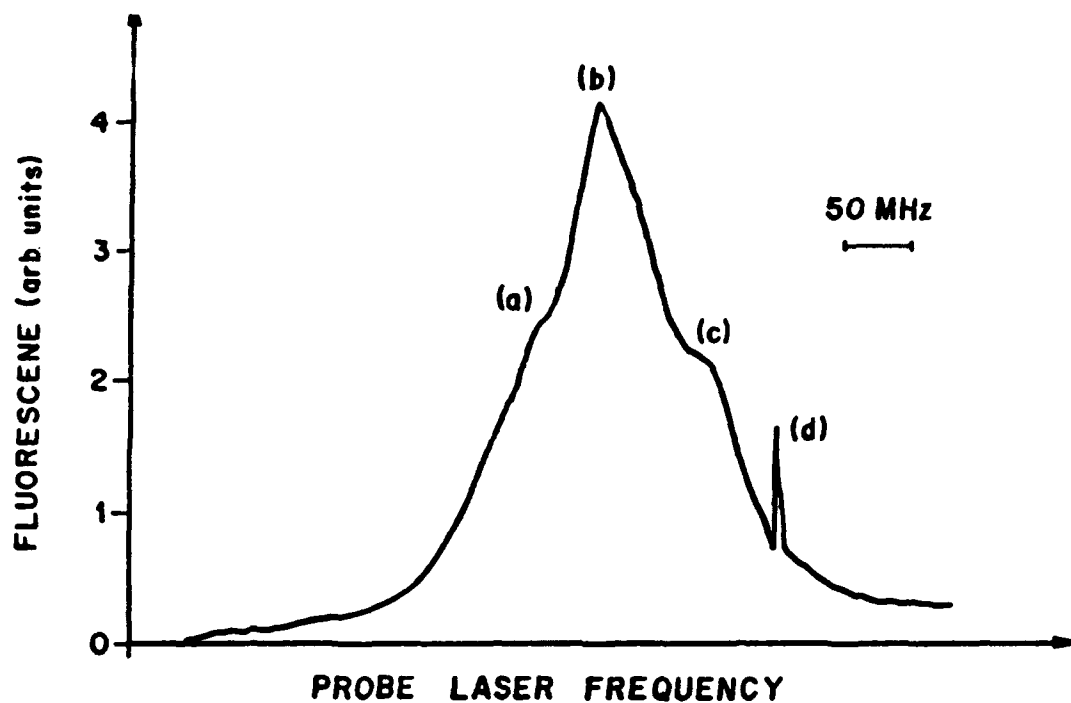


FIG. 1 - Fluorescence of slow atoms in $F = 1$ as a function of the probe laser frequency.

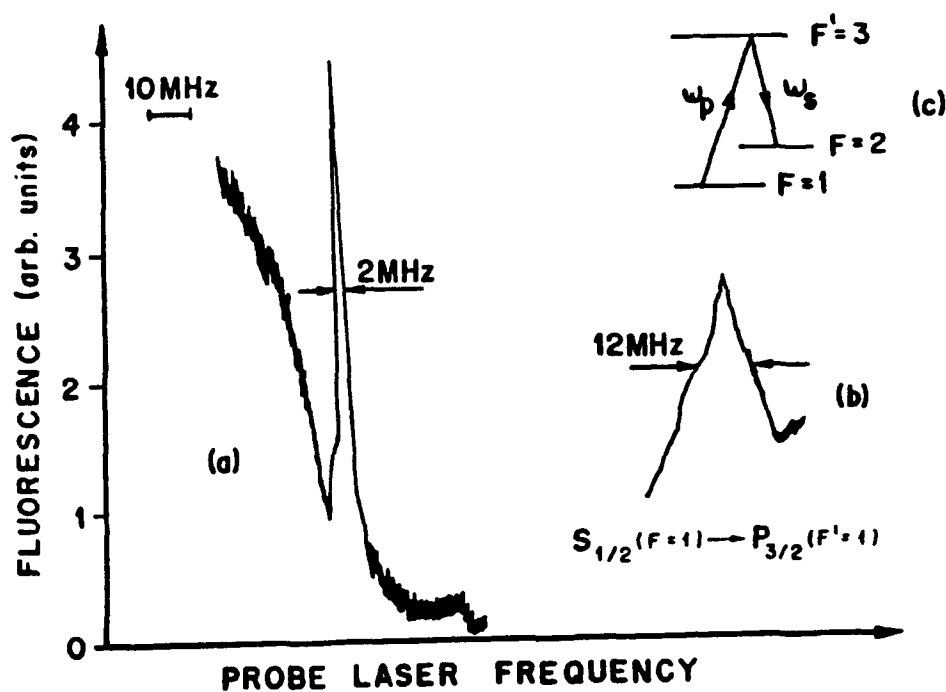


FIG. 2 - (a) Expanded view of peak (d) of fig. 1, (b) natural linewidth obtained with a reference laser beam crossing the atomic beam perpendicularly and (c) A system used to describe the stimulated Raman transition.

Laser Preparation and Probing of Initial and Final Angular Momentum States in the
Collision-Induced Energy Transfer $\text{Ca}(4s4p\ ^3P_1) + \text{He} \rightarrow \text{Ca}(4s4p\ ^3P_2) + \text{He}$

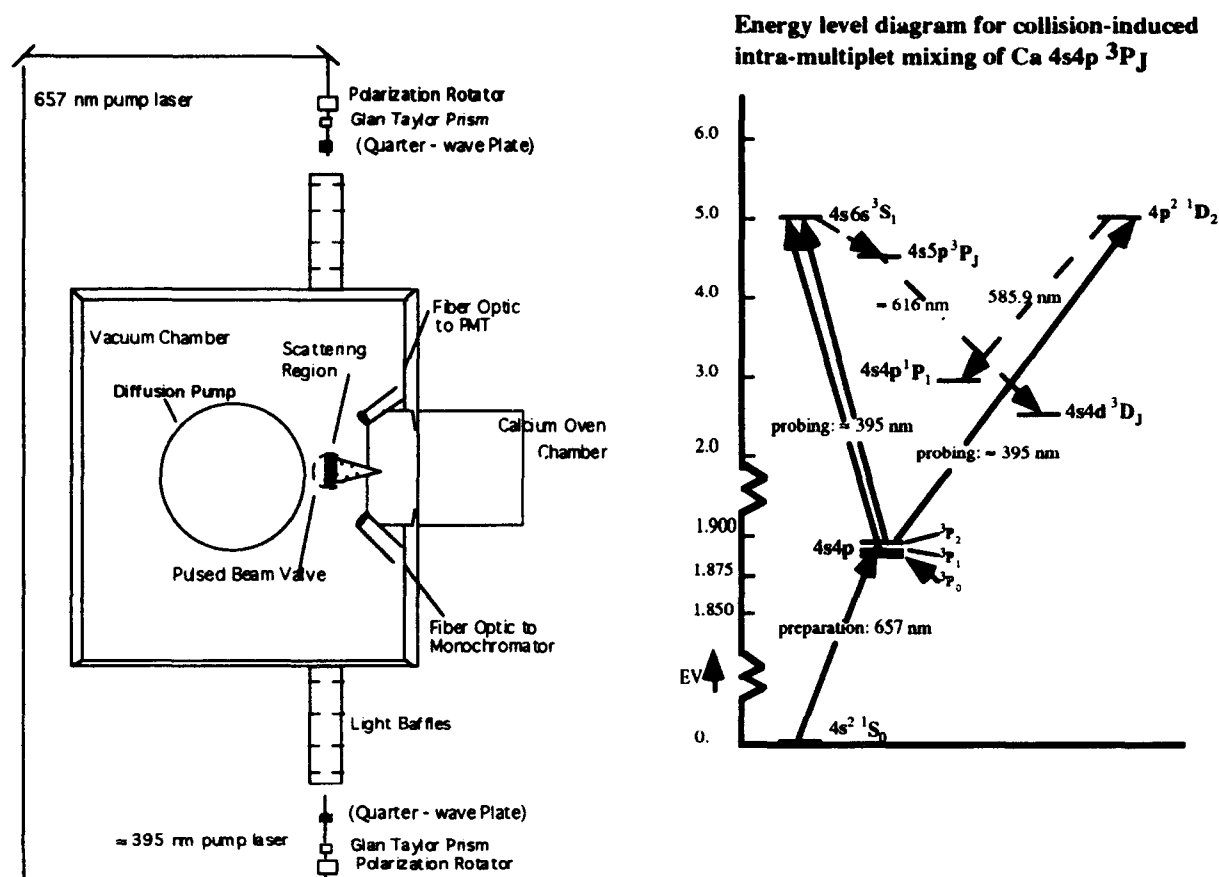
Eileen M. Spain, Christopher J. Smith, Mark J. Dalberth, and Stephen R. Leone

Joint Institute for Laboratory Astrophysics,
National Institute of Standards and Technology,
and the
Department of Chemistry and Biochemistry
University of Colorado
Boulder, Colorado 80309
(303)492-6005

The nature of atomic collisions can be revealed through the preparation and probing of aligned or oriented states. Intense interest in this research topic is evident by the numerous current experimental and theoretical investigations.¹ The results of these studies provide a means of visualizing the important mechanisms and symmetries of the collision process with unprecedented detail.

The mechanism for near-resonant electronic energy transfer in atomic collisions is investigated through a three vector correlation experiment in a crossed beam arrangement. Linearly and circularly polarized lasers are used both to excite and probe the angular momentum states in an electronic energy transfer process. An electronically excited state of atomic Ca ($4s4p\ ^3P_1$) is aligned (oriented) by a laser pulse, and a second, saturating laser pulse probes the final magnetic sublevels of the Ca ($4s4p\ ^3P_2$) state after collision with He. With magnetic sublevel dependence, state-to-state relative cross sections for the collision-induced near-resonant, J mixing process are measured.

Collisions of $\text{Ca}(4s4p\ ^3P_1)$ with He are examined in a crossed beam apparatus shown schematically in the figure below. The relevant energy levels of Ca for this study are depicted below as well. The initial relative velocity vector is defined by the effusive beam of Ca with respect to the pulsed supersonic jet of He. Two collinear and counterpropagating tunable lasers, one for initial excitation of the Ca to the $4s4p\ ^3P_1$ state and one for probing the final angular momentum states, are perpendicular to the plane formed by the crossed Ca and He beams. Therefore, the three relevant vectors in the Ca + He collision system are the initial relative velocity vector and the two vectors representing the polarized excitation and probe laser light.



Following excitation, a small fraction of collisions populate the 3P_2 (and the 3P_0) state of Ca. Laser-induced fluorescence signals from the 3P_2 state are detected as a function of the angles of linear polarization and/or the handedness of circular polarization of the excitation and probe lasers. The four laser configurations employed in this investigation are displayed in the diagram below.

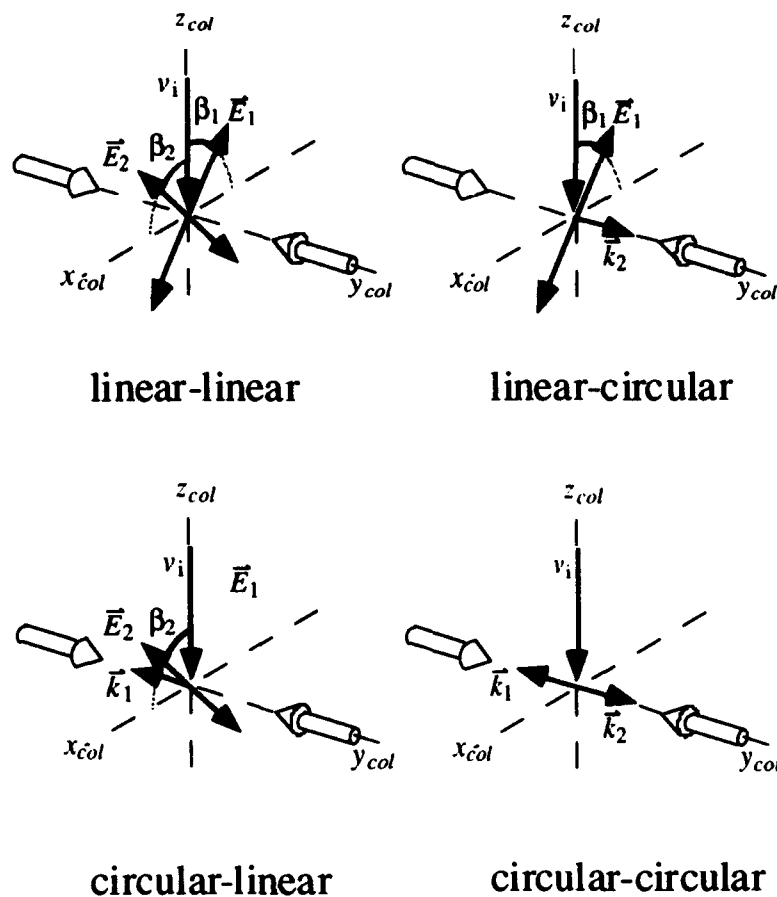
The general expression equating the experimental data to the basic cross sections in the collision frame is given by²

$$\sigma_{j_2 m_2 \leftarrow j_1 m_1}(\Delta\alpha, \beta_1, \beta_2) = \sum_m \rho_{m_1 m_1'}(\alpha_1, \beta_1) \rho_{m_2 m_2'}^*(\alpha_2, \beta_2) \sigma_{j_2 m_2 m_2' \leftarrow j_1 m_1 m_1'}$$

with

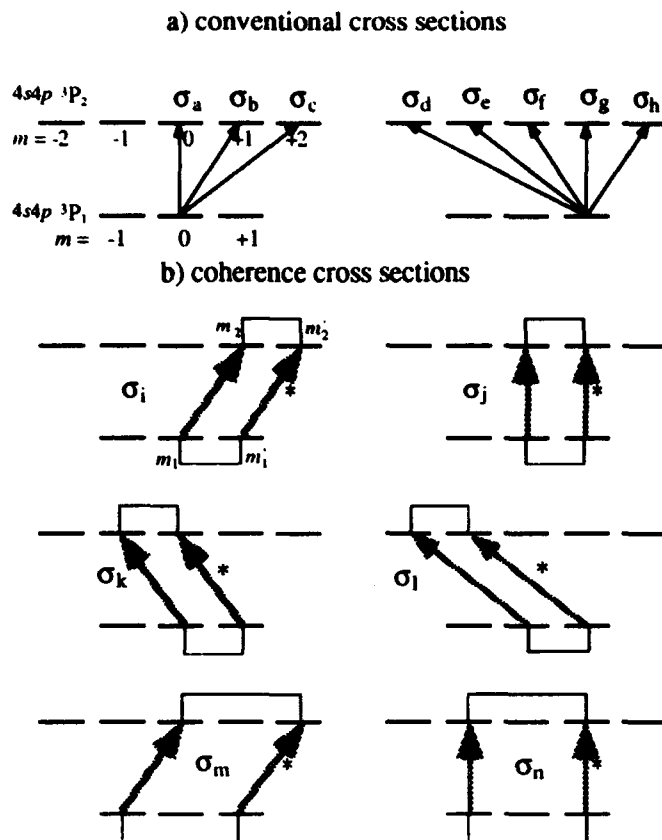
$$\rho_{m_1 m_1'} = D_{m_1 m_i}^{j_1} D_{m_1 m_i}^{j_1*}, \quad \rho_{m_2 m_2'}^* = D_{m_2 m_f}^{j_2*} D_{m_2 m_f}^{j_2}$$

where m_i and m_f are the magnetic quantum numbers defined in the pump and probe laser frames, respectively, m_1 and m_2 are the magnetic quantum numbers defined in the collision frame, and ρ_{mm} are the elements of the density matrix



which describe the $|jm_i\rangle$ or $|jm_f\rangle$ state in the laser frame as a coherent mixture of $|jm\rangle$ states in the collision frame. The cross sections in the collision frame are the fundamental cross sections that we determine. The diagonal elements ρ_{mm} give population information and are termed conventional cross sections. The off-diagonal $\rho_{mm'}$ give coherence or phase information between two initially prepared m states and two final m states, and are termed coherence cross sections.³ The explicit expressions used to analyze the data obtained in the four laser configurations are derived by Driessen and Eno.⁴ A representation of the collisional transitions for conventional and coherence cross sections is provided in the figure below.

A detailed analysis of our findings and an interpretation of the conventional and coherence cross sections will be presented. A brief report of the results is summarized here. For initial 3P_1 preparation with linear polarized light perpendicular to the initial relative velocity vector, the dominant population transfer is from the $m_1=1$ to the $m_2=-1$ and 0 magnetic sublevels of the 3P_2 state. In addition, our results show that the ratio of energy transfer rates to the Ca ($4s4p\ ^3P_2$) state for perpendicular vs. parallel preparation is 1.46 ± 0.04 . Our study of the



alignment effect into the final 3P_0 state suggests striking preservation of the initial asymptotic alignment throughout the collision, resulting in a very large observed effect of $(\sigma^{111}/\sigma^0) = 23 \pm 1$. Further analysis of our results will provide complex valued coherence cross sections that can be interpreted with physical pictures of the changes in orbital shape and direction. A recent *ab initio* calculation of the coherence cross sections in a similar system, Na + He, has been performed.⁵ Insight gained in the Na + He theoretical study will be useful in understanding the experimental results for the Ca + He system.

References

1. see for example: B. Pouilly, J.M. Robbe, and M.H. Alexander, *J. Chem. Phys.* **91**, 1658 (1989); G. Nienhuis, *Phys. Rev. A* **26**, 3137 (1982); G.C. Schatz, L.J. Kovalenko, and S.R. Leone, *J. Chem. Phys.* **91**, 6961 (1989); I. Wallace, J. Kaup, and W.H. Breckenridge, *J. Phys. Chem.* **95**, 8060 (1991); S. Bililign and P.D. Kleiber, *Phys. Rev. A* **42**, 6938 (1990).
2. C.J. Smith, J.P.J. Driessen, L. Eno, and S.R. Leone, *J. Chem. Phys.* **96**, 8212 (1992).
3. J.P.J. Driessen and S.R. Leone, *J. Phys. Chem.* **96**, 6136 (1992).
4. J.P.J. Driessen and L. Eno, *J. Chem. Phys.*, in press.
5. R. de Vivie-Riedle, J.P.J. Driessen, and S.R. Leone, *J. Chem. Phys.*, submitted.

Abello, L. — WA4
 Alijah, Alexander — MB6
 Alfred, D. D. — MB9
 Andrews, Anne M. — TuA4
 Arie, Ady — TuB2
 Asfaw, Araya — WB7

Bagnato, V. S. — ThB3
 Bannai, R. — ThB2
 Barth, H.D. — MA5
 Blake, Geoffrey A. — MB4, TuA
 Bunker, Philip R. — TuA6
 Byer, R. L. — TuB2

Catching, B. F. — ThA3
 Cavanagh, Richard R. — WA3
 Cerny, Timothy M. — MB3
 Chadwick, B. L. — MA5
 Chang, Bor-Chen — TuA3
 Chen, Lingbing — MB8
 Clark, D. — WB1
 Coutaz, J. L. — WA4
 Crim, F. Fleming — MA1

Dalberth, Mark J. — ThB4
 De Lucia, Frank C. — TuA5
 Di Lauro, C. — TuA6
 Dunlop, James R. — TuA3
 Duquette, D. W. — WB3
 Durant, J.L., Jr. — TuB3
 Duxbury, Geoffrey — MB6, ThB2

Ellis, Andrew M. — MB3
 Eschliman, D. S. — WB3
 Eyster, E. E. — WB8, ThA3

Farrow, R. L. — MB2, TuB3
 Fayer, Michael D. — WA1
 Felker, Peter — TuB
 Field, Robert W. — MA2
 Forsman, J. W. — MB2
 Fortna, John — WB7
 Francis, O. P. — WB3
 Fraser, Gerald T. — TuA4
 Fuming, Li — MB8
 Furst, Mitchell L. — MB7

Gancheryonok, Igor I. — WB6
 Gangopadhyay, S. — WB8
 Germer, T. A. — WA3
 Gray, J. A. — TuB3
 Grubbs, W. Tandy — WA2
 Guerin, D. — WB1
 Güttler, Frank — WA5

Hanial, S. S. — WB2
 Heath, James R. — ThA2
 Heilweil, E. J. — WA3
 Hughey, Lanny R. — WB7
 Humm, David C. — WB7
 Hwang, Hyun-Jin — ThA2

Jianzhao, Li — MB8
 Johns, J. W. C. — TuA6

Kanamori, Hideto — MA2
 Kanematsu, Yasuo — WB6
 Klemperer, William — TuA1
 Korsunsky, E. — WB4, WB5
 Kosachiov, D. — WB4, WB5
 Kumar, P. R. Sasi — WB2
 Kuo, Erica W. — ThA2
 Kushida, Takashi — WB6

Lacy, John H. — ThA
 Leone, Stephen R. — ThB4
 Li, Fuming — MB8
 Li, Hao — MB1
 Li, Jianzhao — MB8
 Li, Mingguang — MA2
 Lingbing, Chen — MB8

Mack, J. A. — MB5
 MacPhail, Richard A. — MA3
 Mantz, A. W. — WB1
 McCarthy, Michael C. — MA2
 McKellar, A. R. W. — TuA6
 McLaughlin, K. W. — WB3
 Melikechi, N. — WB8, ThA3
 Milce, A. P. — MA5
 Miller, C. Cameron — MB1
 Miller, Roger E. — TuA2
 Miller, Terry A. — MB3, TuA3
 Miziolek, Andrzej W. — ThB
 Moore, Mary Ann — ThB1
 Morgan, Harry — WB7

Nampoori, V. P. N. — WB2
 Nibler, Joseph W. — WA2
 Nischan, M. — WB1

Orr, B. J. — MA5

Pate, Brooks H. — TuA4
 Philips, Laura A. — MA, MB1
 Pirota, Marco — WA5
 Price, J. M. — MA4, MB5
 Primeau, N. — WA4

Radford, H. E. — ThB1
 Rahn, Larry A. — MB2, TuB1
 Renn, Alois — WA5
 Reutt-Robey, Janice — WA
 Robles, Eric S. J. — MB3
 Rogaski, C. A. — MA4
 Rozhdestvensky, Yu — WB4, WB5

Saykally, Richard J. — ThA2
 Sears, Trevor J. — ThB1
 Sepiol, Jerzy — WA5
 Seyoum, Hailemichael — WB7
 Smith, Christopher J. — ThB4
 Spain, Eileen M. — ThB4

150 / Key to Authors and Presiders

Stephenson, J. C. — WA3
Stockman, Paul — MB4
Suzuki, Sakae — MB4

Tan, Xue-Qing — MB3
Tanaka, Keiichi — ThA2
Thaddeus, Patrick — ThA1
Thorne, L. R. — TuB3

Vallabhan, C. P. G. — WB2
Van Orden, Alan K. — ThA2

Wang, Qi — MB9
Wild, Urs P. — WA5
Williamson, James M. — MB3, TuA3
Wodtke, Alec M. — MA4, MB5

Xiao, Luo — MB8

Youyuan, Zhao — MB8
Yu, R. H. — MB7

Zhao, Youyuan — MB8
Zilio, S. C. — ThB3



Sponsored by
Optical Society of America

In Cooperation with
American Physical Society

HIGH RESOLUTION SPECTROSCOPY POSTDEADLINE PAPERS

PD1	Spectroscopy of Jet-Cooled Ag₂Au , Jacqueline C. Pinegar, Jon D. Langenberg, and Michael D. Morse155
PD2	Bond Energies of Small Transition Metal Cation Clusters , Larry M. Russon, Scott A. Heidecke, Michelle K. Birke, J. Conceicao, P. B. Armentrout, and Michael D. Morse159
PD3	Spectroscopic Analysis of the Transition Metal Aluminides: AlNi, AlCu, and AlZn , Jane M. Behm, Caleb A. Arrington, Thorsten Blume, Jon D. Langenberg, and Michael D. Morse163
PD4	High Resolution Spectroscopy of Ti₂ and AlY at Near-Infrared Frequencies , Caleb A. Arrington, Jon D. Langenberg, Jacqueline C. Pinegar, Michael D. Morse, Mats Doverstål, Bo Lindgren, and Ulf Sassenberg167
PD5	FTIR Spectra and Torsion-Vibration Coupling in ¹³CD₃OH , Li-Hong Xu and R. M. Lees171
PD6	Two-Color Photo-Associative Ionization Collisions between Sodium Atoms , V. Bagnato, L. Marcassa, C. Tao, Y. Wang, and J. Weiner175
PD7	Vibrational Transfer in Collisions of Li₂ A¹ Σ_u⁺(v_i, j_i) with Neon , Peter Gorgone, Scott Davis, Yunxiao Gao, Eric McCall, Mark Rosenberry, and Brian Stewart178
PD8	Intermolecular Interactions in the Fluorene Dimer , Lt. Clark Highstrete and John Wessel182
PD10	Study on Isotope Mass Difference (¹⁶O, ¹⁸O) Effect on CO₂ Laser Oscillation Spectra , Yasuyuki Saito187
PD11	Color Change and Highly Refractory Surfaces of Polycrystalline Silicon of Arsenic Atoms of High Dose Implanted at Low Acceleration Voltage , Yasuyuki Saito191
PD12	Molecular Spectroscopy at Ultracold Temperatures , K. Helmerson, M. Wagshul, P. Lett, S. Rolston, and W. Phillips194
Postdeadline	Author Index198

NOTE: There is no Postdeadline Paper 9

Spectroscopy of Jet-Cooled Ag₂Au

Jacqueline C. Pinegar, Jon D. Langenberg, and Michael D. Morse

University of Utah
 Dept. of Chemistry
 Salt Lake City, UT 84112
 (801)581-4204

While the electronic structure of metallic atoms can be calculated accurately using *ab initio* quantum chemistry, and infinite metallic solids are rather well understood through the methods of solid state physics, metallic clusters ranging in size between these two extremes are understood to a much lesser extent. The study of these small metal clusters provides fundamental information about bonding in metals, such as the contribution of the various orbitals to the bonding and the effect this has on bond strengths and other properties.

In particular, more detailed spectroscopic studies of gas phase metals, in which vibrational structure has been resolved and analyzed, have been accomplished mostly on dimers and trimers. As for metallic trimers, only a few have been successfully investigated in this way. To our knowledge, the only examples are the alkali clusters Li₃,¹ Na₃,²⁻¹¹ and Li_xNa_{3-x},^{12,13} the coinage metal (pseudoalkali) clusters Cu₃,¹⁴⁻¹⁷ Ag₃,¹⁸ Cu₂Ag,¹⁹ Cu₂Au,¹⁹ and CuAgAu,¹⁹ the p-block metals Al₃,²⁰ and Bi₃,²¹ and the transition metal cluster Ni₃.²² The alkali and coinage metal trimers, possessing only one valence electron per atom, have relatively simple electronic structure. This, in combination with the alkali metals having low boiling points allowing a relatively higher pressure of alkali atoms to be generated in an oven, accounts for the greater success in studying them.

The homonuclear alkali and coinage metal trimers are all expected to possess ground electronic states of \tilde{X}^2E' in the D_{3h} point group, deriving from the molecular orbital configuration $a_1'^2e'$. The \tilde{X}^2E' state is orbitally degenerate, and is therefore subject to a Jahn-Teller distortion, lowering the symmetry to C_{2v}, which breaks the degeneracy of the \tilde{X}^2E' state into 2A_1 and 2B_2 . For heteronuclear species, such as Cu₂Ag,¹⁹ Cu₂Au,¹⁹ and in this work, Ag₂Au, the expected symmetry is C_{2v}, and the ground states should either belong to the 2A_1 or 2B_2 symmetry species.

In this study, the Ag₂Au molecules were formed by pulsed laser vaporization (Nd:YAG, 532 nm, 15-20 mJ/mm²) of a 2:1 (molar) alloy of Ag and Au, followed by supersonic expansion in helium carrier gas. Experimental details have been described previously.¹⁹ The excitation laser, a Nd:YAG pumped tunable dye laser was scanned from 16,990 to 18,890 cm⁻¹. A fixed frequency excimer laser (KrF at 5.00 eV) was used for photoionization of the excited molecules. To calibrate the spectrum, four bands were examined under high resolution (≈ 0.04 cm⁻¹). This was accomplished by narrowing the output of the dye laser by insertion of an air-spaced intracavity etalon, which was then pressure scanned with CCl₂F₂ while an absorption spectrum of gaseous I₂ was simultaneously recorded. The I₂ atlas of Gerstenkorn and Luc²³ was used to provide absolute frequency

TABLE I. Vibronic Bands of $^{107}\text{Ag}^{109}\text{Ag}^{197}\text{Au}$.^{a,d}

Band	Measured Frequency (cm ⁻¹) ^b	Isotope shift (cm ⁻¹) ^c	
		$^{107}\text{Ag}_2^{197}\text{Au}$	$^{109}\text{Ag}_2^{197}\text{Au}$
0 _g	17526.72 (1.68)	-0.65 (0.98)	0.07 (2.16)
2 _g	17636.41 (0.92)	-0.44 (0.15)	-1.86 (-0.30)
1 _g	17721.72 (-1.41) ^{d,e}	0.45 (-1.02)	-0.72 (-1.30)
2 _g	17746.04 (0.09)	0.68 (0.22)	-0.85 (0.30)
1 _g 2 _g	17830.52 (-1.41)	1.51 (-0.36)	-0.70 (-1.08)
2 _g	17856.48 (0.09)	0.87 (0.22)	-2.22 (-0.47)
1 _g	17918.40 (-1.58)	1.42 (-0.51)	-1.32 (-1.55)
1 _g 2 _g	17939.73 (-1.01) ^{d,e}	0.72 (-1.09)	-1.39 (-0.98)
2 _g	17966.91 (0.07)
1 _g 2 _g	18026.95 (-0.18)	0.46 (-0.59)	-1.40 (-0.06)
1 _g 2 _g	18049.70 (0.17)	1.30 (0.36)	-2.20 (-0.03)
2 _g	18076.63 (-0.66)	1.07 (-0.57)	-3.07 (-0.27)
1 _g	18115.42 (-0.16) ^d	1.08 (-0.01)	-1.88 (-0.08)
1 _g 2 _g	18134.88 (0.60)	1.44 (0.70)	-0.42 (2.06)
1 _g 2 _g	18158.35 (0.02)	1.56 (0.21)	-1.80 (0.99)
1 _g 2 _g	18221.72 (0.63)	1.12 (0.19)	-2.61 (0.13)
1 _g 2 _g	18241.78 (0.35)	1.63 (0.22)	-2.78 (0.00)
1 _g	18310.76 (0.81)	2.35 (1.37)	-2.52 (0.97)
1 _g 2 _g	18327.01 (0.42) ^{d,e}	1.97 (0.24)	-2.55 (0.31)
1 _g 2 _g	18349.45 (0.87)	1.65 (0.38)	-4.39 (-0.34)
1 _g 2 _g	18413.75 (-0.06)	2.33 (-0.27)	-2.54 (0.20)
1 _g 2 _g	18432.27 (0.18)	2.80 (0.28)	-2.93 (0.22)
1 _g	18504.80 (1.73)	...	-4.34 (0.88)
1 _g 2 _g	18517.75 (0.09)	2.91 (-0.25)	-2.90 (0.30)
1 _g 2 _g	18537.35 (-0.24)	3.50 (0.06)	-3.79 (-0.34)
1 _g 2 _g	18604.45 (-0.83)	4.12 (-0.52)	-4.05 (-1.29)
1 _g 2 _g	18621.47 (-0.04) ^f	3.55 (-0.41)	-3.67 (-0.10)
1 _g 2 _g	18707.40 (-0.09)
1 _g 2 _g	18794.50 (-1.02)	...	-3.80 (-0.33)

^a Vibronic bands were fit to the formula

$$\nu = T_0 + \sum_i [\omega'_i \nu_i + x'_{i1}(\nu_i^2 + \nu_i)] + \sum_{i < j} x'_{ij}[\nu_i \nu_j + (\nu_i + \nu_j)/2].$$

The resulting values of T_0 , ω'_i , ω''_i , x'_{i1} , x'_{i2} , and x'_{ij} are given in Table II, along with their 1σ error limits.

^b Following each observed frequency, the residual $\nu_{\text{obs}} - \nu_{\text{calc}}$ is given in parenthesis.

^c Isotope shifts are given as $\nu(\text{isotope modification}) - \nu(^{107}\text{Ag}^{109}\text{Ag}^{197}\text{Au})$. Following each observed isotope shift, the residual $\nu_{\text{obs}} - \nu_{\text{calc}}$ is given for the fit of that isotopic modification to the formula given in footnote a.

The resulting values of the vibrational constants are given in Table II, along with their 1σ error limits.

^d Lifetimes of the 100, 120, 300, and 320 levels were measured by exciting the 1_g, 1_g2_g, 1_g, and 1_g2_g bands using the time-delayed resonant two-photon method¹⁹. The resulting values are:

$$\tau(100) = 511 \pm 34 \text{ nsec}, \tau(120) = 457 \pm 28 \text{ nsec}, \tau(300) = 658 \pm 128 \text{ nsec}, \text{ and } \tau(320) = 598 \pm 72 \text{ ns}.$$

^e High resolution scan of I₂ was taken ... this transition frequency to calibrate the spectrum.

TABLE II. Fitted vibrational constants for Ag₂Au.^a

Constant	¹⁰⁷ Ag ¹⁰⁹ Ag ¹⁹⁷ Au	¹⁰⁷ Ag ₂ ¹⁹⁷ Au	¹⁰⁷ Ag ₂ ¹⁹⁷ Au
T_0	17525.04 (0.64)	17525.09 (0.46)	17524.63 (0.70)
ω'_1	200.15 (0.49)	199.82 (0.42)	199.83 (0.55)
ω'_2	111.28 (0.62)	111.53 (0.45)	111.23 (0.69)
x'_{11}	-0.62 (0.06)	-0.48 (0.06)	-0.67 (0.07)
x'_{22}	0.00 (0.10)	-0.02 (0.07)	-0.10 (0.10)
x'_{12}	-1.65 (0.09)	-1.53 (0.07)	-1.62 (0.11)

^a All constants are reported in wavenumbers (cm⁻¹), followed by the 1σ error limits in parentheses. These constants were obtained by a least-squares fit of the data of Table I to the expression

$$\nu = T_0 + \sum_i [\omega'_i \nu'_i + x'_{ii}(\nu'^2_i + \nu'_i)] + \sum_{i < j} x'_{ij}[\nu'_i \nu'_j + (\nu'_i + \nu'_j)/2].$$

References:

1. J.-P. Wolf, G. Delacrétaz, and L. Wöste, *Phys. Rev. Lett.* **63**, 1946 (1989).
2. A. Herrman, M. Hoffman, S. Leutwyler, E. Schumacher, and L. Wöste, *Chem. Phys. Lett.* **62**, 216 (1979).
3. G. Delacrétaz and L. Wöste, *Surf. Sci.* **156**, 770 (1985).
4. G. Delacrétaz, E. R. Grant, R. L. Whetten, L. Wöste, and T. W. Zwanziger, *Am. Phys. Soc.* **56**, 2598 (1986).
5. M. Broyer, G. Delacrétaz, P. Labastie, R. L. Whetten, J.-P. Wolf, and L. Wöste, *Z. Phys. D* **3**, 131 (1986).
6. M. Broyer, G. Delacrétaz, P. Labastie, J.-P. Wolf, and L. Wöste, *Phys. Rev. Lett.* **57**, 1851 (1986).
7. M. Broyer, G. Delacrétaz, G.-Q. Ni, J.-P. Wolf, and L. Wöste, *Chem. Phys. Lett.* **145**, 232 (1988).
8. M. Broyer, G. Delacrétaz, G.-Q. Ni, R. L. Whetten, J.-P. Wolf, and L. Wöste, *J. Chem Phys.* **90**, 843 (1989).
9. M. Broyer, G. Delacrétaz, G.-Q. Ni, R. L. Whetten, J.-P. Wolf, and L. Wöste, *J. Chem Phys.* **90**, 4620 (1989).
10. Ph. Dugourd, J. Chevalyere, J. P. Perrot, and M. Broyer, *J. Chem. Phys.* **93**, 2332 (1990).
11. H. J. Foth and W. Demtröder, in *Laser Spectroscopy VIII*, edited by W. Persson and S. Svanberg, (Springer, Berlin, 1987), p.248.
12. M. M. Kappes, *Chem. Rev.* **88**, 369 (1988).
13. P. Radi, Ph.D. thesis, University of Bern, 1986.
14. M. D. Morse, J. B. Hopkins, P. R. R. Langridge-Smith, and R. E. Smalley, *J. Chem. Phys.* **79**, 5316 (1983).
15. W. H. Crumley, J. S. Hayden, and J. L. Gole, *J. Chem. Phys.* **84**, 5250 (1986).
16. E. A. Rohlfing and J. J. Valentini, *Chem. Phys. Lett.* **126**, 113 (1986).
17. M. D. Morse, *Chem. Phys. Lett.* **133**, 8 (1987).
18. P. Y. Cheng and M. A. Duncan, *Chem. Phys. Lett.* **152**, 341 (1988).
19. G. A. Bishea, C. A. Arrington, J. M. Behm, and M. D. Morse, *J. Chem. Phys.* **95**, 8765 (1991).
20. Z. Fu, G. W. Lemire, Y. M. Hamrick, S. Taylor, J. Shui, and M. D. Morse, *J. Chem. Phys.* **88**, 3524 (1989).
21. C. A. Arrington and M. D. Morse, "Spectroscopy of Jet-Cooled Bi₃," in preparation.
22. J. R. Woodward, S. H. Cobb, and J. L. Gole, *J. Phys. Chem.* **92**, 1404 (1988).
23. S. Gerstenkorn and P. Luc, *Atlas du Spectre d'Absorption de la Molecule d'Iode* (CNRS, Paris, 1978).

Bond Energies of Small Transition Metal Cation Clusters

Larry M. Russon, Scott A. Heidecke, Michelle K. Birke, J. Conceicao,
P. B. Armentrout, and Michael D. Morse

University of Utah
Dept. of Chemistry
Salt Lake City, UT 84112
(801) 581-4204

A new experimental apparatus has been constructed for photodissociation spectroscopy of transition metal-containing cations. Predissociation thresholds for Co_2^+ , Co_3^+ , and Ti_2^+ have been observed and values of 2.765 ± 0.001 eV, 2.086 ± 0.002 eV, and 2.435 ± 0.002 eV, respectively, have been determined for the bond energies for these species. These are in good agreement with results obtained by collision-induced dissociation (CID) experiments. Comparison of bond strengths obtained from the observation of predissociation thresholds with those obtained by non-optical methods, such as collision-induced dissociation and Knudsen cell mass spectrometry, have allowed criteria for the interpretation of a predissociation threshold as a bond strength to be developed.

The apparatus employs a laser-vaporization, supersonic expansion source, which produces jet-cooled metal-containing anions, cations, and neutral species. Ion production is sufficient to preclude the need for a secondary ionization mechanism. The molecular beam is skimmed and the cations are extracted using a two-dimensional turning quadrupole.¹ As the ions leave the quadrupole they enter a Wiley-McLaren² time-of-flight source that is adjusted to bring the ion packet to a longitudinal focus in a spectroscopy chamber. Two einzel lenses are used to provide radial focusing. In the spectroscopy chamber the ions are irradiated by the output of a tunable dye laser pumped by an excimer laser operating on XeCl (308 nm), which counterpropagates down the axis of the ion beam. As the ions exit the spectroscopy chamber they pass through a third einzel lens which provides radial focusing at the detector. The ions are then deflected 1.6° to enter a reflectron assembly which separates photo-fragments from any undissociated parents. The ions are detected by a microchannel-plate detector, and the signal is sent to a 40 MHz digital oscilloscope installed in an IBM-compatible, 386-based computer where it is summed and stored for later analysis.

In an investigation of the photodissociation of Co_2^+ at low laser fluences, we have

found an abrupt onset of predissociation in a congested electronic spectrum at an energy of 2.765 ± 0.001 eV ($22,300 \pm 5$ cm⁻¹),³ as shown in Figure 1. This abrupt onset of predissociation probably occurs at the thermodynamic threshold for the production of ground

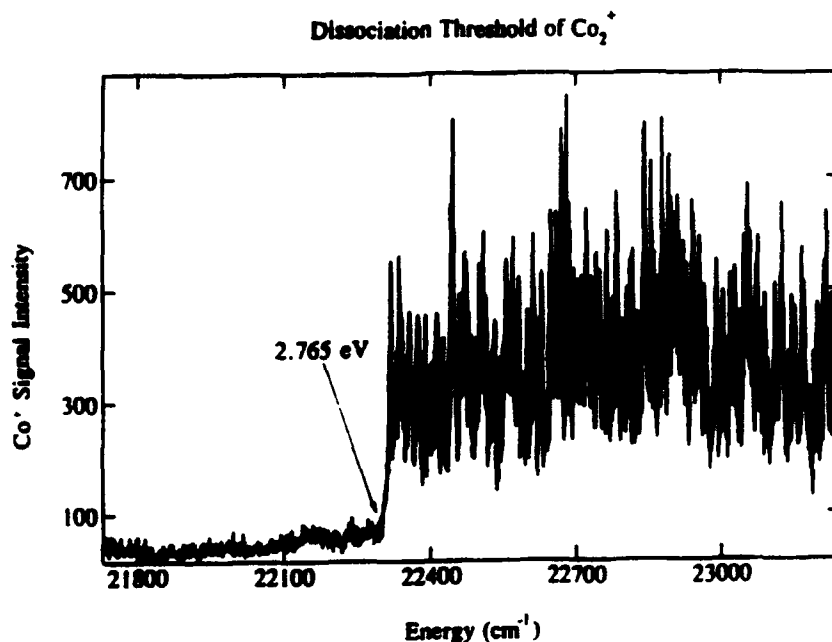


Figure 1. Predissociation threshold of Co₂⁺, obtained using a dye laser fluence of ≈ 5 mJ/cm² of coumarin 460 radiation. From these data a bond strength of $D_0^0(\text{Co}_2^+) = 2.765 \pm 0.001$ eV is deduced.³

state Co and Co⁺, as it agrees very well with the bond strength measured by collision-induced dissociation (CID) methods [$D_0^0(\text{Co}_2^+) = 2.75 \pm 0.10$ eV].⁴ Abrupt onsets of predissociation have been previously observed in our group for many uncharged transition metal diatomics (such as NiPt,⁵ Pt₂,⁶ TiV,⁷ V₂,⁷ TiCo,⁷ and VNi⁷), but this is the first clear-cut case in which this method has succeeded for a diatomic transition metal cation. It appears that this method is perhaps the most precise method generally available for the measurement of bond strengths for such species, provided certain criteria are met. As we have recently discussed,³ a predissociation threshold may be inferred to correspond to the thermodynamic bond strength if:

1. The threshold is sharp and well-defined, without evidence of Franck-Condon difficulties in either the excitation or predissociation step;
2. Dissociation can occur to the ground separated atom limit while preserving good quantum numbers, such as Ω , g/u , and $+/-$;

3a. Either the ground separated atom limit generates a considerable number of molecular potential energy surfaces, some of which may be predicted to be repulsive, or

3b. The ground separated atom limit generates a much larger number of attractive molecular potential energy surfaces, allowing weaker predissociation processes to dominate by sheer strength of numbers.

In the case of Co_2^+ , it may be shown that the ground separated atom limit of Co ($3d^74s^2$, 4F) + Co^+ ($3d^84s^0$, 3F) generates only attractive potential curves,⁸ but the density of electronic states is so huge (3458 distinct potential curves arising within $10,000 \text{ cm}^{-1}$ of the ground separated atom limit) that criterion 3b comes into effect, yielding a facile predissociation process.³ Therefore, we assign the bond strength of Co_2^+ as $D_0^0(\text{Co}_2^+) = 2.765 \pm 0.001 \text{ eV}$.

We have recently found a similar predissociation threshold for Ti_2^+ , shown in Figure 2 below. In this case the threshold for dissociation is not quite so well-defined, leading to an

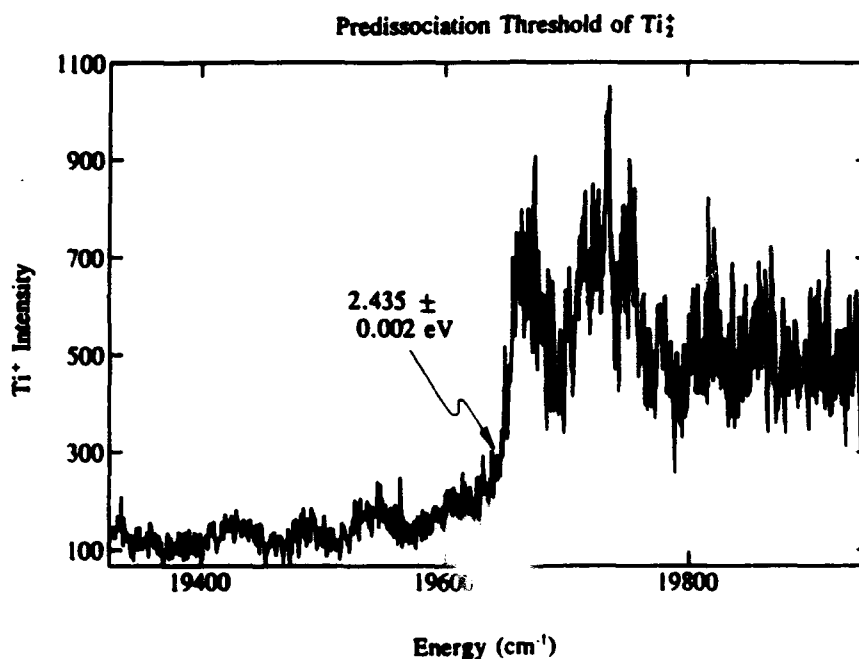


Figure 2. Predissociation threshold of Ti_2^+ , obtained using a dye laser fluence of $\approx 2.7 \text{ mJ/cm}^2$ of coumarin 500 radiation. From these data a bond strength of $D_0^0(\text{Ti}_2^+) = 2.435 \pm 0.002 \text{ eV}$ is deduced.

estimate of $D_0^0(\text{Ti}_2^+)$ of $2.435 \pm 0.002 \text{ eV}$. Again, this compares well with the CID measurement of $D_0^0(\text{Ti}_2^+) = 2.37 \pm 0.07 \text{ eV}$.⁹ It should be noted that our experiment employs a more severe supersonic expansion than that used in the collision-induced dissociation experiments, so the molecules produced in our experiments should possess less internal energy, giving a slightly greater (and more accurate) bond dissociation energy than that

found in the CID experiments. The deviation between the two experiments in the cases of Co_2^+ and Ti_2^+ is indeed in this direction, suggesting incomplete cooling in the CID experiments. In a preliminary experiment we have also located a predissociation threshold in Co_2^+ at approximately 2.086 ± 0.002 eV. This is very promising, since it suggests that these bond strength measurements may be extended to larger clusters. It also suggests that the method may be extended to other polyatomic transition metal molecules which are of considerable interest, such as unsaturated metal-ligand complexes.

References:

1. H. D. Zeman, *Rev. Sci. Instrum.* **48**, 1079 (1977).
2. W. C. Wiley and I. H. McLaren, *Rev. Sci. Instrum.* **26**, 1150 (1955).
3. L. M. Russon, S. A. Heidecke, M. K. Birke, J. Conceicao, P. B. Armentrout, and M. D. Morse, "The Bond Strength of Co_2^+ ," *Chem. Phys. Lett.*, in press.
4. D. A. Hales and P. B. Armentrout, *J. Cluster Science* **1**, 127 (1990).
5. S. Taylor, E. M. Spain, and M. D. Morse, *J. Chem. Phys.* **92**, 2698 (1990).
6. S. Taylor, G. W. Lemire, Y. Hamrick, Z.-W. Fu, and M. D. Morse, *J. Chem. Phys.* **89**, 5517 (1988).
7. E. M. Spain and M. D. Morse, *J. Phys. Chem.* **96**, 2479 (1992).
8. P. B. Armentrout and J. Simons, *J. Am. Chem. Soc.* **114**, 8627 (1992).
9. L. Lian, C.-X. Su, and P. B. Armentrout, *J. Chem. Phys.* **97**, 4084 (1992).

**Spectroscopic Analysis of the
Transition Metal Aluminides: AlNi, AlCu, and AlZn**

Jane M. Behm, Caleb A. Arrington, Thorsten Blume,
Jon D. Langenberg, and Michael D. Morse
Department of Chemistry
University of Utah
Salt Lake City, Utah 84112
(801)581-4204

A systematic gas-phase spectroscopic investigation of the transition metal aluminides has recently been initiated in this laboratory, with the aim of providing fundamental experimental measurements relevant to the chemical bonding between the *p*-block and *d*-block metals. In this study we hope to determine in what cases the aluminum atom bonds to the transition metal through a $p\sigma$ vs. a $p\pi$ approach, and to investigate the possibility of $p\sigma-d\sigma$ and $p\pi-d\pi$ bonds in these mixed main group-transition metal molecules. The fundamental results obtained through the study of the transition metal aluminides may well be relevant to the forces acting between atoms in the bulk alloys of these elements, and this may provide new insights into the metallurgy of aluminum-transition metal alloys.

The experimental technique invoked to investigate these bonding interactions is resonant two-photon ionization (R2PI) spectroscopy. The experimental details of this technique can be found elsewhere.¹ Briefly, the diatomic species of interest is created by laser vaporization of a metal alloy disc, followed by supersonic expansion into vacuum to cool the internal degrees of freedom. The molecular beam travels into an interrogation chamber where the excitation photon is supplied via a photon from a tunable Nd:YAG-pumped dye laser. The second, ionizing photon is then supplied, in most cases, by a fixed-frequency excimer laser operating on KrF (248 nm, 5.00 eV). The ions formed are accelerated up a time-of-flight tube and are detected at a microchannel plate detector. The optical spectra of the species of interest are collected by individually monitoring the ion signals at the particular masses as a function of dye laser frequency. Narrowing of the dye laser linewidth is necessary for high resolution analyses and is accomplished via insertion of an air-spaced intracavity etalon, that is pressure scanned using Freon 12 (CCl₂F₂, DuPont). Absolute line positions are then obtained using the simultaneously recorded I₂ absorption spectrum in conjunction with the I₂ atlas of Gerstenkorn and Luc.² In the instances in which an observed transition does not occur in the limits of the I₂ spectrum, it is necessary to send the output of the dye laser through a stainless steel cell pressurized with approximately 500 psi of H₂ gas. The H₂ Raman shifting process takes place only on the Q(1) line, resulting in radiation that is shifted 4155.163 cm⁻¹ from the fundamental radiation. In addition, a correction for the Doppler shift experienced by the molecules as they travel towards the radiation source at the beam velocity of helium (1.77×10^5 cm/s) is included to provide accurate absolute line positions for all of the rotationally resolved bands.

To our knowledge only one *3d* series transition metal aluminide, AlCu, has been investigated in the gas phase, spectroscopically or otherwise. This molecule was chosen as our starting point due to its simplicity and the fact that we could compare our results with those already collected on this molecule. Results from this study³ confirm that the ground state, as

predicted by theoreticians,^{4,5} is ${}^1\Sigma^+$ deriving from the $3s^2_3d^10_3s^2$ configuration. In this case the $3d^{10}4s^1$ Cu atom combines with the $3s^23p^1$ Al atom with the Al electron in the $p\sigma$ orientation. The filled shell nature of this molecular configuration results in a relatively low density of states that not only allows the chemical bonding of the molecule and the electronic structure of its low-lying electronic states to be thoroughly investigated with the R2PI technique but makes this molecule somewhat tractable for theoreticians as well. Five excited electronic states were observed and characterized, three of which were never previously detected. The spectroscopic constants obtained for the X, A, and B states are in good agreement with those obtained previously in a laser-induced fluorescence study performed by Bondybey *et al.*⁶ In turn, a number of bands from the four unperturbed band systems were rotationally resolved, resulting in a weighted least squares value of the ground state bond length of $r_0 = 2.3389 \pm 0.0005$ Å, also in very good agreement with theoretical values calculated previously.^{5,6,7}

Perhaps the most interesting result is the existence of a new state, the ${}^1\Pi(1)$ state, located at 14892 cm^{-1} . The rotationally resolved spectrum of the 0-0 band is presented below.

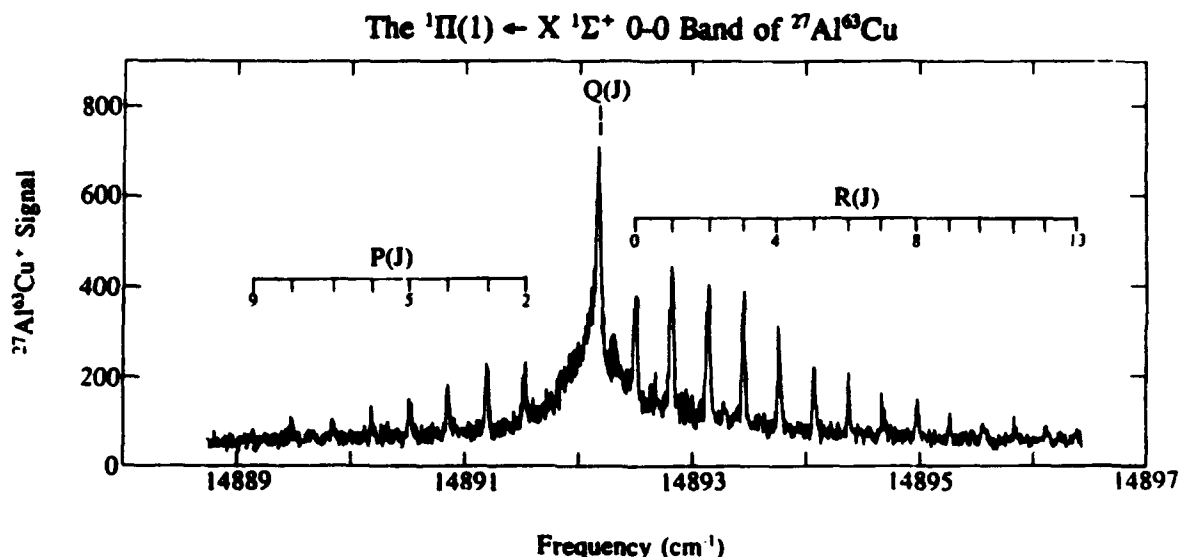


Figure 1. Rotationally resolved spectrum of the 0-0 band of the ${}^1\Pi(1) \leftarrow X {}^1\Sigma^+$ system of ${}^{27}\text{Al}{}^{63}\text{Cu}$.

The excited state bond length is nearly equal to that of the ground state, resulting in a symmetrical fanning out of the R and P branches. The lifetime of this state is $\tau = 77 \pm 1$ μsec as measured by the time-delayed resonant two-photon ionization method, in which the delay between the excitation and ionization lasers is varied, and the ion signal is measured as a function of this delay. Identification of this state as the ${}^1\Pi(1)$ state (versus the ${}^3\Pi$ and ${}^3\Sigma^+$ states that also arise from the ground state separated atom limit) has only very recently been made possible through communications with Bauschlicher and Langhoff⁷ in which they calculate a lifetime of 97 μsec and a T_0 of $\approx 16,000$ cm^{-1} for the ${}^1\Pi$ state.

In contrast to AlCu, the open $3d$ -subshell of nickel leads to many more possibilities for the ground electronic state of AlNi, and contributes to a much greater density of electronic states. Since the predominant bonding is expected to occur through the same $4s\sigma$ - $3p\sigma$ bonding interaction as occurs in AlCu, the interaction of a $3d^9 4s^1$, 3D nickel atom with aluminum would presumably be most favorable for a $p\sigma$ approach of the aluminum to the nickel atom, leading to a ground electronic state deriving from a $3s_{Al}^2 3d_{Ni}^9 (^2D)\sigma^2$ configuration. This is analogous to the $3d_{Ni}^9 (^2D) 3d_{Cu}^{10}\sigma^2$ ground configuration of NiCu,^{8,9} and would lead to $^2\Sigma^+$, $^2\Pi$, and $^2\Delta$ molecular terms, depending on the location of the $3d$ hole on the Ni atom. As in NiCu, the effective positive charge of the aluminum core would be expected to cause these terms to be ordered as $^2\Delta < ^2\Pi < ^2\Sigma^+$, leading to a ground state of $X \ ^2\Delta_{5/2}$.¹⁰ This was verified in the present study¹¹ and although a large density of states in this molecule prohibits a concise elucidation of its electronic structure, the rotational analysis of four discrete transitions has culminated in a measured bond length of 2.3211 ± 0.0007 Å. In addition, the observation of an abrupt predissociation threshold has allowed the dissociation energy of AlNi to be measured.

A comparison of the resonant two-photon ionization spectrum obtained using two different ionization schemes has allowed the ionization potentials of both AlNi and AlCu to be measured. These values may be combined with the respective dissociation energies of the molecules and the atomic ionization potential of Al¹² to arrive at the cationic bond strengths $D_0^0(\text{Al}^+\text{Ni})$ and $D_0^0(\text{Al}^+\text{Cu})$. The overall results of these two studies show AlCu and AlNi to be quite similar in bond length (2.3389 ± 0.0005 vs. 2.3211 ± 0.0007 Å), bond strength (2.315 ± 0.011 vs. 2.434 ± 0.001 eV), ionization potential (7.063 ± 0.012 vs. 6.95 ± 0.09 eV), and cationic bond strength (1.238 ± 0.016 vs. 1.47 ± 0.09 eV). These results provide strong evidence that the chemical bonding is similar in both species (particularly as neutrals).

In contrast to Ni and Cu, Zn has both its $4s$ and $3d$ subshells completely filled, with the first excited separated atom limit lying over $32,000$ cm^{-1} higher in energy.¹² Since the promotion energy required to open the $4s$ subshell is so high, this is the first transition metal aluminide studied that probes the preferential orientation of the lone Al p electron in the presence of a filled $4s^2$ configuration. Furthermore, the contraction of the d orbitals makes them inaccessible for bonding in Zn.

In this study¹³ a puzzling spectrum of several discrete vibronic bands was observed in the energy region from 18400 to 19100 cm^{-1} . Rotational and lifetime analyses of these bands have identified four of the bands as members of a vibronic progression corresponding to a common $\Omega' = 1/2 \leftarrow \Omega'' = 1/2$ electronic transition, designated as $B \ ^2\Pi_{1/2} \leftarrow X \ ^2\Pi_{1/2}$. Three of the remaining bands have been identified as the corresponding $\Omega' = 3/2 \leftarrow \Omega'' = 3/2$ component of the $B \ ^2\Pi_{3/2} \leftarrow X \ ^2\Pi_{3/2}$ electronic transition, while the remaining two bands are believed to belong to an entirely different $\Omega' = 1/2$ electronic state (designated as the A $\Omega' = 0.5$ state). Collection of the spectrum under "hotter" source conditions reveals numerous additional spectroscopic features that after close scrutiny can be attributed to one of the three aforementioned states. A weighted least squares analysis of the ground state bond length yields $r_0 = 2.6944 \pm 0.0003$ Å, significantly longer than that of AlCu or AlNi. In addition, the ground state of AlZn has been unambiguously determined as $^2\Pi_{1/2}$, as is likewise found to be true in preliminary results obtained for AlCa.¹⁴ These studies indicate the preferential orientation of the Al p electron to be $p\pi$ in the presence of a transition metal atom with a filled $4s$ subshell.

References

- ¹Z.-W. Fu, G. W. Lemire, Y. Hamrick, S. Taylor, J.-C. Shui, and M. D. Morse, *J. Chem. Phys.* **88**, 3524-3531 (1988).
- ²S. Gerstenkorn and P. Luc, *Atlas du Spectre d'Absorption de la Molécule d'Iode* (CNRS, Paris, (1978); S. Gerstenkorn and P. Luc, *Rev. Phys. Appl.* **14**, 791 (1979).
- ³J. M. Behm, C. A. Arrington, J. D. Langenberg, and M. D. Morse, manuscript in preparation.
- ⁴C. W. Bauschlicher, Jr., S. R. Langhoff, H. Partridge, and S. P. Walch, *J. Chem. Phys.* **86**, 5603-5612 (1987).
- ⁵M. Bär and R. Ahlrichs, *Chem. Phys. Lett.* **178**, 241-245 (1991).
- ⁶M. F. Cai, S. J. Tsay, T. P. Dzugas, K. Pak, and V. E. Bondybey, *J. Phys. Chem.* **94**, 1313-1316 (1990).
- ⁷C. W. Bauschlicher, Jr. and S. R. Langhoff, personal communication.
- ⁸Z.-W. Fu, and M. D. Morse, *J. Chem. Phys.* **90**, 3417-3426 (1989).
- ⁹E. M. Spain and M. D. Morse, *J. Chem. Phys.* **97**, 4633-4640 (1992).
- ¹⁰E. M. Spain and M. D. Morse, *J. Chem. Phys.* **97**, 4641-4660 (1992).
- ¹¹J. M. Behm, C. A. Arrington, and M. D. Morse, manuscript in preparation.
- ¹²C. E. Moore, *Natl. Bur. Stand. Circ. No. 467* (1971).
- ¹³J. M. Behm, T. Blume, and M. D. Morse, manuscript in preparation.
- ¹⁴J. M. Behm and M. D. Morse, manuscript in preparation.

High Resolution Spectroscopy of Ti_2 and AlY at Near-Infrared Frequencies

Caleb A. Arrington, Jon D. Langenberg, Jacqueline C. Pinegar, and Michael D. Morse

Department of Chemistry
University of Utah
Salt Lake City, Utah 84112
(801) 581-4204

Mats Doverstål, Bo Lindgren, and Ulf Sassenberg

Department of Physics
Stockholm University
Vanadisvägen 9
11346 Stockholm, Sweden

High resolution jet-cooled molecular beam spectroscopy has been effective in revealing the bonding between transition metals. One periodic trend that has developed during the study of small transition metal molecules is the relatively weak bond strength in the early $3d$ transition metals (Sc_2 , Ti_2) in comparison to middle (V_2 , Cr_2) or late (Ni_2 , Cu_2) members of the $3d$ series. This trend of bond strengths in early transition metals is not so pronounced in the $4d$ and $5d$ metals where d -bonding is a major contributor to molecular stability. Low bond strengths in molecules, whether due to poor d overlap or high $s \leftarrow d$ promotion energy, provides a challenge to the spectroscopist. It has been shown that diatomic systems with a large density of electronic states, as is usually the case for open d -subshell molecules, undergo a rapid predissociation ($\tau < 5$ ns) when excited above the lowest dissociation limit.¹ The extreme density of states responsible for predissociation also precludes isolation of single rovibronic states suitable for high resolution spectroscopy at energies near the dissociation limit of these molecules. The spectroscopist interested in investigating species with low bond strengths and high densities of electronic states, as in our investigation of Ti_2 and AlY , is forced to search the low energy near-infrared region for isolated electronic states that are not hopelessly perturbed. In the present near-infrared investigation of Ti_2 and AlY we have employed resonant two photon ionization (R2PI) as the detection strategy for obtaining optical spectra in a jet-cooled molecular beam.

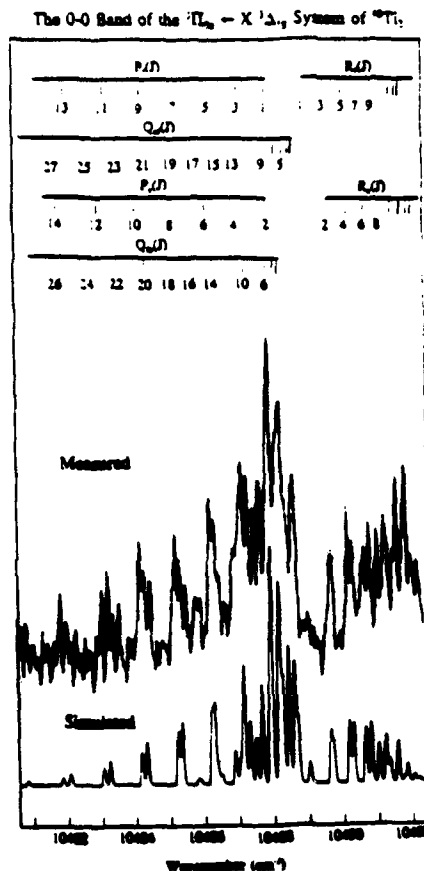
The creation of our jet-cooled molecular beam was accomplished by laser vaporization (Nd:YAG, 532 nm, 15 mJ per pulse) of a Ti rod or an AlY alloy disk. The laser-vaporized metal plasma was entrained in an argon carrier gas 3 cm before supersonic expansion from a 2 mm orifice. Apart from the substitution of argon for helium carrier gas, the experimental details are as described elsewhere.² Argon carrier gas was necessary to more thoroughly cool the molecules, thereby alleviating problems of spectral congestion.

The near-infrared photons required for excitation were generated by Raman shifting the output of a Nd:YAG pumped dye laser operating on laser dyes LDS 698, LDS 750, and LDS 751 using a high pressure (500 psi) H_2 cell 0.75 m in length, giving a Raman shift of 4155.163 cm^{-1} . The second, ionizing photon was generated from an excimer laser operating

on KrF (248 nm, 5.00 eV). In the application of R2PI spectroscopy to low energy excited states, stringent limits are placed on the second, ionizing photon, which must fall between the ionization potential of the molecule (I.P.) and the I.P. minus the energy of the excitation photon. When IR transitions are investigated this energy range can be quite small. For the Ti_2 and AlY molecules we were fortunate that KrF radiation was suitable for ionization.

The near-infrared R2PI investigation of Ti_2 revealed one major vibronic band, shown under high resolution in Figure 1. It is the apparent splitting of the higher rotational lines, most obvious in the P-branch, which enables the unambiguous assignment as ${}^3\Pi_{0u} \leftarrow X {}^3\Delta_{1g}$.

Figure 1. High-resolution R2PI spectrum of ${}^{48}\text{Ti}_2$ near 10488 cm^{-1} .



The mass resolution inherent in the R2PI experiment enabled the various mass combinations of Ti_2 to be monitored individually. For the most abundant isotopic combination, ${}^{48}\text{Ti}_2$ ($I=0$, 54.67% of Ti_2 molecules), nuclear spin statistics require that only levels of one parity type (e or f) exist for even J , while only levels of the opposite parity exist for odd J . Therefore the spectrum of ${}^{48}\text{Ti}_2$ can show no splitting of rotational lines due to lambda doubling, and another explanation for the observed splitting is required. A possible explanation could be an upper or lower state with $\Omega = 0^\pm$, where the + and - components are split by an approximately constant amount. One might then have a $R_2(J)$ line falling near an $R_1(J+1)$ line, for example, leading to the impression of a splitting of an individual line. The *ab initio* studies of Ti_2 performed by Bauschlicher *et al*⁸ suggest a ${}^3\Delta_g$ ground state. Assuming an $X {}^3\Delta_{1g}$ ground state, the Ti_2 spectrum of Figure 1 was fit to a $\Omega=0^\pm_u \leftarrow X {}^3\Delta_{1g}$ transition, giving rotational constants of $B''_0 = 0.18640 \pm 0.00016 \text{ cm}^{-1}$ and

$B_0' = 0.17476 \pm 0.00015 \text{ cm}^{-1}$, and bond lengths of $r_0(X^3\Delta_{1g}) = 1.9422 \pm 0.0008 \text{ \AA}$ and $r_0(^3\Pi_{0g}) = 1.997 \pm 0.009 \text{ \AA}$. These values were used to produce the simulated spectrum in Figure 1, which is in good agreement with the experimental data. Assuming a spin-allowed transition, $^3\Pi_u$ is the only possible choice for the excited $\Omega = 0^\pm$ state.

The bonding of this early transition metal dimer is counterintuitive. One might expect the $3d$ orbital energies to fall in the order $3d\sigma_g < 3d\pi_u < 3d\delta_g < 3d\delta_u^* < 3d\pi_g^* < 3d\sigma_u^*$, so that if exchange effects were to favor unpairing the electrons in one of the d orbitals in the $4s\sigma_g^2 3d\sigma_g^2 3d\pi_u^4$, $^1\Sigma_g^+$ state, it would be the $3d\pi_u^4$ shell that would be cracked open, resulting in a $4s\sigma_g^2 3d\sigma_g^2 3d\pi_u^3 3d\delta_g^1$, $^3\Phi_u$ ground state. The fact that the $3d\sigma_g^2$ shell is opened may indicate that the molecular orbitals are ordered as $3d\pi_u < 3d\sigma_g < 3d\delta_g < 3d\delta_u^* < 3d\sigma_u^* < 3d\pi_g^*$ instead. A possible explanation for the $3d\pi_u < 3d\sigma_g$ energy reordering is that in the early transition metals the molecular orbitals are perturbed by $4s\sigma_g$ - $3d\sigma_g$ mixing, lowering the $4s\sigma_g$ orbital and raising the $3d\sigma_g$ orbital in energy, possibly to the point that it lies above the $3d\pi_u$ orbital. Similar effects occur in early $2p$ series dimers, where $2s\sigma$ - $2p\sigma$ hybridization causes the $2p\pi_u$ orbital to lie lower in energy than the $2p\sigma_g$ orbital in B_2 and C_2 .

As in the case of Ti_2 dimer, AlY was investigated in the near-infrared using R2PI. In this molecule a progression of vibronic bands was observed, shown in Figure 2, leading to fitted spectroscopic constants of $\omega_e' = 279.6 \pm 1.1 \text{ cm}^{-1}$ and $\omega_e x_e' = 4.1 \pm 0.3 \text{ cm}^{-1}$.

$A^3\Sigma^- \leftarrow X^3\Sigma^-$ Vibronic Progression in $^{27}Al^{69}Y$

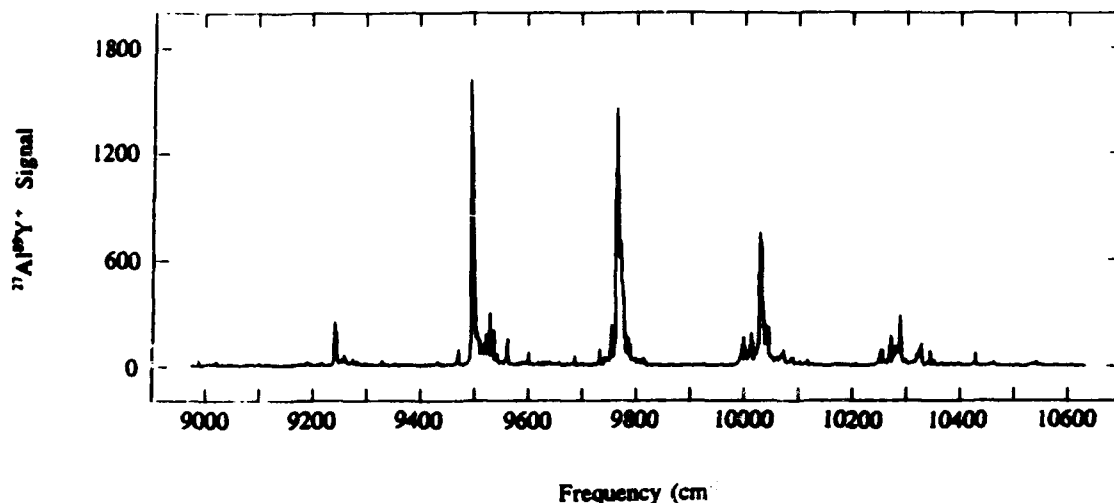


Figure 2. Low-resolution spectrum of $^{27}Al^{69}Y$, showing an intense, regular vibronic progression.

The 0-0, 1-0, and 2-0 bands of this progression have been investigated under high resolution (0.03 cm^{-1}), giving the rotationally resolved spectrum shown in Figure 3 for the 0-0 band. This spectrum clearly lacks a Q-branch, showing that the ground and excited states both possess $\Omega = 0$ (and based on the plausible electronic states, presumably $\Omega = 0^+$). The 0-0, 1-0, and 2-0 bands were fitted to the standard formula, allowing rotational constants to be determined as $B_0' = 0.10117 \pm 0.00015 \text{ cm}^{-1}$ and $B_0'' = 0.09842 \pm 0.00015 \text{ cm}^{-1}$, and confirming the transition as $\Omega=0 \leftarrow \Omega=0$. The $\Omega=0^+$ ground state of AlY is thought to be

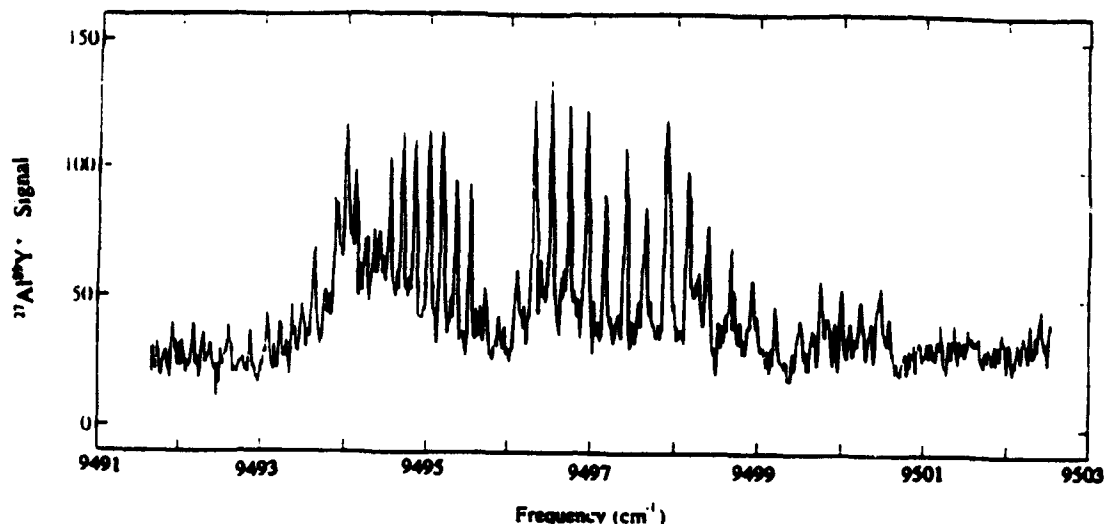
0-0 Band of the A-X System of $^{27}\text{Al}^{69}\text{Y}$ 

Figure 3. High-resolution spectrum of the 0-0 band of AlY near 9496 cm^{-1} , showing the rotational structure expected for an $\Omega = 0 \leftarrow \Omega = 0$ band.

the lowest spin component of a $^3\Sigma$ state, rather than a $^1\Sigma^+$ ground state. The most compelling evidence for this assignment is comparison to the bonding of the cation, AlY^+ . From electron spin resonance (ESR) spectroscopy, AlY^+ molecules isolated in a Ne matrix have been found to have a high spin $^4\Sigma$ ground state.⁴ The dominant configuration contributing to the $^4\Sigma$ ground state is thought to be $3s_{\text{Al}}^2\sigma^1\pi^2$, where both the σ and π orbitals are bonding in character. It is likely that the bonding in neutral AlY is similar, leading to a dominant ground state configuration of $3s_{\text{Al}}^2\sigma^2\pi^2$, $^3\Sigma$. In the case of AlY the ordering of the bonding orbitals is apparently $\sigma < \pi$, consistent with the idea that the $3s$ orbital of aluminum lies too low in energy to strongly mix with the $3p\sigma + 4d\sigma$ orbital of AlY, unlike the situation in Ti_2 where $3d\sigma - 4s\sigma$ mixing is apparently significant.

References

- ¹ E. M. Spain and M. D. Morse, *J. Phys. Chem.* **96**, 2479 (1992).
- ² Z.-W. Fu, G. W. Lemire, Y. M. Hamrick, S. Taylor, J.-C. Shui and M. D. Morse, *J. Chem. Phys.* **88**, 3524 (1988).
- ³ C. W. Bauschlicher, Jr., H. Partridge, S. R. Langhoff and M. Rosi, *J. Chem. Phys.* **95**, 1057 (1991).
- ⁴ L. B. Knight, Jr., R. M. Babb, G. M. King, A. J. McKinley, M. D. Morse and C. A. Arrington, *J. Chem. Phys.* in press.

FTIR Spectra and Torsion-Vibration Coupling in $^{13}\text{CD}_3\text{OH}$

Li-Hong Xu and R.M. Lees

Department of Physics, University of New Brunswick, Fredericton, N.B., Canada E3B 5A3

Tel. (506) - 453 - 4723

I. Introduction

Methanol is one of the simplest molecule capable of large amplitude torsional motion. This couples with the vibrational motions and has significant effects on the infrared spectrum, illustrated at low resolution in Fig. 1 for the $^{13}\text{CD}_3\text{OH}$ isotopomer in the 950-1450 cm^{-1} region. The complex torsion-vibration energy structure of $^{13}\text{CD}_3\text{OH}$ is shown in Fig. 2. Level crossings occur among a variety of states giving numerous Fermi and Coriolis interactions. Thus, methanol offers a good test platform for the study of intramolecular vibrational relaxation (IVR) with torsional effects. Furthermore, the ready availability of different isotopomers allows us to seek insight into individual torsion-vibration interaction mechanisms through the substantial changes in symmetry coordinate mixing and vibrational interaction which occur upon isotopic substitution. So far, different bands of $^{13}\text{CH}_3\text{OH}$, $\text{CH}_3^{18}\text{OH}$, CD_3OH and $^{13}\text{CD}_3\text{OH}$ as well as the normal $^{12}\text{CH}_3^{16}\text{OH}$ species have all been studied by several groups around the world.¹⁻⁷

The vibrational fundamentals are all located below 4000 cm^{-1} . In this work, we recorded Fourier transform spectra for $^{13}\text{CD}_3\text{OH}$ on a modified DA3.002 Bomem instrument from 800-1030 and 1000-1350 cm^{-1} at resolutions of 0.002 and 0.003 cm^{-1} , respectively, with the latter region at higher pressure and path length to enhance the weaker bands. The spectra include the low-lying CD_3 -rocking,⁷ CO-stretching,^{4,5} CD_3 -deformation and OH-bending fundamentals, as shown in Fig. 1. One sees immediately that the low resolution band profiles vary significantly, indicating strong effects from torsion-vibration interaction. This has been difficult to examine explicitly from low-resolution data in the past, but is now becoming possible with high resolution FTIR. The remainder of this paper will discuss each band individually, with particular attention to the torsion-vibration and vibration-vibration interactions.

All of the IR sub-band assignments are based on closed transition combination loops. These utilize ground state wavenumbers derived from the torsion-rotation FIR spectrum, which we have also studied extensively.⁸ The energy patterns for a given state, as shown in Fig. 2 are oscillatory functions of the axial rotational angular momentum K. Two important observables, the amplitude of the oscillation of the torsion-rotation energies with K and the separation between the $n = 0$ and $n = 1$ energy levels, are very sensitive to the torsional barrier height V_3 , hence this parameter plays a major role in the appearance of the band profiles.

II. CD_3 -Rocking Band

Under the low resolution in Fig. 1, the CD_3 -rocking band displays a double-peaked Q branch with about 10 cm^{-1} separation, centred around 851 cm^{-1} . Detailed analysis shows the band to be of parallel a -type but with rather widely spread structure.⁷ The twin peaks in fact arise from a single vibrational mode, and the apparent doublet structure is due simply to strong torsion-vibration interaction in the rocking mode. Fig. 3 illustrates one of the Q-branch peaks at high resolution, showing the individual sub-branches to be well spread out and clearly resolved, unlike the CO-stretch Q branch, indicating substantial changes in torsion-rotation parameters from the ground state. All of the $n=0$ sub-branches have been assigned, and their origins used to

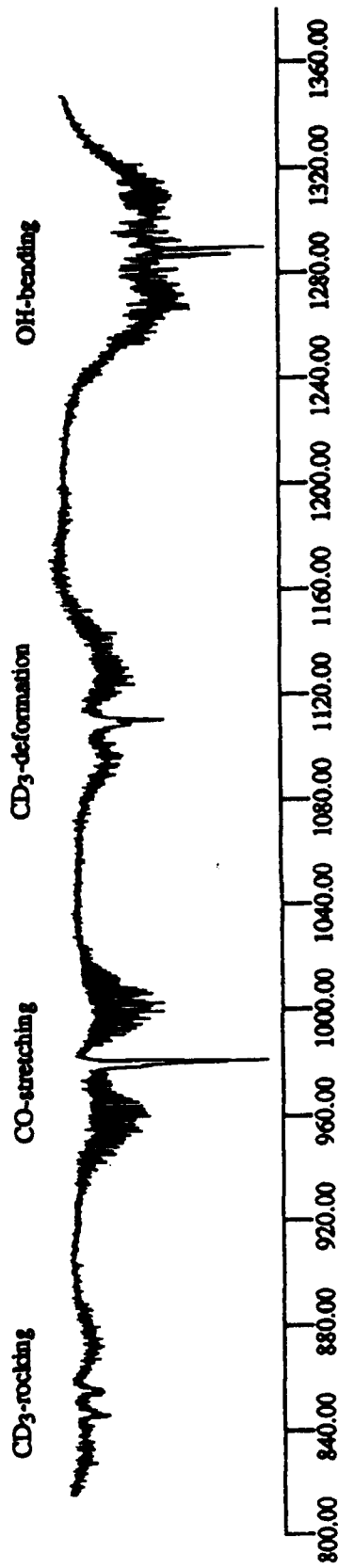


Fig. 1 Low resolution spectrum of $^{13}\text{CD}_3\text{OH}$

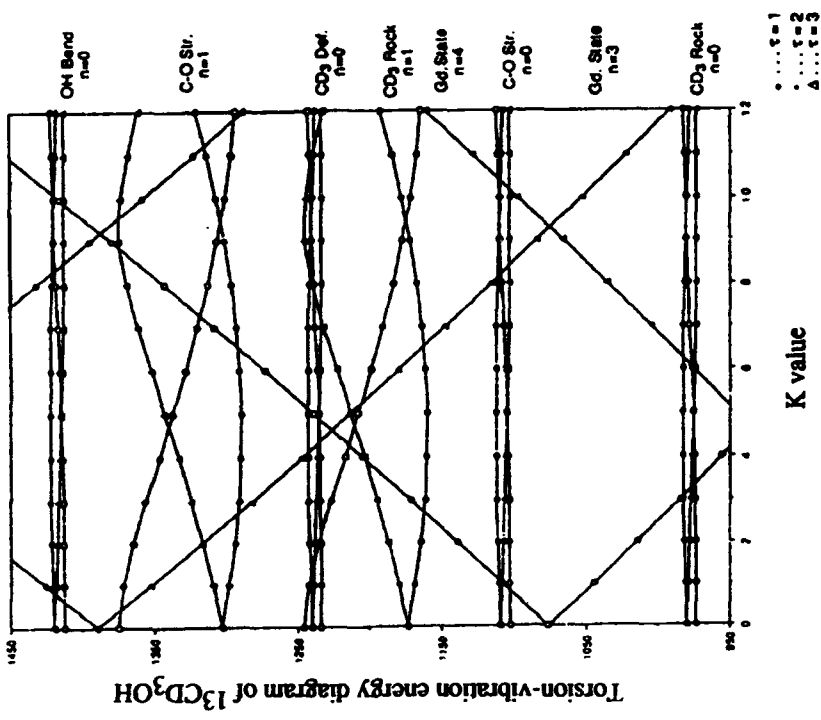


Fig. 2 Torsion-vibration energy diagram of $^{13}\text{CD}_3\text{OH}$

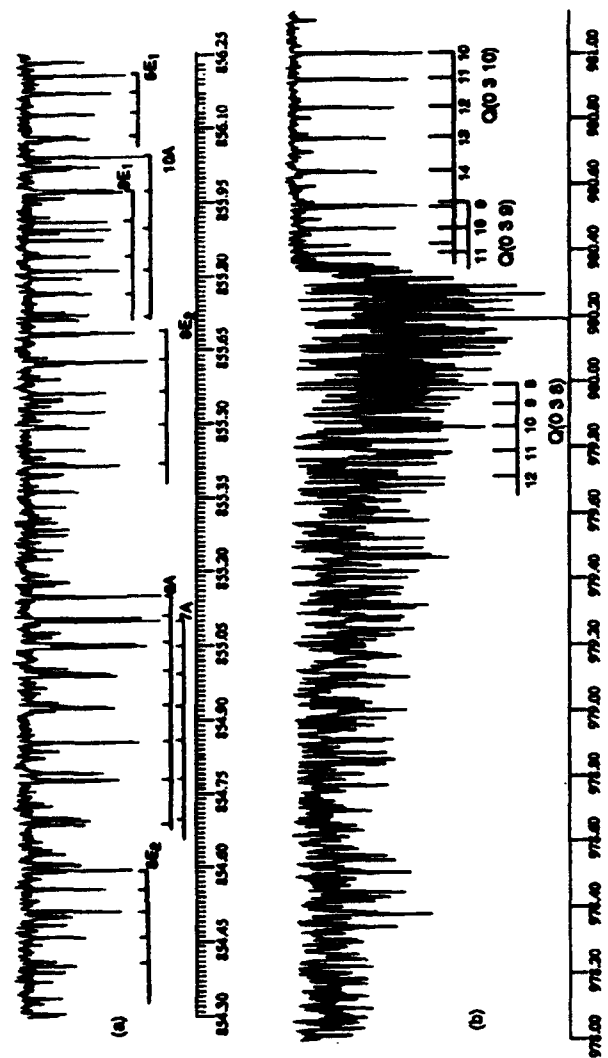


Fig. 3 Comparison of Q branches for (a) CD_3 -rocking, and (b) CO -stretching bands

reconstruct the torsional energy pattern for the excited CD₃-rocking state. Although the normal oscillation with K is not seen, suggesting that something is missing from our Hamiltonian, a smaller apparent amplitude hints at an increased torsional barrier height for the rocking state. This is supported by the observation of several $n = 1$ sub-branches whose origins are located about 50 cm⁻¹ above the main $n = 0$ origins. This 50 cm⁻¹ shift implies an effective V_3 of 483 cm⁻¹ for the rocking state, about 30% higher than the ground state value. In addition, Fermi interactions for the 3A and 6E₁ states are expected due to the level crossings with $n = 3$ ground vibrational levels³ seen in Fig. 2, and these perturbations are indeed observed in our spectrum.

III. CO-Stretching Band

Methanol is an excellent source of FIR laser emission when optically pumped by CO₂ lasers, because the strong CO-stretching absorption band overlaps well with the CO₂ laser bands. Thus, the interest in identifying the FIR laser transitions provides a practical motivation for studying this band.⁹ It is a well behaved a -type band with clear P, Q and R structure, as seen in Fig. 1. The narrow width of the P and R J-multiplets and the highly condensed Q branch in Fig. 3 suggest very similar parameters for the CO-stretch and ground states. Fermi interactions between CO-stretching and $n = 4$ ground vibrational levels^{3,9} are prominent at the Q-branch head in Fig. 3. The $n = 0$ and 1 torsional energy patterns are reproduced by our torsional Hamiltonian but with a general downward shift for the $n = 1$ state. This probably arises from interaction with the OH-bending mode lying close above, as seen in Fig. 2, or through coupling between the CO-stretching and torsional coordinates as proposed by Henningsen and coworkers for CH₃OH.¹⁰

IV. CD₃-Deformation Band

The symmetric CD₃-deformation band is located around 1111 cm⁻¹ with reasonably well behaved a -type features. However, the separation between J-multiplets is larger for the R than the P branch, indicating an increase in rotational B-value in going from ground state to the excited CD₃-deformation state. This results in a very interesting feature for the CD₃-deformation band, a large number of J-localized perturbations which arise because the deformation levels cross from below to above interacting levels of nearby states as J increases. Two types of resonance have been seen in this band, one being Fermi interactions with mainly $n = 4$ torsional levels of the ground vibrational state for medium K, and the other being Coriolis resonance with $n = 1$ levels of the CD₃-rocking state. We observed two sub-branches with long J-progressions which could only be fitted with additional $\Delta K = 1$ matrix elements added, supporting the notion of Coriolis interaction in this state. The $n = 0$ torsional energy pattern is similar to the ground state with a slightly larger amplitude of oscillation of the torsion-rotation energy with K. This corresponds to a decrease of 12% in V_3 from the ground state value.

V. OH-Bending Band

The analysis of this band is still in progress. Our assignments so far show an a -type band structure with the majority of the Q-branch origins concentrated around 1289 cm⁻¹ but others at 1283 cm⁻¹. We believe that the CD₃-rocking and OH-bending motions are significantly coupled, mixing those coordinates in the normal modes. The relatively amorphous shape and lack of well-resolved multiplet structure in the OH-bending band as seen in Fig. 1 may be due to this mixing.

VI. Discussion

Four different fundamental bands have been observed in our FTIR spectral region. It turns out that they are all a -type parallel bands, suggesting that the CO-stretching and probably OH-bending states are bright states feeding intensity into the CD₃-rocking and CD₃-deformation

bands, which were expected to be weak. So far, however, the out-of-plane CD₃-rocking and asymmetric CD₃-deformation states still remain completely dark to our view. The asymmetric CD₃-deformation band has a practical interest since it overlaps the 9.6 μm CO₂ band. Thus, future information on this excited state will likely come through FIR laser assignments, as numerous known lines are optically pumped in this region by strong CO₂ lasers.

So far, our main effort has gone into the assignment of the complex torsion-vibration spectra, with particular attention to searching for perturbations and characterizing the interacting levels. The detailed high resolution study has clearly shown that torsion-vibration interactions in methanol are strong and that they significantly affect the low-resolution band structure and band profiles. Therefore, it seems that it will be necessary to sort out these perturbations before a really reliable force-field analysis is possible.

Our next challenge is to try modelling the perturbations to determine the interaction constants and the unperturbed vibrational energies. From these, we wish to develop a picture of the interacting modes in order to find the true molecular eigenstates. We also hope to develop and test suitable models for the torsion-vibration interaction terms in the molecular Hamiltonian, to examine the extent to which it is possible and reasonable to formulate effective torsion-rotation Hamiltonians which would be valid for each vibrational state. As well, we want to explore the role of torsion in coupling to vibration to seek a more general torsion-vibration potential surface to probe the sensitivity of V₃ to particular vibrational symmetry coordinates.

References

1. I. Mukhopadhyay, "High Resolution Far Infrared and Infrared Spectroscopy and Far Infrared Laser Analysis of C-12 and C-13 Methanols," Ph.D. Thesis, University of N.B., 1986.
2. R.R.J. Goulding, C. Young, R.M. Lees, W. Lewis-Bevan, and J.W.C. Johns, "Doppler-Free Optoacoustic Spectroscopy of O-18 Methanol," *Infrared Phys.* **28**, 297-306 (1988).
3. W.H. Weber and P.D. Maker, "Analysis of Doppler-Limited Spectra of the C-O Stretch Fundamental of CD₃OH," *J. Mol. Spectrosc.* **93**, 131-153 (1982).
4. J.C.S. Moraes, A. Scalabrin, D. Pereira, G. Carelli, N. Ioli, A. Moretti, and F. Strumia, "Spectroscopy of the Excited C-O Stretching Q Branch of ¹³CD₃OH: Measurement and Assignment of New FIR Laser Lines," *Infrared Phys.* **33**, 133-139 (1992).
5. Li-Hong Xu, R.M. Lees, I. Mukhopadhyay, J.W.C. Johns, and G. Moruzzi, "Fourier Transform Spectroscopy of ¹³CD₃OH: The CO-Stretching Fundamental Band," *J. Mol. Spectrosc.* **157**, (1993), in press.
6. G. Moruzzi, F. Strumia, P. Carnesecchi, R.M. Lees, I. Mukhopadhyay and J.W.C. Johns, "Fourier Spectrum of CH₃OH between 950 and 1100 cm⁻¹," *Infrared Phys.* **29**, 583-606 (1989).
7. R.M. Lees, L.H. Xu, K.J. King, J.W.C. Johns, C. Young, and T.J. Lees, "FTIR Spectroscopy of the CD₃-Rocking Bands of CD₃OH and ¹³CD₃OH," 15th Int. Conf. IR & MM Waves, Orlando, Fla., Conf. Digest, ed. R.J. Temkin, Proc. SPIE Vol. **1514**, 726-728 (1990).
8. Li-Hong Xu, R.M. Lees, and J.W.C. Johns, "Torsion-Rotation FIR Spectrum of ¹³CD₃OH," Int. Conf. on Millimeter-Wave and Far-Infrared Technology, Beijing, China, August, 1992, Conf. Digest, ed. G.M. Tucker, pp. 263-266.
9. Li-Hong Xu, R.M. Lees, I. Mukhopadhyay, and J.W.C. Johns, "Fourier Transform Spectroscopy of ¹³CD₃OH: Assignment of Far-Infrared Laser Lines," *J. Mol. Spectrosc.* **153**, 181-196 (1992).
10. H. Rudolph, J. Avery, and J.O. Henningsen, "Torsion-Vibration Interaction in CH₃OH," *J. Mol. Spectrosc.* **117**, 38-45 (1986).

**Two-Color Photo-Associative Ionization Collisions
between Sodium Atoms.**

V. Bagnato¹, L. Marcassa¹, C. Tao, Y. Wang and J. Weiner²

Department of Chemistry and Biochemistry

University of Maryland

College Park, MD 20742

Collisions of ultracold trapped atoms ($T < 1\text{mK}$) have opened a new field of atomic collisions with abundant opportunities for theory and experiments. Photo-associative ionization (PAI) in sodium atoms has been the first two-body collision studied in optical traps¹. In this process two ground state Na atoms absorb two photons during the course of the collisional encounter. The first absorption at long range put the colliding system on an attractive C_3/R^3 potential curve, and the two atoms begin to accelerate toward each other. A second absorption promotes the system to a doubly excited $\text{Na}(3p)+\text{Na}(3p)$ potential curve from which the PAI process takes place at short range.

We have investigated for the first time two-color PAI (TCPAI) of a sample of ultracold sodium atoms held in a magneto-optical trap. Using different combinations of trapping frequency (ω_1), repumper frequency (ω_2), and probe laser frequency (ω_p), we have explored TCPAI by populating different combinations of ground hyperfine levels.

In continuous operation of the MOT, ω_1 is normally tuned about 10 MHz to the red of the $3s^2S_{1/2}(F=2) \rightarrow 3s^2P_{3/2}(F=3)$ transition frequency while ω_2 is tuned near the $3s^2S_{1/2}(F=1) \rightarrow 3s^2P_{3/2}(F=2)$ transition. In this case contribution of both hyperfine ground states are important. The spectrum of TCPAI as a function of ω_p is shown in fig. 1a. The position and general shape of the spectrum is accord with theoretical prediction⁴.

We can also run the experiment in a "chopped MOT" mode in which we cycle the system between periods of trapping and observation. The chopped mode permits preparation of atom samples with nearly pure ground hyperfine $F=1$ or $F=2$ levels. The chopped-mode spectra are shown in Figs 1b and 1c. Evidently manipulation of hyperfine populations radically effects the appearance of the TCPAI spectra. However, from the observations and from comparasion with theory (where applicable) a fairly clear understanding of TCPAI dynamics emerges.

(Financial support from FAPESP , NSF and NIST)

1. Permanent address, Instituto de Fisica e Quimica de S. Carlos, USP, Caixa Postal 369, S. Carlos SP Brasil - 13560
2. On leave at the National Science Foundation, Physics Division, 1800 G Street NW, Washington DC 20550
3. P. Gould, P. Lett, P. Julienne, W. Phillips, H. Thorsheim and J. Weiner, Phys. Rev. Lett. **60**,788 (1988)
4. A. Gallagher, Phys. Rev. A **44**, 4249 (1991)

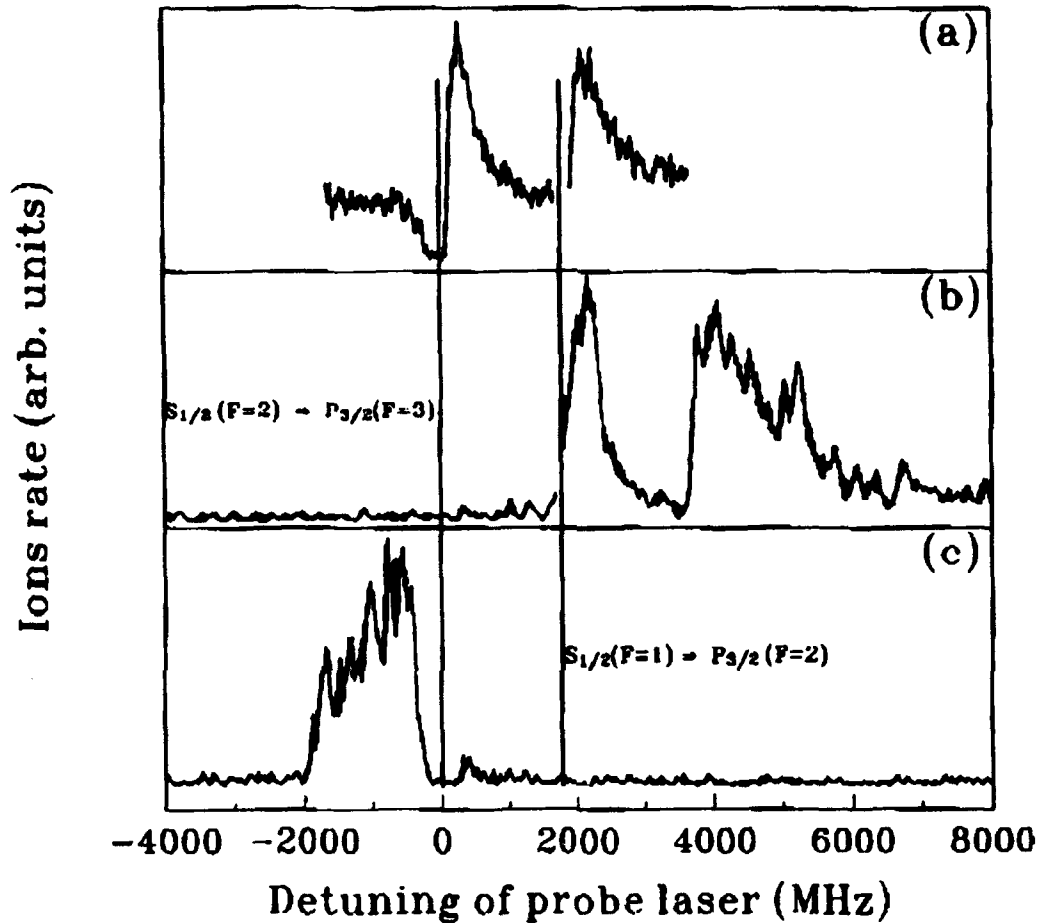


Fig. 1 - PAI ion rate as function of ω_p for different cases. (a) Normal trapping operation, two frequencies are available for the first step (ω_1, ω_2). (b) Process starting with only $F=1$ ground state in the presence of ω_1 and ω_p . (c) Process starting with only $F=2$ ground state atoms in the presence of ω_2 (repumper) and ω_p

Vibrational Transfer in Collisions of $\text{Li}_2 \text{ A}^1\Sigma_u^+(v_i, j_i)$ with Neon

Peter Gorgone, Scott Davis, Yunxiao Gao,
Eric McCall, Mark Rosenberry,
and Brian Stewart

Wesleyan University, Department of Physics
Middletown, CT 06459 (203)347-9411 x3106

We have measured a large number of rate constants for the process



where v_i, j_i, v_f and j_f indicate the initial and final vibrational and rotational quantum numbers of the Li_2 molecule. The experiments were performed in a heated ($\approx 900\text{K}$) cell by the well-known [see e.g. SSP84a] method of preparing excited state population in a single vibrotational level with a single-frequency cw dye laser and dispersing the emission. Strong lines emanating from the laser populated level (*parent lines*) are accompanied by weaker lines (*satellite lines*) from levels populated by collisions with neon. The excited state lifetime provides a clock that establishes single collision conditions. The spectrum is taken at several pressures, and extrapolation to zero pressure yields level-to-level rate constants. A Doppler technique has permitted us to explore the velocity dependence of these rate constants.

Our interest in vibrationally inelastic processes necessitates making measurements over a wide dynamic range, since these highly vibrationally adiabatic collisions account for at most a few percent of the total inelastic rate. We therefore employ a double monochromator and use photon counting, and have worked hard to improve signal rates and decrease background levels by carefully tuning photomultiplier discriminator levels and blocking scattered light. The result is measurements that span five orders of magnitude and clearly reveal the j_f dependence of the vibrationally inelastic rate constants over a range of Δv (see figure 1).

An important goal of these measurements is to elucidate the dependence of inelastic scattering processes on the initial vibrational quantum number v_i . Accordingly, we have taken data with $v_i = 2, 4, 7, 12, 17$ and 24. Results of a preliminary analysis of these data reveal the following points:

1. The rotationally inelastic rate constant is unaffected by increases in initial vibration over the experimental range;
2. The vibrotationally inelastic rate constant rises strongly with increasing v_i , most particularly in the case of $\Delta v = -2$, for which the increase is more than a factor of 50;

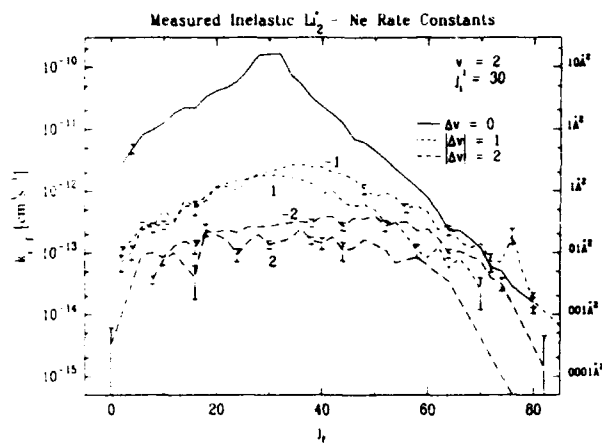


Figure 1: Inelastic rate constants for $v_i = 2, j_i = 30$.

ularly in the case of $\Delta v = -2$, for which the increase is more than a factor of 50;

3. The increase in rate constant with climbing v_i exhibits an abrupt change around $v_i = 7$ which is particularly noticeable for the $\Delta v = -1$ data, for which there is a gap between the low v_i and high v_i rate constants. The discontinuity would be explained by an abrupt decrease in the excited state lifetime above $v = 4$, but the available data [SCM85, PRB85] indicate that there is in general no such change. Similar behavior has been observed in the vibrational deactivation of NO [YKW92], but the explanation invoked by Yang *et al.* of a sudden onset of multiquantum ($|\Delta v| > 1$) transfer cannot be operative here, since the phenomenon is most marked for $\Delta v = 1$. The unexpected behavior has prompted us to design an experiment, now in progress, to fill in the gaps in initial vibrational quantum number and verify our previous measurements.
4. The j_f distributions possess the same shape to within measurement error. This makes the prospect of a universal scaling relation for vibrational transfer seem less remote.

It is noteworthy that our results differ from the (rotationally summed) rate constants determined by Krajnovich *et al.* [KBD89] in the $\text{He} + \text{I}_2$ system. Although their measurements were not absolute, they found that rate constants for $|\Delta v| = 0$ and 1 exhibited nearly the same dependence on v_i , in contrast to the strong differences between $|\Delta v| = 0$ and 1 in our $\text{Li}_2 - \text{Ne}$ data.

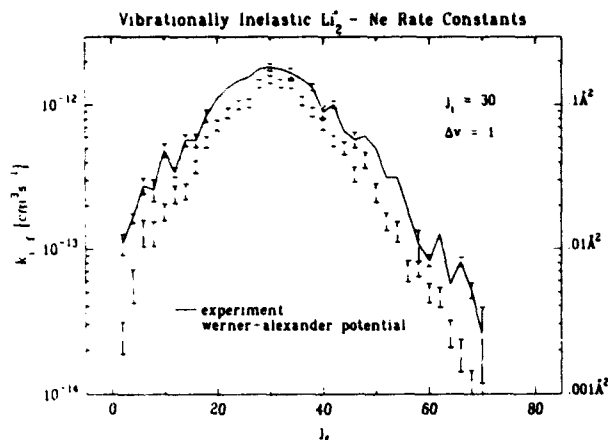


Figure 2: Comparison of experimental and calculated rate constants for $|\Delta v| = 1$.

A high-quality *ab initio* potential for the $\text{Li}_2(\text{A})-\text{Ne}$ system has very recently become available [ALW91]. We have used this potential to calculate classical trajectories with our fast action-angle routine due to Smith [SMI86]. The results of calculations for $v_i = 2$ are shown in figure 2. The agreement is very good; the shape of the j_f distribution in particular agrees nearly perfectly with the measurements. We would like to use this potential to look for the abrupt change seen in the overall size of the experimental rate constants with increasing v_i . Unfortunately, the range of internuclear separations for which the potential was calculated is too small to permit this.

In order to probe the dynamics of the vibrationally inelastic transfer process more deeply than permitted by thermally averaged rate constants, we have measured velocity-dependent cross sections using the Velocity Selection by the Doppler Shift (VSDS) technique [SSP84b]. This method entails measuring the rate constant as a function of detuning from linecenter. Since detuning is related to the component of velocity in the laser direction, a partial velocity selection results; through a deconvolution, the resulting detuning-dependent rate constants yield velocity dependent rate constants and hence cross sections. Our approach to deconvolution, not yet implemented, will be to model the cross sections and calculate the lineshape ratios. We will choose a functional form for the cross section and adjust it iteratively until lineshape ratios computed from it match our data. We are currently working on establishing the proper basis for the construction of the cross sections. In the meantime, we can calculate simulated

lineshape ratios from cross sections obtained from classical trajectories and compare them. Cross sections, data and simulations are shown in figures 3 and 4. It is already clear from this limited analysis that the experimental vibrationally inelastic cross sections exhibit threshold behavior similar to that exhibited by the calculated cross sections.

Our measurements, particularly our velocity-resolved cross sections, coupled with the r -dependent *ab initio* potential of Alexander and Werner, provide a benchmark system for the quantum mechanical computation of vibrationally inelastic cross sections. There are at present very few vibrating atom-diatom potentials (e.g. N_2-He [BCW86]) and for those potentials there is a dearth of detailed experimental data on vibrationally inelastic scattering. The agreement between rotationally inelastic rate constants calculated using this potential [ALW91] and experimental rate constants obtained by the same method as employed by us [SSP84] is essentially perfect; this fact plus the close agreement between our classical rate constants and our data lead us to hope that a quantum mechanical calculation will be carried out soon.

Further testing of this potential would be provided by comparison of measured and calculated angle differential cross sections. McCaffery and co-workers have recently developed a technique that makes it possible to extract differential cross sections from double resonance signals [REM92,MRW88]. Figure 5 shows the vibrationally inelastic angle differential cross section from classical trajectories for $v_i = 2$, $j_i = 30$, and several different values of Δj . The prominent forward peak associated with the classical rotational rainbow at small $|\Delta j|$ is replaced by backward scattering at large negative Δj and by sideways scattering at large positive Δj . Moskowits [MOS90] has proposed a three dimensional model that accurately reproduces measured vibrotationally inelastic differential cross sections in the system Na_2-X and permits association of features on the potential surface with features in the differential cross section. We intend to apply this model to $\text{Li}_2(\text{A})-\text{Ne}$ scattering in order to understand the form of the differential cross sections we calculate and measure and also in the hope of extending a recent suggestion for the inversion of differential cross sections [MCA91] to vibrationally inelastic scattering.

We intend to extend our measurements much closer to the dissociation limit. At $v = 24$ the vibrational level spacing has declined by only 28%

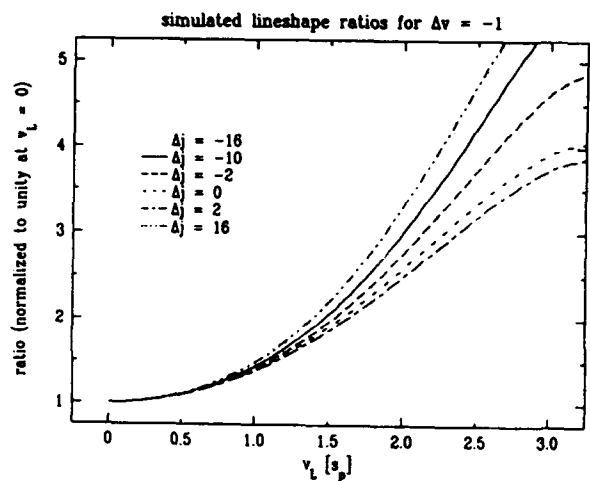
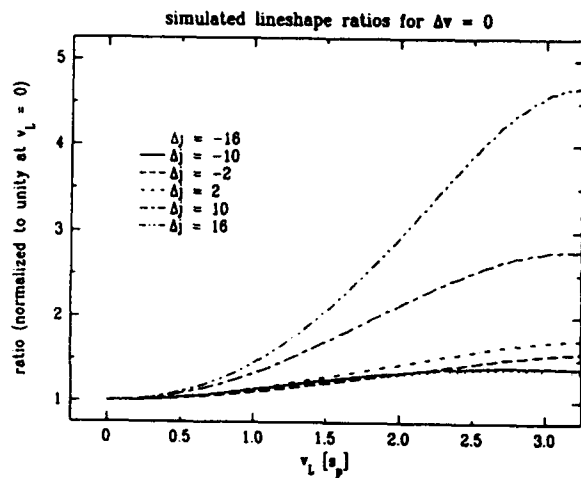
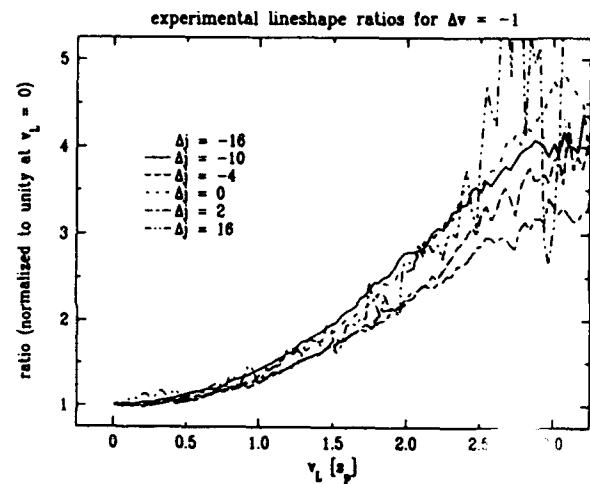
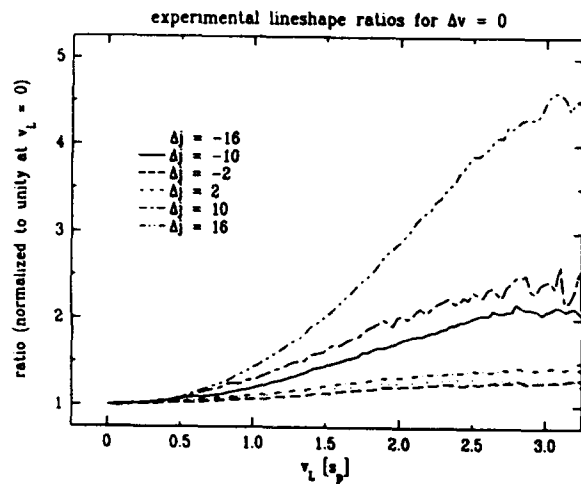
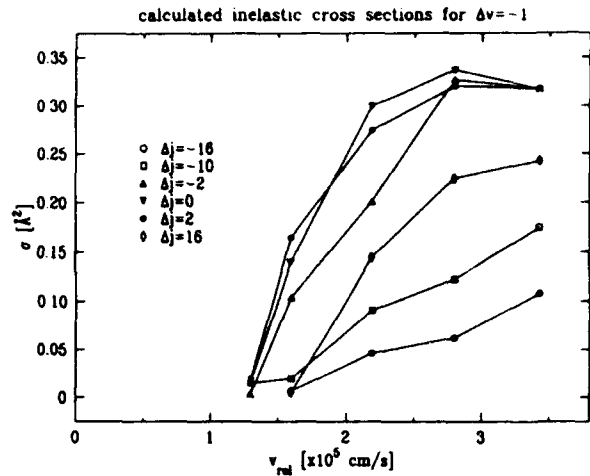
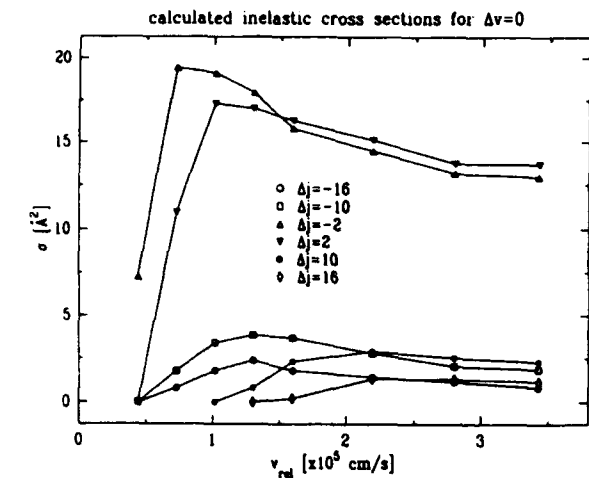


Figure 3: Calculated velocity-dependent cross sections and experimental and calculated lineshape ratios for $\Delta v = 0$. Velocity is in units of mean thermal velocity.

Figure 4: Calculated velocity-dependent cross sections and experimental and calculated lineshape ratios for $\Delta v = -1$.

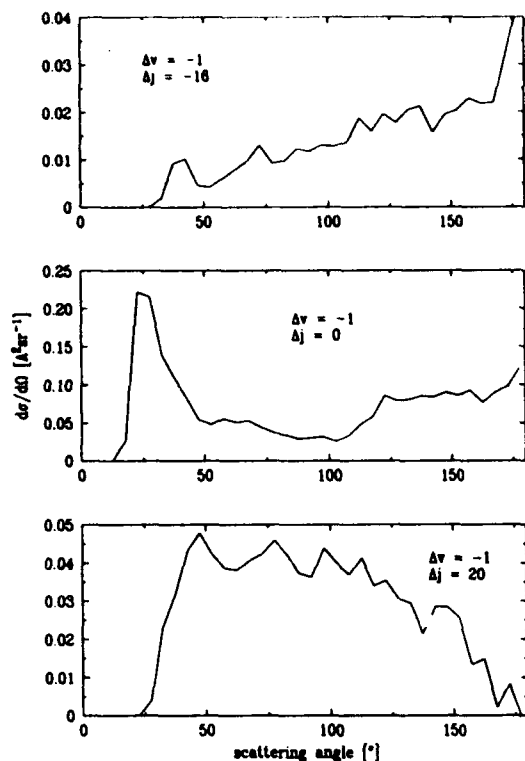


Figure 5: Differential cross sections from classical trajectories on the Werner-Alexander potential.

from its value at $v = 0$. To achieve higher v will require Franck-Condon pumping and a second laser to excite the inverted X state vibrational population distribution. In this way we intend to extend our study as close as possible to the dissociation continuum. A part of this study will entail extending the known spectroscopy of the A state, which currently terminates at $v=25$ [KUH77], although the A state possesses 41 bound vibrational levels. We anticipate that this will be a straightforward process, since perturbations are few and local in this state [SCM85]. If we can excite levels near to dissociation in this manner, we can learn about the transition from vibrationally adiabatic to sudden behavior. This will provide a concrete experimental test of the observation of Nesbitt and Hynes, based on classical trajectories, that average energy transfer as a fraction of local oscillator spacing obeyed a power law for highly excited oscillators [NEH82].

References

- ALW91 M. H. Alexander and H.-J. Werner, *J. Chem. Phys.*, **95**, p. 6524 (1991).
 BCW86 A. J. Banks, D. C. Clary, and H.-J. Werner, *J. Chem. Phys.*, **84**, p. 3788 (1986).
 KBD89 D. J. Krajnovich, K. W. Buts, H. Du, and C. S. Parmenter, *J. Chem. Phys.*, **91**, p. 7705 (1989).
 KUH77 P. Kusch and M. M. Hessel, *J. Chem. Phys.*, **67**, p. 586 (1977).
 MCA91 A. J. McCaffery and Z. T. Alwahabi, *Phys. Rev. A*, **43**, p. 611 (1991).
 MOS90 W. P. Moskowitz, Ph. D. Thesis, M.I.T., 1990 (unpublished).
 MRW88 A. J. McCaffery, K. L. Reid, and B. J. Whitaker, *Phys. Rev. Lett.*, **61**, p. 2085 (1988).
 NEH82 D. J. Nesbitt and J. T. Hynes, *J. Chem. Phys.*, **76**, p. 6002 (1982).
 PRB85 W. Preuss and G. Baumgartner, *Z. Physik*, **A320**, p. 125 (1985).
 REM92 K. L. Reid and A. J. McCaffery, *J. Chem. Phys.*, **96**, p. 5789 (1992).
 RFK87 L. B. Ratcliff, J. L. Fish, and D. L. Konowalow, *J. Mol. Spectrosc.*, **122**, p. 293 (1987).
 RUB90 H.-G. Rubahn, *J. Chem. Phys.*, **92**, p. 5384 (1990).
 SCM85 I. Schmidt-Mink and W. Meyer, *Chem. Phys. Lett.*, **121**, p. 49 (1985).
 SMI86 N. Smith, *J. Chem. Phys.*, **85**, p. 1987 (1986).
 SSP84a T. P. Scott, N. Smith, and D. E. Pritchard, *J. Chem. Phys.*, **80**, p. 4841 (1984).
 SSP84b N. Smith, T. P. Scott, and D. E. Pritchard, *J. Chem. Phys.*, **81**, p. 1229 (1984).
 YKW92 X. Yang, E. H. Kim, and A. M. Wodtke, *J. Chem. Phys.*, **96**, p. 5111 (1992).

INTERMOLECULAR INTERACTIONS IN THE FLUORENE DIMER

Lt. Clark Highstrete
USAF Space and Missile System Center
El Segundo, CA 90245

and

John Wessel
The Aerospace Corporation
P. O. Box 92957
Los Angeles, CA 90009

INTRODUCTION

Excited state interactions in molecular dimers and higher clusters are of increasing spectroscopic interest because the interactions reveal the nature of the intermolecular potential and provide geometrical information about clusters. Cold clusters were prepared in a supersonic beam and studied by fluorescence excitation and photoionization and spectroscopies. Past studies revealed that benzene dimers are characterized by weak intermolecular interactions in the first excited state, whereas naphthalene dimers undergo strong excimer formation that results in broad electronic spectra. Prior reports² indicated that fluorene dimers fluoresce efficiently from a lower energy excimer state.

RESULTS

The photoionization spectrum recorded in our laboratory was relatively broad compared to the published fluorescence excitation spectrum, which was sharp and highly chaotic in structure. Attempts to increase cooling of the molecular beam were not effective in reducing linewidths to those reported previously for the corresponding fluorescence excitation spectrum. Therefore, we implemented a fluorescence detection system that was optimized for cooling capability. Photoexcitation was detected by monitoring excimer emission at wavelengths red shifted from the dimer absorption spectrum.

The resulting highly resolved spectra, shown in Figure 1, are far more regular and have drastically different structure than those reported previously. They provide clear evidence of complex intermolecular interactions. Although it can be difficult to exclude contributions from higher mass species when using conventional fluorescence excitation methods, it is not a significant problem in this case because the monomer transitions are sharp and readily identified, the dimer lines have uniform pressure dependence, and the higher clusters are of low abundance, as established from photoionization spectra.

The most prominent feature of the dimer spectrum is the complex origin system shown in Figure 1. We designate the origin band system to be the lowest energy group of components which span the range from 298 to 297 nm. The structure is highly reproducible. The higher energy components, which are separated by intervals corresponding to monomer intramolecular vibrations of 208, 405, and 736 cm^{-1} , appear to be simple overlapping doublets. If there is substructure, it is concealed by the overall linewidths.

DISCUSSION

The fluorene dimer spectrum shown in Figure 1 reveals a classical example of dimer excitonic interaction in the intermediate coupling limit. This was predicted in early papers by McClure³, and Davydov⁴. In our analysis, based on the simple exciton model approach, the intermolecular interactions in the origin system are modulated by the vibronic strength associated with an intermolecular vibrational mode. The vibrationless origin consists of two weak components, at 33564 and 33572 cm^{-1} . The splitting between them represents a portion of the overall excitonic coupling, which is distributed over all the totally symmetric vibronic band structure. The $\nu' = 1$ intermolecular vibrational level has the largest Franck-Condon factor, therefore it is subject to greatest intermolecular interaction. This is responsible for the large splitting between the intense 33567 and 33584 cm^{-1} components. The pairs of weaker components at 33572 and 33591 cm^{-1} and at 33598 and 33603 cm^{-1} represent the $\nu' = 2$ and $\nu' = 3$ levels. The splittings in each pair are roughly proportional to the intensities, as required in the exciton model provided the Condon approximation and multipolar interaction models apply. The nearly equal intensities of the doublets suggests that the dimer molecules are effectively symmetry equivalent, with long in-plane transition dipole moments oriented at large angles (about 90 degrees).

Based on these assignments, we obtain an intermolecular progression of 11 cm^{-1} , extending over the sequence from $v' = 0 - 4$, with a standard deviation of 0.7 cm^{-1} . This frequency is consistent with the intermolecular stretching vibration of a fluorene vander Waals dimer.

The observed spectra do not provide direct evidence of the excimer state. In essence, all the excitonic interactions for this species are expressed in a highly regular origin band system. The rapidly increasing linewidths within this system are consistent with a rate of vibrational redistribution that increases with energy or with indirect coupling to lower lying excimer states. The higher energy intramolecular vibrational features are correlated with totally symmetric monomer vibrational species. In the traditional weak coupling vibronic interaction picture excitonic interactions occur for these levels. The splittings should be proportional to band intensity. The vibrational transitions have low intensity relative to the origin system, therefore splittings are predicted to be small. .

In conclusion, the fluorene dimer spectrum represents a classic case of intermediate excitonic coupling. It represents the clearest example known of dimer excitonic coupling. These large molecules behaves as regularly as one would expect a simple dimer composed of diatomic molecules! Currently we are implementing improved cooling in the photoionization configuration in order to ascertain if, under ideal cooling conditions, the photoionization spectrum converges with the fluorescence excitation spectrum. The existing results suggest that the photoionization spectrum contains discrete, low amplitude structure corresponding to the features of the fluorescence excitation spectrum, superimposed on a broad, continuum background that is centered on the origin band. The broad background is repeated in some of the intermolecular vibrational bands. Provisionally, we associate the broad structure with rapid biexcitonic autoionization, as was observed for the naphthalene trimer⁵. However, in the latter case, the continuum was less prominent. Final confirmation of these results awaits measurement of mixed isotopic spectra using mass selective detection.

In summary, the results show that there is a modest displacement between the fluorene molecules along an intermolecular coordinate in the S_1 dimer state, relative to the ground state. The excitonic interactions are consistent with a pure S_1 interaction and there is no clearcut spectral evidence in this region of the excimer state. This suggests that excimer formation involves a different set of precursor molecular states.

Figure

1. Photoexcitation spectrum of the fluorene dimer S_1 -- S_0 origin region recorded by monitoring the excimer emission. Fluorene dimers were cooled in a supersonic beam expansion.

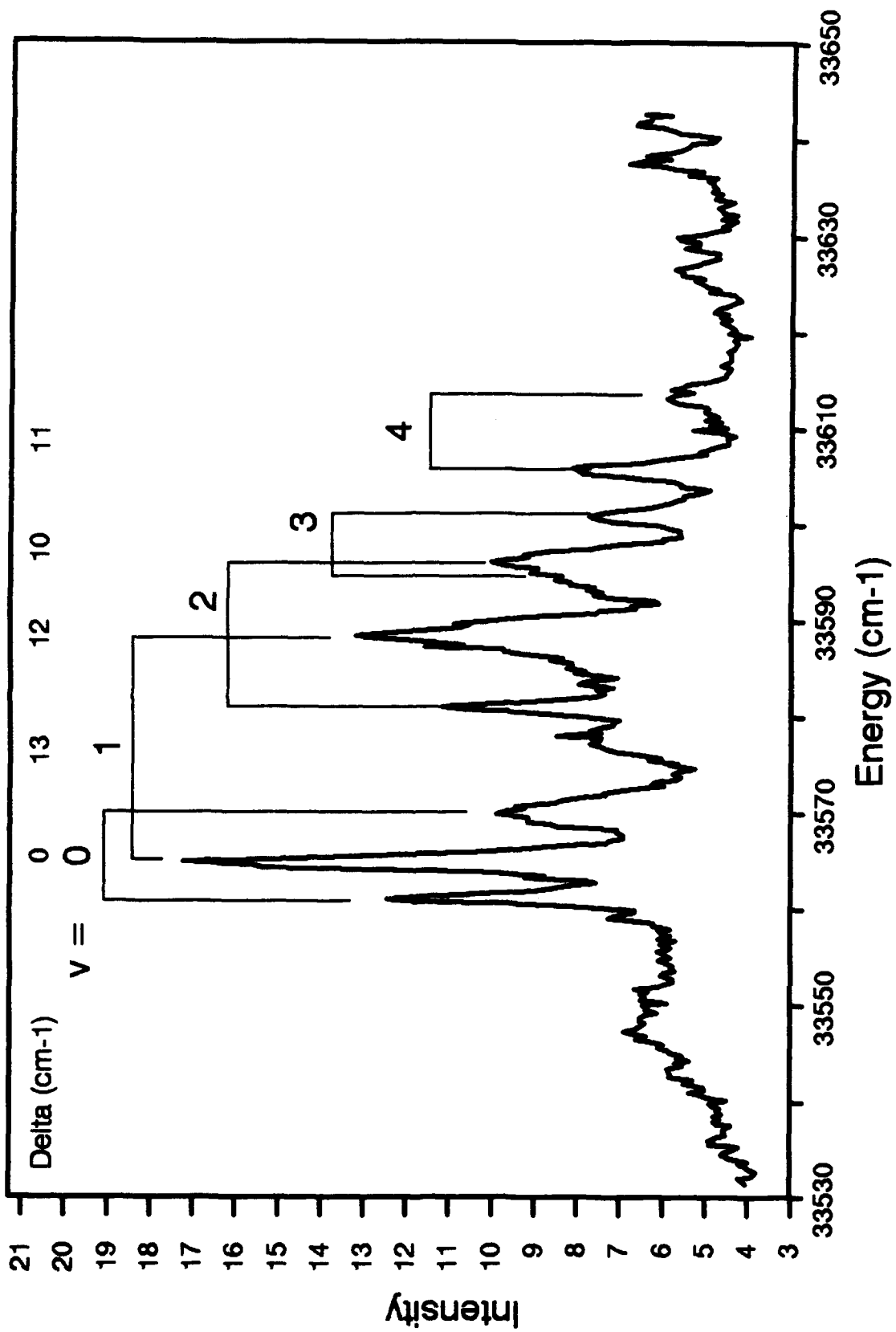
¹Supported by the Department of Energy, Office of Health and Environment, Grant DE-FG03-86ER60391.

²H. Saigusa and M. Itoh, *J. Phys. Chem.* **89**, 5486, (1985); H. Saigusa and E. C. Lim, *J. Phys. Chem.* **94**, 2631 (1990).

³D. S. McClure, *Solid State Phys.* **8**,1 (1958).

⁴A. S. Davydov, *Theory of Molecular Excitons*, McGraw-Hill, New York, New York (1962).

⁵J. Wessel, *Phys. Rev. Lett.* **64**, 2046 (1990).



Study on isotope mass difference (^{16}O , ^{18}O) effect on
 CO_2 laser oscillation spectra

Yasuyuki SAITO

Domicile and actual address: Apartment Sanyu-Kopo Room No.202, Hazawa-cho 342,
 Kanagawa-ku Yokohama 221, Japan (Correspondent address: Microelectronics Center
 Tamagawa Works, Toshiba Corp., 1, Komukai Toshiba-cho, Saiwai-ku, Kawasaki 210, Japan)

Abstract

It is difficult to explain continuity between $^{12}\text{C}^{16}\text{O}_2$ - $^{12}\text{C}^{18}\text{O}_2$ laser oscillation spectra due to only oxygen isotope-mass-difference (^{16}O , ^{18}O) effect on rotation energy level of fine structure for 00^0_1 to 10^0_0 of transition of CO_2 molecules. In order to explain fine structure interval of CO_2 laser oscillation spectra, it is necessary to consider CO_2 molecule shape of smaller O=C bond length (this means smaller rotation inertia moment of a CO_2 molecule) through nuclear characteristics (for example, gravity center, shape, spin) in a CO_2 molecule.

The author offered the possibility of isotope effect in CO_2 molecules on continuity between CO_2 laser oscillation spectra.1-4) The continuous spectra of CO_2 molecule laser was shown.5,6) However, in spite of the conceptually same conditions of the previous reports 5,6), separated oscillation spectrum lines of CO_2 molecule lasers were shown.1-3,7,8) Therefore, on the basis of the offered idea 1-4) that isotopes in a CO_2 molecule laser act as important role for CO_2 molecule laser oscillation spectra, from the viewpoint of mass difference between an ^{16}O and ^{18}O atoms, the actual CO_2 molecule laser oscillation spectrum lines was considered.

Isotopes in CO_2 molecules exist as shown in Table I.9) In the present study, $^{12}\text{C}^{16}\text{O}_2$ and $^{12}\text{C}^{18}\text{O}_2$ molecules were selected from isotope-contained CO_2 molecules as shown in Fig.1 in order to compare calculation data with the experiment data 3,6,7).

Table I. Isotopes in CO_2 molecules [not radioactive] (Ref.9)

Element	Carbon		Oxygen		
	^{12}C	^{13}C	^{16}O	^{17}O	^{18}O
Isotope					
Mass	12	13	16	17	18
Natural existence ratio (%)	98.892	1.108	99.759	0.037	0.204

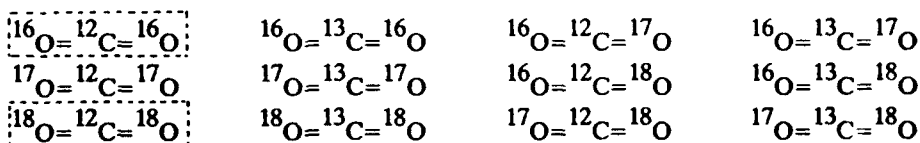


Fig.1. Isotope combinations in carbon dioxide molecules.

We observed the separated fine structure laser oscillation of transition 00^0_1 band to 10^0_0 band for for the author's previous experiment 3) such as shown in the previous reports 7,8) in spite of entirely different conditions. Thus, we take a theme on the CO_2 molecule band transition of 00^0_1 to 10^0_0 band for $^{12}\text{C}^{16}\text{O}_2$ and $^{12}\text{C}^{18}\text{O}_2$ molecules as shown in Fig.2. It is thought that the origin of the fine structure of CO_2 molecule laser oscillation spectrum lines is rotation of a CO_2 molecule as shown in Fig.2.

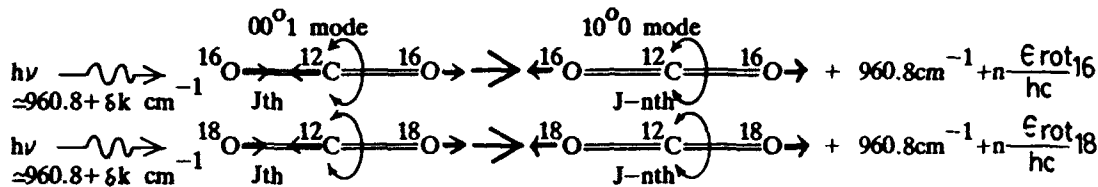


Fig.2. Transitions from $^{12}\text{C}^{16}\text{O}_2$ 00^0_1 , $^{12}\text{C}^{18}\text{O}_2$ 00^0_1 rotation mode to $^{12}\text{C}^{16}\text{O}_2$ 10^0_0 , $^{12}\text{C}^{18}\text{O}_2$ 10^0_0 rotation mode.

Energy level of J th rotational level from the 0 th rotational level is given by

$$F(J) \approx BJ(J+1). \quad (1.7)$$

Here, B is $\hbar^2/2I$. I is inertia moment of a CO_2 molecule. $\hbar = h/2\pi$. h is a Planck constant. We take carbon nuclear position in a CO_2 molecule as the center of gravity as shown in Fig.3.

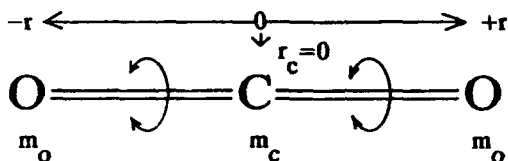


Fig.3. Mass and coordinates of a carbon dioxide molecule for rotation mode. m_o : oxygen mass, m_c : carbon mass. r : vector, $|r|$ =bond length of $\text{O}=\text{C}$. r_c : vector, $|r_c|$ =distance from the coordinate of C to gravity center. $r_c=0$ nearly means rotation of a hard uniform cylinder.

The coordinate \bar{x} of the center of gravity is 0, because $r_c=0$ and

$$\bar{x} = (m_o r - m_o r + m_c r_c) / (2m_o + m_c) = 0. \quad (2.9)$$

Inertia moment I is given by

$$I = \sum m_i x_i^2 - M \bar{x}^2 = 2m_o r^2 + m_c r_c^2 = 2m_o r^2. \quad (3.9)$$

For example, when natural oxygen mass is 16.00445 ($16 \times 0.99759 + 17 \times 0.00037 + 18 \times 0.00204$), inertia moment is $43.06 \text{ amu} \text{ \AA}^2$. Bond length of $\text{O}=\text{C}$ is 1.16 \AA .

The inertia moment I_{16} of $^{12}\text{C}^{16}\text{O}_2$ is $2 \times 16 \times 1.16 \text{ \AA}^2 = 43.06 \text{ amu} \text{ \AA}^2 = 43.06 \times 10^{-20} / 6.023 \times 10^{26} \text{ Kgm}^2 = 7.15 \times 10^{-46} \text{ Kgm}^2$. I_{18} of $^{12}\text{C}^{18}\text{O}_2$ is $2 \times 18 \times 1.16 \text{ \AA}^2 = 8.04 \times 10^{-46} \text{ Kgm}^2$. B in Eq.(1) is given by

$$B \text{ of } ^{12}\text{C}^{16}\text{O}_2 = \hbar^2/2I_{16} = 7.77 \times 10^{-24} \text{ J}, \quad B_{16} = 7.77, \text{ and} \quad (4a).$$

$$B \text{ of } ^{12}\text{C}^{18}\text{O}_2 = \hbar^2/2I_{18} = 6.91 \times 10^{-24} \text{ J}, \quad B_{18} = 6.91. \quad (4b).$$

The difference $\Delta \epsilon_{jth}$ between J th laser oscillation energy level from 00^0_1 to 10^0_0 and $J+1$ th one is given by

$$\begin{aligned} \Delta \epsilon_{jth} &\approx \{h\nu_{00^0_1} + BJ(J+1)\} - \{h\nu_{10^0_0} + BJ(J-1)\} \\ &= h(\nu_{00^0_1} - \nu_{10^0_0}) + 2BJ = h\Delta\nu + 2BJ. \text{ Here, } \Delta\nu = \nu_{00^0_1} - \nu_{10^0_0} \text{ and } J=2n \text{ (n:1,2,3,..).} \end{aligned} \quad (5)$$

Fine structure wavelength difference is given by

$$\begin{aligned} \Delta\lambda &= \lambda_{j\text{th}}^{-1} - \lambda_{j+1\text{th}}^{-1} = hc(1/\Delta\epsilon_{j\text{th}} - 1/\Delta\epsilon_{j+1\text{th}}) = hc4B/(h\nu + 4nB)^2 [1 + 4B(h\nu + 4nB)^{-1}] \\ &= hc4B(h\nu)^{-2} = \lambda^2 4B(hc)^{-1} = (10.4 \times 10^{-4})^2 \text{ cm}^2 \times 4 \times B_{16\text{or}18} \times 10^{-24} / hc \\ &= 21.77 \times 10^{-8} B_{16\text{or}18} \text{ (cm)}, \quad c: 2.999 \times 10^{10} \text{ cm/sec.} \quad (6) \end{aligned}$$

Therefore, $\Delta\lambda_{16}$ for $^{12}\text{C}^{16}\text{O}_2 \approx 0.017\mu\text{m}$ and $\Delta\lambda_{18}$ for $^{12}\text{C}^{18}\text{O}_2 \approx 0.015\mu\text{m}$. The calculated oscillation spectrum line differences of both $^{12}\text{C}^{16}\text{O}_2$ and $^{12}\text{C}^{18}\text{O}_2$ are about $0.017\mu\text{m}$ and $0.015\mu\text{m}$ for each branch spectra line.

This result suggests a few meanings for CO_2 molecule laser oscillation spectra. One: From the calculation result and the previous report's result 6), we can conclude that the spectra in Fig.4 is from $^{12}\text{C}^{16}\text{O}_2$ molecule gas without oxygen isotope.

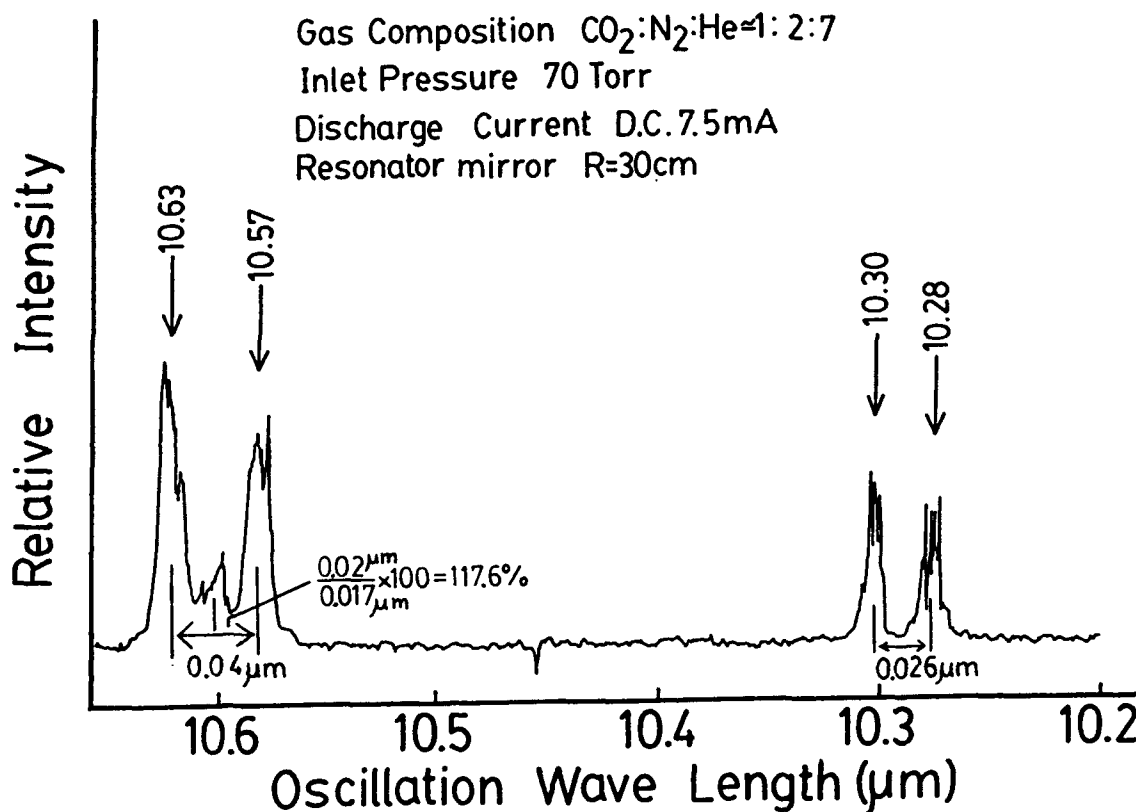


Fig.4. Separated spectra of a gas-flow small waveguide carbon dioxide laser. From Ref.3.

Two: However, these calculated values are 17.6% smaller than those of the previous report 7) and the spectra in Fig.4. This discrepancy requires small inertia moment I of Eq.(3). This means that if oxygen effective mass for CO_2 laser oscillation is the same as the oxygen effective mass for CO_2 molecule thermodynamic heat capacity, the excited effective bond length of $\text{C}=\text{O}$ for inertia moment I is shorter than 1.16\AA . It may be necessary to consider

excited CO_2 molecule shape of smaller $\text{O}=\text{C}$ bond length (this means smaller inertia moment of a CO_2 molecule) through nuclear characteristics (for example, gravity center, shape, spin) in CO_2 molecule. Three: The wavelength difference for $^{12}\text{C}^{16}\text{O}_2$ molecule laser is only 13% different from that for $^{12}\text{C}^{18}\text{O}_2$ molecule laser. Therefore, it seems that the continuity between all branch fine structures of oscillation spectra as shown in Fig.5 can not be obtained from the mass difference effect of $^{12}\text{C}^{16}\text{O}_2$ and $^{12}\text{C}^{18}\text{O}_2$ existence even though the continuity between some branches can be possible.

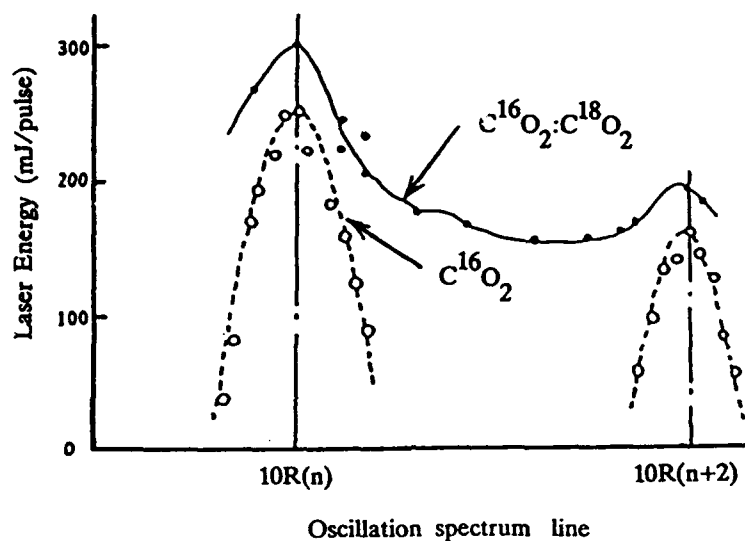


Fig.5. Continuous spectra of a $^{12}\text{C}^{16}\text{O}_2$ and $^{12}\text{C}^{18}\text{O}_2$ mixed gas high pressure grating laser. From Ref.6 (cf. Ref.5).

References

1. Y.Saito and T.Manabe, Extended Abstracts (The 39th Spring Meeting, 1992); The Jpn.Appl. Phys.Soc. and Related Societies, 28p-D-2, p.867 (JSAP Cat.Num.: AP921108-03).
2. Y.Saito and T.Manabe, presented by the 1992 Interdisciplinary Laser Science Conference (ILS-VIII) in session E4 [TuPP](Zia Room): Gas and Free Electron Lasers (in Albuquerque, NM) at 15.00 p.m. on 22nd Sept., 1992. The American Physical Society, Bulletin Vol.37, No.4, p. 1215.
3. Y.Saito, submitted to Applied Optics
4. Y.Saito, unpublished (1982).
5. K.Hotta, Extended Abstracts (The 37th Autumn Meeting, 1976), Jpn.Appl.Phys.Soc., 2p-N-5, p.309 (Japanese).
6. M.Hagiwara, H.Tanaka, M.Hasegawa, Y.Yato, H.Tashiro, M.Igarashi, and T.Yamada, Extended Abstracts (The 38th Spring Meeting, 1991); The Jpn.Appl.Phys.Soc. and Related Societies, 29p-E-5, p.896 (JSAP Cat.Num.: AP911109-03) (Japanese).
7. C.K.N. Patel, Phys.Rev.136, A1187 (1964).
8. Y.Saito, Y.Kinoshita, T.Sato, and T.Manabe, in Extended Abstracts (The 40th Spring Meeting, 1993); The Jpn.Appl.Phys.Soc. and Related Societies.
9. S.Chikazumi, K.Kigoshi, and S.Tanuma, Revised Modern Knowledge on Elements (Japanese, Revised 1st Ed., Tokyoshoseki, 1985, Tokyo), p.20 and p.24.
10. J.H.Knox, Molecular Thermodynamics (English Ed. John Wiley and Sons, Ltd. 1971. Translated into Japanese by I.Nakagawa and his colleagues. Tokyo-Kagakudojin. 1974), major related sections: 6.2, 6.3, 9.3, 9.4, and 11.3 on a carbon dioxide molecule.

Color change and highly refractory surfaces of polycrystalline silicon of arsenic atoms of high dose implanted at low acceleration voltage. as the interesting object of the Raman spectroscopy.

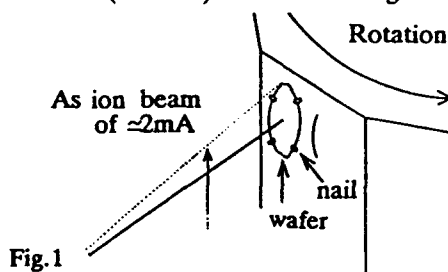
Yasuyuki SAITO

Nichiden-Toshiba Info.Syst. (NTIS) res.lab. in Toshiba Horikawa-cho Works, 72, Horikawa-cho, Saiwai-ku, Kawasaki 210, Japan. (now Microelectronics ctr. Tamagawa Works, Toshiba Corp., 1 Komukai Toshiba-cho, Saiwai-ku, Kawasaki 210, Japan. Correspondence address)

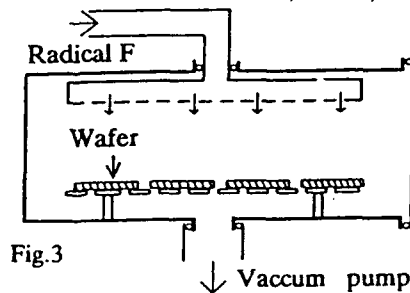
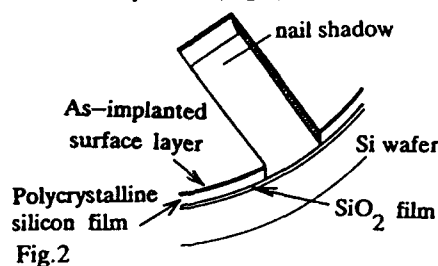
Abstract

Polycrystalline silicon surface of arsenic atoms of $\approx 10^{15} \text{ cm}^{-2}$ implanted at 40keV showed color change from gold to light-red under a fluorescent light and highly refractory obstacle against exposure etching of radical fluorine excited with microwave. The refractory surface mechanism may be related to the fastening of vibration of lattice Si atoms of polycrystalline silicon. This is an interesting object for analysis of the Raman spectroscopy.

On the way to examining a very large scale integration circuit (VLSI) making process on silicon wafers 1-5), high dose ($\approx 10^{15} \text{ cm}^{-2}$) of high current ($\approx \text{mA}$, typical: 2mA) arsenic implantation at 40keV with a Lintott series-3 apparatus 6-10) was applied to n-type electrically-active shallow impurity doping of polycrystalline silicon films of low-pressure chemical vapor deposition method (LPCVD) as shown in Fig.1.



After high dose and low acceleration voltage arsenic implantation into LPCVD polycrystalline silicon films of $\approx 4000 \text{ \AA}$ on SiO_2 -covered Si wafers, it was found that there were shadows of susceptor nails 11) and there was color change 12). The color change was from gold to light-red under a fluorescent light.13) The parts of the nail shadows (Fig.2) were easily etched with the exposure (Fig.3) of radical fluorine excited with microwave 14).15-17)



Molecular Spectroscopy at Ultracold Temperatures

K. Helmerson, M. Wagshul, P. Lett, S. Rolston, and W. Phillips
National Institute of Standards and Technology, Physics A-167
Gaithersburg, MD 20899
(301) 975-4266

Associative ionization (AI) in sodium ($\text{Na} + \text{Na} + 2 h\nu \rightarrow \text{Na}_2^+ + e^-$) has been a convenient reaction in which to study excited state collisions under "ultracold" conditions (≤ 1 mK) because the reaction product is easily identified and collected with high signal-to-noise. Previous studies [1] have revealed evidence of molecular intermediate-state resonances under high-intensity laser conditions. Theoretical analysis [2] has associated this structure with singly- and doubly-excited Na_2 intermediate states. In this work, we present a new technique utilizing a switched magneto-optical trap (MOT) to make clean measurements of the spectrum of associative ionization in a regime where we can identify the peaks as being associated with states of the Na_2 molecule. In addition, our technique reveals new structure in the spectrum of AI versus laser frequency, pointing out the previously unappreciated importance of atomic hyperfine structure in the reaction.

In previous experiments studying AI we found resonance structure indicative of molecular intermediate states. In those measurements the laser that was used for exciting the colliding atoms also provided the confinement. Thus, scanning the laser changed the temperature and the density of atoms as well as the excitation frequency. The laser necessarily had to be kept at quite high intensity to confine the atoms, thereby broadening the spectrum. In addition, the trap could not be tuned to the blue of resonance and its design inherently limited us to rather small numbers of atoms. The new experiments reported here are performed with a MOT providing the confinement and with an added excitation laser probing the AI spectrum. The MOT lasers are alternated with the swept excitation laser and an ion counting system is gated open only during the time that the single frequency excitation laser is on.

Figure 1 displays a partial spectrum of associative ionization of ultracold sodium versus the frequency of a probe laser. The region displayed is red of the $3S_{1/2}, F=2 \rightarrow 3P_{3/2}, F'=3$ transition and the resonance structures evident have been tentatively identified with intermediate molecular states. The extremely unusual conditions of ultracold collisions offers us the opportunity to perform such free-bound-free spectroscopy. These conditions allow us to study photo-associative spectroscopy extremely close to the dissociation limit.

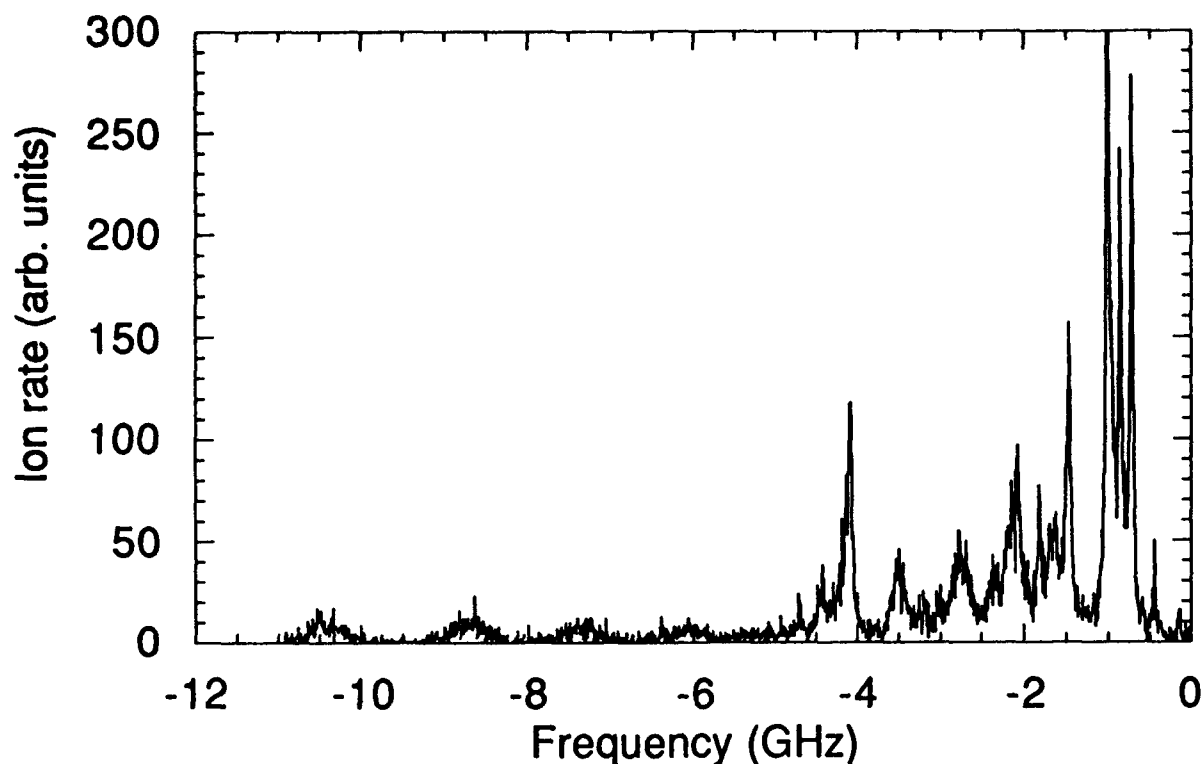


Figure 1. Spectrum of associative ionization versus laser detuning from the $F=2 \rightarrow F'=3$ transition frequency.

We have also utilized the switched MOT technique to obtain AI spectra blue of the $3S_{1/2}, F=2 \rightarrow 3P_{3/2}, F'=3$ transition. Figure 2b shows the results. A clear peak in the AI rate, beginning half way between the two resonances is seen. This feature is interpreted as follows. Two atoms collide, one in the $F=1$ ground hyperfine state and one in the $F=2$ state. Two photons at a frequency half way between the two resonance frequencies is just able to excite the atom pair to an excited $P + P$ state (which undergoes AI) through the indicated intermediate (see figure 3). This channel dominates because the excitation occurs at small enough internuclear separation that spontaneous decay is unimportant. Light slightly to the blue of this frequency is also able to excite the complex to higher lying continuum states. Detailed structure within this broad peak is interpretable in terms of intermediate bound state resonances.

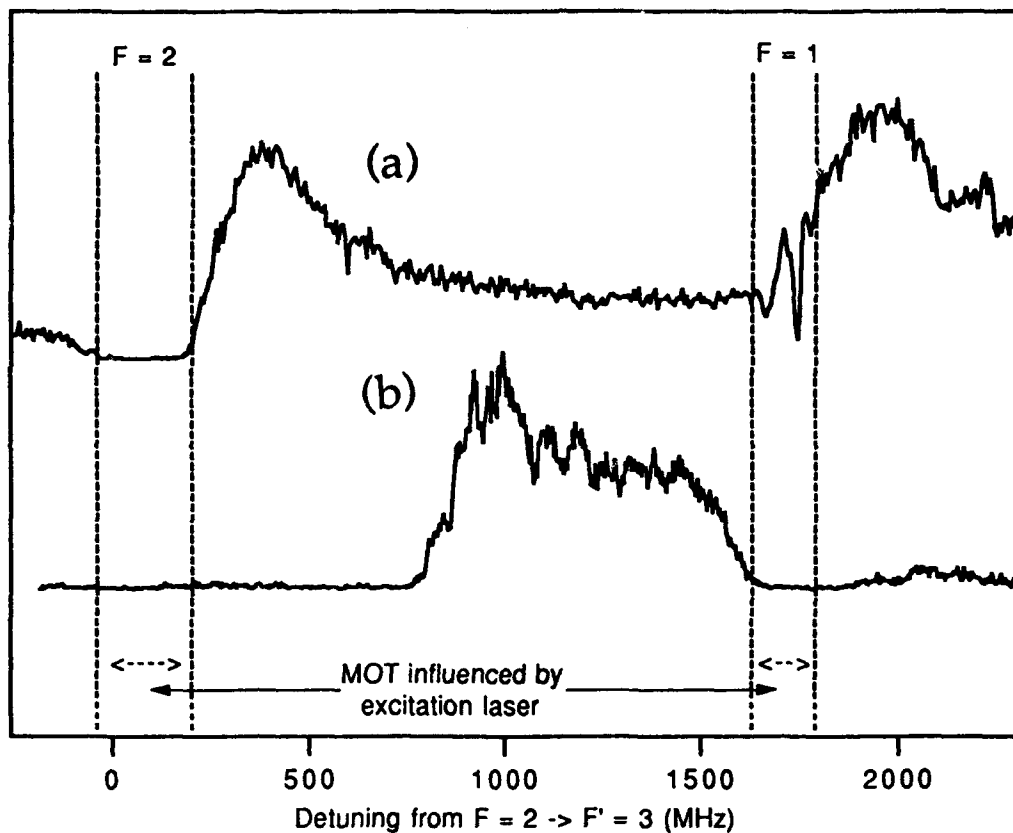


Figure 2 AI spectrum versus probe laser frequency. The position of the $F = 2 \rightarrow F' = 3$ and the $F = 1 \rightarrow F' = 2$ transition frequencies are indicated. a) MOT, including sidebands, on continuously. b) MOT and probe alternated.

We find that collision processes can be radically affected by the presence of small amounts of light at additional frequencies. In fact, the presence of the MOT lasers, although much weaker than the probe, cause rather severe and unexpected optical pumping and two-color enhancements in the AI rate, making interpretation extremely difficult. Figure 2a shows the spectrum of AI as the excitation laser is swept with the MOT on. The new resonance feature obtained with the switched MOT technique has been obscured. Also indicated in figure 2a are the regions over which the excitation laser has a clear influence on the MOT.

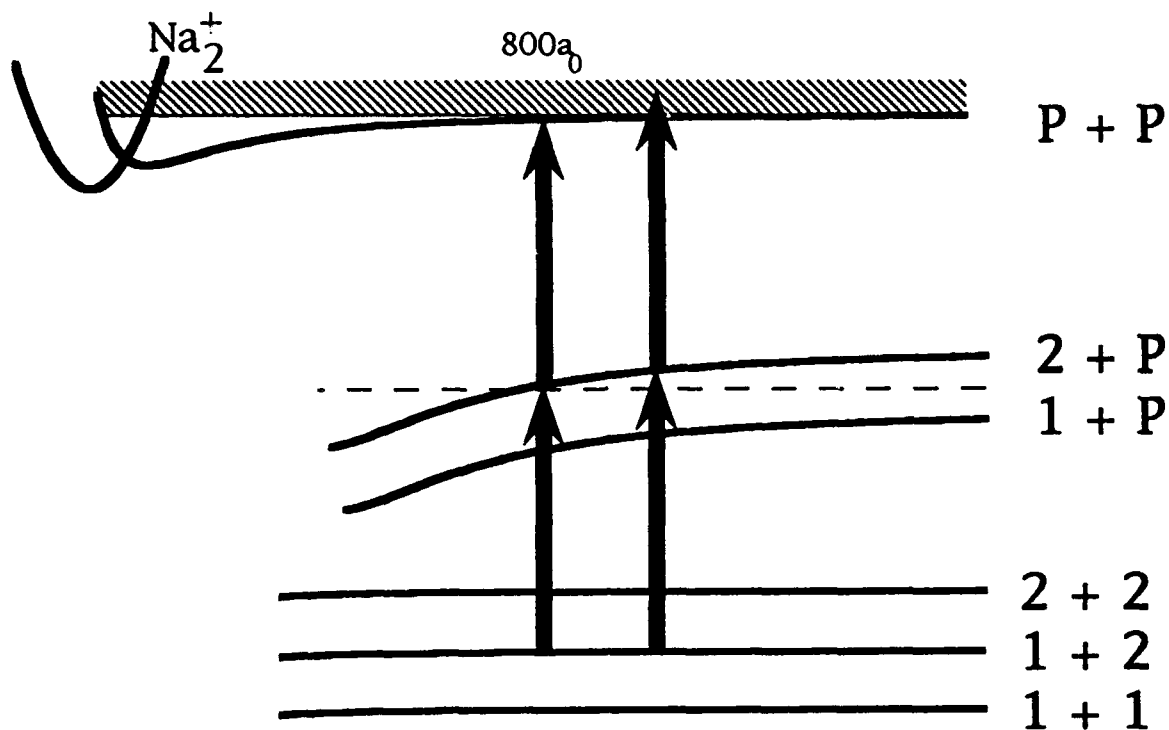


Figure 3 Sketch of the potential curves indicating the ground state hyperfine levels ($F = 1$ or 2), the excited states (P) and the transitions studied.

We would like to thank P. Julienne and R. Heather for helpful discussions. This work was supported by ONR.

- References:
1. P. Lett, P. Jessen, W. Phillips, S. Rolston, C. Westbrook and P. Gould, *Phys Rev. Lett.* **67**, 2139 (1991).
 2. P. Julienne and R. Heather, *Phys. Rev. Lett.* **67**, 2135 (1991), R. Heather and P. Julienne, *Phys. Rev. A*, (to be published).

Armentrout, P. B. — 159

Arrington, Caleb A. — 163, 167

Bagnato, V. — 175

Behm, Jane M. — 163

Birke, Michelle K. — 159

Blume, Thorsten — 163

Conceicao J. — 159

Davis, Scott — 178

Doverstål, Mats — 167

Gao, Yunxiao — 178

Gorgone, Peter — 178

Heidecke, Scott A. — 159

Helmerson, K. — 194

Highstrete, Lt. Clark — 182

Langenberg, Jon D. — 155, 163, 167

Lees, R. M. — 171

Lett, P. — 194

Lindgren, Bo — 167

Marcassa, L. — 175

McCall, Eric — 178

Morse, Michael D. — 155, 159, 163, 167

Phillips, W. — 194

Pinegar, Jacqueline C. — 155, 167

Rolston, S. — 194

Rosenberry, Mark — 178

Russon, Larry M. — 159

Saito, Yasuyuki — 187, 191

Sassenberg, Ulf — 167

Stewart, Brain — 178

Tao, C. — 175

Wagshul, M. — 194

Wang, Y. — 175

Weiner, J. — 175

Wessel, John — 182

Xu, Li-Hong — 171